TECHNISCHE UNIVERSITÄT DRESDEN

The multi Davydov-Ansatz:

Apoptosis of moving Gaussian basis functions

with applications to open quantum system dynamics

Dissertation
zur Erlangung des wissenschaftlichen Grades
Doctor rerum naturalium

vorgelegt von

Michael Werther
geboren am 03.02.1984 in Rudolstadt

Professur für Quanten-Vielteilchentheorie
Institut für Theoretische Physik
Fachrichtung Physik
Fakultät für Mathematik und Naturwissenschaften
Technische Universität Dresden
2020

Eingereicht am 21.04.2020

1. Gutachter: Prof. Dr. Jan Carl Budich
2. Gutachter: Prof. Dr. Uwe Manthe

Verteidigt am 30.07.2020

Abstract

We utilize the multi Davydov-Ansatz, an Ansatz of the bosonic many-body wave function in terms of moving Gaussian basis functions, to illuminate several aspects of open quantum system dynamics and quantum many-body theory. By two artifices alongside the time-dependent variational principle we extract from this Ansatz, commonly considered ill-behaved and not converging, a highly stable and converging method. Its extremely favourable scaling of the numerical effort with the number of degrees of freedom facilitates exploration of the zero and non-zero temperature physics of both system and environment of open quantum systems in the strong coupling regime, even in cases where the system is laser-driven.

The discovery that strongly coupling a system to an environment may, apart from the introduction of dissipation and decoherence also serve as a resource for the system has fuelled the research on strongly correlated open quantum systems. Although the advent of ultra powerful data processors enables advanced methods to tackle these systems, their explicit treatment without further assumptions remains an eminently challenging task. With the multi Davydov-Ansatz we numerically exactly calculate the dynamics of various open systems coupled strongly to an environment. In particular, we illuminate diverse aspects of laser-driven molecular dynamics in dissipative environments.

Based on a rigorous investigation of the time-dependent variational principle for moving Gaussian basis functions, we systematically develop a linear algebra formulation of the system of equations of motion for the Ansatz parameters. On its basis we precisely isolate the origin of the issues related to the multi Davydov-Ansatz and solve the long-standing convergence problem of the method by a regularization termed apoptosis. We show exemplary for the ohmic and sub-ohmic Spin-Boson model that apoptosis renders the multi Davydov-Ansatz a highly stable method with an outstanding speed of convergence, suited to numerically exactly reproduce the dynamics of the model at surprisingly humble numerical effort even for strong coupling strengths.

Furthermore, since they are not suited to efficiently reproduce Fock number states in many-body systems, we shed some light on possible extensions of the Gaussian basis functions in the multi Davydov-Ansatz in terms of displaced number states and in terms of squeezed states. In particular we argue that due to the emergence of an inappropriate number of equations of motion, there is no straightforward generalization of the multi Davydov-Ansatz by displaced number states.

For the purpose of further optimization of the multi Davydov-Ansatz, we investigate in detail the impact on the numerical effort of different representations of an open system's environment. In particular, different frequency discretizations for given continuous spectral densities are examined with respect to the speed of convergence of the system dynamics to the continuum limit. We utilize a Windowed Fourier Transform as an a priori measure for the quality of the discretized representation of bath correlations. Furthermore, efficient representations of the environment for shifted initial conditions in general and non-zero temperature in particular are found systematically.

As an alternative representation of an environment of mutually uncoupled harmonic oscillators, we investigate an environment represented in terms of a linear chain of effective modes. In this context we detail how to consistently reformulate the effective mode representation in second quantization, removing inadvertent double excitations introduced by the original formulation. We show that the

alternative representation is beneficial in cases where the bath spectral density is highly structured, while for the ohmic and sub-ohmic spectral density of the Spin-Boson model it is of no advantage.

Once we have identified the numerically most efficient representation of the environment, we apply the multi Davydov-Ansatz in order to illuminate several aspects of open quantum system dynamics whose investigation has previously remained occlusive. In particular, the access to the exact dynamics of the environmental degrees of freedom allows to shed light on the question for the channels through which energy can be interchanged between system and environment in the considered systems.

Firstly, in a system-bath setup we survey the vibrational relaxation dynamics of deuterium dimers at a silicon surface. The investigation of the relaxation dynamics requires the quantum mechanical treatment of multiple system levels, which in turn prohibits a treatment of the environmental dynamics on a perturbative level. We demonstrate that the multi Davydov-Ansatz allows for a numerically exact calculation of the system dynamics with multiple system levels and a huge number of surface vibrations explicitly taken into account. Furthermore, due to the structure of the spectral density of the environment, the effective mode representation allows for this system to dramatically reduce the numerical effort.

Secondly we shall investigate in detail the relaxation dynamics of an exciton in a one-dimensional molecular crystal. Since the strong coupling regime renders highly complicated the phonon dynamics, apoptosis turns out to be inevitably required in order to reliably converge the system dynamics. We show that the multi Davydov-Ansatz equipped with apoptosis allows for an extremely efficient calculation of the exciton and phonon dynamics, for both large hopping integrals and large molecular crystals.

Furthermore we illuminate diverse aspects of laser-driven molecular dynamics in a dissipative environment. By restriction to two electronic energy levels we determine the channels through which system and environment interchange energy in the vicinity of an avoided crossing in a dissipative Landau-Zener model. In particular, we reveal that the final transition probability can be tuned by coupling to the environment for both diagonal and off-diagonal coupling. By appropriately adjusting the initial excitation of the system, the final transition probability is shown to converge to a fixed value for increasing coupling.

Finally, we investigate in detail laser-induced population transfer by rapid adiabatic passage in a dissipative environment. By application of the multi Davydov-Ansatz it is shown for zero as well as for non-zero temperature that strongly coupling the system to an environment can serve as a resource for the population inversion. In particular, we shall examine how the coupling to the environment compensates for the decay channels in the system even if the laser pulse is only weakly chirped.

Zusammenfassung

Wir verwenden den multi Davydov-Ansatz, einen Ansatz der bosonischen Vielteilchen-Wellenfunktion mit frei beweglichen Gausschen Basisfunktionen, um verschiedene Aspekte der Dynamik offener Quantensysteme und der Quanten-Vielteilchen-Theorie zu untersuchen. Vermittels zweier Kunstgriffe im zeitabhängigen Variationsprinzip extrahieren wir aus diesem Ansatz, der üblicherweise als instabil und nicht konvergierend angesehen wird, eine hochgradig stabile und schnell konvergierende Methode. Die extrem günstige Skalierung des numerischen Aufwands der Methode mit der Zahl der Freiheitsgrade ermöglicht die Erforschung der System- als auch Umgebungs-Physik von offenen Quantensystemen bei starker Kopplung. Da des Weiteren sowohl zeitlich veränderliche Systeme als auch nicht verschwindende Temperaturen leicht in den Formalismus des multi Davydov-Ansatzes integrierbar sind, können sogar lasergetriebene Systeme bei endlichen Temperaturen und starker Kopplung untersucht werden. Die Kopplung eines Systems an eine Umgebung dient typischerweise der Beschreibung dissipativer Prozesse und führt zu Dekohärenz im System. Zwar hat die Entdeckung, dass eine solche starke Kopplung an eine Umgebung auch eine Ressource für die Systemdynamik darstellen kann, die Forschung an stark korrelierten offenen Quantensystemen befeuert. Doch trotz der Entwicklung ultraleistungsfähiger Datenprozessoren stellt die explizite Berechnung der Dynamik solcher Systeme ohne weitere einschränkende Annahmen noch immer eine überaus schwierige Aufgabe dar. Der multi Davydov-Ansatz befähigt uns, die Dynamik verschiedener stark gekoppelter offener Quantensysteme numerisch exakt zu berechnen. Mit seiner Hilfe beleuchten wir insbesondere diverse Aspekte lasergetriebener Moleküldynamik in dissipativen Umgebungen.

Basierend auf einer mathematisch rigorosen Untersuchung des zeitabhängigen Variationsprinzips für frei bewegliche Gausssche Basisfunktionen entwickeln wir systematisch eine Formulierung des Systems von Bewegungsgleichungen für die Ansatzparameter vermittels linearer Algebra. Diese ermöglicht sowohl die exakte Bestimmung der Ursachen der Instabilitäten und des Konvergenzproblems des multi Davydov-Ansatzes als auch deren Auflösung, welche wir im Falle des Konvergenzproblems als Apoptosis bezeichnet haben. Wir zeigen exemplarisch für das ohmsche und sub-ohmsche Spin-Boson Modell dass der multi Davydov-Ansatz durch Apoptosis zu einer hochgradig stabilen Methode mit hervorragender Konvergenzgeschwindigkeit wird, welche geeignet ist die Dynamik des Modells sogar für starke Kopplung mit geringem numerischem Aufwand exakt zu reproduzieren.

Da weiterhin die Gausschen Basisfunktionen im multi Davydov-Ansatz nicht geeignet sind, um die Fock-Besetzungszahlzustände in Quanten-Vielteilchensystemen effizient darzustellen, erläutern wir mögliche Erweiterungen derselben durch verschobene Besetzungszahlzustände und gequetschte Zustände. Dabei zeigen wir insbesondere die Unmöglichkeit einer direkten Verallgemeinerung des multi Davydov-Ansatzes durch verschobene Besetzungszahlzustände, da sich bei ihrer variationellen Ableitung eine ungeeignete Ansatz von Bewegungsgleichungen ergibt.

Zum Zwecke der weiteren Optimierung des multi Davydov-Ansatzes untersuchen wir detailliert den Einfluss verschiedener Darstellungen der Umgebung auf den numerischen Aufwand der Methode. Dazu analysieren wir für gegebene kontinuierliche Spektraldichten verschiedene Diskretisierungen der Frequenzachse hinsichtlich deren Konvergenzgeschwindigkeit der Systemdynamik gegen den Kontinuums-

Limes. Eine Fourier-Fensterfunktion dient dabei als Maß für die Qualität der diskretisierten Darstellung der Bad-Korrelationen. Des Weiteren leiten wir systematisch effiziente Darstellungen der Umgebung für verschobene Anfangsbedingungen im Allgemeinen und endliche Temperatur im Speziellen her.

Als eine alternative Darstellung der Umgebung durch miteinander nicht wechselwirkende harmonische Oszillatoren untersuchen wir auch Umgebungen die als eine lineare Kette effektiver Moden gegeben sind. In diesem Kontext zeigen wir, wie das Auftreten unerwünschter Doppelanregungen in der ursprünglichen Formulierung durch eine konsistente Herleitung der effektiven Darstellung in zweiter Quantisierung verhindert werden kann. Wir demonstrieren, dass die effektive Darstellung für hochgradig strukturierte Spektraldichten vorteilhaft ist, während sie für die ohmsche und sub-ohmsche Spektraldichte des Spin-Boson Modells keinen Vorteil bietet.

Sobald wir die numerisch effizienteste Darstellung der Umgebung identifiziert haben, untersuchen wir unter Anwendung des multi Davydov-Ansatzes bisher unerforschte Aspekte der Dynamik offener Quantensysteme. Dabei nutzen wir den Zugang zur exakten Dynamik der Umgebung zur Identifikation der Kanäle, durch welche System und Umgebung in den betrachteten offenen Quantensystemen Energie austauschen können.

Zum einen erforschen wir in einem System-Bad-Kontext die Schwingungs-Relaxationsdynamik von Deuterium-Dimeren an einer Silizium-Oberfläche. Die Tatsache, dass die Untersuchung der Dynamik dieses Systems die quantenmechanische Einbeziehung vieler System-Level erfordert, macht eine störungstheoretische Behandlung der Umgebungsdynamik unmöglich. Wir demonstrieren, dass vermittels des multi Davydov-Ansatzes eine numerisch exakte Berechnung der Systemdynamik unter Einbeziehung vieler System-Level und einer sehr großen Anzahl von Oberflächen-Schwingungen möglich ist. Wegen der Struktur der Spektraldichte der Umgebung kann der numerische Aufwand für die Berechnung der Dynamik durch die Darstellung in effektiven Moden drastisch reduziert werden.

Zweitens untersuchen wir detailliert die Relaxationsdynamik eines Exzitons in einem eindimensionalen Molekül-Kristall. Wir zeigen, dass die zuverlässige Konvergenz der Systemdynamik Apoptosis zwingend erfordert, da wegen der starken Kopplung die Phononendynamik hochgradig kompliziert ist. Wir demonstrieren, dass der multi Davydov-Ansatz kombiniert mit Apoptosis eine extrem effiziente Berechnung der Exziton- und Phononendynamik sowohl für große Übergangsintegrale als auch ausgedehnte Molekülkristalle ermöglicht.

Drittens beleuchten wir diverse Aspekte lasergetriebener Moleküldynamik in dissipativen Umgebungen. Unter Beschränkung auf zwei elektronische Energie-Level bestimmen wir die Kanäle, durch welche System und Bad in der Umgebung einer vermiedenen Kreuzung im dissipativen Landau-Zener Modell Energie austauschen. Wir zeigen insbesondere, dass die Übergangswahrscheinlichkeit durch diagonale und neben-diagonale Kopplung eingestellt werden kann, und dass durch geeignete initiale Anregung des Systems die Übergangswahrscheinlichkeit mit wachsender Kopplung gegen einen festen Wert konvergiert.

Schließlich untersuchen wir im Detail laserinduzierten Populationstransfer vermittels schnellen adiabatischen Durchgangs in einer dissipativen Umgebung. Wir zeigen durch Anwendung des multi Davydov-

Ansatzes dass sowohl für Temperatur Null als auch für endliche Temperatur die starke Kopplung des Systems an eine Umgebung als Ressource für Populationsinversion dienen kann. Wir untersuchen dabei insbesondere, wie die Kopplung an die Umgebung die Zerfallskanäle sogar im Falle schwach gechirpter Laserpulse kompensiert.

Contents

1. Introduction

In the early 1970s it was not yet understood how chemical energy, released by hydrolysis of ATP into ADP, was converted into mechanical energy during the muscle contraction in vertebrates. In his influential works [1, 2] Davydov explained muscle contraction on the basis of his earlier works on excitation transport in crystals. Considering the muscle as a linear chain of peptides, he assumed that the chemical energy excited the C=O group of a single peptide bond, causing a distortion of the protein while continuing to the next peptide bond. By a mechanism of self-trapping he explained that the size of the region under excitation did not spread but remained constant [3, 4]. Thus the excitation could be modeled as a coherent state and was later called (Davydov-)soliton in reminiscence of [5].

A coherent state is obtained by displacing in phase space the ground state of the quantum harmonic oscillator. In a quadratic potential coherent states evolve in time as if they were classical particles [6]. Alongside with them fulfilling the minimum Heisenberg uncertainty, coherent states have proven a powerful tool to forge the bridge between quantum and classical mechanics. They exhibit, however, further intriguing properties which render them appealing candidates also for fully-quantum real-time propagation. In this spirit Davydov applied coherent states in his work, and likewise will we pursue along these lines.

In order to solve the time-dependent Schrödinger equation (TDSE), Davydov postulated two types of wave-functions (later called D1 and D2) in terms of coherent states and showed, that indeed it was a solution to Hamilton's equations under some additional assumptions at temperature $T = 0$. In a subsequent paper Davydov investigated the soliton motion with thermal oscillations of the peptides taken into account [7] utilizing a thermally averaged Hamiltonian. The subsequent exposition on the thermal stability of the soliton caused the 'crisis of bio-energy', since at standard conditions the lifetime of C=O vibrations relative to the time for transforming their energy into disordered heat motion was found to be only $10^{-10} - 10^{-12}$s. The nonlinear equations of motion Davydov used had soliton-like solutions only when solved in the adiabatic limit corresponding to $T = 0$. However, the questions of existence and importance of the Davydov soliton remained controversial for $T > 0$, because numerical simulations and theoretical calculations done by independent research groups reached diametrically opposed conclusions [8–12]. They were summarized in [13], yet the discourse reaches to present days (see e.g. [14, 15]).

Also on a more theoretical level, Davydov's ideas were further investigated. The authors of [16] showed that none of Davydov's Ansätze could actually account for the exact solution of the TDSE by using the similarity of Davydov's Hamiltonian with the Fröhlich Hamiltonian arising in polaron theory [17]. It was furthermore shown that the application of Hamilton's equations had to be replaced by the variational principle [18, 19], and that temperature could not be included by the averaged Hamiltonian method [20–22].

After several rather silent years, in 2010 the first work appeared which utilizes Davydov's idea under the alias 'Davydov-Ansatz' as a numerical tool for the approximate solution of the TDSE [23].

In subsequent works [24–26], the method was refined and further developed to include multiple coherent states [27], the so-called multi Davydov-Ansatz - surprisingly enough seemingly unaware of works employing an Ansatz in terms of multiple freely moving Gaussian basis functions in the multi-configurational time-dependent Hartree (MCTDH) community [28–30]. Developed independently in parallel, the methods exhibit rather divergent formalisms. It will be one of the main foci of this work to include both into a united framework, profiting from and to be profitable for both sides.

This work consists of four main chapters. In the first chapter, the theoretical ground is prepared for the subsequent chapters. While there is much more that could be said about the concepts introduced there, the focus will be on the aspects which will be needed later on to solve open quantum system dynamics, accompanied by hints for further reading. The material is completed by further details in the appendix.

In the second chapter we will set the stage by considering the variational multi-configurational Gaussian Ansatz (vMCG) of the bosonic many body wave function in terms of freely moving coherent states. We will satisfy the desire for a clear presentation of the derivation of equations of motion for the parameters in an as simple and as general as possible setting. By carving out as precisely as possible the structure of these equations, we will show how to circumvent the issues related to the Ansatz by two minimally invasive artifices. While one of these artifices is adopted from the multi-configurational time-dependent Hartree method (MCTDH), the other one is fully innovative and has been termed 'apoptosis'. Contact is drawn to semiclassical and other methods with the main focus on attempts to circumvent the original method's weaknesses. We investigate possible generalizations of the vMCG method by application of squeezed states and displaced number states on the background of the inefficiency of the representation of Fock number states by the vMCG method. As a generalization of the vMCG method to open quantum system settings, the multi Davydov-Ansatz formalism is included into the framework constructed so far. Finally, it is outlined how to efficiently treat with the multi Davydov-Ansatz non-zero temperature by Monte-Carlo sampling.

In the third chapter the impact of the regularizations outlined in the second chapter will be investigated in detail. It will be shown that the multi Davydov-Ansatz equipped with the regularizations outlined in the second chapter is suited to propagate in real-time the full system-plus-bath wave-function with extremely small computational effort. To this end, the multi Davydov-Ansatz will firstly be applied to the Quantum Rabi model. The impact of the regularization in the case of vanishing coefficients is investigated for a single environmental mode in the strong coupling regime. Secondly, the maybe simplest model of an open quantum system, the Spin-Boson model, will serve as a testbed for apoptosis, in the ohmic and in the sub-ohmic regime at weak as well as strong coupling. Once the reliability of the concept is proven, the quality of different discretizations with respect to the speed of convergence to the continuum limit of a continuous spectral density is examined. We will show that the aspiration for an a priori measure of the quality of the discretization can be satisfied by the Windowed Fourier transform (WFT). While coherent states allow for a straightforward description of non-zero temperature physics, no attention has been paid so far to the corresponding subtleties arising in the context of a sub-ohmic spectral density. We will show how to concisely extend the description

to these contexts. Again in the spirit of reduction of the numerical effort, we outline subsequently how to transform the environment, typically given by a set of uncoupled modes each of which is coupled separately to the system, into a linear chain of effective modes where only the first mode is coupled to the system. In particular, the quality of the optimal discretization of the spectral density found from the WFT will be contrasted with this effective mode representation (EMR). Rounding off the considerations regarding the Spin-Boson model, we will show that the multi Davydov-Ansatz is suited to calculate the critical coupling strength for the quantum phase transition from the delocalized to the localized regime in the case of ohmic damping.

The fourth chapter is devoted to the application of the developed methodology. We will see that the regularizations found in the second chapter are inevitably required for the method to produce reliable results. We will investigate two settings where the spectral density is already given in discretized form and thus not requiring a continuum limit as well as two settings where the spectral density is given in continuous form. In a setup where the spectral density is given in discretized form we will firstly determine the vibrational relaxation dynamics of deuterium dimers in the presence of a silicon surface, utilizing a novel Hamiltonian exact up to second order in the environmental coordinates [31]. As we shall outline, the model does not allow for a treatment on a perturbative level. Thus we will apply the multi Davydov-Ansatz in order to calculate the system dynamics with multiple system levels and a huge number of surface vibrations explicitly taken into account. We will outline how to drastically reduce the numerical effort by transforming the environment with the EMR. We will secondly push the limits for the investigation of the relaxation dynamics of an exciton hopping on a linear molecular chain utilizing the Holstein polaron model into previously unknown territory by calculating the long-time dynamics for large exciton hopping elements and strong coupling strengths. Turning our back to un-driven cases, we will show subsequently how to use the multi Davydov-Ansatz for the investigation of laser-driven molecular dynamics. In a first setup we will investigate the impact of environmental excitation on the transition probability in a Landau-Zener system coupled to a dissipative environment. We will show that the multi Davydov-Ansatz is suited to reliably reproduce the analytically given long-time limit of the staying probability for multiple modes given in terms of a continuous ohmic spectral density. In a second setup we will show that the dissipative environment, given in terms of a super-ohmic continuous spectral density, can be used as a resource for population inversion if coupled strongly to a two-level system subject to chirped femtosecond laser excitations.

The appendix complements the work by additional detailed calculations and numerical details. This work was started in Oct. 2016, 30 years after the first appearance of Davydov's Ansatz [3], and finished in 2020, 10 years after Davydov's ideas had firstly been used under the alias 'Davydov-Ansatz' as numerical tool [23].

2. Prerequisites

In this section the foundations will be laid for all theoretical tools needed later in this thesis. Special emphasis is laid on properties of coherent states (CS), which have been known to exhibit outstanding theoretical physical properties for a very long time [6]. Their localized nature will render them appealing candidates for real-time propagation in bosonic many-body setups. CS arise naturally in the context of the quantum harmonic oscillator, which is why the treatment of the latter is the spark from which the light will emanate in this work.

2.1. Harmonic oscillator basics

The Hamilton operator of the one-dimensional harmonic oscillator with mass m and frequency ω reads

$$\hat{\mathcal{H}}_{\mathrm{HO}} = \frac{\hat{p}^2}{2m} + \frac{1}{2}m\omega^2\hat{q}^2. \tag{2.1}$$

The position operator $\hat{q}$ and the momentum operator $\hat{p}$ fulfill the canonical commutation relation

$$[\hat{q}, \hat{p}] = \mathrm{i}\hbar, \tag{2.2}$$

where $[\cdot, \cdot]$ denotes the commutator, $[\hat{A}, \hat{B}] = \hat{A}\hat{B} - \hat{B}\hat{A}$ for operators $\hat{A}, \hat{B}$. By $\hbar$ we denote the reduced Planck constant. By introducing the operators

$$\hat{a} = \sqrt{\frac{m\omega}{2\hbar}}\left(\hat{q} + \mathrm{i}\frac{\hat{p}}{m\omega}\right), \qquad \hat{a}^\dagger = \sqrt{\frac{m\omega}{2\hbar}}\left(\hat{q} - \mathrm{i}\frac{\hat{p}}{m\omega}\right), \tag{2.3}$$

the differential analysis, required to solve for the spectrum of $\hat{\mathcal{H}}_{\mathrm{HO}}$, can be traded for operator algebra. From the canonical commutation relation (2.2) one obtains

$$\left[\hat{a}, \hat{a}^\dagger\right] = \hat{1} \tag{2.4}$$

for the commutator of the operators (2.3). With the help of the inverse of (2.3),

$$\hat{q} = \sqrt{\frac{\hbar}{2m\omega}}\left(\hat{a}^\dagger + \hat{a}\right), \qquad \hat{p} = \sqrt{\frac{\hbar m\omega}{2}}\mathrm{i}\left(\hat{a}^\dagger - \hat{a}\right), \tag{2.5}$$

the Hamilton operator (2.1) can be rewritten as

$$\hat{\mathcal{H}}_{\mathrm{HO}} = \hbar\omega\left(\hat{a}^\dagger\hat{a} + \frac{1}{2}\right). \tag{2.6}$$

It can then be shown that the spectrum of the (Hermitian) number-operator $\hat{\mathcal{N}}_{\mathrm{HO}} = \hat{a}^{\dagger}\hat{a}$ is $\mathbb{N}$ (see eg. [32] for details). Consequently, the eigenvalues of $\hat{\mathcal{H}}_{\mathrm{HO}}$ are

$$E_n = \hbar\omega \left(n + \frac{1}{2} \right), \qquad n \in \mathbb{N}. \tag{2.7}$$

Furthermore, the corresponding eigenspaces are not degenerate, such that the normalized eigenstates can be denoted by $|n\rangle$ and are mutually orthogonal,

$$\hat{\mathcal{H}}_{\mathrm{HO}} |n\rangle = E_n |n\rangle, \qquad \langle m|n\rangle = \delta_{mn}. \tag{2.8}$$

The $|n\rangle$ are termed number states, and since they obey (see [32])

$$\hat{a}^{\dagger} |n\rangle = \sqrt{n+1} |n+1\rangle, \tag{2.9}$$

$$\hat{a} |n\rangle = \sqrt{n} |n-1\rangle, \tag{2.10}$$

the operators $\hat{a}^{\dagger}$ and $\hat{a}$ are called ladder operators. Two consecutive number states $|n\rangle$ and $|n+1\rangle$ differ by $\hbar\omega$ in energy, thus $\hat{a}^{\dagger}$ creates and $\hat{a}$ annihilates a phonon of energy $\hbar\omega$. Consequently, $\hat{a}^{\dagger}$ is termed creation operator and $\hat{a}$ annihilation operator. Since $\hat{a}^{\dagger}\hat{a}$ is Hermitian, one infers from the spectral theorem (see e.g. [33]) that the number states fulfill the closure relation

$$\hat{1} = \sum_{n=0}^{\infty} |n\rangle \langle n|. \tag{2.11}$$

The position representation of the number states, obtained by solving the time-independent Schrödinger equation in terms of q, reads

$$\langle q|n\rangle = \left(\frac{m\omega}{\pi\hbar} \right)^{\frac{1}{4}} (2^n n!)^{-\frac{1}{2}} \, \mathrm{e}^{-\frac{\xi^2}{2}} H_n(\xi), \qquad \xi = \sqrt{\frac{m\omega}{\hbar}} q, \tag{2.12}$$

where $H_n(x)$ denotes the n-th Hermite polynomial [34]. The probability density $|\langle q|n\rangle|^2$ is plotted in the left panel of Fig. 2.1 as function of q for the first five number states. While the ground state probability distribution $|\langle q|0\rangle|^2$ of the quantum harmonic oscillator is a Gaussian function of mean 0 and width $\sqrt{\frac{\hbar}{2m\omega}}$ and thus localized around $q = 0$, with increasing n the number states $|n\rangle$ become more and more delocalized.

The momentum representation of the number states can be obtained up to a normalization prefactor by formally substituting $q \to p$ and $m\omega \to \frac{1}{m\omega}$ in Eq. (2.12),

$$\langle p|n\rangle = (-\mathrm{i})^n \left(\frac{1}{m\omega\pi\hbar} \right)^{\frac{1}{4}} (2^n n!)^{-\frac{1}{2}} \, \mathrm{e}^{-\frac{y^2}{2}} H_n(y), \qquad y = \sqrt{\frac{1}{\hbar m\omega}} p. \tag{2.13}$$

Note that the prefactor is required in order for the two representations to be Fourier transforms of each other by the Fourier transform

$$f(p) = \frac{1}{\sqrt{2\pi\hbar}} \int\limits_{-\infty}^{\infty} \mathrm{d}q \, \mathrm{e}^{-\mathrm{i}pq/\hbar} f(q), \qquad f(q) = \frac{1}{\sqrt{2\pi\hbar}} \int\limits_{-\infty}^{\infty} \mathrm{d}p \, \mathrm{e}^{\mathrm{i}pq/\hbar} f(p). \qquad (2.14)$$

The set of all possible states of the quantum harmonic oscillator has the structure of a Hilbert space, i.e. a complex vector space equipped with a scalar product. Since the number states constitute a countable basis of this Hilbert space, they allow for utilization of linear algebra concepts. While this is often helpful, in many contexts it is desirable to work with *localized* basis states instead. The coherent states, introduced in the next section, constitute such a set of localized basis functions.
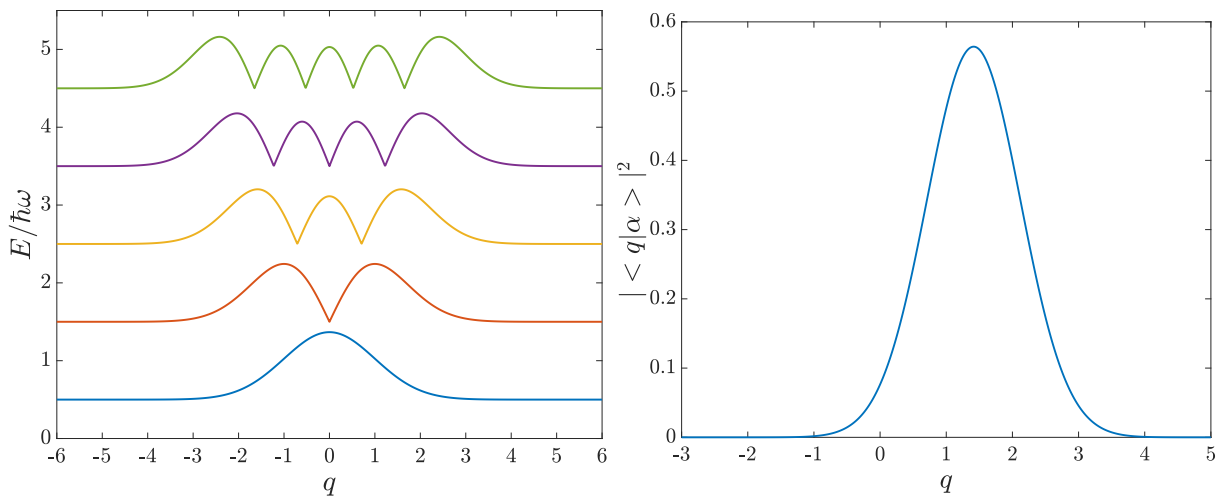
Figure 2.1.: Left panel: probability density $|\langle q|n\rangle|^2$ as function of q in units where $\hbar = \omega = m = 1$ for the first 5 number states: $n = 0$ (blue solid), $n = 1$ (red solid), $n = 2$ (yellow solid), $n = 3$ (violet solid) and $n = 4$ (green solid). Ordinate is the corresponding energy in units of $\hbar\omega$. Right panel: probability density $|\langle q|\alpha\rangle|^2$ of a coherent state for $\alpha = 1 + \mathrm{i}$ as function of q in arbitrary units.

2.2. Canonical coherent states of the harmonic oscillator

CS arise naturally in the context of the quantum harmonic oscillator. They are defined as the eigenstates of the annihilation operator $\hat{a}$, defined in (2.3). By expansion in terms of number states, one finds that the spectrum of $\hat{a}$ is $\mathbb{C}$, that the corresponding eigenspaces are not degenerate, and that the normalized eigenstates read [35]

$$|\alpha\rangle = \mathrm{e}^{-\frac{|\alpha|^2}{2}} \sum_{n=0}^{\infty} \frac{\alpha^n}{\sqrt{n!}} |n\rangle, \qquad \alpha \in \mathbb{C}. \qquad (2.15)$$

Although the harmonic oscillator ground state $|0\rangle$ and the CS $|0\rangle$ coincide, the notations $|n\rangle$ for the number states and $|\alpha\rangle$ for CS can be ambiguous due to $\mathbb{N} \subset \mathbb{C}$. It will, however, directly be indicated

what is meant, if it is not clear from the context. From Eq. (2.15) the overlap $\langle n|\alpha \rangle$ of a coherent state with a number state is given by

$$\langle n|\alpha \rangle = \mathrm{e}^{-\frac{|\alpha|^2}{2}} \frac{\alpha^n}{\sqrt{n!}}. \tag{2.16}$$

The position representation of the CS can be obtained by utilization of the generating function of the Hermite polynomials [34]:

$$\langle q|\alpha \rangle = \left(\frac{m\omega}{\pi\hbar}\right)^{\frac{1}{4}} \exp\left[-\frac{m\omega}{2\hbar}\left(q - \sqrt{\frac{2\hbar}{m\omega}}\alpha\right)^2 + \frac{\alpha^2 - |\alpha|^2}{2}\right] \tag{2.17}$$

$$= \left(\frac{m\omega}{\pi\hbar}\right)^{\frac{1}{4}} \exp\left[-\frac{|\alpha|^2}{2} - \frac{x^2}{2} + \sqrt{2}x\alpha - \frac{\alpha^2}{2}\right], \qquad x = \sqrt{\frac{m\omega}{\hbar}}q. \tag{2.18}$$

The momentum representation, obtained either by Fourier transform of (2.18) or by using (2.13) and the generating function of the Hermite polynomials, reads

$$\langle p|\alpha \rangle = \left(\frac{1}{\pi\hbar m\omega}\right)^{\frac{1}{4}} \exp\left[-\frac{|\alpha|^2}{2} - \frac{y^2}{2} - \sqrt{2}\mathrm{i}y\alpha + \frac{\alpha^2}{2}\right], \qquad y = \sqrt{\frac{1}{\hbar m\omega}}p. \tag{2.19}$$

Thus, by virtue of (2.18) and (2.19), CS are Gaussians in phase space, centered at

$$\alpha = \sqrt{\frac{m\omega}{2\hbar}}\left(\alpha_1 + \frac{\mathrm{i}}{m\omega}\alpha_2\right). \tag{2.20}$$

Insertion of (2.20) into (2.18) yields the usual expression

$$\langle q|\alpha \rangle = \left(\frac{m\omega}{\pi\hbar}\right)^{\frac{1}{4}} \exp\left[-\frac{m\omega}{2\hbar}\left(q - \alpha_1\right)^2 + \mathrm{i}\alpha_2\left(q - \frac{1}{2}\alpha_1\right)\right], \tag{2.21}$$

from which the width and the center of the Gaussian can be read off immediately. The probability density $|\langle q|\alpha \rangle|^2$ as a function of q is plotted for $\alpha = 1 + \mathrm{i}$ in the right panel of Fig. 2.1, again revealing the Gaussian nature of the coherent states: the probability density $|\langle q|\alpha \rangle|^2$ of a coherent state $|\alpha \rangle$ is a Gaussian distribution of mean α_1 and width $\sqrt{\frac{\hbar}{2m\omega}}$.

The Wigner distribution function [36] $\rho(p, q)$ of the density $\hat{\rho} = |\alpha \rangle \langle \alpha|$ corresponding to the CS $|\alpha \rangle$ can be calculated as

$$\rho(p, q) = \hbar^{-1} \int \mathrm{d}\tau \, \exp\left[\frac{\mathrm{i}}{\hbar}p\tau\right] \langle q + \frac{\tau}{2}| \hat{\rho} |q - \frac{\tau}{2}\rangle \tag{2.22}$$

$$= \frac{2}{\hbar} \exp\left[-\left(x - \sqrt{2}\,\mathrm{Re}\,(\alpha)\right)^2 - \left(y + \sqrt{2}\,\mathrm{Im}\,(\alpha)\right)\right], \qquad x = \sqrt{\frac{m\omega}{\hbar}}q, \, y = \sqrt{\frac{1}{\hbar m\omega}}p, \tag{2.23}$$

where we have inserted (2.18). Here, $\mathrm{Re}\,()$ denotes the real part and $\mathrm{Im}\,()$ the imaginary part. As to be expected, this is a Gaussian in phase space centered at (2.20). We infer that CS are, in contrast to the number states, highly localized quantum objects: 99.9% of a CS's weight is in the phase space region $\left\{ (q,p) \,|\, \frac{m\omega}{\hbar} q^2 + \frac{1}{\hbar m \omega} p^2 \leq r^2,\, r = 2.63 \right\}$. This localization will turn out highly advantageous in bosonic many-body setups, but it comes at the price that the CS are not orthogonal. On the contrary, the overlap of two arbitrary CS does not vanish due to

$$\langle \alpha | \beta \rangle = \exp\left[\alpha^* \beta - \frac{1}{2}\left(|\alpha|^2 + |\beta|^2 \right) \right]. \tag{2.24}$$

The absolute value of the overlap of two CS as a function of $\mathrm{Re}\,(\alpha)$ and $\mathrm{Im}\,(\alpha)$ is plotted in Fig. 2.2. It reveals that, although two arbitrary CS have non-vanishing overlap, the overlap decreases
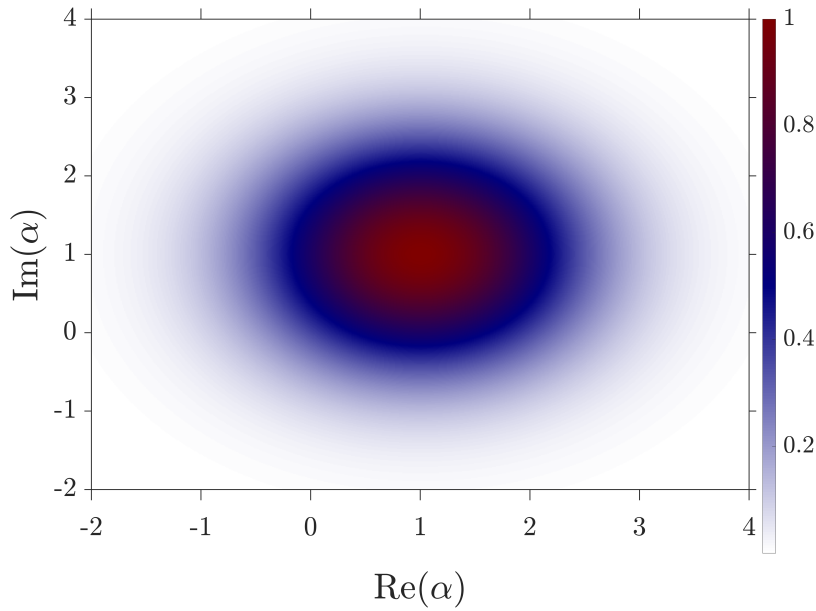
Figure 2.2.: Absolute value of the overlap $\langle \alpha | \beta \rangle$ of two CS for fix $\beta = 1 + \mathrm{i}$ as function of $\mathrm{Re}\,(\alpha)$ and $\mathrm{Im}\,(\alpha)$.

exponentially with the distance of the CS - in compliance with their localized nature.
From the integral identity

$$\int_{\mathbb{C}^2} \mathrm{d}\alpha\, (\alpha^*)^m \alpha^n \mathrm{e}^{-|\alpha|^2} = \int_0^\infty \mathrm{d}|\alpha|\, |\alpha|^{m+n+1} \mathrm{e}^{-|\alpha|^2} \int_0^{2\pi} \mathrm{d}\theta\, \mathrm{e}^{\mathrm{i}(m-n)\theta} = \pi n! \delta_{mn} \tag{2.25}$$

and by insertion of (2.11) readily follows the closure relation

$$\hat{1} = \frac{1}{\pi} \int_{\mathbb{C}^2} \mathrm{d}\alpha\, |\alpha\rangle \langle \alpha |, \tag{2.26}$$

where $\mathrm{d}\alpha = \mathrm{d}\,\mathrm{Re}\,(\alpha)\,\mathrm{d}\,\mathrm{Im}\,(\alpha)$ and the integral has to be performed over the whole complex plane. In contrast to the number states which form a countable basis of the Hilbert space of the harmonic oscillator, coherent states form an uncountable basis and thus have to form an overcomplete set of states. One consequently expects the closure relation (2.26) to exhibit redundancies, something we address in Sec. 2.3.

Furthermore, while working in the context of number states allows for utilization of linear algebra concepts, working in the context of coherent states allows for utilization of concepts of functional analysis. Thus, for a single harmonic oscillator, the former is in most contexts obviously much simpler to work with. We shall see, however, that this is not the case for multiple harmonic oscillators in open quantum system settings, where the powerful tools of the latter play a dominant role.

Another important aspect makes coherent states appealing candidates for basis functions one would like to work with. The CS are considered *the* most classical quantum objects [6], due to two important properties. Firstly, they exhibit the minimum possible quantum uncertainty $\Delta q \Delta p = \frac{\hbar}{2}$ according to the Heisenberg uncertainty principle,

$$\Delta q = \sqrt{\langle\alpha|\,\hat{q}^2\,|\alpha\rangle - \left[\,\langle\alpha|\,\hat{q}\,|\alpha\rangle\,\right]^2} = \sqrt{\frac{\hbar}{2m\omega}}, \qquad \Delta p = \sqrt{\langle\alpha|\,\hat{p}^2\,|\alpha\rangle - \left[\,\langle\alpha|\,\hat{p}\,|\alpha\rangle\,\right]^2} = \sqrt{\frac{\hbar m\omega}{2}}.$$
$$(2.27)$$

Secondly, the CS stays a CS under the action of the propagator of the harmonic oscillator,

$$\exp\left[-\frac{\mathrm{i}}{\hbar}\omega\hat{a}^\dagger\hat{a}t\right]|\alpha\rangle = \exp\left[-\frac{\mathrm{i}}{\hbar}\omega\hat{a}^\dagger\hat{a}t\right]\exp\left[-\frac{|\alpha|^2}{2}\right]\sum_{n=0}^{\infty}\frac{\alpha^n}{\sqrt{n!}}\,|n\rangle \tag{2.28}$$

$$= \exp\left[-\frac{|\alpha|^2}{2}\right]\sum_{n=0}^{\infty}\frac{\left(\alpha\mathrm{e}^{-\mathrm{i}\omega t/\hbar}\right)^n}{\sqrt{n!}}\,|n\rangle \tag{2.29}$$

$$= |\alpha\mathrm{e}^{-\mathrm{i}\omega t/\hbar}\rangle, \tag{2.30}$$

which moves on an ellipse in phase space, as the classical harmonic oscillator [37]. Coherent states thus appear as the most appropriate tool to draw contact between quantum and classical mechanics. While we will work in the full quantum context throughout this thesis, the intimate relation with (semi-) classical methods will always shine through.

We have seen in section 2.1 that the ground state $|0\rangle$ of the harmonic oscillator is a Gaussian centered at $(0,0)$ in phase space. A coherent state can thus be viewed as the ground state displaced in phase space. Indeed, the CS $|\alpha\rangle$ is generated by the action of the displacement operator

$$\hat{D}_\alpha := \exp\left[\alpha\hat{a}^\dagger - \alpha^*\hat{a}\right] \tag{2.31}$$

on the ground state,

$$|\alpha\rangle = \hat{D}_\alpha\,|0\rangle. \tag{2.32}$$

This can easily be verified by rewriting the displacement operator (2.31) with the help of the Baker-Campbell-Hausdorff formula in normal ordered form,

$$\hat{D}_\alpha = \exp\left[-\frac{1}{2}\,|\alpha|^2\right]\exp\left[\alpha\hat{a}^\dagger\right]\exp\left[-\alpha^*\hat{a}\right],\tag{2.33}$$

and comparison with (2.15),

$$|\alpha\rangle = \exp\left[-\frac{|\alpha|^2}{2}\right]\exp\left[\alpha\hat{a}^\dagger\right]|0\rangle.\tag{2.34}$$

Furthermore, the displacement operator is unitary since a shift by $-\alpha$ inverts a shift by α,

$$\hat{D}_\alpha^\dagger = \hat{D}_\alpha^{-1} = \hat{D}_{-\alpha}.\tag{2.35}$$

Clearly, two subsequent shifts can be combined into one single shift. Indeed, as can be seen from the Baker-Campbell-Hausdorff formula, the composition of two displacement operators is, apart from an exponential factor, again a displacement operator,

$$\hat{D}_\alpha\hat{D}_\beta = \exp\left[\frac{1}{2}\left(\alpha\beta^* - \alpha^*\beta\right)\right]\hat{D}_{\alpha+\beta}.\tag{2.36}$$

A central element of the calculus we will employ later on is the commutation of the displacement operator with the creation and annihilation operators. It can be derived from the Baker-Campbell-Hausdorff formula and reads

$$\hat{D}_\alpha^\dagger\hat{a}\hat{D}_\alpha = \hat{a} + \alpha, \qquad \hat{D}_\alpha^\dagger\hat{a}^\dagger\hat{D}_\alpha = \hat{a}^\dagger + \alpha^*.\tag{2.37}$$

In Sec. 2.6 we will need the displacement operator expressed in terms of position and momentum operator. By insertion of (2.20) for α and (2.3) for the creation and annihilation operator, we may easily derive the desired representation. It reads

$$\hat{D}_\alpha = \exp\left[\mathrm{i}\left(\alpha_2\hat{q} - \alpha_1\hat{p}\right)\right].\tag{2.38}$$

We will employ the coherent states as basis functions for real-time propagation in bosonic many-body systems. If the system's potential is harmonic, as e.g. for the harmonic oscillator (2.1), the system comprises a natural frequency ω, defining the width of the CS in phase space. In cases where the potential is not harmonic, however, the width of the CS is a free parameter. Then it is convenient to calculate the overlap $\langle\alpha,\omega|\beta,\gamma\rangle$ of two CS of different phase-space positions α,β and widths ω,γ.

This can be carried out analytically in position representation, since by (2.18)

$$\langle \alpha, \omega | \beta, \gamma \rangle = \int\limits_{-\infty}^{\infty} \mathrm{d}q \; \langle \alpha, \omega | q \rangle \, \langle q | \beta, \gamma \rangle \tag{2.39}$$

$$= \sqrt{\frac{2\sqrt{\omega\gamma}}{\omega + \gamma}} \exp\left[\frac{1}{2(\omega + \gamma)} \left(2\omega(\alpha^*)^2 + 2\gamma\beta^2 + 4\sqrt{\omega\gamma}\alpha^*\beta \right.\right.$$

$$\left.\left. - (\omega + \gamma)\left(|\alpha|^2 + |\beta|^2 + (\alpha^*)^2 + \beta^2 \right) \right) \right]. \tag{2.40}$$

As desirable, Eq. (2.40) reduces to the standard overlap (2.24) for $\omega = \gamma$.

Apart from the ones outlined so far, the CS have a vast number of other interesting properties. An exquisite assortment is given in [38]. Here, the focus is on application of CS as time-dependent basis functions, thus the following important aspects will be selected: the completeness of CS (see Sec. 2.3) and representation of the canonical density operator in terms of CS (see Sec. 2.4). Furthermore, as promising generalizations of the concept of CS, squeezed states are introduced in Sec. 2.5 while displaced number states are introduced in Sec. 2.6.

2.3. Overcompleteness of CS and the Segal-Bargmann transformation

In order to examine the completeness of CS in more detail, we wish to apply concepts of functional analysis to the setting of the quantum harmonic oscillator. To this end we consider the space of analytic functions on phase space $\mathbb{C}$, i.e. the space of complex functions that are locally given by a convergent power series with complex coefficients. It is easy to verify that the operators $\hat{b} := \sqrt{\hbar}\partial_z$ and $\hat{c} := \frac{1}{\sqrt{\hbar}}z$, acting as partial derivative and multiplication respectively, fulfill the analog of the canonical commutation relation

$$\left[\hat{b}, \hat{c} \right] = \hat{1}. \tag{2.41}$$

This analogy is suited to translate the standard functional analysis setup to the quantum mechanics setup of the harmonic oscillator, since the Stone-von Neumann theorem [39, 40] ensures the unitary equivalence of the two representations. Indeed, Bargmann showed in [41] that with the inner product

$$\langle f | g \rangle = \frac{1}{\pi\hbar} \int\limits_{\mathbb{C}} \mathrm{d}z \, \mathrm{e}^{-\frac{|z|^2}{\hbar}} f^{\dagger}(z) g(z), \tag{2.42}$$

these two operators can be made adjoints of each other,

$$\hat{b}^{\dagger} = \hat{c}, \tag{2.43}$$

and that the space of analytic functions satisfying $\langle f|f \rangle < \infty$ thus attains the structure of a Hilbert space, named Segal-Bargmann space H_{SB}. The unitary Segal-Bargmann transformation (SBT)

$$A : L^2(\mathbb{R}) \to H_{\mathrm{SB}}, \qquad (Af)(z) = \int\limits_{\mathbb{R}} \mathrm{d}x \, \mathrm{e}^{-\frac{1}{2}\left(|z|^2 - 2\sqrt{2}zx + |x|^2\right)} f(x) \tag{2.44}$$

maps a wave function in position representation to an analytic function in the Segal-Bargmann space. In (2.44) we have introduced the symbol $L^2(\mathbb{R})$ for the Hilbert space of the quantum harmonic oscillator, considered as the space of square integrable functions on $\mathbb{R}$.

The unitary transformation (2.44) may be extended straightforwardly to operators by setting $A(\hat{B}) := A(\hat{B}(A^{-1}))$ for any operator $\hat{B}$ acting on the Hilbert space $L^2(\mathbb{R})$. It can be shown that in this way the SBT maps the annihilation operator $\hat{a}$ onto $\hat{b}$ and the creation operator $\hat{a}^\dagger$ onto $\hat{c}$, respectively (see [42] for further details).

An important property of the transformation (2.44) is that it maps the ground state $|0\rangle$ to the identity function. Hence, for any state $|\Psi\rangle$ of the quantum harmonic oscillator may be expanded in terms of number states by the closure relation (2.11),

$$|\Psi\rangle = \sum_{n=0}^{\infty} \Psi_n |n\rangle = \sum_{n=0}^{\infty} \frac{\Psi_n}{\sqrt{n!}} (\hat{a}^\dagger)^n |0\rangle \,, \tag{2.45}$$

the SBT maps this wave function to a power series,

$$(A|\Psi\rangle)(z) = \sum_{n=0}^{\infty} \frac{\Psi_n}{\sqrt{n!}} A\left((\hat{a}^\dagger)^n\right) A|0\rangle = \sum_{n=0}^{\infty} \frac{\Psi_n}{\sqrt{n!}} z^n. \tag{2.46}$$

Thus, in the spirit of the SBT the expansion of a wave function in terms of the number states is the analog of expanding the wave-function in terms of a power series. The coherent states can be considered to directly mediate this analogy, since for any CS $|z\rangle$ it holds that

$$\langle \Psi | z \rangle = \sum_{n=0}^{\infty} \langle \Psi | n \rangle \langle n | z \rangle = \mathrm{e}^{-\frac{|z|^2}{2}} \sum_{n=0}^{\infty} \frac{\langle \Psi | n \rangle}{\sqrt{n!}} z^n. \tag{2.47}$$

In addition, the property of $|\alpha\rangle$ being an eigenvector of $\hat{a}$,

$$\hat{a} |\alpha\rangle = \alpha |\alpha\rangle \tag{2.48}$$

along with

$$\hat{a}^\dagger \mathrm{e}^{\frac{|\alpha|^2}{2}} |\alpha\rangle = \partial_\alpha \mathrm{e}^{\frac{|\alpha|^2}{2}} |\alpha\rangle \tag{2.49}$$

again emphasize appealingly that the coherent states mediate the analogy of the Segal-Bargmann transformation (2.44).

The SBT enables us to directly include complex functional analysis tools into quantum mechanics. In particular, the authors of [43] show with a straightforward proof by means of complex functional analysis that the CS are vastly overcomplete: the CS on a lattice $L_{z,\gamma} := \{z + \gamma(m + in) \,|\, m, n \in \mathbb{Z}\}$ in the complex plane form an overcomplete set if and only if $0 < \gamma \leq \sqrt{\pi}$. Thus completeness holds for a phase-space lattice of coherent states if and only if the density of states per Planck unit cell is equal to or greater than one. A corresponding graphical illustration is given in 2.3. This result will play a very important role in numerical applications later on.

Furthermore, with the SBT, it is simple to prove that the CS are *supercomplete*, i.e. the CS
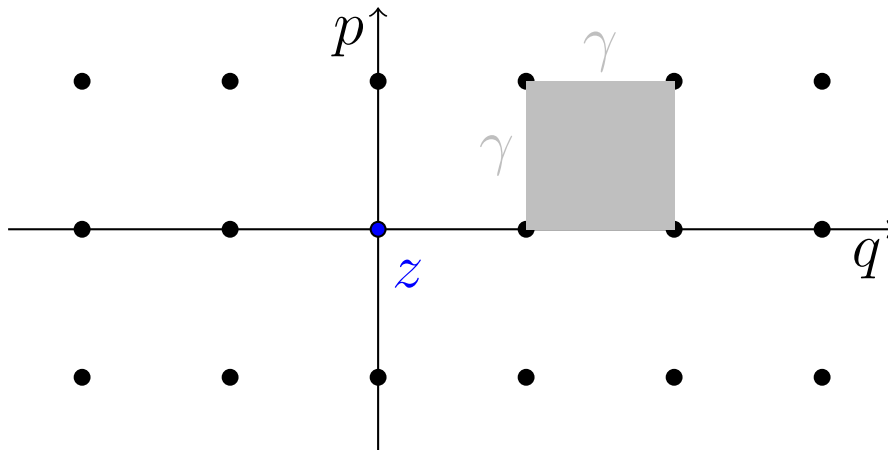
Figure 2.3.: Overcompleteness of CS: if the area of the phase-space region shaded in grey is at most π (i.e. a Planck unit cell), the CS corresponding to the lattice form an overcomplete set.

corresponding to any (non-constant) convergent series in $\mathbb{C}$ form a complete set (see, e.g., [44]). Prominent examples are the CS on a circle and on a line.

In the context of the completeness of the number states it is not surprising that a countable set of CS suffices to represent unity. In numerical applications, however, taking into account infinitely many basis functions is not possible in general. Since it is at the heart of any method which employs coherent states as basis functions, we wish to represent unity in terms of a finite number of coherent states, at least approximately. Since the CS $\{|\alpha_k\rangle \,|\, k \in \mathbb{N}\} := \{|\alpha\rangle \,|\, \alpha \in L_{z,\gamma}\}$ on an appropriate lattice $L_{z,\gamma}$ in the complex plane form an overcomplete set, they have to obey a closure relation,

$$\hat{1} = \sum_{k,l \in \mathbb{N}} A_{kl} \,|\alpha_k\rangle \langle\alpha_l| . \tag{2.50}$$

With the matrix elements of the overlap matrix $S_{ij} := \langle\alpha_i|\alpha_j\rangle$, (2.50) results in

$$S_{ij} = \sum_{k,l \in \mathbb{N}} A_{kl} S_{ik} S_{lj}, \tag{2.51}$$

which gives $\boldsymbol{S} = \boldsymbol{SAS}$ rewritten in matrix form. Consequently $\boldsymbol{A} = \boldsymbol{S}^{-1}$, and we deduce

$$\hat{1} = \sum_{k,l \in \mathbb{N}} \left(\boldsymbol{S}^{-1} \right)_{kl} |\alpha_k\rangle \langle\alpha_l| , \qquad \boldsymbol{S}_{kl} = \langle\alpha_k|\alpha_l\rangle . \tag{2.52}$$

To be precise, this is valid only in the case where the overlap matrix $\boldsymbol{S}$ is invertible. It will turn out that the requirement of invertibility is an extremely crucial point if coherent states are applied as freely moving basis functions. Consequently one would wish to circumvent the inversion. One can indeed show that the inverse $\boldsymbol{S}^{-1}$ can be replaced with the identity matrix if the coherent states are taken on a tight frame [45] instead of the grid $L_{z,\gamma}$ introduced above. Unfortunately this requires a huge number of CS and does thus not appear suited to tackle many-body setups, in general.

We shall see that the non-orthogonality of the coherent states causes the major issue which their application suffers from. On the contrary their vast overcompleteness, highlighted in this section and intimately related to this non-orthogonality, will be the corner stone of their extremely favourable complexity scaling with the number of particles.

2.4. Density operator representation in terms of CS

Later in this thesis, we aim at application of coherent states in setups of nonzero temperature. Thus in this section we introduce the basic concepts of formulation of density operators in terms of coherent states. The properties of a system of constant particle number being in thermodynamic equilibrium with an energy reservoir at temperature T are described by the canonical density operator

$$\hat{\rho}_\beta = \left(\text{tr} \left[\exp\left(-\beta\hat{\mathcal{H}} \right) \right] \right)^{-1} \exp\left(-\beta\hat{\mathcal{H}} \right) , \tag{2.53}$$

where

$$\beta = (k_{\text{B}} T)^{-1} \tag{2.54}$$

is the inverse temperature, k_{B} the Boltzmann constant and $\hat{\mathcal{H}}$ is the Hamiltonian of the system.

We will exclusively be concerned with setups in which the system is given by a set of harmonic oscillators. Thus we assume the Hamiltonian $\hat{\mathcal{H}}$ to be the harmonic oscillator Hamiltonian (2.6) in which we omit the ground state energy without loss of generality. By

$$\exp\left[-\beta\hbar\omega\hat{a}^\dagger\hat{a} \right] |n\rangle = \exp\left[-\beta\hbar\omega n \right] |n\rangle \tag{2.55}$$

one finds the canonical density of the harmonic oscillator in number state representation

$$\hat{\rho}_\beta = Z(\beta) \sum_{n=0}^{\infty} \text{e}^{-\beta\hbar\omega n} |n\rangle \langle n| , \tag{2.56}$$

where the inverse partition function $Z(\beta)$ is given by

$$Z(\beta) = 1 - \mathrm{e}^{-\beta\hbar\omega}. \tag{2.57}$$

The inverse temperature $\beta \to \infty$ as $T \to 0$, and thus the system is in the (pure) ground state $\hat{\rho}_\beta = |0\rangle\langle 0|$ at zero temperature.

Let us for the moment consider again a system governed by a general density operator $\hat{\rho}$. The attempt to generate a phase space probability density by using the diagonal elements of $\hat{\rho}$ in the CS basis (2.15) gives rise to the definition of the Q-function [46]

$$Q(\alpha, \alpha^*) = \frac{1}{\pi}\langle\alpha|\hat{\rho}|\alpha\rangle. \tag{2.58}$$

Since it is positive and normalized the Q-function can be viewed as a kind of probability density. Indeed, averages of antinormally ordered products of creation and annihilation operators can be calculated from the Q-function via

$$\mathrm{tr}\left[(\hat{a})^r(\hat{a}^\dagger)^s\hat{\rho}\right] = \int\limits_{\mathbb{C}} \mathrm{d}\alpha\,\alpha^r(\alpha^*)^s Q(\alpha, \alpha^*). \tag{2.59}$$

Resting on the overcompleteness of the CS (see Sec. 2.3), the Q-function has, among others, the interesting property to completely determine the density operator (see e.g. [46] for details).

Accordingly, Glauber [47] and Sudarshan [48] showed that a wide variety of density operators $\hat{\rho}$ can be written as diagonal ensemble of CS,

$$\hat{\rho} = \int\limits_{\mathbb{C}} \mathrm{d}\alpha\,P(\alpha, \alpha^*)|\alpha\rangle\langle\alpha|, \tag{2.60}$$

where P is called the P-function. An enlightening treatise of its properties can be found in [49]. The P-function plays a role similar to the one of the Q-function for expectation values of normally ordered products of creation and annihilation operators,

$$\mathrm{tr}\left[(\hat{a}^\dagger)^r(\hat{a})^s\hat{\rho}\right] = \int\limits_{\mathbb{C}} \mathrm{d}\alpha\,(\alpha^*)^r\alpha^s P(\alpha, \alpha^*). \tag{2.61}$$

It is straightforward to show, by insertion of (2.58) and (2.60), that Q- and P-function are related via

$$\exp\left(|\lambda|^2\right)\int\limits_{\mathbb{C}} \mathrm{d}\alpha\,\exp\left[\lambda\alpha^* - \lambda^*\alpha\right]Q(\alpha, \alpha^*) = \int\limits_{\mathbb{C}} \mathrm{d}\alpha\,\exp\left[\lambda\alpha^* - \lambda^*\alpha\right]P(\alpha, \alpha^*). \tag{2.62}$$

Since $\lambda\alpha^* - \lambda^*\alpha$ is purely imaginary, the integrals are Fourier transforms in two variables, $\mathrm{Re}\,(\alpha)$ and $\mathrm{Im}\,(\alpha)$. By transforming back, one obtains the more direct relation

$$Q(\alpha, \alpha^*) = \frac{1}{\pi^2} \int_{\mathbb{C}} \mathrm{d}\lambda \int_{\mathbb{C}} \mathrm{d}\beta \, \exp\left(-|\lambda|^2 + \lambda\,(\beta^* - \alpha^*) - \lambda^*\,(\beta - \alpha)\right) P(\beta, \beta^*) \tag{2.63}$$

$$= \frac{1}{\pi} \int_{\mathbb{C}} \mathrm{d}\beta \, \exp\left[-|\beta - \alpha|^2\right] P(\beta, \beta^*). \tag{2.64}$$

Accordingly, one obtains

$$P(\alpha, \alpha^*) = \frac{1}{\pi^2} \int_{\mathbb{C}} \mathrm{d}\lambda \int_{\mathbb{C}} \mathrm{d}\beta \, \exp\left(|\lambda|^2 + \lambda\,(\beta^* - \alpha^*) - \lambda^*\,(\beta - \alpha)\right) Q(\beta, \beta^*), \tag{2.65}$$

but the λ-integration can not be performed directly since the integral does not exist due to the exponential prefactor. For specified $\hat{\rho}$, however, the β-integration can be performed first, possibly compensating for the prefactor. In particular, this is the case for the canonical density of the harmonic oscillator.

For the thermal state (2.56), the corresponding Q-function Q_β can be easily calculated from (2.15),

$$Q_\beta(\alpha, \alpha^*) = \frac{Z(\beta)}{\pi} \sum_{n=0}^{\infty} \mathrm{e}^{-\beta\hbar\omega n} \mathrm{e}^{-|\alpha|^2} \frac{|\alpha|^{2n}}{n!} = \frac{Z(\beta)}{\pi} \exp\left[-|\alpha|^2 Z(\beta)\right]. \tag{2.66}$$

Plugging this into (2.65), the P-function can be calculated,

$$P_\beta(\alpha, \alpha^*) = \frac{1}{\pi^2} \int_{\mathbb{C}} \mathrm{d}\lambda \, \exp\left(|\lambda|^2 - \lambda\alpha^* + \lambda^*\alpha\right) \exp\left(-\frac{|\lambda|^2}{Z(\beta)}\right) \tag{2.67}$$

$$= \frac{\mathrm{e}^{\beta\hbar\omega} - 1}{\pi} \exp\left[-|\alpha|^2 \left(\mathrm{e}^{\beta\hbar\omega} - 1\right)\right]. \tag{2.68}$$

Thus, for the canonical density of the harmonic oscillator the P-function P_β in (2.68) is a complex Gaussian distribution with mean 0 and variance $\frac{1}{2}\left(\mathrm{e}^{\beta\hbar\omega} - 1\right)^{-1}$. For zero temperature, this width becomes zero and thus the distribution becomes a δ-peak at zero. On the contrary, for nonzero temperature the width diverges for $\omega \to 0$ meaning that oscillators of small frequency can be strongly displaced. This will play an important role in later applications.

The Gaussian nature of the distribution (2.68) concedes the treatment of nonzero temperature setups by Monte-Carlo sampling, allowing for a highly efficient computation of the integral in (2.60) in many-body setups. For further options to treat nonzero temperature by means of coherent states see [50].

2.5. Ideal squeezed states

We have seen that the coherent states constitute a vastly overcomplete set of states in the quantum harmonic oscillator's Hilbert space. The width $\sqrt{\frac{\hbar}{m\omega}}$ of a coherent state's wave function is fixed by the mass m and frequency ω of the oscillator. Still it may be desirable to have a set of states with the width as a free parameter, whereas the minimum uncertainty property of coherent states is required unaffected. The squeezed states, to be introduced below, constitute such a set of states, with a squeezing parameter which allows to tune the degree of localization in position or momentum even below $\sqrt{\frac{\hbar}{2}}$. The localization in the other quadrature is then such that the overall uncertainty is minimal, $\Delta p \Delta q = \frac{\hbar}{2}$.

Squeezed states $|\xi, \alpha\rangle$ are defined as

$$|\xi, \alpha\rangle = \hat{S}_\xi \hat{D}_\alpha |0\rangle , \tag{2.69}$$

where $\hat{D}_\alpha$ is the displacement operator defined in Sec. 2.2 and $\hat{S}_\xi$ is the squeezing operator defined as

$$\hat{S}_\xi = \exp\left[\frac{1}{2}\left(\xi^*(\hat{a})^2 - \xi(\hat{a}^\dagger)^2\right)\right] . \tag{2.70}$$

Consequently, a squeezed state is obtained by first displacing the vacuum and then squeezing the result.

Analogously to the displacement operator (2.35), the squeezing operator is unitary,

$$\hat{S}_\xi^\dagger = \hat{S}_\xi^{-1} = \hat{S}_{-\xi}. \tag{2.71}$$

We now aim at the derivation of the position representation of a squeezed state, where we follow the argumentation of [51]. To this end, we rewrite the squeezing operator with the help of the Baker-Campbell-Hausdorff formula in normal ordered form [52]

$$\hat{S}_\xi = \exp\left[-\frac{1}{2}(\hat{a}^\dagger)^2 e^{i\phi} \tanh r\right] (\cosh r)^{-\left(\hat{a}^\dagger \hat{a} + \frac{1}{2}\right)} \exp\left[\frac{1}{2}(\hat{a})^2 e^{-i\phi} \tanh r\right] , \tag{2.72}$$

where $\xi = re^{i\phi}$. We thus find that the squeezed ground state $|\xi, 0\rangle = \hat{S}_\xi |0\rangle$ is given by

$$|\xi, 0\rangle = \frac{1}{\sqrt{\cosh r}} \exp\left[-\frac{1}{2}e^{i\phi} \tanh r(\hat{a}^\dagger)^2\right] |0\rangle . \tag{2.73}$$

While squeezing and displacement operator do not commute, they can be interchanged as

$$\hat{S}_\xi \hat{D}_\alpha = \hat{D}_{\alpha'} \hat{S}_\xi, \qquad \alpha' = \alpha \cosh r - \alpha^* e^{i\phi} \sinh r. \tag{2.74}$$

Thus we can derive from the squeezed ground state (2.73) the general form of a squeezed state by application of the displacement operator $\hat{D}_{\alpha'}$,

$$|\xi,\alpha\rangle = \frac{1}{\sqrt{\cosh r}} \exp\left[-\frac{1}{2}|\alpha'|^2 + \alpha'\hat{a}^\dagger - \frac{1}{2}\mathrm{e}^{\mathrm{i}\phi}\tanh r\left(\hat{a}^\dagger - (\alpha')^*\right)^2\right]|0\rangle, \tag{2.75}$$

where α' is given by (2.74). One immediately infers that (2.75) reduces to the expression of a coherent state (2.34) in the case of zero squeezing $\xi = 0$, since then $\alpha' = \alpha$, $\cosh r = 1$ and $\tanh r = 0$.

We have finally arrived at a form analogous to (2.34), with the annihilation operator dislodged from the expression. This form is especially suited to calculate the overlap with a number state,

$$\langle n|\xi,\alpha\rangle = \frac{\left(\frac{1}{2}\mathrm{e}^{\mathrm{i}\phi}\tanh r\right)^{\frac{n}{2}}}{\sqrt{n!\cosh r}} \exp\left[-\frac{1}{2}\left(|\alpha|^2 - \alpha^2\mathrm{e}^{\mathrm{i}\phi}\tanh r\right)\right] H_n\left(\frac{\alpha}{\sqrt{2\mathrm{e}^{\mathrm{i}\phi}\cosh r\sinh r}}\right). \tag{2.76}$$

One may verify that this reduces to the overlap of a coherent state with a number state (2.16) for zero squeezing $\xi = 0$ by inferring

$$\lim_{x\to 0}\sqrt{x^n}H_n\left(\frac{\alpha}{\sqrt{x}}\right) = \alpha^n \tag{2.77}$$

from the fact that the Hermite polynomial H_n has degree n.

Finally, by utilization of the generating function of the Hermite polynomials H_n we find the position representation of the squeezed states as [53]

$$\langle q|\xi,\alpha\rangle = \sum_{n=0}^{\infty} \langle q|n\rangle\langle n|\xi,\alpha\rangle = \frac{\exp\left(-\frac{1}{2}\alpha_1\alpha_2\right)}{\pi^{\frac{1}{4}}\sqrt{S(1+2\mathrm{i}\kappa)}} \exp\left[-\left(\frac{1}{2S^2(1+2\mathrm{i}\kappa)} - \mathrm{i}\kappa\right)(q-\alpha_1)^2 + \mathrm{i}\alpha_2 q\right], \tag{2.78}$$

where $\kappa = \frac{\mathrm{Im}(\xi)\sinh r}{2rS}$ and $S = \cosh r + \frac{\mathrm{Re}(\xi)}{r}\sinh r$ and α is defined as in (2.20). Taking ξ to be real and positive and setting $s = \mathrm{e}^\xi$ yields

$$\langle q|\xi,\alpha\rangle = \left(\frac{1}{\pi s^2}\right)^{\frac{1}{4}}\exp\left[-\frac{1}{2s^2}(q-\alpha_1)^2 - \mathrm{i}\alpha_2 q\right], \tag{2.79}$$

which is obviously a Gaussian distribution with mean α_1 determined by the displacement α and width $s = \mathrm{e}^\xi$ determined by the squeezing parameter ξ. The relationship $s = \mathrm{e}^\xi$ confirms that squeezing with $-\xi$ indeed compensates for squeezing with ξ in nice compliance with Eq. (2.71).

We have in mind the application of squeezed states to real-time propagation in bosonic many-body systems. While the squeezed states obviously fulfill a closure relation analogous to the one of the coherent states (see Eq. (2.26)),

$$\frac{1}{\pi}\int_{\mathbb{C}}\mathrm{d}\alpha\,|\xi,\alpha\rangle\langle\xi,\alpha| = \hat{S}_\xi\left[\frac{1}{\pi}\int_{\mathbb{C}}\mathrm{d}\alpha\,|\alpha\rangle\langle\alpha|\right]\hat{S}_\xi^\dagger = \hat{1}, \tag{2.80}$$

the additional squeezing parameter renders more flexible the set of possible states compared to the canonical coherent states. We can think of the squeezed states as a set of states being even more overcomplete than the coherent states. The calculations we have executed so far in this section reveal, however, that this additional flexibility comes at the price of a much more complicated algebra for the squeezed states.

In the applications we have in mind, we will need to calculate the commutation relations of the squeezing parameter with the creation and annihilation operator. Derived from the Baker-Campbell-Hausdorff formula, they read

$$\hat{S}^\dagger \hat{a} \hat{S} = \hat{a} \cosh r + \hat{a}^\dagger \mathrm{e}^{\mathrm{i}\phi} \sinh r, \qquad \hat{S}^\dagger \hat{a}^\dagger \hat{S} = \hat{a}^\dagger \cosh r + \hat{a} \mathrm{e}^{-\mathrm{i}\phi} \sinh r. \tag{2.81}$$

We may expect two subsequent squeezes by ξ_1 and ξ_2 to be condensable into a single squeezing by a certain ξ_3. Indeed, the composition of two squeezing operators reads [54]

$$\hat{S}_{\xi_1} \hat{S}_{\xi_2} = \hat{S}_{\xi_3} \left(\frac{1 + t_1 t_2^*}{1 + t_1^* t_2} \right)^{\frac{1}{2}(\hat{a}^\dagger \hat{a} + \frac{1}{2})}, \qquad t_j = \mathrm{e}^{\mathrm{i}\phi_j} \tanh r_j \text{ for } \xi_j = r_j \mathrm{e}^{\mathrm{i}\phi_j}, \tag{2.82}$$

where $\xi_3 = \frac{t_1 + t_2}{1 + t_1^* t_2}$. Formula (2.82) is consistent since it reduces to $\hat{S}_{\xi_1} \hat{S}_{\xi_2} = \hat{1}$ for $\xi_1 = -\xi_2$ since then $t_1 = -t_2$.

Many of the formulas in this section have been joined from different standard text books and publications. It is their complicated character which makes the squeezed states hard to work with in second quantized form. By assuming the squeezing parameter ξ to be real and positive, all presented formulas simplify tremendously. This is why, in order to do real-time propagation, applications typically resort to this specification.

Let us now highlight a second possible generalization to coherent states, the so-called displaced number states.

2.6. Displaced number states

A vast number of generalizations of the concept of coherent states can be found in the literature (see e.g. [55]). Apart from the previously introduced ideal squeezed states also squeezed number states have been considered [53, 56, 57]. Since it combines a delocalization scheme with delocalized functions, their application as time-dependent basis functions in real-time propagation problems does not seem promising to us. We have seen in Secs. 2.1 and 2.2 that with increasing n the number states $|n\rangle$ become more and more delocalized, while the coherent states α are highly localized for any α. Thus we may expect neither for large n nor for bosonic many-body problems the coherent states to be well suited to approximate the number states. We shall see later that a possible expedient is the application of displaced number states, which basically are the number states displaced in phase space.

Displaced number states $|\alpha, n\rangle$ are defined as

$$|\alpha, n\rangle := \hat{D}_\alpha |n\rangle \, , \tag{2.83}$$

where $|n\rangle$ are the number states of the harmonic oscillator and $\hat{D}_\alpha$ is the displacement operator defined in (2.31). While we have applications with fixed n but time-dependent α in mind, the parameters n and α allow in principle to tune between canonical coherent states ($n = 0$) and number states ($\alpha = 0$). By utilization of the properties of the Hermite polynomials, from (2.12) and (2.38) one may easily find the position representation of a number state. It reads

$$\langle q|\alpha, n\rangle = \left(\frac{m\omega}{\pi\hbar}\right)^{\frac{1}{4}} (2^n n!)^{-\frac{1}{2}} \exp\left[-\frac{m\omega}{2\hbar}(q - \alpha_1)^2 + \mathrm{i}\alpha_2 \left(q - \frac{1}{2}\alpha_1\right)\right] H_n\left(\frac{m\omega}{\hbar}(q - \alpha_1)\right), \tag{2.84}$$

where α is given by (2.20). The position representation (2.84) reduces to the position representation of coherent states, Eq. (2.21), for $n = 0$, as well as to the one of the number states, Eq. (2.12), for $\alpha = 0$.

We concentrate here on the properties of displaced number states which will be important for later applications. A profound essay on many further properties of displaced number states can be found in [58].

While the number states are orthogonal, this does in general not hold for displaced number states. We furthermore expect the overlap $\langle m, \alpha|\beta, n\rangle$ of two displaced number states not to be as localized as the one of two coherent states. By using the composition rule of displacement operators (2.36) we find that the overlap of two displaced number states is given by

$$\langle m, \alpha|\beta, n\rangle = \exp\left[\frac{1}{2}(\alpha^*\beta - \alpha\beta^*)\right] \langle m| \hat{D}_{\beta-\alpha} |n\rangle$$

$$= \exp\left[\alpha^*\beta - \frac{1}{2}\left(|\alpha|^2 + |\beta|^2\right)\right] \begin{cases} \sqrt{\frac{n!}{m!}}(\beta - \alpha)^{m-n} L_n^{m-n}\left(|\beta - \alpha|^2\right), & m \geq n \\ \sqrt{\frac{m!}{n!}}(\alpha^* - \beta^*)^{n-m} L_m^{n-m}\left(|\beta - \alpha|^2\right), & n \geq m \end{cases}. \tag{2.85}$$

The calculation of the overlap $\langle m| \hat{D}_{\beta-\alpha} |n\rangle$ is transferred to App. A. The expression of the overlap (2.85) reduces to the overlap of coherent states (2.24) for $m = n = 0$, and to δ_{mn} for the number states in the case of $\alpha = \beta = 0$.

In the left panel of Fig. 2.4 the probability density $|\langle q|\alpha, n\rangle|^2$ for fixed α of a displaced number state is shown as function of q for the first five integers. The right panel of Fig. 2.4 shows the absolute value $|\langle m, \alpha|\beta, n\rangle|$ of the overlap of two displaced number states, for $m = 3, n = 2$ and fixed β as function of $\mathrm{Re}(\alpha)$ and $\mathrm{Im}(\alpha)$. It shows the rotational symmetry of the overlap which is apparent if one considers the absolute value of (2.85).

It is clear that the displaced number states constitute an overcomplete set of states. For the applications we have in mind it is important to have available a representation of unity in terms of
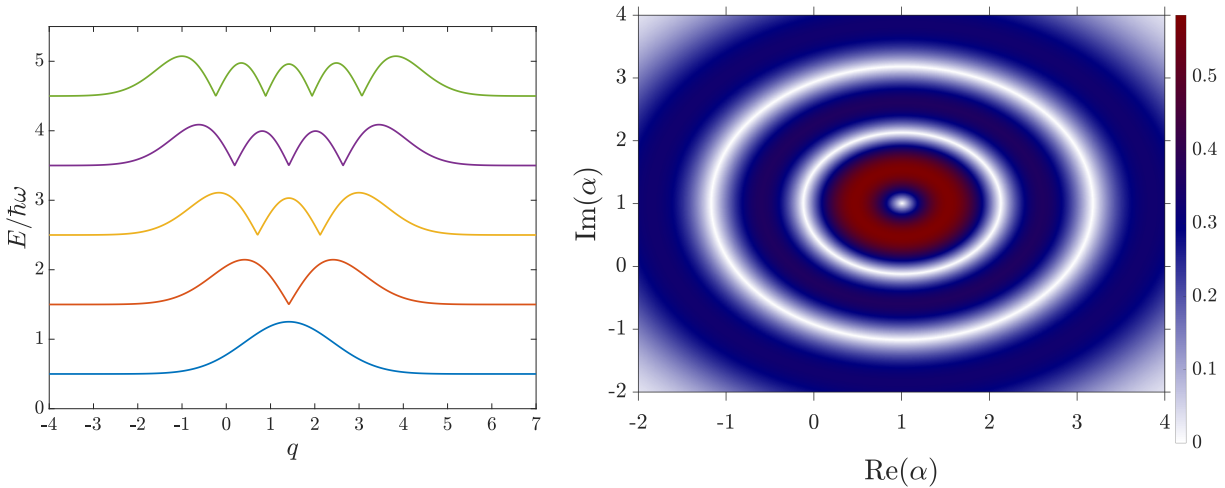
Figure 2.4.: Left panel: probability density $|\langle q|\alpha,n\rangle|^2$ of a displaced number state for fixed $\alpha = 1+\mathrm{i}$ as function of q in arbitrary units for the first 5 numbers: $n = 0$ (blue solid), $n = 1$ (red solid), $n = 2$ (yellow solid), $n = 3$ (violet solid) and $n = 4$ (green solid). Ordinate is the corresponding energy in units of $\hbar\omega$. Right panel: absolute value $|\langle m,\alpha|\beta,n\rangle|$ of the overlap of two displaced number states, for $m = 3, n = 2$ and fixed $\beta = 1+\mathrm{i}$ as function of $\mathrm{Re}\,(\alpha)$ and $\mathrm{Im}\,(\alpha)$.

the displaced number states. While it is straightforward to show that

$$1 = \sum_{n=0}^{\infty} |\alpha,n\rangle \langle \alpha,n|, \tag{2.86}$$

it turns out tedious to show that

$$1 = \frac{1}{\pi} \int_{\mathbb{C}} \mathrm{d}\alpha \; |\alpha,n\rangle \langle \alpha,n|. \tag{2.87}$$

Since there is no proof to be found in the literature, the latter is shown in App. A.

We have introduced so far primarily three sets of states which we plan to apply in order to examine the real-time dynamics of bosonic many-body systems: the canonical coherent states, the squeezed states and the displaced number states. Although the canonical coherent states are the least general ones of these, it will turn out that they result in the by far best suited formalism. Before we come to this, in the next section we shall address the question how to determine the time-evolution of these states in order to as good as possible reproduce the exact system dynamics.

2.7. On the variational principle

In only a very small number of bosonic many-body systems the exact system dynamics can be calculated straightforwardly by expansion of the wave-function in terms of an orthogonal basis. This is due to the exponential scaling of the basis size with the number of degrees of freedom: if n basis

functions shall be taken into account for a single degree of freedom, then the tensor-product basis for N particles consists of n^N basis functions. In order to circumvent this problem, we shall seek for a wave-function in terms of parametrized basis functions. Although still convergence has to be checked by increasing the number of basis functions, one may hope to circumvent the exponential scaling issue by a clever parametrization of the wave function which explores the relevant region of phase space with only a few basis functions.

While orthogonal basis functions have been utilized extremely successfully in this context by the multi-configurational time-dependent Hartree method (MCTDH) and the multi-layer variant (ML-MCTDH) [59–62], we here utilize the non-orthogonal sets of states introduced so far (see Secs. 2.2, 2.6 and 2.5) by assuming the respective parameters which define the states to be time-dependent. The closure relation, shown to hold for each of the sets, ensures that the system's initial state can be represented in terms of the parametrized wave function. Then we will be concerned with the question how to determine the time-evolution of the parameters such that the parametrized wave-function *optimally* follows the exact system dynamics, where the adverb *optimally* is to be specified.

We assume, as general as possible, a parametrization of the wave-function in terms of a set of complex time-dependent parameters $\{a_1, \ldots, a_n\} \subset \mathbb{C}$,

$$|\Psi(t)\rangle = |\Psi(a_1(t), \ldots, a_n(t))\rangle. \tag{2.88}$$

We will in the sequel suppress the explicit notion of the argument t in $|\Psi(t)\rangle$.

It is of utmost importance that any such parametrization equips the set of states M, defined as

$$M := \{|\Psi(a_1, \ldots, a_n)\rangle \,|\, a_1, \ldots, a_n \in \mathbb{C}\}, \tag{2.89}$$

with the structure of a complex manifold [63]. This means that the set of states M is locally homeomorph to $\mathbb{C}^n$, which is not true for the full Hilbert space, in general. For each fixed point $(a_1, \ldots, a_n) \in \mathbb{C}^n$ the local homeomorphism allows for translation of the concept of partial derivatives from $\mathbb{C}^n$ to M. Consequently one can define the tangent space $T(M, (a_1, \ldots, a_n))$ on the set of states M, spanned by the partial derivatives ∂_{a_i}.

Since the set of states in general is a subspace of the full system's Hilbert space, one can not hope for the Ansatz wave function (2.88) to exactly follow the system dynamics. Rather, by increasing the number of basis functions included in the Ansatz, i.e. by increasing the number of parameters, one has to check for convergence. On the route to convergence it is desirable to determine the time-evolution of the parameters a_i such that the wave-function (2.88) evolves according to a certain optimality condition. In order to specify this condition, we assume that the system dynamics is governed by some Hamiltonian $\hat{\mathcal{H}}$, for which we would like to solve the TDSE

$$i\hbar \partial_t |\Psi\rangle = \hat{\mathcal{H}} |\Psi\rangle. \tag{2.90}$$

While the action $\hat{\mathcal{H}} \left| \Psi(a_1, \ldots, a_n) \right\rangle$ of the Hamiltonian on the Ansatz wave function is exactly calculable, finding the time-derivatives of the parameters is an optimization problem. We define it in terms of variational calculus: the time-derivatives $\dot{a}_i$ are determined such that

$$\partial_t \left| \Psi \right\rangle = \sum_{i=1}^{n} \dot{a}_i \partial_{a_i} \left| \Psi \right\rangle \tag{2.91}$$

obeys some variational principle.

In this context, three variational principles are commonly referred to in the literature: the McLachlan variational principle [64] (MVP), the time-dependent variational principle [65] (TDVP) and the Dirac-Frenkel variational principle [66] (DFVP). A nice overview along with further interesting details of the respective principle can be found in [67].

Firstly, in McLachlan's version of the variational principle, the time-derivatives are determined such that $||\mathrm{i}\hbar\Psi - \hat{\mathcal{H}}\Psi||^2$ is minimized on M. It can easily be shown that this leads to

$$\mathrm{Im} \left(\left\langle \delta\Psi \right| \mathrm{i}\hbar\partial_t - \hat{\mathcal{H}} \left| \Psi \right\rangle \right) = 0. \tag{2.92}$$

Here, the variation $\left| \delta\Psi \right\rangle$ denotes the possible variations of the parametrized wave function, obtained by varying the parameters.

Secondly, in the TDVP, the time-derivatives of the parameters are determined from the requirement of the action

$$S = \int \mathrm{d}t \, L, \qquad L = \left\langle \Psi \right| \mathrm{i}\hbar\partial_t - \hat{\mathcal{H}} \left| \Psi \right\rangle \tag{2.93}$$

to be stationary, $\delta S = 0$ (along with some fixed boundary conditions), leading to

$$\mathrm{Re} \left(\left\langle \delta\Psi \right| \mathrm{i}\hbar\partial_t - \hat{\mathcal{H}} \left| \Psi \right\rangle \right) = 0. \tag{2.94}$$

Thirdly, the DFVP states directly and without derivation from a specific extremal condition that

$$\left\langle \delta\Psi \right| \mathrm{i}\hbar\partial_t - \hat{\mathcal{H}} \left| \Psi \right\rangle = 0. \tag{2.95}$$

Obviously the TDVP and the MVP can be derived from the DFVP, while it is not obvious that the reverse holds as well. Assuming the parameters $a_1, \ldots, a_n$ in (2.88) to be real, it can be shown that a sufficient condition for the equivalence of the different versions of the variational principle is that M can be parametrized by pairs of real *complementary* parameters (see [68] for details and for the definition of complementary parameters). We translate the result of [68] to the present context by combining complementary pairs of parameters to complex ones, leading to the important theorem:

The three variational principles MVP, TDVP and DFVP are equivalent if M can be parametrized by

complex parameters a_i such that $|\Psi\rangle$ fulfills the Cauchy-Riemann equations

$$\frac{\partial}{\partial a_i^*}|\Psi\rangle = 0. \tag{2.96}$$

We have argued above that M is locally homeomorph to $\mathbb{C}^n$. In this sense the requirement for $|\Psi\rangle$ to fulfill the Cauchy-Riemann equations (2.96) coincides with the requirement of $|\Psi\rangle$ being parametrizable as an analytic function on M.

It is of utmost importance to note that the previous theorem does not imply that for a given parametrization which does not fulfill condition (2.96) the three variational principles MVP, TDVP and DFVP are not equivalent. In fact we shall see that a wave function parametrized in terms of coherent states does actually not fulfill condition (2.96) - but it can be reparametrized to fulfill this condition. We shall furthermore see that for a wave function parametrized by displaced number states neither condition (2.96) nor the equivalence of the three variational principles hold. This hints that the above theorem is indeed an equivalence. Finally we will see that for a wave function parametrized in terms of squeezed states, resorting to real squeezing parameters ensures the equivalence of the three variational principles.

For all three variational principles the equations of motion for the parameters can be obtained by expressing the variation $|\delta\Psi\rangle$ in terms of the parameter variations δa_i and assuming the latter's mutual independence (see Sec. 3.1 for details). The definition of the action S in the TDVP (see eq. (2.93)), however, allows to derive the equations of motion on a different route.

From the Lagrangian density (2.93) the Euler-Lagrange equations can easily be derived (see e.g. [69]). They read

$$\frac{d}{dt}\frac{\partial L}{\partial \dot{u}} - \frac{\partial L}{\partial u} = 0. \tag{2.97}$$

Here, u has to be replaced by all parameters a_i *and their complex conjugates*.

Since the Euler-Lagrange equations have to be derived from the 'pure form' of the variational principle, one expects the effort invested in this derivation to pay off when computing the equations of motion (EOM) for the parameters. Peculiarly, the contrary is the case: computing the EOM in the Euler-Lagrange formalism turns out highly arduous. Furthermore, the Euler-Lagrange formalism heavily disguises the structure which is apparent on the level of the pure variational principle. Moreover, differing from (2.93) also a Lagrangian density

$$L = \frac{i\hbar}{2}\left[\langle\Psi|\dot{\Psi}\rangle - \langle\dot{\Psi}|\Psi\rangle\right] - \langle\Psi|\hat{\mathcal{H}}|\Psi\rangle \tag{2.98}$$

is used in the literature. In [70] we have investigated different aspects of the Euler Lagrange formalism as applied to wave functions parametrized by coherent states. Especially the usefulness of (2.98) in the context of normalized wave functions has been detailed there.

Since conservation of the normalization of the wave function is a requirement one would naturally impose on (almost) any propagation scheme, we examine it in more detail for the propagation of

parametrized wave functions in terms of the variational principle. Indeed, it can be shown that the normalization of a wave function whose parameter's time evolution is determined from the DFVP is conserved if the corresponding set of states M contains rays, i.e. if $\alpha u \in M$ for all $\alpha > 0, u \in M$ (see [67] for details). Since any parametrization which we employ here fulfills this condition, the previous statement ever ensures the conservation of the normalization of the wave function.

It has been amplified nicely in [71] for an Ansatz in terms of coherent states that the Euler-Lagrange and the pure variational formalism indeed yield identical equations of motion. Although we have utilized the Euler Lagrange formalism in many applications, we concentrate here on the application of the DFVP due to the former's tediousness and the latter's simplicity and straightforwardness.

We have now completed the discourse on theoretical tools required to employ coherent states as time-dependent basis functions. In the next chapter, we will detail how to apply these tools in order to obtain from the coherent states a highly functional method called multi Davydov-Ansatz.

3. Real time propagation with CS

As we have seen in the previous chapter, the CS have a vast number of interesting properties. What makes them appealing candidates for basis functions for real-time propagation for a large number of degrees of freedom is their overcompleteness and their local nature (see Secs. 2.1 and 2.3). Since the CS are localized, matrix elements of potentials only known locally can easily be calculated. This is of utmost importance in so-called on the fly methods, where the potential is determined simultaneously with the propagation of the equations of motion. From the overcompleteness, on the other hand, we may expect the number of basis functions required to adequately reproduce the exact wave function to be reasonably small in high-dimensional problems. Already in the early stages of quantum mechanics people have tried to utilize CS as basis functions in order to approximately solve the TDSE. Semiclassical methods founded their triumphal march on the classical properties of CS, namely their minimal uncertainty (2.27) and their classical time-evolution under the action of the harmonic oscillator propagator (2.30). Emanating from the correspondence principle and influential works of Gutzwiller [72–75], Miller [76–79], Marcus [80–85], Heller [86] and many others, the method was ennobled by Herman [87, 88], Kluk [89] and others [90, 91]. While the initial value representation remained Achilles' heel of the method, requiring a vast oversampling of the initial state, attempts to write the wave function as an exact expansion in terms of CS emerged in parallel [86, 92–94]. While CS are utilized today in many different contexts, two main groups exist (to our best knowledge) which employ CS as moving basis functions in combination with the full variational principle. Firstly, the group of Yang Zhao has contributed valuable work in the field. Secondly, the group of Irene Burghardt has contributed many precious works employing sets of moving CS as basis functions. This group has from the very beginning publicly risen to the challenge of certain issues intimately related to the method [95] and outlined in detail below. After systematically deriving the equations of motion from the variational principle we shall highlight how to solve these issues. Two artifices will be shown to suffice in order to circumvent them, rendering extremely stable and reliable the formerly highly unstable method. On its basis, the multi Davydov-Ansatz being a straightforward generalization of the basic method to more general systems is introduced. Furthermore, also squeezed states and displaced number states will be investigated with respect to their potential as time-dependent moving basis functions. Finally it is outlined how to treat non-zero temperature systems with the multi Davydov-Ansatz.

3.1. Variational principle with CS

We set the stage by first considering an N-particle Hilbert space and a dynamics being governed by the Hamiltonian $\hat{\mathcal{H}} = \sum_{j=1}^{N} \hat{H}_j + \sum_{i<j} \hat{W}_{ij}$, with one-particle Hamiltonians $\hat{H}_j$ and two-particle interactions $\hat{W}_{ij}$.

A straightforward numerical calculation of the exact dynamics in terms of the number states, introduced in Sec. 2.1, is in most cases out of reach due to the exponential scaling of the basis size with

the number N of particles. In order to circumvent this issue, we aim at utilization of an appropriate parametrization along with the application of a variational principle, outlined in Sec. 2.7.

We shall focus on the parametrization of the wave function in terms of coherent states (see Sec. 2.2) since it will turn out that for these - in contrast to the displaced number states and for the squeezed states - the three variational principles MVP, TDVP and DFVP are equivalent. We shall furthermore see that the overcompleteness of the CS is at the heart of their extremely favourable scaling with the number of degrees of freedom.

Any result from Chap. 2 straightforwardly generalizes to the setting of N degrees of freedom. Specifically, N-mode coherent states

$$|\boldsymbol{\alpha}\rangle := \bigotimes_{n=1}^{N} |\alpha_n\rangle, \qquad \boldsymbol{\alpha} = (\alpha_1, \ldots, \alpha_N) \in \mathbb{C}^N, \tag{3.1}$$

are multi-dimensional Gaussians in phase space,

$$\langle \mathbf{q}|\boldsymbol{\alpha}\rangle = \left(\prod_{n=1}^{N} \frac{m_n \omega_n}{\pi \hbar}\right)^{\frac{1}{4}} \exp\left[\sum_{n=1}^{N}\left(-\frac{|\alpha_n|^2}{2} - \frac{\xi_n^2}{2} + \sqrt{2}\xi_n\alpha_n - \frac{\alpha_n^2}{2}\right)\right], \qquad \xi_n = \sqrt{\frac{m_n \omega_n}{\hbar}}q_n, \tag{3.2}$$

whose overlap is given by

$$\langle \boldsymbol{\alpha}|\boldsymbol{\beta}\rangle = \prod_{n=1}^{N} \langle \alpha_n|\beta_n\rangle = \exp\left[\sum_{n=1}^{N}\left(\alpha_n^*\beta_n - \frac{1}{2}\left(|\alpha_n|^2 + |\beta_n|^2\right)\right)\right]. \tag{3.3}$$

Any wave function $|\Psi\rangle$ in the N-particle Hilbert space can be written in terms of multi-mode coherent states by utilization of the N-mode analog of the closure relation (2.26),

$$|\Psi\rangle = \frac{1}{\pi^N} \int_{\mathbb{C}^N} \mathrm{d}\boldsymbol{\alpha} \,\langle \boldsymbol{\alpha}|\Psi\rangle\, |\boldsymbol{\alpha}\rangle. \tag{3.4}$$

By straightforward discretization of (3.4), one deduces that an Ansatz for the wave function in terms of multi-mode CS of multiplicity M is given by

$$|\Psi_{\mathrm{CS}}^{\mathrm{M}}(t)\rangle = \sum_{k=1}^{M} A_k(t)\, |\boldsymbol{\alpha}_k(t)\rangle. \tag{3.5}$$

Here, $A_k(t)$ are time-dependent complex coefficients, while $\boldsymbol{\alpha}_k(t)$ are time-dependent N-dimensional complex displacements. We shall refer to this Ansatz as the variational multi-configurational Gaussian (vMCG) Ansatz.

Clearly, the integral entering Eq. (3.4) is an N-fold product of independent integrals each of whose integration has to be performed over the complex plane. A discretization of each single integral, however, is not at all expedient since then one was back at exponential scaling. Rather, the discretization

(3.5) comprises the expectation that our unconsciousness about a single particles dynamics will be taken care of by the variational principle. Speaking more generically: in order to reproduce the exact dynamics it may be that for certain particles a single coherent state is enough, while for others multiple coherent states may be needed. Although it is not known a priori for which of the particles which number of coherent states is needed, we may well leave this issue to the variational principle since it optimizes the dynamics in this respect.

Let us now investigate the structure of the vMCG Ansatz (3.5) in more detail.

3.1.1. Gauge freedom in the vMCG Ansatz

For the following, it is of utmost importance that there is a gauge freedom in the vMCG Ansatz (3.5) in the sense that the wave function (3.5) is invariant with respect to (time-dependent) linear transformations of the CS basis. Let Q be a nonsingular transformation matrix, then the wave function remains unchanged if A_k and $|\boldsymbol{\alpha}_k\rangle$ are replaced by

$$A_k \to \tilde{A}_k = \sum_{l=1}^{M} A_l \left(Q^{-1}\right)_{lk} \qquad \text{and} \qquad |\boldsymbol{\alpha}_k\rangle \to |\tilde{\boldsymbol{\alpha}}_k\rangle = \sum_{l=1}^{M} Q_{kl} |\boldsymbol{\alpha}_l\rangle. \tag{3.6}$$

This is analogous to the multi-configurational time-dependent Hartree approach[59, 60] (MCTDH), where the gauge freedom is used to significantly simplify the equations of motion.

Let us first consider diagonal transformations Q, which effectively amount to multiplication of each CS with a possibly time-dependent non-zero C-number. Due to the normalization factor of the CS, the Ansatz (3.5) does not obey relation (2.96),

$$\frac{\partial}{\partial \alpha_i^*} |\Psi_{\text{CS}}^{\text{M}}\rangle \neq 0. \tag{3.7}$$

But, transforming coefficients and displacements according to (3.6) by the transformation

$$Q_{kl} := \begin{cases} \exp\left[\frac{1}{2}\sum_{n=1}^{N} |\alpha_{kn}|^2\right], & k = l \\ 0, & k \neq l \end{cases} \tag{3.8}$$

results in the same wave function, yet it obeys property (2.96) because the normalization terms are canceled. Thus, although the Ansatz (3.5) does not obey the relation (2.96), it can be reparametrized such that condition (2.96) is fulfilled. Hence, according to Sec. 2.7, the three variational principles are equivalent for the wave function Ansatz (3.5). On the basis of this equivalence holding, we may propagate the parameters of the vMCG Ansatz by the DFVP on a thorough ground.

Apart from the vMCG Ansatz (3.5) also other discretizations of (3.4) are possible. While in order to avoid exponential scaling a discretization of each single integral entering (3.4) is not expedient, separate discretization of certain parts of the system may well be appropriate. Thus let us, in the spirit of MCTDH, split the full Hilbert space artificially into (at least) two parts, e.g. by combining

'physical' or 'logical' coordinates,

$$H = H_1 \otimes H_2. \tag{3.9}$$

Then, the wave-function may be expanded in terms of CS in each subspace separately,

$$|\Psi(t)\rangle = \left(\sum_{k=1}^{M_1} A_k \, |\boldsymbol{\alpha}_k\rangle \right) \left(\sum_{j=1}^{M_2} B_j \, |\boldsymbol{\beta}_j\rangle \right). \tag{3.10}$$

While this decomposition in comparison to (3.5) introduces further coefficients, it allows for optimization in each subspace separately. To be more precise: while the additional equations for the additional coefficients come at marginal computational cost, the dimension of the space in which the displacements have to be propagated can be halved. This constitutes an extraordinary advantage in the MCTDH method. But, in tremendous contrast to the latter, the basis functions employed here are not orthogonal. Consequently, in order to obtain the equations in the reduced space, a corresponding overlap matrix has to be inverted. Since its invertibility can not always be guaranteed, this unfortunately compensates for the gained effort. Apart from the requirement of a priori guessing a decomposition of the full Hilbert space, this introduces further instabilities into the method and hence we refrain from following this route.

By further exploiting the gauge freedom of the vMCG method, the authors of [28, 29, 71, 96, 97] have successfully included the vMCG method into the MCTDH formalism. By allowing not only diagonal but more general transformations, one may mutually orthogonalize sets of CS. This is being done in the so-called Gaussian-MCTDH (GMCTDH) method). Here, however, we will take an alternative route here and show that with the improvements of the vMCG Ansatz, outlined in Secs. 3.3.1 and 3.3.2 suffice to yield a method working smoothly also without application of more general transformations.

3.1.2. Equations of motion for the vMCG Ansatz

Before we explicitly derive the equations of motion for the vMCG method, let us briefly mention that the set of states

$$M := \left\{ \sum_{k=1}^{M} A_k \, |\boldsymbol{\alpha}_k\rangle \mid A_k \in \mathbb{C}, \boldsymbol{\alpha}_k \in \mathbb{C}^N \right\} \tag{3.11}$$

corresponding to the vMCG Ansatz (3.5) obviously contains rays, i.e. $\beta u \in M$ for all $\beta \in \mathbb{C}, u \in M$. Hence the norm of the Ansatz wave function (3.5) is conserved if its parameters are propagated according to the DFVP (see Sec. 2.7).

Now that we know that for the Ansatz (3.5) all three variational principles are equivalent, and that the wave function's norm is conserved if propagated with any of these, we may set about explicit

calculation of the equations of motion. Due to its simplicity and straightforwardness, we shall apply the DFVP.

The variation of the Ansatz (3.5) reads

$$\langle \delta \Psi_{\mathrm{CS}}^{\mathrm{M}} | = \sum_{l=1}^{M} \langle \boldsymbol{\alpha}_l | \left\{ \delta A_l^* + A_l^* \sum_{n=1}^{N} \left[\left(-\frac{1}{2} \alpha_{ln} + \hat{a}_n \right) \delta \alpha_{ln}^* - \frac{1}{2} \alpha_{ln}^* \delta \alpha_{ln} \right] \right\}, \tag{3.12}$$

where the variation with respect to the displacements is most easily calculated from (2.34). All appearing variations are mutually independent. Thus the equations of motion read

$$\langle \boldsymbol{\alpha}_l | \, \mathrm{i}\partial_t - \hat{\mathcal{H}} \, | \Psi_{\mathrm{CS}}^{\mathrm{M}} \rangle = 0, \tag{3.13}$$

$$A_l^* \langle \boldsymbol{\alpha}_l | \, \hat{a}_j \left(\mathrm{i}\partial_t - \hat{\mathcal{H}} \right) | \Psi_{\mathrm{CS}}^{\mathrm{M}} \rangle = 0, \tag{3.14}$$

where Eq. (3.13) was obtained from the variations of the coefficients, (3.14) was obtained from the variations of the displacements, and where the first equation was used to simplify the second one. By insertion of the explicit expression for the time-derivative of the Ansatz wave function

$$\partial_t | \Psi_{\mathrm{CS}}^{\mathrm{M}} \rangle = \sum_{k=1}^{M} \left\{ \dot{A}_k + A_k \sum_{n=1}^{N} \left[-\frac{1}{2} \left(\alpha_{kn} \dot{\alpha}_{kn}^* + \dot{\alpha}_{kn} \alpha_{kn}^* \right) + \dot{\alpha}_{kn} \hat{a}_n^\dagger \right] \right\} | \boldsymbol{\alpha}_k \rangle, \tag{3.15}$$

equations (3.13,3.14) read

$$\mathrm{i} \sum_{k=1}^{M} \left\{ \dot{A}_k + A_k \sum_{n=1}^{N} \left[-\frac{1}{2} \left(\alpha_{kn} \dot{\alpha}_{kn}^* + \dot{\alpha}_{kn} \alpha_{kn}^* \right) + \dot{\alpha}_{kn} \alpha_{ln}^* \right] \right\} \langle \boldsymbol{\alpha}_l | \boldsymbol{\alpha}_k \rangle = \langle \boldsymbol{\alpha}_l | \, \hat{\mathcal{H}} \, | \Psi_{\mathrm{CS}}^{\mathrm{M}} \rangle, \tag{3.16}$$

$$\mathrm{i} A_l^* \sum_{k=1}^{M} \left\{ \alpha_{kj} \left(\dot{A}_k + A_k \sum_{n=1}^{N} \left[-\frac{1}{2} \left(\alpha_{kn} \dot{\alpha}_{kn}^* + \dot{\alpha}_{kn} \alpha_{kn}^* \right) + \dot{\alpha}_{kn} \alpha_{ln}^* \right] \right) + A_k \dot{\alpha}_{kj} \right\} \langle \boldsymbol{\alpha}_l | \boldsymbol{\alpha}_k \rangle$$
$$= A_l^* \langle \boldsymbol{\alpha}_l | \, \hat{a}_j \hat{\mathcal{H}} \, | \Psi_{\mathrm{CS}}^{\mathrm{M}} \rangle. \tag{3.17}$$

Eqs. (3.16,3.17) are the central working equations of this thesis. They constitute a system of highly nonlinear ordinary differential equations, which one attempts to solve numerically in two steps:

(i) solve the *linear* system of equations for the vector containing derivatives of the parameters

(ii) integrate the vector

While step (ii) is just a matter of appropriate technical equipment, step (i) may be problematic. Firstly, any numerical solver requires the linear system to be in standard form

$$\boldsymbol{M} \vec{x} = \vec{b}. \tag{3.18}$$

It is not straightforward how to do so due to the complex conjugates of the derivatives of the displacements $\dot{\alpha}_{kn}^*$. Secondly, if the linear system was in standard form, moreover its unique solubility

would be required. It will turn out that this is actually *very often not the case*. However, these two problems are so severe that an own section is attributed to each of them (see the next two sections).

3.2. Standard form of the linear system

In order to bring the system (3.16,3.17) into standard form, the most obvious approach would be to split real and imaginary parts. Besides this being cumbersome, it would completely disguise the structure of the coefficient matrix. With the intention to avoid splitting of real and imaginary parts, the authors of [29, 30] therein and in subsequent works [71, 95–100] employ an Ansatz

$$|\Psi(t)\rangle = \sum_{k=1}^{M} B_k(t) \exp\left[\mu_k(t)\right] |\boldsymbol{\beta}_k(t)\rangle , \tag{3.19}$$

where

$$|\boldsymbol{\beta}_k\rangle = \bigotimes_{n=1}^{N} |\beta_{kn}\rangle , \qquad |\beta_{kn}\rangle = \exp\left[\beta_{kn}\hat{a}_n^\dagger\right]|0\rangle \tag{3.20}$$

are *unnormalized* CS and $\mu_k(t)$ are additional parameters. Then, $\dot{\mu}_k$ replaces the problematic terms in the EOM,

$$\sum_{k=1}^{N} \left[-\frac{1}{2}\left(\beta_{kn}\dot{\beta}_{kn}^* + \dot{\beta}_{kn}\beta_{kn}^*\right)\right] \to \dot{\mu}_k, \tag{3.21}$$

which stem from the normalization of the CS. However, keeping in mind the gauge freedom elaborated on at the beginning of Sec. 3.1, it is little surprising that no additional equations can be obtained for the μ_k from the variational principle. The equations one obtains actually coincide with those for the coefficients (3.16). Consequently it is argued that one is free to choose $\dot{\mu}_k = 0$, and one sets

$$\mu_k(t) = -\frac{1}{2}\sum_{n=1}^{N} |\beta_{kn}(t)|^2 \tag{3.22}$$

as the appropriate normalization of the CS at each time step. This procedure is inconsistent, since then neither $\dot{\mu}_k = 0$ nor is independent variation of μ_k and β_{kn} justified. Surprisingly enough, there is a vast number of publications where this method is applied, admittedly suffering from certain instabilities which are nevertheless attributed to the issues outlined in the next section.

Let us now outline how to consistently bring system (3.16,3.17) into standard form. The key observation is that

$$X_k := \dot{A}_k + A_k \sum_{n=1}^{N} \left[-\frac{1}{2}\left(\alpha_{kn}\dot{\alpha}_{kn}^* + \dot{\alpha}_{kn}\alpha_{kn}^*\right)\right] \tag{3.23}$$

is only dependent on the index k, and appears equally in (3.16) and in (3.17). Consequently, having to solve the linear system (3.16,3.17) for the unknowns $\dot{A}_k$ and $\dot{\alpha}_{kn}$ is replaced by having to solve the system

$$\mathrm{i} \sum_{k=1}^{M} \left\{ X_k + A_k \sum_{n=1}^{N} \dot{\alpha}_{kn} \alpha_{ln}^* \right\} \langle \boldsymbol{\alpha}_l | \boldsymbol{\alpha}_k \rangle = \langle \boldsymbol{\alpha}_l | \hat{\mathcal{H}} | \Psi_{\mathrm{CS}}^{\mathrm{M}} \rangle \,, \tag{3.24}$$

$$\mathrm{i} A_l^* \sum_{k=1}^{M} \left\{ \alpha_{kj} \left(X_k + A_k \sum_{n=1}^{N} \dot{\alpha}_{kn} \alpha_{ln}^* \right) + A_k \dot{\alpha}_{kj} \right\} \langle \boldsymbol{\alpha}_l | \boldsymbol{\alpha}_k \rangle = A_l^* \langle \boldsymbol{\alpha}_l | \hat{a}_j \hat{\mathcal{H}} | \Psi_{\mathrm{CS}}^{\mathrm{M}} \rangle \tag{3.25}$$

for the unknowns X_k and $\dot{\alpha}_{kn}$. Advantageously, it is immediate how to bring the latter in standard form (3.18). Subsequent to its numerical solution, $\dot{A}_k$ can easily be calculated from X_k and $\dot{\alpha}_{kn}$ according to (3.23).

This whole idea actually rests upon the gauge freedom of the vMCG Ansatz (see Sec. 3.1.1) and the transformation (3.8), since X_k originates from coefficients transformed according to (3.8) forth and back,

$$X_k = Q_{kk} \partial_t \left(Q^{-1} \right)_{kk} A_k, \qquad Q_{kk} = \exp \left[\frac{1}{2} \sum_{n=1}^{N} |\alpha_{kn}|^2 \right]. \tag{3.26}$$

Clearly, application of unnormalized CS *without* introduction of the μ_k parameters would as well eliminate the complex conjugates of the displacements' derivatives from the EOM (see [70] for further details). This again corresponds to the gauge (3.8),

$$A_k \rightarrow \tilde{A}_k = \left(Q^{-1} \right)_{kk} A_k, \qquad Q_{kk} = \exp \left[\frac{1}{2} \sum_{n=1}^{N} |\alpha_{kn}|^2 \right], \tag{3.27}$$

but without transforming back as in (3.26). Disadvantageously in this case the coefficients may become large: given a certain magnitude for the coefficients A_k in (3.27), the transformed coefficients $\tilde{A}_k$ have to scale reciprocally as $\tilde{A}_k = Q_{kk} A_k$. Since this is numerically less stable, the procedure which introduces the X_k will be favored in the sequel.

Now that we have shown how to bring the system of equations of motion into standard form, we illuminate in more detail the second problem mentioned in Sec. 3.1.2: the regularity of the coefficient matrix.

3.3. Regularity of the coefficient matrix

We shall now address the main issue which real-time propagation with CS has suffered from for the last decades: the invertibility of the coefficient matrix. We will show that the effort invested in the previous section to bring the system (3.16,3.17) into standard form (3.18) will pay off here. From the system (3.24,3.25) we infer that the coefficient matrix is (almost) singular if

(a) any of the coefficients $A_l \approx 0$, since then the corresponding N equations (3.25) read $0 \approx 0$,

(b) for any two CS $\boldsymbol{\alpha}_{l_1} \approx \boldsymbol{\alpha}_{l_2}$ ($l_1 \neq l_2$), since then two of the equations (3.24) and $2N$ (pairwise) equations (3.25) are (almost) equal, called the *linear dependency problem.*

(a) is related to the type of the Ansatz (3.5) being kind of a scalar product between the vector containing the coefficients and the 'vector' containing the coherent states. Adopting the language of (ML-)MCTDH [60], we will speak of the CS $|\boldsymbol{\alpha}_l\rangle$ as *unpopulated* if $A_l \approx 0$. Clearly then the position and the evolution of the CS $|\boldsymbol{\alpha}_l\rangle$ is rather arbitrary. Indeed, the authors of [101–103] have shown that one may infer directly from the TDSE that in the case $A_l = 0$ the time evolution of the corresponding displacements α_{ln} cannot be given by any first-order differential equation. Consequently, canceling A_l^* in (3.25) is not expedient. Rather, some workaround has to be found. In [60] the authors propose to regularize the (positive semidefinite) *single-particle density matrix*

$$\boldsymbol{\rho}_{lk} = A_l^* A_k \tag{3.28}$$

according to

$$\boldsymbol{\rho} \rightarrow \boldsymbol{\rho} + \varepsilon \exp\left[-\frac{\boldsymbol{\rho}}{\varepsilon}\right], \qquad \varepsilon \ll 1. \tag{3.29}$$

As can be seen by diagonalization of $\boldsymbol{\rho}$ this amounts in replacing the eigenvalues $\lambda \geq 0$ of $\boldsymbol{\rho}$ according to

$$\lambda \rightarrow \lambda + \exp\left[-\frac{\lambda}{\varepsilon}\right], \qquad \varepsilon \ll 1, \tag{3.30}$$

analogously to the proceeding given in [102, 103].
While calculation of the matrix exponential may be computationally expensive, one may also resort to regularization of $\boldsymbol{\rho}$ according to

$$\boldsymbol{\rho} \rightarrow \boldsymbol{\rho} + \varepsilon \mathbb{1}, \qquad \varepsilon \ll 1, \tag{3.31}$$

where $\mathbb{1}$ is the identity matrix.
Furthermore, in [101] the author proposes to resort to second-order differential equations. Due to the nonorthogonality of the CS, this is not feasible in our case. Instead, we would like to resort to a regularization according to (3.29), but special care has to be taken due to the nonorthogonality of the coherent states. In the next section, we highlight how to carefully regularize the equations (3.24, 3.25) according to (3.29) or (3.31), while in Sec. 3.3.2 we address case (b) of two CS coming close.

3.3.1. Regularization in the case of vanishing coefficients

It will be convenient to express the ingredients entering the equations (3.24, 3.25) by matrix operations. To this end we denote the Hadamard product (elementwise multiplication) by $\circ$, the tensor product

by $\otimes$, by $\mathbb{1}_n$ the $n \times n$ unit matrix, and by $1_{m \times n}$ the matrix in $\mathbb{C}^{m \times n}$ which consists of only ones. Then we define the matrix $\boldsymbol{F}$ of displacements

$$\boldsymbol{F}_{kn} := \alpha_{kn}, \tag{3.32}$$

and the vector of coefficients

$$A \in \mathbb{C}^{M \times 1}. \tag{3.33}$$

Then the coefficient matrix $\boldsymbol{M}$ of system (3.24, 3.25) in standard form, up to the pre-factor i, reads

$$\boldsymbol{M} = \begin{pmatrix} \boldsymbol{S} & \boldsymbol{L}_2 \\ \boldsymbol{L}_2^\dagger & \boldsymbol{L}_3 \end{pmatrix}, \tag{3.34}$$

where the matrix $\boldsymbol{\rho}$ is defined by Eq. (3.28), the overlap matrix $\boldsymbol{S}$ is defined as

$$\boldsymbol{S}_{lk} = \langle \boldsymbol{\alpha}_l | \boldsymbol{\alpha}_k \rangle, \tag{3.35}$$

and

$$\boldsymbol{L}_2 = \left(\boldsymbol{F}^* \otimes A^T \right) \circ \left(1_{1 \times N} \otimes \boldsymbol{S} \right), \tag{3.36}$$

$$\boldsymbol{L}_3 = \left[1_{1 \times N} \otimes \boldsymbol{F}^T \otimes 1_{M \times 1} \right] \circ \left[1_{N \times 1} \otimes \boldsymbol{F}^* \otimes 1_{1 \times M} \right) \right] \circ \left[1_{N \times N} \otimes (\boldsymbol{\rho} \circ \boldsymbol{S}) \right] + \mathbb{1}_N \otimes (\boldsymbol{\rho} \circ \boldsymbol{S}). \tag{3.37}$$

It has been claimed in [95] that for the unpopulated CS, regularization of $\boldsymbol{L}_3$ *en bloc* would result in a stable algorithm. On the contrary, our implementations show that doing so results in further instabilities since it effects not only the coefficients (present in $\boldsymbol{\rho}$) but also the displacements (present in $\boldsymbol{F}$ and $\boldsymbol{S}$). Regularizing not carefully enough thus leads to further instabilities since it indirectly changes the present positions of the coherent states.

Conversely, the explicit form of $\boldsymbol{M}$ given in (3.34) nicely highlights via (3.37) how to carefully regularize. Regularizing only $\boldsymbol{\rho}$ in (3.37) according to (3.29) or (3.31) in the case of (almost) vanishing coefficients does not indirectly affect the positions of the CS, and thus does not introduce further instabilities into the propagation scheme. Indeed it turns out to be highly stable, which we will detail in Sec. 4.3.1.

3.3.2. Apoptosis of CS

In this section, we address issue (b) of Sec. 3.3. If two CS come close, $\boldsymbol{\alpha}_{l_1} \approx \boldsymbol{\alpha}_{l_2}$, their roles are not unique and consequently their derivatives can not be determined uniquely, rendering (almost) singular the coefficient matrix $\boldsymbol{M}$. This setup does not occur if orthogonal states are propagated, thus we can not lend further help from MCTDH where the wave function is expanded in terms of (layers of) orthogonal basis states. If $\boldsymbol{\alpha}_{l_1} \approx \boldsymbol{\alpha}_{l_2}$, only two of the equations (3.24) become equal, while $2N$ of the equations (3.25) become pairwise equal. The physical problems which one attempts

to tackle with the help of CS and Ansatz (3.5) are typically high-dimensional, since one hopes their vast overcompleteness to beat the exponential scaling of orthogonal basis sets. But it is especially these high-dimensional problems where CS coming close is the dominant issue [104]. Furthermore, in unfortunate synergy with the latter, we may expect the issue generically to occur if enough CS are included to ensure convergence [105], since then they are dense enough to exhibit redundancies. Thus CS generically come close as soon as convergence with respect to the number of CS is reached and hence full convergence is out of reach. Frustratingly enough in most applications only a few CS suffice to be already close to convergence.

In order to circumvent this problem, plenty of effort such as re-expansion schemes [106], multiplication of the CS with orthogonal polynomials [107, 108], orthogonalizing momentum-symmetrized Gaussians [109] and projector splitting [110] has been invested. Nevertheless, each of these methods suffers itself from further issues (loss of norm conservation in the case of re-expansion, complication of EOM and indeterminateness of coefficients in the case of orthogonal polynomials, etc).

A first immediate observation is related to the dimension of the matrices entering $\boldsymbol{M}$ which are affected by the closeness of CS. $\boldsymbol{\alpha}_{l_1} \approx \boldsymbol{\alpha}_{l_2}$ produces (almost) equal rows in $\boldsymbol{F}$ and $\boldsymbol{S}$ (see (3.34)-(3.37)). While we may hope to regularize the overlap matrix $\boldsymbol{S} \in \mathbb{C}^{M \times M}$ along similar lines as the density matrix $\boldsymbol{\rho} \in \mathbb{C}^{M \times M}$ in Sec. 3.3, this is unlikely to succeed for $\boldsymbol{F} \in \mathbb{C}^{M \times N}$ since in typical setups $M \ll N$.

The second immediate observation is related to the subsequent desire to remove one of the corresponding rows $l_{1/2}$ from $\boldsymbol{F}$. It is the linearity in the variations of (3.12) and the linearity in the displacements' derivatives of (3.15) which is the key to implement this removal. Assume that the two CS $|\boldsymbol{\alpha}_{l_1}\rangle$ and $|\boldsymbol{\alpha}_{l_2}\rangle$ move from a certain time t_0 on *connectedly*, i.e. without changing their relative position. Mathematically this means that the N free parameters of one of them, say $\boldsymbol{\alpha}_{l_2}$, are replaced by the parameters of the other one:

$$\boldsymbol{\alpha}_{l_2}(t) = \boldsymbol{\alpha}_{l_1}(t) + \boldsymbol{C}, \tag{3.38}$$

for $t \geq t_0$, where $\boldsymbol{C} = \boldsymbol{\alpha}_{l_2}(t_0) - \boldsymbol{\alpha}_{l_1}(t_0)$ is a constant. Consequently $\delta\alpha_{l_1,j} = \delta\alpha_{l_2,j}$ and $\dot{\alpha}_{l_1,j} = \dot{\alpha}_{l_2,j}$ for all j. At the level of the coefficient matrix $\boldsymbol{M}$, this indeed amounts to deleting the N rows/columns corresponding to the displacements $\alpha_{l_2,j}$ and replacing the N rows/columns corresponding to $\alpha_{l_1,j}$ with the sum of both from time t_0 on. The idea originates from [70] where we have used a similar idea to obtain equations for CS on a fixed grid which we have termed the D1.5 Ansatz.

$\boldsymbol{\alpha}_{l_2}$ may from time t_0 on be regarded as dislodged, since its N free parameters are removed. We have name this programmed death for the ensemble's benefit apoptosis [111]. Still the corresponding coefficient A_{l_2} remains as a free parameter which is highly advantageous, because, in contrast to a complete removal of the CS $|\boldsymbol{\alpha}_{l_2}\rangle$, the norm of the Ansatz wave function is naturally conserved (no re-expansion is necessary) and no instabilities are introduced. Hence apoptosis is compatible with any adaptive integrator and can be done on the fly. Furthermore, keeping the coefficient comes at marginal computational cost since usually $M \ll N$.

We relate the time t_0 at which apoptosis shall occur to the distance $d(|\boldsymbol{\alpha}_{l_1}\rangle, |\boldsymbol{\alpha}_{l_2}\rangle)$ given by the 2

product metric on $\mathbb{C}^N$,

$$d(|\boldsymbol{\alpha}_{l_1}\rangle, |\boldsymbol{\alpha}_{l_2}\rangle) = \sqrt{\sum_{n=1}^{N} |\alpha_{l_1,n} - \alpha_{l_2,n}|^2}. \tag{3.39}$$

This is obviously equivalent to relating it with the absolute value of the overlap, see (3.3). For a given threshold $\varepsilon \ll 1$, apoptosis is implemented if $d(|\boldsymbol{\alpha}_{l_1}\rangle, |\boldsymbol{\alpha}_{l_2}\rangle) < \varepsilon$. The distance threshold on the one hand should be chosen according to timeliness of apoptosis. If it is too small, the integrator will get stuck as if no apoptosis had been implemented. On the other hand, in order to keep flexibility maximal, ε should not be too large. Keeping the threshold in a range $0.01 \leq \varepsilon \leq 0.1$ works nicely in all cases studied so far.

Furthermore, it may happen that multiple CS approach each other during propagation, and apoptosis of more than one CS could be required at a time step. Finding those CS which are close to each other is implemented using a connected-component search in graphs [112]. Then, each connected component has to be replaced by one of its members only à la (3.38).

Any calculation performed in the context of this thesis indicates that an increasing number of CS does not necessarily lead to an increasing number of apoptosis events. This is again intimately related to the overcompleteness of the CS: one CS's motion in phase space is complicated and dependent on the position of all other CS. Actually propagation with increased multiplicity M may cope without apoptosis, or with more or fewer CS connected. Thus, in the presence of apoptosis convergence can be checked by increasing the multiplicity M in a systematic way (see Sec. 4.3.2. However, in cases of very long propagation times, it seems also possible to exploit the CS's flexibility and to split the propagation interval into parts. Then, convergence for each part could be ensured independently by insertion of new CS at appropriate positions (see Sec. D) at each part's beginning.

In our tests, the integrator steps typically decrease significantly in the event of two CS coming close. This is exemplary shown in the left panel of Fig. 3.1, where without apoptosis the integrator finally gets stuck, meaning that the step size is too small to obtain results within reasonable time. With apoptosis implemented, the integrator steps also decrease in the event of two coherent states coming close, but always recovers after apoptosis has occurred (see right panel of Fig. 3.1. The specific details (time to recovery, step-size of the integrator etc.) depend on the setting and the specific choice of the regularization threshold ε. Converged results are obtained although the flexibility of the remaining CS is decreased. Furthermore it seems likely for some of the coefficients of connected CS to decrease after apoptosis, which would require a stronger regularization of the density matrix $\boldsymbol{\rho}$. This has, however, not been observed in our tests.

We shall show that apoptosis succeeds in the regularization of CS as moving basis functions, rendering extremely stable the formerly highly unstable method. We round out this part of the theory section by taking the chance to detail the route from the full variational principle to Semiclassics (Sec. 3.4), highlighting further attempts to resolve the convergence issue of CS. Furthermore, we address the so-called Davydov-Ansatz which generalizes the Ansatz (3.5) by orthogonal basis expansion for systems
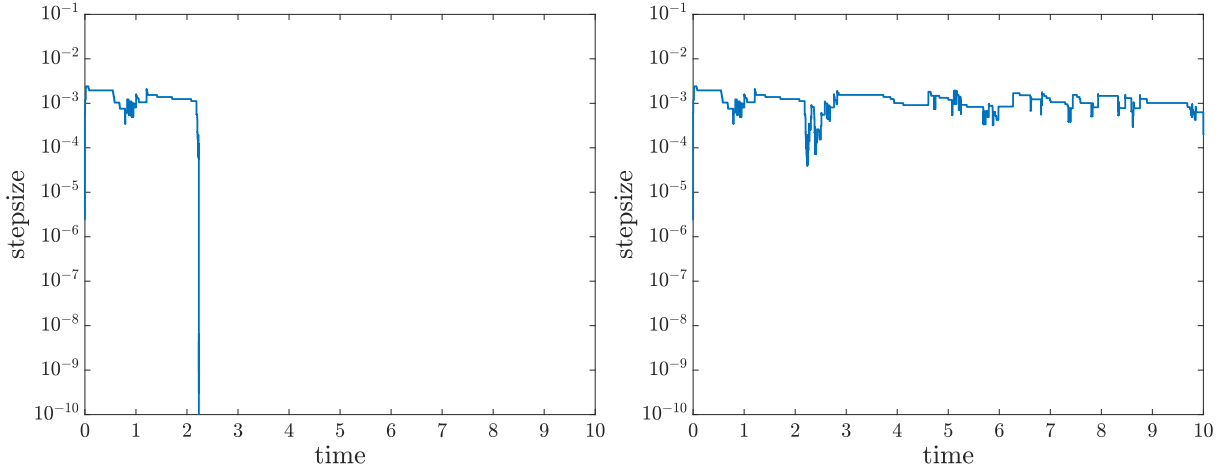
Figure 3.1.: Typical evolution of integrator steps (here for the 1D Morse potential with well depth $D = 150$ and potential width $\alpha = 0.288$ (see App. B), for multiplicity $M = 49$). In the event of two CS approaching at t_0 (here at $t_0 \approx 2.2$), the integrator steps decrease significantly, rendering impossible a further proceeding of the integrator (left panel). With apoptosis implemented (right panel), the integrator steps also decrease at t_0, but the integrator soon recovers, allowing for continuation of the propagation.

of finite Hilbert space dimension in open quantum system settings (see Sec. 3.6). Especially it will be exemplified how to apply the Davydov-Ansatz to cases of nonzero temperature.

3.4. The route to Semiclassics

Being aware of the issues related to the fully variational vMCG method and the lack of these issues in semiclassical methods due to the fact that classical trajectories never intersect (see below), quite some effort has been invested in order to find a middle course combining the advantages of both. For the sake of highlighting these courses, we reproduce here the route from the vMCG to the semiclassical Herman-Kluk (HK) method.

For the simplicity of notation, the case $N = 1$ is considered in this section. Generalization to $N > 1$ is straightforward. Without loss of generality we assume that the Hamilton operator of our system of interest is in normal-ordered form,

$$\hat{\mathcal{H}} = H(\hat{a}^\dagger, \hat{a}), \tag{3.40}$$

where all powers of $\hat{a}^\dagger$ precede all powers of $\hat{a}$. With (2.48) it is immediate that the matrix elements of the Hamiltonian then read

$$\langle \alpha_l | \hat{\mathcal{H}} | \alpha_k \rangle = H(\alpha_l^*, \alpha_k) \langle \alpha_l | \alpha_k \rangle. \tag{3.41}$$

For a normally ordered Hamiltonian (3.40),

$$\left[\hat{a}, \hat{\mathcal{H}}\right] = \frac{\partial \hat{\mathcal{H}}}{\partial \hat{a}^\dagger},$$

(3.42)

where also the left-hand side is normally ordered. This can most easily be argued by induction, by letting $\hat{\mathcal{H}} = \left(\hat{a}^\dagger\right)^n$ without loss of generality. Consequently the system of differential equations (3.24,3.25) reads

$$i\sum_{k=1}^{M} \left[X_k + A_k \dot{\alpha}_k \alpha_l^*\right] \langle \alpha_l | \alpha_k \rangle = \sum_{k=1}^{M} A_k H\left(\alpha_l^*, \alpha_k\right) \langle \alpha_l | \alpha_k \rangle,$$

(3.43)

$$iA_l^* \sum_{k=1}^{M} \left[\alpha_k X_k + A_k \left(1 + \alpha_k \alpha_l^*\right) \dot{\alpha}_k\right] \langle \alpha_l | \alpha_k \rangle = A_l^* \sum_{k=1}^{M} A_k \left[H\left(\alpha_l^*, \alpha_k\right) \alpha_k + \frac{\partial H\left(\alpha_l^*, \alpha_k\right)}{\partial \alpha_l^*}\right] \langle \alpha_l | \alpha_k \rangle.$$

(3.44)

The authors of [113] have noted that in the case of multiplicity $M = 1$, Eq. (3.44) with the help of Eq. (3.43) reduces to

$$i\dot{\alpha} = \frac{\partial H(\alpha^*, \alpha)}{\partial \alpha^*},$$

(3.45)

i.e. a purely classical equation of motion for the coherent state parameter. Nevertheless Eq. (3.45) may differ from classical Hamiltons equations even in the case when the potential has a classical analog. This is shown exemplary in App. B for the 1D Morse potential.

Different authors have utilized the idea of using equation (3.45) (see, e.g. [114, 115]). One possible approximation on the route to semiclassics is to propagate all the coherent state parameters $\alpha_k(t)$ according to the classical equation, but to keep the fully variational equations of motion for the coefficients $A_k(t)$. The corresponding method, the coupled coherent state method (CCS), was first proposed in [116, 117]. Propagating the CS on classical trajectories prevents any issue related to CS coming too close (see Sec. 3.3.2): in Hamilton-type systems of differential equations, trajectories can never cross since this would contradict the uniqueness of the solution (see e.g. [118]). This, however, comes at the price of leaving the full variational realm. While the variational principle ensures that increasing the multiplicity M increases the quality of the approximation towards the exact result, no such convergence is ensured in the CCS method. Especially it turns out that in numerical applications one has to start with a finite swarm of CS localized in a physically relevant region of phase space initially. Because their centers move classically, there are still situations (e.g. tunneling) in which the CS will not reach relevant regions at later stages.

Further ideas have emerged in the periphery of CCS. For instance, propagating random grids of CS guided by Ehrenfest trajectories [119], locally coupled CS [120], propagating the CS along Bohmian trajectories [121] etc. Also static grids of CS have been used. This either requires a priori knowledge about the wave function's support during propagation, or a highly dense and vastly extended grid. Both is not possible in high dimensional problems. Also hybrid methods have emerged where the

CS are to be propagated fully quantum mechanically, but as soon as two CS come close they are propagated according to the classical equation (3.45), see e.g. [122].

Even further away from the full variational method are semiclassical methods. They rest upon the fact that classical trajectories can never intersect (see above) and Liouville's theorem of conservation of phase-space volume [123]. From these one infers that the points α_t, propagated classically from a set of initial points α_0, cover the whole phase space if the initial ones do so. Consequently the corresponding CS $|\alpha_t\rangle$ are overcomplete,

$$1 = \frac{1}{\pi} \int \mathrm{d}\alpha_t \ |\alpha_t\rangle \langle\alpha_t| . \tag{3.46}$$

In order to derive the semiclassical Herman-Kluk (HK) propagator [87–89], one writes the wavefunction by insertion of the closure relations (2.26) and (3.46) as

$$|\Psi(t)\rangle = \int \mathrm{d}\alpha_0 \ \int \mathrm{d}\alpha_t \ |\alpha_t\rangle \langle\alpha_t| \exp\left[-\frac{\mathrm{i}}{\hbar}\hat{\mathcal{H}}t\right] |\alpha_0\rangle \langle\alpha_0| . \tag{3.47}$$

The authors of [124] have shown that replacing the coherent state matrix element of the propagator with its semiclassical approximation, and performing the α_t integral with stationary phase approximation, the HK propagator can be obtained. Resting upon the same foundation, alternative routes to the HK propagator have also been proposed (see e.g. [90, 91]) along with a detailed analysis of approximations necessary in order to obtain it ([125]). In the HK-method all the dynamical input that enters the final expression is local, classical information: the classical trajectories 'do not talk to each other'. This means that, in contrast to the CCS method, not only the trajectories but also the coefficients in the CS expansion are evolving independently from each other. The fact that only uncoupled ordinary differential equations have to be solved in the HK case is a big advantage numerically. This, however, comes at the price that the stability information can increase exponentially in chaotic systems and therefore a lot of trajectories (CS) are usually needed for convergence [126].

While application of the variational principle ensures that increasing the multiplicity M increases the quality of the approximation towards the exact result, no such fundamental mechanism is at hand in the CCS and HK methods. In the CCS method it is just known that the method is exact *in the continuum limit*: if each point α_0 in phase space would be propagated, then the result was exact. Although interesting attempts to solve for these issues exist [127], usually many trajectories have to be propagated which do not to contribute to the result at all.

Along with coherent states (termed frozen Gaussians in this context), also squeezed states (termed thawed Gaussians) have been applied (see, e.g.,[37]). While the possibility for the CS to squeeze is expected to decrease the number of basis functions required for convergence, it renders the corresponding method even more unstable in the full variational case. Clearly, the additional freedom also introduces more uncertainty in the case of vanishing coefficients as well as close to convergence. Interestingly it has also proven not to work satisfactorily in semiclassical methods [128].

Finishing the detour to semiclassical methods we return to the main route of the vMCG method. We shall detail how to apply the concepts of the vMCG method in more general contexts.

3.5. Variational principle with DNS and squeezed states

Now that we have detoured to semiclassical methods we come back to the main road and the vMCG method. Bosonic many body problems are central in solid state and condensed matter physics. Although solid state physics Hamiltonians as the Bose-Hubbard model [129–132] are still challenging frameworks, they appear ideal for treatment with CS. We will outline, however, the limitations of the vMCG method with respect to these applications. The vMCG formalism has been applied to this class of problems if the initial state is a CS [133]. But initial conditions often include single number state distributions on lattices, e.g. each even lattice site shall be occupied etc [131]. In order to apply the vMCG method to these problems, an efficient representation of Fock number states in terms of multi mode CS would be nice to be at hand. Unfortunately, the standard representation, obtained by insertion of the completeness relation (2.26) for CS,

$$|n\rangle = \frac{1}{\pi} \int\limits_{\mathbb{C}} \mathrm{d}\alpha \, \langle\alpha|n\rangle \, |\alpha\rangle \qquad (3.48)$$

yields a distribution $|\langle\alpha|n\rangle| = \exp\left[-|\alpha|^2/2\right]\frac{|\alpha|^n}{\sqrt{n!}}$ in the complex plane which is rotationally symmetric, not allowing for efficient Monte-Carlo integration for multiple modes. Although the two-dimensional integral in (3.48) can be traded for a one-dimensional integral (see [36]), this does not resolve for the issue of rotational symmetry. The impossibility of an efficient representation of number states in terms of CS is rooted in the CS being highly localized while the number states are not (see Sec. 2.2).

An expedient is offered by utilization of displaced number states (DNS), introduced in Sec. 2.6. For the simplicity of notation we restrict the following considerations to the single mode case $N = 1$. Generalization to multiple modes is straightforward. Due to the closure relation (2.87), an Ansatz for the wave function in terms of DNS reads

$$|\Psi_{\mathrm{DNS}}^{\mathrm{M}}(t)\rangle = \sum_{k=1}^{M} A_k(t) \, |\alpha_k(t), n\rangle \,, \qquad (3.49)$$

with time dependent complex coefficients and time dependent complex displacements α_k, which one may hope to converge to the exact result as $M \to \infty$. On the one hand, the Ansatz (3.49) circumvents the problem of sampling for the initial value representation since $|\Psi(0)\rangle = |n\rangle$ for $A_k(0) = \delta_{k,1}, \alpha_1(0) = 0$. On the other, we shall outline subsequently that the equations of motion obtained for the Ansatz

in terms of DNS, are not well behaved. The variation reads

$$\langle\delta\Psi_{\mathrm{DNS}}^{\mathrm{M}}| = \sum_{l=1}^{M} \langle n| \left\{\delta A_l^* + A_l^* \left[\hat{D}_{\alpha_l}^\dagger \left(-\frac{1}{2}\alpha_l + \hat{a}\right)\delta\alpha_l^* + \left(-\frac{1}{2}\alpha_l^* - \hat{a}^\dagger\right)\hat{D}_{\alpha_l}^\dagger\delta\alpha_l\right]\right\}, \tag{3.50}$$

and thus, by assuming the variations to be mutually independent, *three* sets of equations emerge,

$$\langle\alpha_l, n|\, \mathrm{i}\partial_t - \hat{\mathcal{H}}\, |\Psi_{\mathrm{DNS}}^{\mathrm{M}}\rangle = 0, \tag{3.51}$$

$$A_l^* \langle\alpha_l, n|\, \hat{a}\left(\mathrm{i}\partial_t - \hat{\mathcal{H}}\right)|\Psi_{\mathrm{DNS}}^{\mathrm{M}}\rangle = 0, \tag{3.52}$$

$$A_l^* \langle n|\, \hat{a}^\dagger \hat{D}_{\alpha_l}^\dagger \left(\mathrm{i}\partial_t - \hat{\mathcal{H}}\right)|\Psi_{\mathrm{DNS}}^{\mathrm{M}}\rangle = 0, \tag{3.53}$$

where the first equations were used to simplify the second and third ones. Although equations of motion have been derived for DNS in the literature [50, 134, 135], they focused on derivation of the equations of motion by the time-dependent variational principle, overseeing that variation with respect to the parameters *and* their complex conjugates have to be carried out. Consequently, the third equation (3.53) has not been taken into account there. The set of equations reduces to the system (3.13,3.14) in the case of $n = 0$. Nevertheless, system (3.51-3.53) overdetermines the displacements and coefficients, and in no obvious way is one of them a combination of two others. The reason is deeply rooted in the variational principle: due to the appearance of the complex conjugates of the displacements in combination with the annihilation operator in the wave function (3.49), it can not be parametrized such that it fulfills the Cauchy-Riemann equations (2.96). This is in contrast to the case $n = 0$, for which we have shown in Sec. 3.1 that it can be parametrized such that it fulfills the Cauchy-Riemann equations. Thus we conclude that for the Ansatz (3.49) the three variational principles are not equivalent, see Sec. 2.7. Furthermore, neither in resorting only to the real part nor to the imaginary part does the set of equations (3.51-3.53) offer a way out, since in any case the resulting number of equations is not appropriate to uniquely determine the complex coefficients and displacements. Summarizing, the equations of motion for the parameters in the Ansatz (3.49) for $n \neq 0$ can not be derived from the variational principle in a consistent way, and thus the Ansatz is in general not suited to account for dynamics in high-dimensional solid state physics problems. It is especially not possible to circumvent the curse of dimensionality in the sampling of the integral (3.48) by derivation of generalized equations of motion from the Ansatz (3.49).

In the case of multiplicity $M = 1$ and a single environmental mode, squeezed states introduced in Sec. 2.5 have been utilized in [37] in order to do real-time propagation of the Quantum Rabi model (see also Sec. 4.3.2.1). As can be expected from the considerations of Sec. 2.5 and be seen in [37], the formalism is highly complicated. It has to remain an open question whether the results of [37] are generalizable straightforwardly to $M > 1$ and multiple modes $N > 1$ if the squeezing parameters is allowed to be complex. Unpublished results from the Burghardt community exist which claim to have generalized the squeezed states (so-called thawed Gaussians) to cases where $M, N > 1$ for real squeezing parameters. In the light of the above considerations it is doubtful that the variational

principle formalism can be applied such that the issue of a third equation emerging for the DNS can be prevented for the squeezed states. In particular, the representation (2.75) seems appropriate for this purpose, but it does not allow to straightforwardly calculate commutation relations with the creation and annihilation operators. Research in this direction is in progress in our group. However, we refrain from implementation of both the DNS and the squeezed states subsequently but utilize the CS as basis functions. We outline in the next section how to apply the latter in a more general context.

3.6. The multi Davydov-Ansatz

It is obviously a matter of the underlying system whether the vMCG Ansatz (3.5) is a promising parametrization of the wave function. While, due to their overcompleteness, in principle any wave function may be expressed in terms of CS, the vMCG Ansatz is particularly promising for bipartite systems one of whose parts' dynamics is *exactly* solvable by coherent states. As we have seen in Sec. 2.2, coherent states are the exact solution of the TDSE for the quantum harmonic oscillator. Thus, we will mainly aim at the investigation of *open quantum systems* which are composed of a system of interest part (the 'system') and a part of uncoupled harmonic oscillators (the 'environment'). Then the two components being coupled renders the overall system dynamics non-trivial.

Although the vMCG Ansatz is promising for the environment-component, this does not have to be the case for the system-part. Especially in cases where the latter's Hilbert space has finite dimension N_S, expansion in terms of a finite orthonormal basis $\{|\phi_n\rangle \,|\, n = 1, \ldots, N_S\}$ appears preferable.

Thus, expanding the environment in the spirit of the vMCG Ansatz and the system in terms of a finite orthonormal basis, two straightforward generalizations of the vMCG Ansatz are conceivable. Firstly, by pairing each coherent state with a general system wave function, the Ansatz

$$|\Psi_{\mathrm{D2}}^{\mathrm{M}}(t)\rangle = \sum_{k=1}^{M} \left(\sum_{n=1}^{N_S} A_{kn}(t) \,|\phi_n\rangle \right) |\boldsymbol{\alpha}_k(t)\rangle \tag{3.54}$$

arises. We shall term this the multi (Davydov) D2-Ansatz [27], correspondingly also termed 'single-set' [95].

Secondly, by pairing each coherent state with one system basis function, the Ansatz

$$|\Psi_{\mathrm{D1}}^{\mathrm{M}}(t)\rangle = \sum_{k=1}^{M} \sum_{n=1}^{N_S} A_{kn}(t) \,|\phi_n\rangle \,|\boldsymbol{\alpha}_{kn}(t)\rangle \tag{3.55}$$

emerges. We shall term this the multi (Davydov) D1-Ansatz, correspondingly termed 'multi-set'.

The application of an orthonormal system basis allows to straightforwardly generalize the equations of motion (3.24, 3.25) as well as the considerations of Secs. 3.1 - 3.3 to the present setting. In particular,

the general equations (3.13, 3.14) are replaced by

$$\langle\phi_n|\,\langle\boldsymbol{\alpha}_l|\,\mathrm{i}\partial_t - \hat{\mathcal{H}}\,|\Psi_{\mathrm{D2}}^{\mathrm{M}}\rangle = 0, \tag{3.56}$$

$$\sum_{n=1}^{N_S} A_{ln}^* \,\langle\phi_n|\,\langle\boldsymbol{\alpha}_l|\,\hat{a}_j\left(\mathrm{i}\partial_t - \hat{\mathcal{H}}\right)|\Psi_{\mathrm{D2}}^{\mathrm{M}}\rangle = 0 \tag{3.57}$$

for the multi D2-Ansatz, and by

$$\langle\phi_n|\,\langle\boldsymbol{\alpha}_{ln}|\,\mathrm{i}\partial_t - \hat{\mathcal{H}}\,|\Psi_{\mathrm{D1}}^{\mathrm{M}}\rangle = 0, \tag{3.58}$$

$$A_{ln}^* \,\langle\phi_n|\,\langle\boldsymbol{\alpha}_{ln}|\,\hat{a}_j\left(\mathrm{i}\partial_t - \hat{\mathcal{H}}\right)|\Psi_{\mathrm{D2}}^{\mathrm{M}}\rangle = 0 \tag{3.59}$$

for the multi D1-Ansatz. A detailed derivation of the equations of motion for both the multi D1 and the multi D2-Ansatz is gathered in App. C, and an implementable form in terms of matrix operations is derived in App. C.1 for the D2 and in App. C.2 for the D1-Ansatz.

Since the displacements carry the additional index of the sum over the system basis states, the multi D1-Ansatz is considered to be more flexible than the multi D2-Ansatz [95, 136]. As all our calculations show (see Sec. 4.3.2.2), this is actually not the case. Rather is the multi D1-Ansatz disadvantageous compared to the multi D2-Ansatz in certain settings, to be detailed readily.

The number of parameters in the multi D2-Ansatz of multiplicity M is $M \cdot N_S + M \cdot N$, while in the multi D1-Ansatz of multiplicity M it is $M \cdot N_S \cdot (N + 1)$. Here, N is the number of environmental modes. Consequently, a multi D1-Ansatz of multiplicity M has as many free parameters as a multi D2-Ansatz of multiplicity $M \cdot N_S$. Subsequent calculations (see Sec. 4.3.2.2) will show that the number of parameters needed if the multi D2-Ansatz is employed is never smaller than the number of parameters needed for the multi D1-Ansatz.

At a first glance, this seems contradictory since obviously the multi D2-Ansatz (3.54) is less general than the multi D1-Ansatz: the latter reduces to the former by requiring

$$\boldsymbol{\alpha}_{nk} = \boldsymbol{\alpha}_k. \tag{3.60}$$

Similarly, however, one may argue that the D1-Ansatz can be derived from the D2-Ansatz by requiring

$$A_{nk} = \delta_{nk}, \tag{3.61}$$

provided $M = n \cdot N_S$ is a multiple of N_S.

A first hint to understand the difference between the multi D1 and D2-Ansatz is to examine their respective behavior in the context of the issue of vanishing coefficients, discussed in Sec. 3.3.1. Assume that the dynamics is such that one basis state of the orthogonal system basis, say $|\phi_1\rangle$, is highly stable for a long time $t \in [0, T]$,

$$\langle\phi_j|\Psi(t)\rangle = 0, \qquad j = 2, \ldots, N_S, \quad t \in [0, T]. \tag{3.62}$$

For instance, the Landau Zener system, investigated in Sec. 5.3, constitutes such a system in which one of the standard basis functions is long-time stable. Then in the D1-Ansatz $A_{kj}(t) = 0$ for all $k = 1, \ldots, M$, $j = 2, \ldots, N_S$, $t \in [0, T]$, rendering highly singular the coefficient matrix since all corresponding displacements are arbitrary. As can be seen by comparing Eqs. (3.57) and (3.59), this is not the case for the D2-Ansatz.

A second hint is given by the natural bipartiteness of the open system. An arbitrary wave function $|\Psi\rangle$ in the corresponding Hilbert space can be written as

$$|\Psi\rangle = \int \mathrm{d}\boldsymbol{\alpha} \sum_{n=1}^{N_S} A_{\boldsymbol{\alpha},n} |\phi_n\rangle |\boldsymbol{\alpha}\rangle. \tag{3.63}$$

Consequently, we may expect the D2-Ansatz (3.54) to converge to the exact result as $M \to \infty$. Since the D1-Ansatz reduces to the D2-Ansatz given that (3.60), we may also expect the D1-Ansatz to converge to the exact result, but only provided that (3.60) holds. With respect to the system's bipartiteness, the D2-Ansatz appears much more natural.

Putting it again differently: while in the D2-Ansatz the CS $|\boldsymbol{\alpha}_k\rangle$ is optimized under the premise that the corresponding system part is arbitrary, in the D1-Ansatz it is optimized under the premise that its system compagnon is a certain given basis state. It is hence not clear a priori (and will be examined in Sec. 4.3.2.2) whether the quality of the D1-Ansatz depends on the choice of the system basis. On the contrary, from the Ansatz (3.54) one readily infers that the quality of the D2-Ansatz does not depend on the choice of the system basis.

In order to account for the dynamics of open quantum systems we will, according to the previous considerations, always apply the multi D2-Ansatz, while the D1-Ansatz is merely used for comparison in Sec. 4.3.2.1. However, a natural requirement to an open quantum system is the environment to be in thermodynamic equilibrium with an energy reservoir at temperature T. We shall outline in the next section how to treat the nonzero temperature case with the multi D2-Ansatz.

3.7. The multi Davydov-Ansatz at non-zero temperature

In the context of the environment being in thermodynamic equilibrium with an energy reservoir at temperature T it is also termed a (heat-) bath. In order to investigate systems where the bath's temperature is finite (i.e. not zero), we aim at generalization of the multi D2-Ansatz to these setups. The state of a system at temperature T is in general a statistical ensemble of pure states and is thus described appropriately by a density operator $\hat{\rho}$, the time-evolution of which is governed by the Liouville-von Neumann equation

$$\mathrm{i}\hbar \partial_t \hat{\rho} = \left[\hat{\mathcal{H}}, \hat{\rho}\right]. \tag{3.64}$$

Here, $\hat{\mathcal{H}}$ is the possibly time-dependent full system plus environment Hamiltonian. Intending to tackle Eq. (3.64) on the wave function level, we have investigated different approaches to generalize the multi

D2-Ansatz formalism to baths at finite temperature [50]. It turns out, however, that for numerical purposes finite temperature is best incorporated by a stochastic initial value sampling [137].

The total state at finite temperature may be written as

$$\hat{\rho}(t) = \hat{U}\rho(0)\hat{U}^\dagger, \tag{3.65}$$

where $\hat{U}$ is the time evolution operator corresponding to the full Hamiltonian,

$$\hat{U} = \mathcal{T}\exp\left[-\frac{\mathrm{i}}{\hbar}\int\limits_0^t \mathrm{d}t'\,\hat{\mathcal{H}}(t')\right]. \tag{3.66}$$

Here, we have introduced the time-ordering operator $\mathcal{T}$ [126].

We assume that the initial state is factorized, $\hat{\rho}(0) = \hat{\rho}_{\mathrm{sys}}(0) \otimes \hat{\rho}_{\mathrm{bath}}(0)$. Since the bath is comprised of harmonic oscillators assumed to be at temperature T initially, the bath part of the initial density is given by the multi-mode analog of the thermal state (2.56), $\hat{\rho}_{\mathrm{bath}}(0) = \hat{\rho}_\beta$, with β being the inverse temperature (2.54).

In order to express the thermal state in terms of multi-mode CS, we may analogously to (2.60) use the multi-mode analog of the (Glauber-Sudarshan) P-representation introduced in Sec. 2.4,

$$\hat{\rho}_\beta = \int\limits_{\mathbb{C}} \mathrm{d}\boldsymbol{\alpha}\, P_\beta\left(\boldsymbol{\alpha}, \boldsymbol{\alpha}^*\right) |\boldsymbol{\alpha}\rangle\langle\boldsymbol{\alpha}|. \tag{3.67}$$

Here, analogously to (2.68) the multi-mode P-function is given by

$$P_\beta\left(\boldsymbol{\alpha}, \boldsymbol{\alpha}^*\right) = \prod_n \frac{\mathrm{e}^{\beta\omega_n} - 1}{\pi}\exp\left[-|\alpha_n|^2\left(\mathrm{e}^{\beta\omega_n} - 1\right)\right], \tag{3.68}$$

which is a multidimensional complex Gaussian distribution.

It is the decomposition (3.67) of the initial thermal state in terms of coherent states along with the Gaussian nature of the P-function (3.68) which facilitate application of Monte-Carlo sampling of the integral, and thus propagation on the wave function level even in cases where the bath's temperature is finite. If the initial system state is a pure state, reading

$$\hat{\rho}_{\mathrm{sys}}(0) = |\Psi_{\mathrm{sys}}(0)\rangle\langle\Psi_{\mathrm{sys}}(0)|, \tag{3.69}$$

then the total state takes the form

$$\hat{\rho}(t) = \mathcal{M}_{\boldsymbol{\alpha}}\left(\hat{U}|\Psi_{\mathrm{sys}}(0)\rangle\langle\Psi_{\mathrm{sys}}(0)| \otimes |\boldsymbol{\alpha}\rangle\langle\boldsymbol{\alpha}|\hat{U}^\dagger\right) = \mathcal{M}_{\boldsymbol{\alpha}}\left(|\Psi_{\mathrm{D2}}^{\mathrm{M}}(\boldsymbol{\alpha}, t)\rangle\langle\Psi_{\mathrm{D2}}^{\mathrm{M}}(\boldsymbol{\alpha}, t)|\right) \tag{3.70}$$

of a stochastic average $\mathcal{M}_{\boldsymbol{\alpha}}$ over independently sampled complex valued Gaussian random variables $\boldsymbol{\alpha}$ with zero mean and variance

$$\sigma_n^2 = \frac{1}{2}(e^{\beta\omega_n} - 1)^{-1}. \tag{3.71}$$

In (3.70) we have assumed that the propagation $\hat{U}\,|\Psi_{\text{sys}}(0)\rangle\,|\boldsymbol{\alpha}\rangle$ of the whole state, with the bath being initially in the stochastic state $|\boldsymbol{\alpha}\rangle$, can be identified with the multi D2 state $|\Psi_{\text{D2}}^{\text{M}}(\boldsymbol{\alpha}, t)\rangle$ subject to the same initial condition. This is reasonable if each realization is ensured to be converged with respect to the multiplicity M, i.e. to the number of coherent states.

In particular, the expectation value of an operator $\hat{O}_{\text{S}}$ acting only on the system Hilbert space is given by

$$\langle\hat{O}_{\text{S}}\rangle = \mathcal{M}_{\boldsymbol{\alpha}}\,\langle\Psi_{\text{D2}}^{\text{M}}(\boldsymbol{\alpha}, t)|\,\hat{O}_{\text{S}}\,|\Psi_{\text{D2}}^{\text{M}}(\boldsymbol{\alpha}, t)\rangle\,, \tag{3.72}$$

where we have used the specific form of the multi D2-Ansatz (3.54). Thus, utilization of the P-function (3.68) allows to randomly sample from the Gaussian distribution and to independently propagate each sample by the multi D2-Ansatz. The total state (3.70) as well as expectation values (3.72) are then given by an average over these samples.

In this chapter we have investigated general aspects of the real-time propagation in terms of the vMCG Ansatz (3.5) along with the application of the variational principle. We have outlined how to carefully regularize the ρ-matrix in the case of vanishing coefficients, and apoptosis in the case of coherent states approaching. As completion of the discourse on previous attempts to circumvent these issues, we have rounded out this part by an excursion to semiclassical methods. In order to tackle open quantum system settings we have highlighted how to generalize the vMCG Ansatz to the multi D1 and D2-Ansatz. Finally we have theoretically argued that the multi D2-Ansatz should be preferred over the multi D1-Ansatz and shown how to treat nonzero bath setups by the multi D2-Ansatz on the wave function level.

Before we come to more complex problems we shall firstly apply the method to the Spin-Boson model, assumed to be the ideal test-bed due to its intricacy in combination with the wealth of available results.

4. Open Quantum Systems

Quantum mechanical systems must be regarded as open systems, because, on the one hand, any empirical test of the statistical predictions on a quantum system requires one to couple it to a macroscopic measurement device. On the other hand, any realistic system is subject to a coupling to environmental degrees of freedom which in turn act back on the system.

The quantum-mechanical approach to description of dissipative systems is via coupling of the system to an environment. While the whole framework, consisting of system and environment, then will obey the fundamental rule of energy conservation, the system of interest may loose energy to the environment. But, due to the Poincaré recurrence theorem (see e.g. [138]), also the reversed process may occur within finite time. Hence, in order to describe 'proper' dissipation, the environment must be large enough such that the time it takes for energy to flow back from the environment into the system is large or 'practically infinity'. But also on the contrary, thermal and quantum fluctuations in the environment cause fluctuations in the system, which results in Brownian motion and may also induce further effects in the system (see also below). Especially, a quantum system which becomes entangled with an environment exhibits decoherence. This is of particular interest in the field of quantum information, where phase coherence between two qubit states is used as resource [139–141]. No real-world system is completely isolated from its environment, making dissipation, fluctuation and decoherence omnipresent in physics and chemistry. In particular this is quantified by the fluctuation-dissipation theorem [142], which relates the fluctuations in a system that obeys detailed balance with the response of the system to external perturbations [143].

In most applications, the environment is uncontrollable, its dynamics is not tractable and/or of no interest. Reduced density operator approaches thus aim for an effective description of the reduced dynamics [143–161] in terms of master equations. In contrast to the whole framework consisting of system and environment, the time-evolution of the reduced density operator is not unitary in general. Furthermore, the derivation and implementation of such master equations usually requires several assumptions as e.g. Markovianity (no memory), rendering the reduced dynamics valid only for a certain parameter regime. Alternatively, a wealth of methods has been developed to compute the dynamics of the composite system including environmental degrees of freedom [59, 60, 127, 134, 162–169]. Unlike effective reduced evolution approaches, they do not aim at the derivation of an equation of motion for the reduced density matrix, but rather are based on an explicit calculation of the system and bath dynamics.

There is a growing number of open systems where the environment cannot adequately be described as memoryless [170]. These include micromechanical resonators [171], quantum dots [172, 173], superconducting qubits [174], and single photon sources needed for quantum communication [175]. Furthermore, structured environments are ubiquitous in problems involving the strong interplay of vibrational and electronic states, e.g. natural photosynthetic systems [176], semiconductor quantum dots [177–179], non-adiabatic processes in physical chemistry [180] and non-equilibrium energy trans-

port in molecular systems [181].

The open system's environment may under mild assumptions be taken as a set of mutually uncoupled oscillators, each of which couples via its position to the system [182]. Under the further assumption that the system couples bilinearly to the environmental oscillators' positions, the coupling between the system and the environment can be quantified in terms of a continuous spectral density (SD) $J(\omega)$ defined for all frequencies $\omega \in [0, \infty]$. Its functional form may then be chosen such that in the classical limit a Langevin equation for the system is recovered. For a given set of environmental oscillators quantified by their respective frequencies ω_n, the spectral density specifies the bilinear coupling λ_n of the oscillator of frequency ω_n to the system. We shall then aim at the investigation of the system dynamics in the *continuum limit*, i.e. for all frequencies $\omega \in [0, \infty]$ present in the environment.

The Spin-Boson model, composed of a two-level system and an environment, constitutes the simplest non-trivial open quantum system. Despite its simplicity it is numerically demanding and shows a rich variety of interesting physical phenomena. In this chapter we use the multi Davydov method to solve the Spin-Boson model numerically exactly for both, a zero and non-zero temperature initial bath state. After introducing the basics of open quantum systems in Sec. 4.1, we will in Sec. 4.2 perform a classical limit of the latter, demonstrating that in this limit classical dissipation emerges. Subsequently we shall firstly examine in detail the effect of the regularizations outlined in Chaps. 3.3.1 and 3.3.2 for a given discretization of the SD. Once we have shown that with these regularizations the multi Davydov method is suited to exactly reproduce the Spin-Boson dynamics, we shall investigate secondly the problem of finding a discretization to the SD which results in a good approximation of the dynamics, especially for a small number of bath modes. We utilize the windowed Fourier transform (WFT), a useful representation of bath correlations which indicates a priori the quality of a given discretization. The results, found for the Spin-Boson model, have the potential to judge the quality of approximations with respect to the exact dynamics also for other systems. This might be useful for many methods other than the ones presented here, that are based on a discretization of the bath. With the goal of further reducing the number of environmental oscillators required to reproduce the continuum limit dynamics, we will investigate in detail the dynamics of the environmental oscillators. We will find that special care has to be taken in the case of polarized initial conditions and for nonzero temperature, in the sub-ohmic case of the Spin-Boson model. Furthermore, we will thirdly utilize the effective mode representation (EMR), an alternative representation of the environment in terms of a chain of effective modes.

The Spin-Boson model undergoes a quantum phase transition from a localized to a delocalized regime with the coupling strength between system and environment being the transition's order parameter. While the value of the critical coupling can be calculated analytically in some settings, we will finally numerically determine the precise value of the critical coupling in a case where no such analytical value is known. Units in which $\hbar = 1$ will be used throughout.

We shall subsequently give a general introduction to open quantum systems. We will in particular motivate the physical relevance of these systems by drawing contact with the classical limit in which many quantities arise naturally. The following sections mainly serve as a proof of concept for the

methodology introduced in Sec. 3.1. Firstly, for the Quantum Rabi model, the results obtained from the multi Davydov-Ansatz will be compared to an expansion in terms of number states. Special emphasis is on the investigation of the impact of the regularization in the case of vanishing coefficients outlined in Sec. 3.3.1. Secondly, many calculations have already been performed for the SBM and are thus at our disposal. Results obtained with the multi Davydov-Ansatz will be compared to these. Especially the apoptosis procedure outlined in Sec. 3.3.2 will be examined in detail here. It will become apparent that the two regularizations turn the method commonly considered ill-behaved into a well behaved reliable high-precision tool. While in the first parts, Secs. 4.3.1 and 4.3.2, we will work in a fixed setting, in the subsequent sections we will examine in detail the ingredients which determine this setting. In particular, we will examine different routes along which the numerical effort may be reduced. Firstly, we will investigate different discretizations of the frequency axis in Sec. 4.4. Furthermore, in Sec. 4.5 we shall outline how to circumvent an oversampling of small frequencies for polarized initial conditions and non-zero temperature in the sub-ohmic case. Thirdly and finally, we will transfer the SBM into a linear chain of effective modes as outlined in Sec. 4.6 and investigate the resulting dynamics. We shall see that, for the SBM, the effective representation does not yield substantial advantage.

4.1. System-Bath Hamiltonian

An open quantum system introduces a natural bipartiteness of the whole framework consisting of system and environment. In order to account for this bipartiteness we denote by $\hat{\mathcal{H}}_\mathrm{S}$ the Hamiltonian of the system part and by $\hat{\mathcal{H}}_\mathrm{B}$ the Hamiltonian of the environmental (bath-) part. It is natural to require system and environment to interact with each other, rendering non-trivial the overall system-bath dynamics. Thus, taking into account interactions between the two parts, the total Hamiltonian reads

$$\hat{\mathcal{H}} = \hat{\mathcal{H}}_\mathrm{S} + \hat{\mathcal{H}}_\mathrm{B} + \hat{\mathcal{H}}_\mathrm{int}. \tag{4.1}$$

We assume the environment to be modelled by a set of N mutually uncoupled harmonic oscillators of frequencies ω_n, $n = 1, \ldots, N$. The bath Hamiltonian in second quantized form is then given by

$$\hat{\mathcal{H}}_\mathrm{B} = \sum_{n=1}^N \omega_n \hat{a}_n^\dagger \hat{a}_n, \tag{4.2}$$

where $\hat{a}_n^\dagger$ and $\hat{a}_n$ are creation and annihilation operators of the n-th mode. We have neglected the oscillators' ground state energies (2.6) since they only contribute a constant term to the Hamiltonian, which does thus only contribute an overall phase to the system dynamics. Furthermore, the mass m_n of the n-th oscillator is included according to (2.3) into the definition of the creation and annihilation operators.

Proceeding according to [182] we furthermore require the system to couple linearly to the positions

of the bath oscillators. Then the system-bath interaction Hamiltonian reads

$$\hat{\mathcal{H}}_{\mathrm{int}} = \hat{L} \sum_{n=1}^{N} \lambda_n \left(\hat{a}_n^\dagger + \hat{a}_n \right), \tag{4.3}$$

where $\hat{L}$ is the system coupling operator,

$$\hat{\mathcal{H}}_{\mathrm{I}} = \sum_{n=1}^{N} \lambda_n \left(\hat{a}_n^\dagger + \hat{a}_n \right) \tag{4.4}$$

is the bath coupling operator, and λ_n specifies the coupling strength of the n-th mode to the system. In order for the full Hamiltonian to be Hermitian, the coupling operator is assumed to be Hermitian,

$$\hat{L} = \hat{L}^\dagger. \tag{4.5}$$

The Hamiltonian we will be working on here thus takes the general Caldeira-Leggett form [182]

$$\hat{\mathcal{H}} = \hat{\mathcal{H}}_{\mathrm{s}} + \sum_{n=1}^{N} \omega_n \hat{a}_n^\dagger \hat{a}_n + \hat{L} \sum_{n=1}^{N} \lambda_n \left(\hat{a}_n^\dagger + \hat{a}_n \right). \tag{4.6}$$

The couplings λ_n can be quantified in terms of a continuous SD $J(\omega)$, which can be chosen such that in the classical limit an equation of Langevin type for the system emerges (see Sec. 4.2) and is an input parameter of the model. Then J is related to the couplings λ_n by requiring

$$J(\omega) = \pi \sum_{n=1}^{N} \lambda_n^2 \delta(\omega - \omega_n), \tag{4.7}$$

from which for a given set of frequencies $\{\omega_n \,|\, n = 1, \ldots, N\}$ the couplings λ_n can be calculated by integration of (4.7) over a small interval $[\omega_n - \delta, \omega_n + \delta]$ containing only the frequency ω_n,

$$\lambda_n^2 = \frac{1}{\pi} \int\limits_{\omega_n-\delta}^{\omega_n+\delta} \mathrm{d}\omega \, J(\omega). \tag{4.8}$$

Since the couplings are determined by (4.8) only up to a pre-factor of absolute value 1, we expect the model properties not to change if all couplings are multiplied by such a pre-factor.

In order to avoid ultraviolet divergences, the SD $J(\omega)$ may have *effective support* only on a finite sub-interval $[0, \Omega] \subseteq [0, \infty]$. This means that $J(\omega) > \varepsilon$ only for $\omega \in [0, \Omega]$, for a given $\varepsilon \ll 1$. Although it is in general neither possible to directly numerically calculate the system dynamics if all frequencies $\omega \in [0, \Omega]$ nor if countably many frequencies $\{\omega_n \,|\, n = 1, \ldots, \infty\} \subseteq [0, \Omega]$ are present in the environment, we shall aim at investigation of the system dynamics in the continuum limit, i.e. for all frequencies $\omega \in [0, \Omega]$ present in the environment. To this end we will propagate with the Hamiltonian (4.6), i.e. with a fixed number N of environmental modes, and then numerically check convergence

for $N \to \infty$ where the ω_n sufficiently densely cover the interval $[0, \Omega]$ in the limit $N \to \infty$.

Instead of explicit declaration of the frequencies ω_n the discretization of the frequency axis can alternatively be specified indirectly by a frequency density (FD) $\rho_{\mathrm{f}}(\omega)$. A normalized frequency density $\int_0^{\infty} \mathrm{d}\omega\, \rho_{\mathrm{f}}(\omega) = 1$ allows to divide the ω-axis into parts of equal weight with respect to the FD. For x_n chosen such that

$$\int_0^{x_n} \mathrm{d}\omega\, \rho_{\mathrm{f}}(\omega) = \frac{n}{N+1}, \qquad n = 0, \ldots, N, \tag{4.9}$$

the intervals $[x_{n-1}, x_n]$ for $n = 1 \ldots N$ have the same weight $\frac{1}{N+1}$ with respect to the FD ρ_{f}. The actual frequency for the n-th mode can in general be somewhere inside the n-th interval. Usually one fixes the position to the median with respect to the FD which results in the condition

$$\int_0^{\omega_n} \mathrm{d}\omega\, \rho_{\mathrm{f}}(\omega) = \frac{2n-1}{2(N+1)}, \qquad n = 1, \ldots, N, \tag{4.10}$$

from which by inversion the mode frequency ω_n can be calculated.

The corresponding coupling strength then follows according to (4.8), where it is ensured that only the frequency ω_n is in the interval $[x_{n-1}, x_n]$. Hence

$$\lambda_n^2 = \frac{1}{\pi} \int_{x_{n-1}}^{x_n} \mathrm{d}\omega\, J(\omega) \quad . \tag{4.11}$$

Three remarks are in place. Firstly, the factor $\frac{1}{\pi}$ originates from the defining relation of the approximation of the continuous SD given by (4.7). Secondly, it is as justified to fix the position of the frequency ω_n to the median with respect to the FD of the interval $[x_{n-1}, x_n]$ according to (4.10) as to fix it anywhere else in this interval. Especially, by fixing the frequencies as the left boundaries of the intervals, one may calculate the frequencies from

$$\int_0^{\omega_n} \mathrm{d}\omega\, \rho_{\mathrm{f}}(\omega) = \frac{n}{N+1}, \qquad n = 1, \ldots, N. \tag{4.12}$$

Thirdly, in differential form condition (4.9) reads $(x_n - x_{n-1})\rho_{\mathrm{f}}(\omega_n) = \frac{1}{N+1}$, and (4.11) then becomes $\lambda_n^2 = \frac{1}{\pi}(x_n - x_{n-1})J(\omega_n)$, leading to the couplings

$$\lambda_n^2 = \frac{J(\omega_n)}{(N+1)\pi\rho_{\mathrm{f}}(\omega_n)}, \tag{4.13}$$

frequently used in the literature[134, 163, 166, 183].

In order to better understand the role of the SD, we show in the next section that the classical limit of the Hamiltonian (4.6) yields a stochastic differential equation of Langevin type for the system degrees

of freedom. The damping kernel entering this Langevin equation is intimately related to the SD.

4.2. The road to classical dissipation

In this section we will perform a classical limit of the open quantum system (4.6) revealing that in this limit the Hamiltonian (4.6) yields a classical Langevin equation. In particular, the environmental fluctuations yield a stochastic force acting on the system degree of freedom. The SD of the system is related to and thus allows to specify the damping kernel of the Langevin equation. Furthermore, the emergence of the so-called counter term is discussed.

In order to perform the classical limit of (4.6) we consider in the following a one-dimensional system of a particle with mass $M = 1$ with position q and momentum p, moving in some (possibly time-dependent) potential $V(q, t)$. This system is described by a Hamilton operator

$$\hat{\mathcal{H}}_{\mathrm{s}} = \frac{1}{2}\hat{p}^2 + V(\hat{q}, t). \tag{4.14}$$

Under the assumption that the system-bath coupling be linear in the system coordinate (for detailed justification of this assumption, see [182]), the system coupling operator

$$\hat{L} = \hat{q}. \tag{4.15}$$

The corresponding classical Hamilton's equations of motion for the full classical Hamiltonian corresponding to (4.6) in mass weighted coordinates read

$$\ddot{q} + V'(q, t) = \sum_{n=1}^{N} c_n q_n, \tag{4.16}$$

$$\ddot{q}_n + \omega_n^2 q_n = c_n q. \tag{4.17}$$

Here, $V'(q, t)$ denotes the derivative of the potential with respect to q, and

$$c_n = \sqrt{2\omega_n}\lambda_n \tag{4.18}$$

are the coupling constants.

The inhomogeneous equations (4.17) for the bath oscillators are driven by the system displacement. These equations can formally be solved with the Green's function for the harmonic oscillator,

$$G_n(t) = \Theta(t)\frac{\sin(\omega_n t)}{\omega_n}, \tag{4.19}$$

which results in

$$q_n(t) = q_n(0)\cos(\omega_n t) + \frac{p_n(0)}{\omega_n}\sin(\omega_n t) + \frac{c_n}{\omega_n}\int_0^t ds\,\sin\left[\omega_n(t-s)\right]q(s). \tag{4.20}$$

Performing integration by parts on the integral, and insertion of the result into (4.16) finally yields a stochastic equation of Langevin type for the system coordinate

$$\ddot{q} + \int_0^t ds\,\gamma(t-s)\dot{q}(s) + V'(q,t) - \gamma(0)q = \Gamma(t). \tag{4.21}$$

Here the so-called damping-kernel $\gamma(t)$ is given by

$$\gamma(t) = \sum_{n=1}^{N}\frac{c_n^2}{\omega_n^2}\cos\left(\omega_n t\right), \tag{4.22}$$

while

$$\Gamma(t) = \sum_{n=1}^{N}c_n\left[\cos\left(\omega_n t\right)\left(q_n(0) + \frac{c_n q(0)}{\omega_n^2}\right) + \frac{p_n(0)}{\omega_n}\sin\left(\omega_n t\right)\right] \tag{4.23}$$

is a force acting on the system which can be shown to obey Gaussian statistics [143].
The damping kernel is related to the continuous SD since one infers from the discretization (4.7) of the SD and (4.18) that

$$\gamma(t) = \sum_{n=1}^{N}\frac{c_n^2}{\omega_n^2}\cos(\omega_n t) = \frac{2}{\pi}\int_0^\infty d\omega\,\frac{J(\omega)}{\omega}\cos(\omega t). \tag{4.24}$$

Thus specification of the SD suffices in order to define the damping kernel. Especially for the choice $J(\omega) = \frac{\gamma_0}{4}\omega$ for the continuous SD, one infers that the damping kernel then is memoryless,

$$\gamma(t) = \frac{2}{\pi}\int_0^\infty d\omega\,\frac{J(\omega)}{\omega}\cos(\omega t) = \gamma_0\delta(t). \tag{4.25}$$

The Langevin equation (4.21) thus describes ohmic dissipation in this case. As already pointed out earlier, the SD has to have effective support only on a sub-interval of $[0,\infty]$ in order to avoid ultraviolet divergences. According to the previous considerations, a SD $J(\omega) \sim \omega$ equipped with an appropriate high-frequency cutoff is called *ohmic*.
Furthermore, the bilinearity of the interaction results in the additional term $-\gamma(0)q$ in (4.21), which

renormalizes the potential according to

$$V(q,t) \to V(q,t) - \frac{1}{2}q^2 \sum_{n=1}^{N} \frac{c_n^2}{\omega_n^2}. \tag{4.26}$$

In order to compensate for this renormalization one introduces the so-called counter term (see [182] for further details) in the quantum system Hamilton operator (4.6)

$$\hat{\mathcal{H}}_{\mathrm{CT}} = \frac{1}{2}\hat{q}^2 \sum_{n=1}^{N} \frac{c_n^2}{\omega_n^2} = \hat{q}^2 \frac{1}{\pi} \int_0^\infty \mathrm{d}\omega \, \frac{J(\omega)}{\omega}. \tag{4.27}$$

In the second equality, we have inserted the discretization (4.7) of the SD and the couplings (4.18) in position representation. The counter term acts only on the system Hilbert space, and one replaces

$$\hat{\mathcal{H}}_{\mathrm{S}} \to \hat{\mathcal{H}}_{\mathrm{S}} + \hat{\mathcal{H}}_{\mathrm{CT}}, \tag{4.28}$$

with which one attempts to cancel any effect other than dissipation and random forcing originating from the coupling of the system to the environment.

The counter term (4.27) straightforwardly generalizes to cases where the Hamiltonian has the more general form (4.6) than the one considered in this section (replace $\hat{L}^2$ with $\hat{q}^2$).

The integral

$$\Lambda = \frac{1}{\pi} \int_0^\infty \mathrm{d}\omega \, \frac{J(\omega)}{\omega} \tag{4.29}$$

on the right hand side of Eq. (4.27) is a measure for the system-bath coupling. It arises in electron transfer theory [184–186] where it analogously is a measure for the overall electronic–nuclear coupling. Being the energy corresponding to the transfer of a unit charge, it is termed reorganization energy.

Now that we have detailed the origin of the ohmic form of the continuous SD and the counter term from the classical limit, we return to the full quantum case.

4.3. The impact of apoptosis and regularization of the ρ-matrix

The multi Davydov-Ansatz is commonly known to suffer from severe instabilities. Even with straightforward regularizations implemented, whether a propagation completes or not is just a matter of luck: while for certain numbers M of CS employed and certain positions of the initially unpopulated CS a numerical propagation may successfully complete, a slight change in the multiplicity M or the positions of the initially unpopulated CS may lead to termination of the propagation due to tiny integrator steps before completion. This instability is commonly considered intimately related to the method, which is why one - despite its amazingly slow growth of the numerical effort with the number of environmental modes - considers the method to be better avoided.

In this section we shall investigate in detail the impact of the regularizations of the vMCG Ansatz outlined in Secs. 3.3.1 and 3.3.2 on the multi Davydov-Ansatz. While the regularization in the case of vanishing coefficients plays the dominant role if the environment consists of just a few modes (see Sec. 3.3.1), singularity of the coefficient matrix (3.34) in the case of two CS approaching is the dominant issue in settings with a large number of modes (see Sec. 3.3.2). Thus we will consider two settings here for an open system given by a single qubit.

Firstly, we investigate the impact of regularization in the case of vanishing coefficients in the quantum Rabi model for a single environmental oscillator in Sec. 4.3.1. We will find that regularization of the coefficient matrix (3.34) *en bloc* (see Sec. 3.3.1) introduces further instabilities and that it is of utmost importance to regularize carefully by only regularizing the ρ-matrix.

Secondly, we investigate the impact of apoptosis in the case of two CS approaching in the Spin-Boson model for multiple environmental oscillators in Sec. 4.3.2. We will find that with apoptosis implemented each propagation completes successfully.

We shall show that the combination of both regularizations renders highly stable the multi Davydov-Ansatz and thus allows for convergence of the multi Davydov method to arbitrary precision. Further details regarding the implementation of the multi Davydov-Ansatz are gathered in App. D.

4.3.1. Multi Davydov-Ansatz for the Quantum Rabi model

In order to investigate the impact of the regularization of the coefficient matrix (3.34) in the case of vanishing coefficients, let us consider a two-level system coupled to only a single environmental mode. This model, known as the quantum Rabi model, has been introduced in [187, 188] to describe the effect of a rapidly varying, weak magnetic field on an oriented atom possessing nuclear spin. The model is obtained by treating the field as classically rotating. Then the system Hamiltonian is given by

$$\hat{\mathcal{H}}_{\mathrm{S}} = \frac{\Delta}{2}\hat{\sigma}_x, \tag{4.30}$$

and the coupling operator is given by

$$\hat{L} = \frac{1}{2}\hat{\sigma}_z. \tag{4.31}$$

Here, $\hat{\sigma}_x$ and $\hat{\sigma}_z$ are the Pauli spin matrices and Δ is the level splitting. The bath Hamiltonian and the environmental coupling operator corresponding to (4.2) and (4.4) are given by

$$\hat{\mathcal{H}}_{\mathrm{B}} = \omega\hat{a}^\dagger\hat{a} \tag{4.32}$$

and

$$\hat{\mathcal{H}}_{\mathrm{I}} = \lambda(\hat{a}^\dagger + \hat{a}), \tag{4.33}$$

respectively, for a single environmental mode. A photonic realization of the Rabi model has been found recently [189], and nice reviews of the model along with further properties and experimental realizations can be found in [190, 191]. Most importantly, all parameters of the Rabi model are tunable in experimental realizations.

We do not resort to an analytical solution to the quantum Rabi model, presented in [192], since a numerically exact and quickly calculable solution is available if one expands the wave-function in terms of number states $|j\rangle$ and truncates the series at finite N_n:

$$|\Psi(t)\rangle = \sum_{j=0}^{N_n} \left(A_j(t) \left|+\right\rangle + B_j(t) \left|-\right\rangle \right) |j\rangle. \tag{4.34}$$

A straightforward calculation with the Hamilton operator (4.6) yields

$$\hat{\mathcal{H}} |\Psi\rangle = \sum_{j=0}^{N_n} \left[\left(\frac{\Delta}{2} \left(A_j \left|-\right\rangle + B_j \left|+\right\rangle \right) + \omega j \right) |j\rangle \right.$$
$$\left. + \frac{\lambda}{2} \left(A_j \left|+\right\rangle - B_j \left|-\right\rangle \right) \left(\sqrt{j+1} \left|j+1\right\rangle + \sqrt{j} \left|j-1\right\rangle \right) \right]. \tag{4.35}$$

Insertion into the TDSE and projection onto $\langle j| \langle\pm|$ yields the system

$$\mathrm{i}\dot{\vec{y}} = \boldsymbol{M}\,\vec{y} \tag{4.36}$$

for $\vec{y} = (A_1, \ldots, A_N, B_1, \ldots, B_N)$, with the time-independent matrix

$$M = \begin{pmatrix} \boldsymbol{m}_1 & \boldsymbol{m}_2 \\ \boldsymbol{m}_2 & \boldsymbol{m}_3 \end{pmatrix}, \tag{4.37}$$

where

$$\boldsymbol{m}_1 = \begin{pmatrix} 0\omega & \frac{\lambda}{2}\sqrt{0} & 0 & 0 \\ \frac{\lambda}{2}\sqrt{1} & 1\omega & \frac{\lambda}{2}\sqrt{1} & \\ 0 & \frac{\lambda}{2}\sqrt{2} & 2\omega & \frac{\lambda}{2}\sqrt{2} \\ & & & \ddots \end{pmatrix}, \tag{4.38}$$

$$\boldsymbol{m}_2 = \mathrm{diag}\left[\frac{\Delta}{2}, \ldots, \frac{\Delta}{2} \right], \tag{4.39}$$

and

$$
\boldsymbol{m}_3 = \begin{pmatrix} 0\omega & -\frac{\lambda}{2}\sqrt{0} & 0 & 0 \\ -\frac{\lambda}{2}\sqrt{1} & 1\omega & -\frac{\lambda}{2}\sqrt{1} & \\ 0 & -\frac{\lambda}{2}\sqrt{2} & 2\omega & -\frac{\lambda}{2}\sqrt{2} \\ & & & \ddots \end{pmatrix}. \tag{4.40}
$$

The solution is given by

$$
\vec{y}(t) = \exp\left[-\mathrm{i}\boldsymbol{M}t\right]\vec{y}(0), \tag{4.41}
$$

where the matrix exponential can be calculated in many different ways [193, 194]. Convergence then has to be checked with respect to the number of included number states N_n.

Subsequently we compare the numerical exact result with the one obtained by the multi Davydov-Ansatz. Special emphasis is on the investigation of the regularization of the coefficient matrix (3.34) in the case of (almost) vanishing coefficients. To this end we consider the demanding setting given in [190]. There the strong coupling regime has been explored. Both presented settings provide an optimal test bed for the regularization to be investigated since many initially unpopulated CS are to be employed, $M \gg N$, and consequently not apoptosis but vanishing coefficients is expected to be the dominant issue. We investigate the effect of regularization of the matrices $\mathbf{S}$, $\mathbf{L}_3$ and $\boldsymbol{\rho}$ (see Sec. 3.3.1 and Eq. 3.34) by adding a multiple of the identity to them.

The initial state is assumed to be $|\Psi(0)\rangle = \frac{1}{\sqrt{2}}\Big(|+\rangle + |-\rangle \Big) |0\rangle$, i.e. the system is in the equator of the Bloch sphere while the environmental oscillator is in its ground state initially. The oscillator frequency is set to $\omega = 1$ and the coupling $\lambda = 4$. In the first setting, $\Delta = 0.2$ while in the second setting $\Delta = 4$. The multi Davydov-Ansatz has been employed with a multiplicity $M = 20$. Further details of the implementation are summarized in App. D.

Table 4.1.: Comparison of regularizations for different setups

regularization			$\Delta = 0.2$		$\Delta = 4$	
$\boldsymbol{\rho}$	$\mathbf{S}$	$\mathbf{L}_3$	Fig.	deviation d	Fig.	deviation d
no	no	weak	4.1 left	0.048	X	X
no	no	strong	4.1 middle	3.369	4.3 left	2.377
no	weak	weak	4.1 right	0.045	X	X
no	weak	strong	4.2 left	3.369	4.3 middle	2.259
no	strong	weak	4.2 middle	1.354	4.3 right	1.196
weak	no	no	4.2 right	0.008	4.4	0.111

Impact of different regularizations of the matrices $\boldsymbol{\rho}$ (see Eq. (3.28)), $\mathbf{S}$ (see Eq. (3.35)) and $\mathbf{L}_3$ (see Eq. (3.37)) entering the coefficient matrix (3.34). The entry X indicates that the propagation could not be completed, and the deviation d is given by (4.42).

The results are gathered in Figs. 4.1 - 4.4 where the expectation value $s_x(t) := < \hat{\sigma}_x > = \langle \Psi(t) | \hat{\sigma}_x | \Psi(t) \rangle$ of $\hat{\sigma}_x$ is plotted as function of time. Table 4.1 summarizes the results obtained by regularizing the matrices $\mathbf{S}$, $\mathbf{L}_3$ and $\boldsymbol{\rho}$ in Eq. (3.34) by respectively adding the identity times 10^{-4} (strong) and times 10^{-8} (weak) to some of them. The entry X indicates that the propagation could not be completed. By neither regularizing $\boldsymbol{\rho}$ nor $\mathbf{L}_3$, none of the propagations completed, and thus these lines have been omitted from Tab. 4.1. The same holds true for strongly regularizing $\mathbf{S}$ and $\mathbf{L}_3$ which gave completely unreasonable results. In order to better quantify the impact of the regularizations, the deviation d from the exact result, given by the distance

$$d = \sum_{m=1}^{N_t} |s_x^{\mathrm{approx}}(t_m) - s_x^{\mathrm{exact}}(t_m)| \tag{4.42}$$

for a discretization $(t_1, \ldots, t_{N_t})$ of the time-interval $[0, 20]$ is also given.

From Figs. 4.2 (right panel) and 4.4 and Table 4.1 we find that weakly regularizing $\boldsymbol{\rho}$ suffices in order to obtain converged results in both settings, while none of the remaining possibilities listed in Tab. 4.1 lead to converged results in both setups. Furthermore, the instability of the other regularizations can be carved out in even more detail by increasing the multiplicity M which only in the case of regularization of the $\boldsymbol{\rho}$-matrix leads to a decay in the distance d.

This exemplary shows what we generally found for all performed numerical calculations: as theoretically outlined in Sec. 3.3.1 carefully regularizing only the $\boldsymbol{\rho}$-matrix is suited to tackle the issue of vanishing coefficients without introducing further instabilities. We conclude that the regularization of the ρ-matrix as outlined in Sec. 3.3.1 is the minimally invasive regularization best suited for the propagation of CS in the case of (almost) vanishing coefficients.
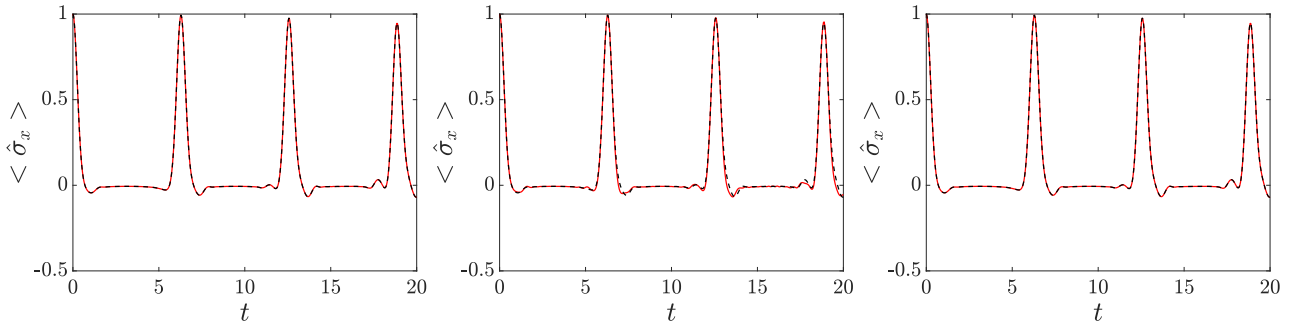
Figure 4.1.: Expectation value of $\hat{\sigma}_x$ as function of time for the first setting $\Delta = 0.2$, for different regularizations. Results obtained from the multi Davydov-Ansatz with multiplicity $M = 20$ (red solid) are compared to the exact result (black dashed) Left panel: only $\mathbf{L}_3$ weakly regularized. Middle panel: only $\mathbf{L}_3$ strongly regularized. Right panel: $\mathbf{S}$ and $\mathbf{L}_3$ weakly regularized.

While we have detailed the impact of the regularization of the $\boldsymbol{\rho}$-matrix in the case of vanishing coefficients in this section, we shall now investigate in more detail the effect of apoptosis in the case of two CS approaching. To this end, we will switch to multiple environmental modes in the Spin-Boson model.
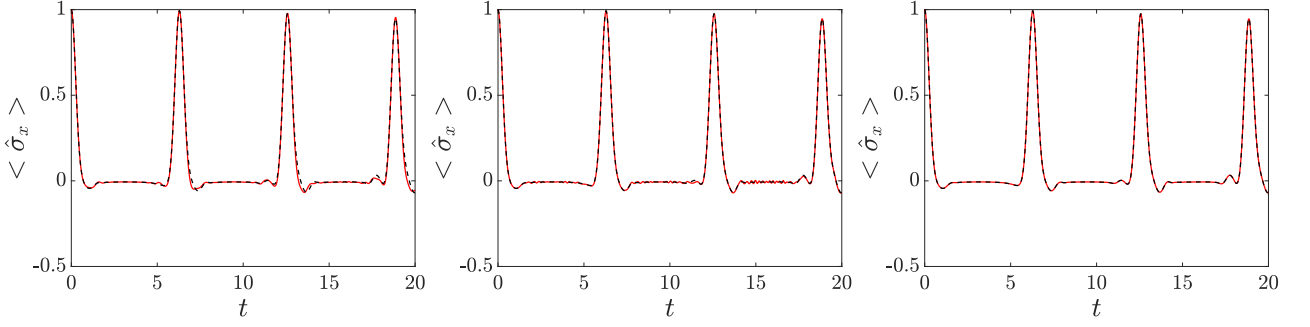
Figure 4.2.: As in Fig. 4.1, but for different regularizations. Left panel: **S** weakly and **L₃** strongly regularized. Middle panel: **S** strongly and **L₃** weakly regularized. Right panel: only **ρ** weakly regularized.
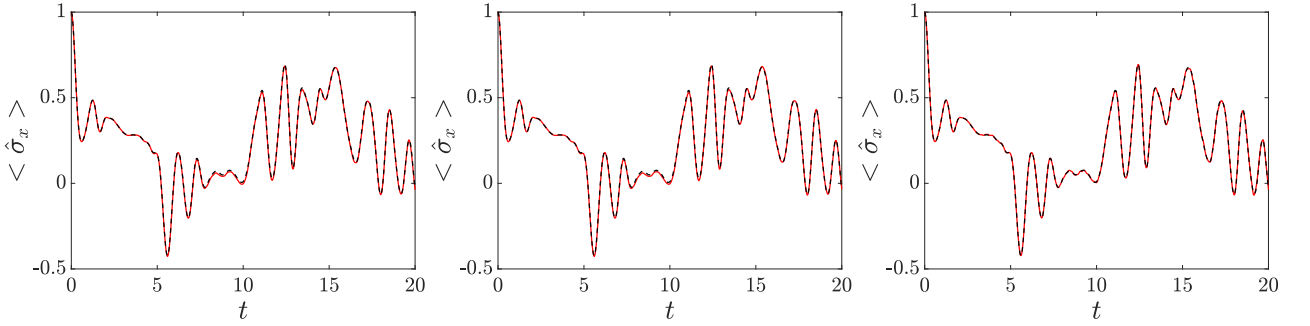
Figure 4.3.: As in Fig. 4.1, but for different regularizations. Left panel: only **L₃** strongly regularized. Middle panel: **S** weakly and **L₃** strongly regularized. Right panel: **S** strongly and **L₃** weakly regularized.
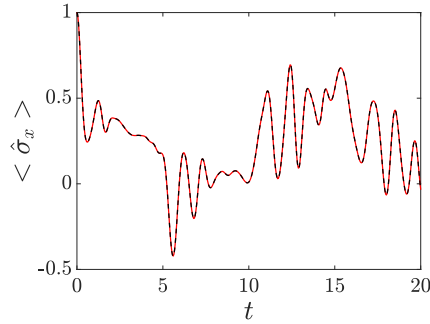
Figure 4.4.: As in Fig. 4.1, but only **ρ** weakly regularized.

4.3.2. Multi Davydov-Ansatz and the Spin-Boson model

In order to examine in more detail the impact of apoptosis, outlined in Sec. 3.3.2, we transition from the simple quantum Rabi model with only a single environmental mode (see the previous section) to the Spin-Boson model (SBM) where the environment comprises many modes, since different coherent states approaching is expected to be the dominant issue for multiple modes. Typically different CS come close if convergence with respect to the number M of CS is reached, rendering impossible further systematic convergence by increasing the multiplicity. In other words: if with a certain multiplicity

M the result obtained with the multi Davydov-Ansatz is *close* to convergence, propagation with increased *M* will typically fail due to tiny integrator steps caused by CS approaching.

On the contrary, we shall see that with apoptosis implemented, convergence can be systematically reached by increasing *M*. It will turn out that in the Spin-Boson model the region of convergence of the multi Davydov-Ansatz can be reached extremely quickly, i.e. for surprisingly small *M*. Since the implementation of apoptosis allows to further converge the result, we will obtain converged results in various parameter regimes for astonishingly small computational effort. Thus by apoptosis the multi Davydov-Ansatz can be tuned into a reliable high-precision tool suited to tackle open quantum system dynamics at almost every level.

It is hard to graphically show the impact of apoptosis. The dynamics of the coherent states in the multi Davydov-Ansatz is highly non-linear, thus whether and for which coherent states apoptosis is needed depends on the setup and the positions of the initially unpopulated CS. In order to give a complete description of an apoptosis event, one consequently has to include the initial positions of all the coherent states, the integrator tolerances etc., which is tedious due to the high dimension of the environmental phase space. Thus we refrain from specifying the time of apoptosis events and rather resort to a presentation of systematically converged results which indirectly confirms the reliability of the method. In order to do so, we examine the Spin-Boson model in various parameter regimes.

The Spin-Boson model (SBM) constitutes the simplest non-trivial open quantum system, a two-level system coupled non-trivially to an environmental bath. It has been the subject of research for many decades [26, 163, 166, 168, 195–197]. While it arises naturally in contexts where the system comprises intrinsically just two levels, a vast number of more complex systems can be described by the SBM. This can be accomplished firstly if the system comprises multiple levels which one artificially restricts in the low-temperature limit to only the lowest-lying two ones, as e.g. in the case of a NH_3-molecule coupled to the radiation field. Generally, even in cases where the system has a continuous degree of freedom with which is associated a potential with two separate minima, restriction to a two-level system can be accomplished by only taking into account the ground states in the two separate minima [198].

Due to its generality, the SBM has found wide application, e.g. for the incoherent tunneling of bistable defects in metals [199] and amorphous systems as metallic glass [200], electron and proton transfer in solvent environments [201], and macroscopic quantum tunneling in superconducting circuits [202]. In addition, the SBM is relevant in describing exciton transport in biological complexes [203, 204], especially in photosynthetic reactions [205, 206], and in quantum computing [207].

In the case of ohmic damping (see Sec. 3.4 and below) the SBM can be shown to be equivalent with the anisotropic spin-1/2 Kondo model in one dimension [208, 209]. The Kondo model describes a magnetic impurity coupled to a Fermi sea, and below an ultraviolet energy scale set by the Fermi energy the equivalence can be formulated explicitly through bosonization [210–212]) of the SBM. Thus, for strong coupling, the SBM may be utilized to describe the emergence of Kondo screening clouds [157].

Recently, a new experimental setup was implemented [213] which realizes the ohmic SBM with an

environmental coupling tunable from weak to ultrastrong [214]. Furthermore, in [215], a qubit ultra-strongly coupled to a single oscillator mode was demonstrated. Although plenty of research has been done on the model in recent years, only a very early review of the SBM exists [198].

The Hamilton operator of the two-level system reads

$$\hat{\mathcal{H}}_{\mathrm{S}} = \frac{\varepsilon}{2}\hat{\sigma}_z + \frac{\Delta}{2}\hat{\sigma}_x, \tag{4.43}$$

where ε is the detuning between the two wells and Δ is the tunneling matrix element. This generalizes the system Hamiltonian of the quantum Rabi model (4.30), where again $\hat{\sigma}_z$ and $\hat{\sigma}_x$ are Pauli spin matrices. We assume the environment to be sensitive to the system position, i.e. the coupling operator is given by

$$\hat{L} = \frac{1}{2}\hat{\sigma}_z. \tag{4.44}$$

We recall that the full system-bath Hamiltonian is given by (4.6).

Despite the seeming simplicity of the Spin-Boson model, its exact numerical solution requires advanced methods, e.g., the multi-layer multi-configurational time-dependent Hartree (ML-MCTDH) method, hierarchical equations of motion [154, 216] (HEOM), time-evolving matrix product operators [31] (TEMPO), or others [164, 217] while still being numerically demanding. Consequently, certain aspects of the SBM are still not yet fully understood.

For the Spin-Boson model, the counter-term (4.27) introduced in Sec. 4.2 is a multiple of the identity,

$$\hat{\mathcal{H}}_{\mathrm{CT}} = \frac{1}{4}\hat{L}^2 \sum_{n=1}^{N} \frac{\lambda_n^2}{\omega_n} = \frac{1}{4}\sum_{n=1}^{N} \frac{\lambda_n^2}{\omega_n}, \tag{4.45}$$

and thus does not affect the dynamics. Introducing the counter term at the level of the Caldeira Leggett model (4.6) and then reducing to the simplified SBM does obviously not yield the same as introducing the counter term at the level of the already reduced SBM. To our best knowledge, this inconsistency has not been addressed in the literature.

A continuous SD $J(\omega) \sim \omega$, equipped with an appropriate cutoff in order to avoid ultraviolet divergences (see Sec. 4.1), leads to ohmic dissipation in the classical limit (see Sec. 4.2). By equipment of J with an exponential cutoff, the SD

$$J(\omega) = \frac{\pi}{2}\alpha\omega e^{-\omega/\omega_c}, \tag{4.46}$$

is consequently called ohmic. Here, α is the Kondo parameter which specifies the overall system-bath coupling strength and ω_c specifies the high-frequency cutoff. The ohmic SD can be generalized by allowing it to obey an arbitrary power-law,

$$J(\omega) = \frac{\pi}{2}\alpha\omega_c^{s-1}\omega^s e^{-\omega/\omega_c}, \tag{4.47}$$

which reduces to (4.46) in the case of $s = 1$. For $s < 1$ the SD is referred to as sub-ohmic, while for $s > 1$ it is called super-ohmic. Numerical solutions for a wide variety of parameters, commonly considered as 'the' exact solution for the Spin-Boson model, have been calculated for zero temperature by means of the ML-MCTDH method and presented in [163] for the ohmic and in [166] for the sub-ohmic case. We shall use these numerical results as reference and compare them to the results obtained from the multi Davydov-Ansatz in the ohmic (Sec. 4.3.2.1) as well as in the sub-ohmic (Sec. 4.3.2.2) case. We restrict ourselves to the case of zero detuning $\varepsilon = 0$. Then by setting Δ as the unit of energy, the Spin-Boson model has only two free parameters, the cutoff frequency ω_c and the Kondo parameter α. In this section, the system is assumed to be in its excited state and the bath to be in the ground state initially,

$$|\Psi(0)\rangle = |\mathbf{0}\rangle |+\rangle . \tag{4.48}$$

Further details concerned with the positions of initially unpopulated CS are summarized in App. D.

4.3.2.1. Spin-Boson model in the ohmic regime

In this section we aim at comparison of the dynamics obtained from the multi D2-Ansatz with the results given in [163]. To this end, we assume the SD to be of ohmic form (4.46) and discretize the frequency axis by a FD given by

$$\rho_{\mathrm{f}}(\omega) = \frac{1}{\omega_c} \exp\left[-\frac{\omega}{\omega_c}\right]. \tag{4.49}$$

The frequencies and couplings, calculated from (4.12) and (4.13) respectively, read

$$\omega_n = -\omega_c \ln\left[1 - \frac{n}{N+1}\right], \quad \lambda_n = \sqrt{\frac{\alpha\omega_c}{2(N+1)}\omega_n}, \qquad n = 1, \ldots, N. \tag{4.50}$$

We will consider here couplings $\alpha \in \{0.1, 0.5\}$ and cutoffs $\omega_c \in \{10\Delta, 40\Delta\}$. Convergence with respect to the number of bath modes N and the number of CS employed in the multi Davydov-Ansatz will be checked, where we aim at reproduction of the results for the expectation value $< \hat{\sigma}_z > = \langle\Psi(t)| \hat{\sigma}_z |\Psi(t)\rangle$ of $\hat{\sigma}_z$ given in [163] in the time interval $t\Delta \in [0, 25]$ within line width.

The results are shown in Figs. 4.5 - 4.8. The speed of convergence with respect to M is remarkable. While for small coupling $\alpha = 0.1$ three CS, i.e. $M = 3$ is enough to converge the result, even in the strong coupling case ($\alpha = 0.5$) only six multi-mode CS are required to converge the result. We will see, however, that in the sub-ohmic regime, more CS are required for converged results (see Sec. 4.3.2.2). Furthermore, we observe that the number N of bath modes required to converge to the continuum limit is not excessively large. Rather, at most $N = 400$ modes suffice for convergence. As we shall see in Sec. 4.4 this is intimately related to the specific choice of the FD. It will turn out that the FD (4.49) applied here is extremely favourable in this respect.

In order to converge the results, apoptosis is needed frequently. We point out again that without
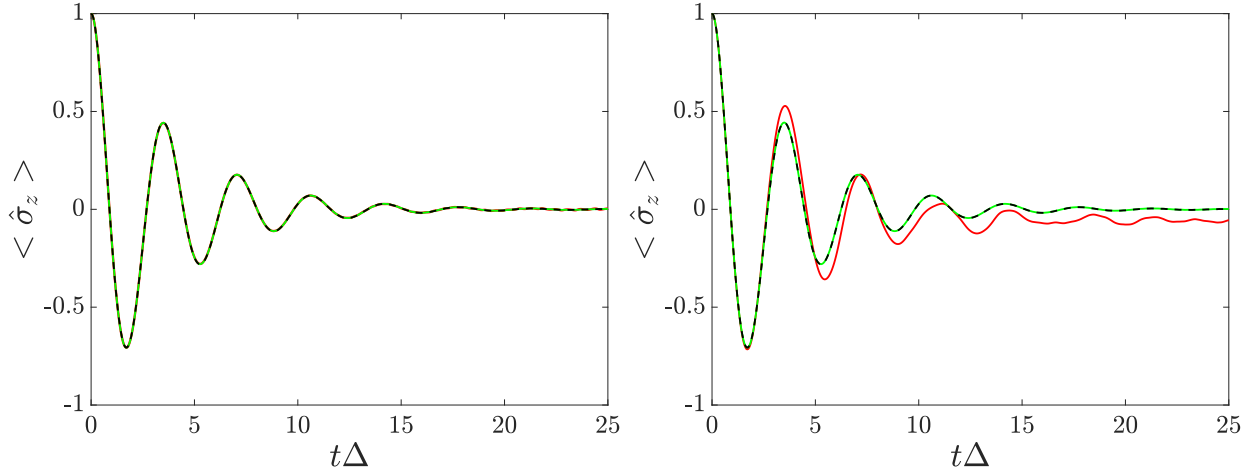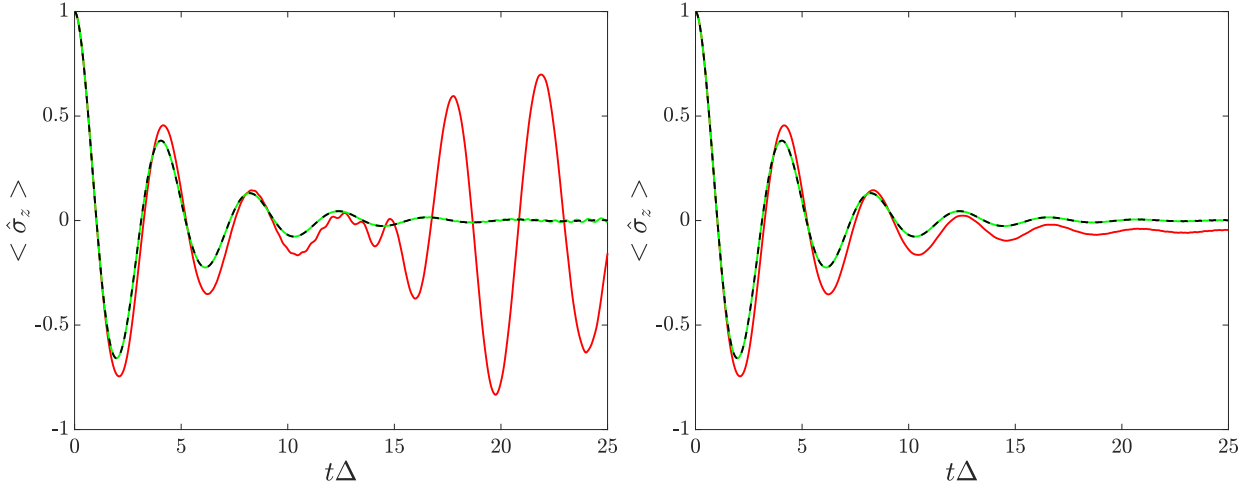
Figure 4.5.: Convergence of the multi D2-Ansatz for $\omega_c = 10\Delta$, $\alpha = 0.1$. Left panel convergence wrt. N: $N = 100$ (red solid), $N = 200$ (green solid), $N = 300$ (black dashed), for $M = 5$. Right panel convergence wrt. M for $N = 300$: $M = 3$ (red solid), $M = 4$ (green solid), $M = 5$ (black dashed).
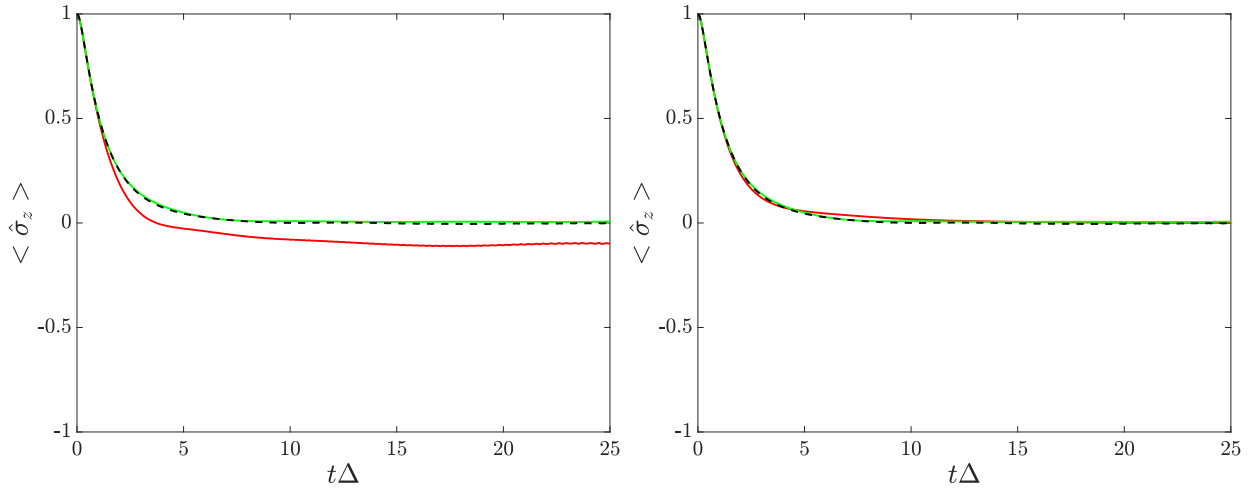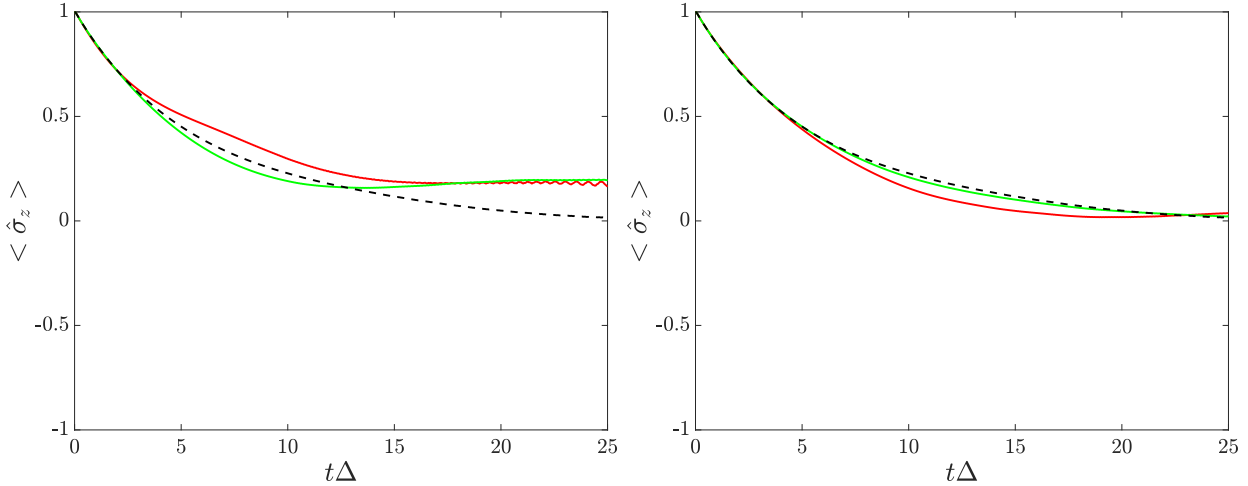

Figure 4.6.: Convergence of the multi D2-Ansatz for $\omega_c = 10\Delta$, $\alpha = 0.5$. Left panel convergence wrt. N: $N = 100$ (red solid), $N = 200$ (green solid), $N = 300$ (black dashed), for $M = 6$. Right panel convergence wrt. M for $N = 300$: $M = 4$ (red solid), $M = 5$ (green solid), $M = 6$ (black dashed).

apoptosis implemented still some of the results may be obtained for certain positions of the initially unpopulated CS. Finding these positions is cumbersome, and sometimes none of the attempts seems to work. On the contrary, with apoptosis implemented, *each* of the propagations successfully completes independently from the positions of the initially unpopulated CS. It is indeed much more convenient and time-saving to have apoptosis implemented. Furthermore, the results show that although apoptosis decreases the flexibility of the multi Davydov-Ansatz, convergence occurs systematically by increasing the multiplicity M. We conclude that apoptosis is minimally invasive and suited to stabilize the formerly highly unstable method.

By plotting the absolute value of the displacements as a function of the number n of the mode and the

Figure 4.7.: Convergence of the multi D2-Ansatz for $\omega_c = 40\Delta$, $\alpha = 0.1$. Left panel convergence wrt. N: $N = 100$ (red solid), $N = 200$ (green solid), $N = 300$ (black dashed), for $M = 4$. Right panel convergence wrt. M for $N = 300$: $M = 3$ (red solid), $M = 4$ (green solid), $M = 5$ (black dashed).

Figure 4.8.: Convergence of the multi D2-Ansatz for $\omega_c = 40\Delta$, $\alpha = 0.5$. Left panel convergence wrt. N: $N = 200$ (red solid), $N = 300$ (green solid), $N = 400$ (black dashed), for $M = 6$. Right panel convergence wrt. M for $N = 400$: $M = 4$ (red solid), $M = 5$ (green solid), $M = 6$ (black dashed).

index k labeling the multiplicity, for different times, in Figs. 4.9 - 4.12 we can read off the channels through which the energy flows from the system to the bath. It is remarkable that even for short times all the bath modes contribute to the dynamics (we have not plotted the absolute values of the coefficients since we expect all multi-mode CS to contribute from the small multiplicity $M = 4$). Furthermore comparison of the left panels of Figs. 4.9,4.10 with the left panels of Figs. 4.11,4.12 shows the effect of the cutoff frequency on the dynamics of the bath: the larger the cutoff (at the same number of modes), the more are the modes distributed in a larger region of the frequency axis and thus fewer modes lie in the region of the system frequency. Hence fewer modes effectively couple
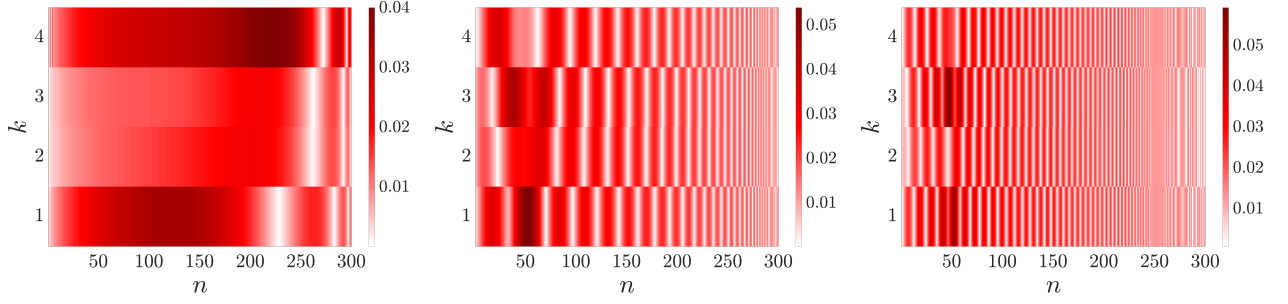
Figure 4.9.: Displacements for the ohmic case for $N = 300$ bath modes and multiplicity $M = 4$ at different times: left panel $t\Delta = 0.5$, middle panel $t\Delta = 5$, right panel $t\Delta = 15$. Further parameters read $\omega_c = 10\Delta$, $\alpha = 0.1$.
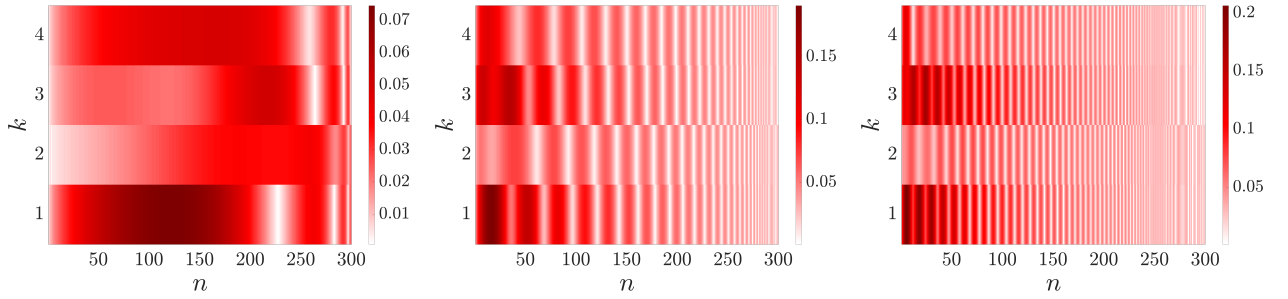

Figure 4.10.: Displacements for the ohmic case for $N = 300$ bath modes and multiplicity $M = 4$ at different times: left panel $t\Delta = 0.5$, middle panel $t\Delta = 5$, right panel $t\Delta = 15$. Further parameters read $\omega_c = 10\Delta$, $\alpha = 0.5$.
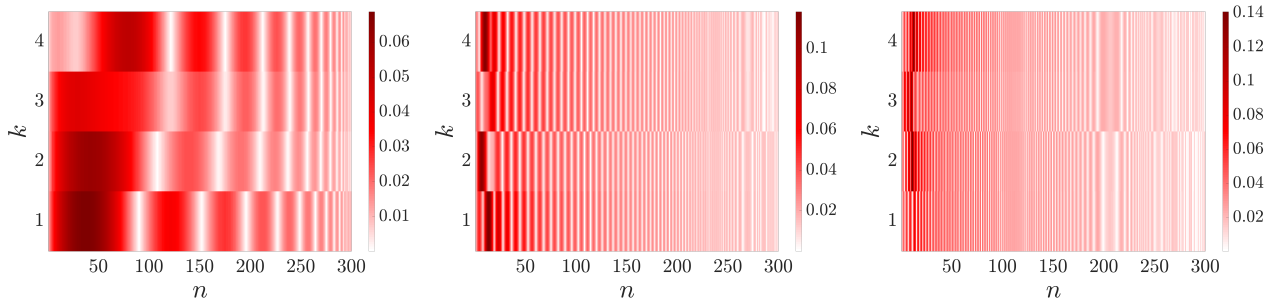
Figure 4.11.: Displacements for the ohmic case for $N = 300$ bath modes and multiplicity $M = 4$ at different times: left panel $t\Delta = 0.5$, middle panel $t\Delta = 5$, right panel $t\Delta = 15$. Further parameters read $\omega_c = 40\Delta$, $\alpha = 0.1$.

to the system mode, and the dynamics is slower, in coincidence with a comparison of Figs. 4.5,4.6 and 4.7,4.8. This pursues in the dynamics for larger times, as for large coupling the energy is concentrated in the small frequency modes (see Fig. 4.12) for large cutoff, while the energy stays distributed for small cutoff (see Fig. 4.10), for large coupling.

In order to better understand the dynamics of the bath, we have plotted in Fig. 4.13 the energy
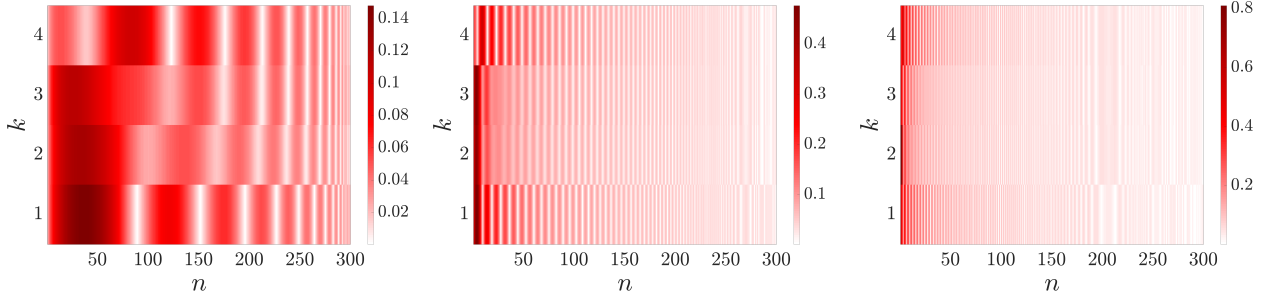
Figure 4.12.: Displacements for the ohmic case for $N = 300$ bath modes and multiplicity $M = 4$ at different times: left panel $t\Delta = 0.5$, middle panel $t\Delta = 5$, right panel $t\Delta = 15$. Further parameters read $\omega_c = 40\Delta$, $\alpha = 0.5$.

density

$$\rho_{\mathrm{B}}^{\mathrm{E}}(\omega_n, t) := \rho_{\mathrm{f}}(\omega_n) \langle \Psi(t)| \, \omega_n \hat{a}_n^\dagger \hat{a}_n \, |\Psi(t)\rangle \tag{4.51}$$

of the bath and in Fig. 4.14 the energy density

$$\rho_{\mathrm{int}}^{\mathrm{E}}(\omega_n, t) := \rho_{\mathrm{f}}(\omega_n) \langle \Psi(t)| \, \hat{\sigma}_z \lambda_n \left(\hat{a}_n^\dagger + \hat{a}_n \right) |\Psi(t)\rangle \tag{4.52}$$

of the interaction. For small coupling, the energy is mainly concentrated in the small frequencies of the bath (see right panel of Fig. 4.13). With growing coupling strength the energy is stronger distributed among the different modes in the system. We see from Figs. 4.13, 4.14 that density of bath and interaction are complementary with each other. The picture which we draw from the displacements is confirmed here: in the ohmic case, for strong coupling all modes share the energy equally. As we shall see in Sec. 4.3.2.2, this is not the case for sub-ohmic dissipation.
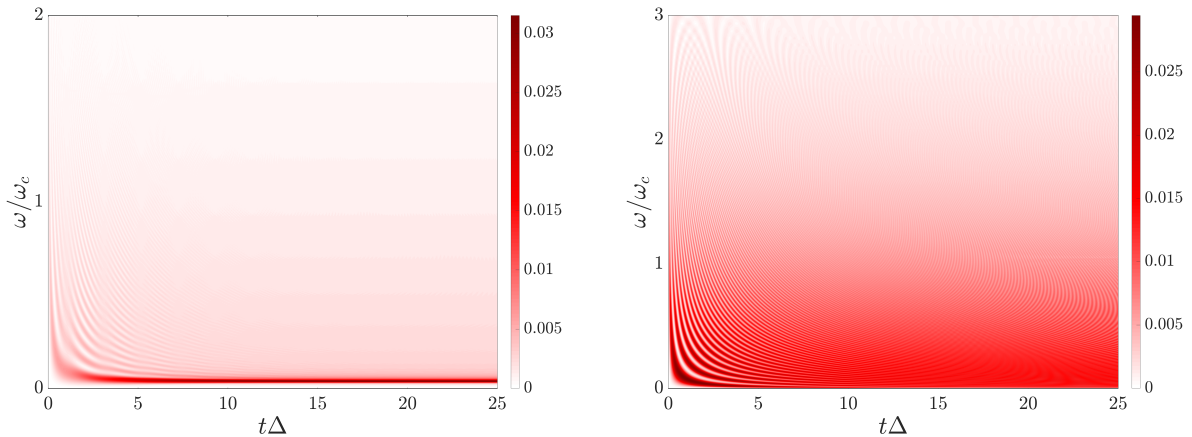
Figure 4.13.: Energy density (4.51) of the bath as function of ω and time t. Left panel $\alpha = 0.1$, right panel $\alpha = 0.5$, with cutoff $\omega_c = 40\Delta$.

In the present setting we also substantiate the theoretical considerations of Sec. 3.6 with respect to
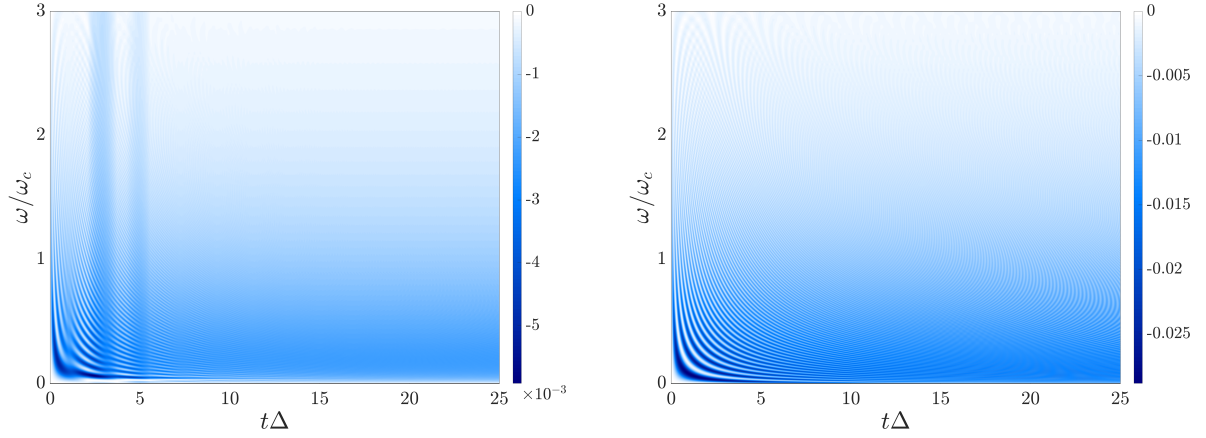
Figure 4.14.: Energy density (4.52) of the interaction as function of ω and time t. Left panel $\alpha = 0.1$, right panel $\alpha = 0.5$, with cutoff $\omega_c = 40\Delta$.

the differences between the D1 and the D2-Ansatz. Confirming these considerations, we shall show that the D2-Ansatz outperforms the D1-Ansatz and that thus the former should be preferred over the latter. In the multi D2-Ansatz, used to numerically calculate the results presented so far, we have utilized as system basis the eigenbasis of $\hat{\sigma}_z$, i.e. the standard basis $\{(1,0)^T, (0,1)^T\}$ of $\mathbb{R}^2$. By utilization of the D2-Ansatz with alternative basis choices we find that the results do not differ from the ones presented so far for different choices of the system basis. Concerning the multi D1-Ansatz, however, for different choices of the system basis we find different results. In Fig. 4.15 we compare
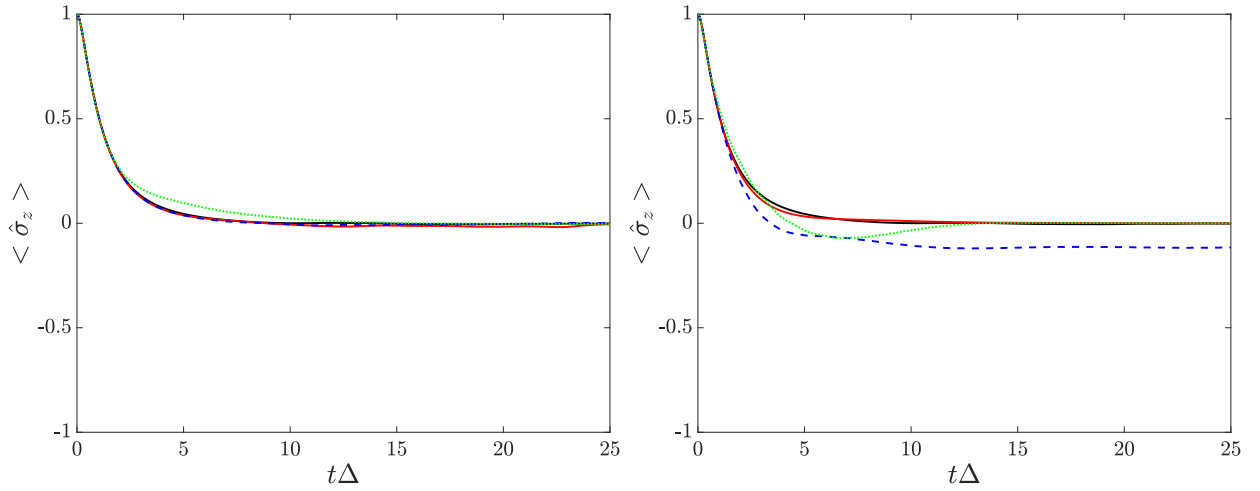
Figure 4.15.: Multi D2 vs D1-Ansatz. Left panel: Comparison of D1 in eigenbasis of $\hat{\sigma}_z$ with converged D2 result (black solid), for $N = 400$ bath modes: $M = 2$ (green dotted), $M = 3$ (blue dashed), $M = 4$ (red solid). Right panel: Comparison of D1 in eigenbasis of $\hat{\sigma}_x$ with converged D2 result (black solid), for $N = 400$ bath modes: $M = 2$ (green dotted), $M = 3$ (blue dashed), $M = 4$ (red solid).

different types of the D1-Ansatz with the numerically exact result of the D2-Ansatz which we found in Sec. 4.3.2. It turns out firstly that the D1-Ansatz converges slower than the D2-Ansatz. While the

multi D1-Ansatz with multiplicity $M = 4$ (employing eight multi-mode CS) is not yet fully converged, the multi D2-Ansatz with multiplicity $M = 6$ (employing six multi-mode CS) is fully converged. It turns out that the multi D1-Ansatz with multiplicity $M = 6$ is fully converged as well, which confirms the theoretical considerations of Sec. 3.6. Furthermore disadvantageously it turns out that the quality of the D1 result depends on the chosen basis. If the eigenbasis of $\hat{\sigma}_x$ is chosen, results are even worse than those obtained if the eigenbasis of $\hat{\sigma}_z$ is chosen. On the contrary and as expected from Sec. 3.6, this is not the case for the D2-Ansatz which yields *identical* results whichever system basis is chosen. For this reason, we will from now on perform any calculation with the D2-Ansatz.

In this section we have investigated the ohmic Spin-Boson model, which is in the context of master equation approaches considered less complicated than the sub-ohmic case. We shall in the next section apply the multi D2-Ansatz to this more challenging regime.

4.3.2.2. Spin-Boson model in the sub-ohmic regime

In this section, we examine the sub-ohmic regime of the Spin-Boson model and aim at comparison of the dynamics obtained from the multi D2-Ansatz with the results given in [166]. To this end, we assume the SD to be of sub-ohmic form (4.47) for $s < 1$ and again discretize the frequency axis by a FD given by (4.49). The frequencies and couplings, calculated from (4.12) and (4.13) respectively, read

$$\omega_n = -\omega_c \ln\left[1 - \frac{n}{N+1}\right], \quad \lambda_n = \sqrt{\frac{\alpha\omega_c^{2-s}}{2(N+1)}\omega_n^s}, \qquad n = 1, \dots, N. \tag{4.53}$$

We will consider here the case of $s = 0.5$ with couplings $\alpha \in \{0.05, 0.2\}$ for small cutoff $\omega_c = 10\Delta$ and $\alpha \in \{0.025, 0.1\}$ for large cutoff $\omega_c = 40\Delta$. Again convergence with respect to the number of bath modes N and the number of CS employed in the multi Davydov-Ansatz was checked, with the goal of reproduction of the results for the expectation value $<\hat{\sigma}_z> = \langle\Psi(t)|\,\hat{\sigma}_z\,|\Psi(t)\rangle$ of $\hat{\sigma}_z$ given in [166] in the time interval $t\Delta \in [0, 25]$ within line width.

The results are shown in Fig. 4.16, where the polarization $\langle\hat{\sigma}_z\rangle := \langle\Psi(t)|\,\hat{\sigma}_z\,|\Psi(t)\rangle$ as well as the entropy $S(t)$ are plotted. The entropy is defined as

$$S(t) = -\mathrm{tr}_\mathrm{S}\left[\hat{\rho}_\mathrm{S}(t)\ln\hat{\rho}_\mathrm{S}(t)\right], \tag{4.54}$$

where the reduced density matrix is calculated by a trace over the bath degrees of freedom,

$$\rho_\mathrm{S}(t) = \mathrm{tr}_\mathrm{B}\hat{\rho}(t). \tag{4.55}$$

It is a measure for the entanglement between system and bath. Again, the speed of convergence with respect to the multiplicity M is remarkable, yet not as brilliant as in the ohmic regime (see the previous section). While a smaller number $N = 200$ of modes is required in the sub-ohmic regime to converge to the continuum limit, the dynamics of these modes turns out more complicated, requiring

more CS to converge with respect to the multiplicity M compared to the ohmic regime. Because of this more complicated dynamics, events of two CS approaching occur more frequently. Consequently, apoptosis is needed more frequently in the sub-ohmic regime. However, the calculations performed in this regime confirm that the number of CS coming close during propagation is not related to the multiplicity M nor the coupling strength in an obvious way. Propagation with increased M may cope without apoptosis, or with more or fewer CS connected. Thus, in the presence of apoptosis convergence can be checked by increasing the multiplicity M in a systematic way. The results reveal that although apoptosis events decrease the flexibility of the CS, results still nicely converge by increasing M.
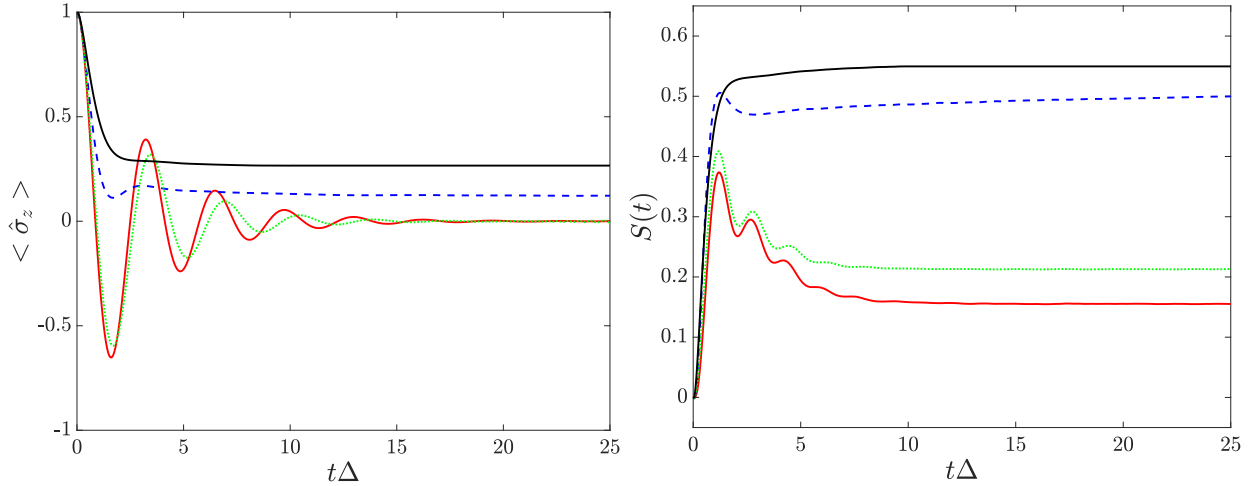
Figure 4.16.: Results in the sub-ohmic regime for $N = 200$. $\omega_c = 10\Delta$, $\alpha = 0.05$ converged with $M = 16$ (red solid) and $\alpha = 0.2$ converged with $M = 24$ (blue dashed). $\omega_c = 40\Delta$, $\alpha = 0.025$ converged with $M = 16$ (green dotted) and $\alpha = 0.1$ converged with $M = 28$ (black solid). Dynamics of the polarization $< \hat{\sigma}_z(t) >$ (left panel), entropy $S(t)$ (right panel).

Also in this case we investigate the dynamics of the displacements more closely. Results are plotted in Figs. 4.18 - 4.21 for different values $\alpha \in \{0.05, 0.2\}$ for small cutoff $\omega_c = 10\Delta$ and $\alpha \in \{0.025, 0.1\}$ for large cutoff $\omega_c = 40\Delta$. The rather strange formations seen in the left panels of these figures are reminiscent of the initial positions of the unpopulated displacements. We firstly see that the cutoff frequency has the same impact as in the ohmic case, namely that fewer modes effectively couple to the system mode, and that hence the dynamics is slower. Furthermore, the small modes are much more pronounced than in the ohmic case, meaning that the energy which flows from the system is concentrated in the small modes. This is shown exemplary in Fig. 4.17, where the energy density (4.51) of the interaction is plotted. By comparing with Fig. 4.14 in the ohmic case we see that in the ohmic case on the contrary all modes are equally pronounced.

It could even be suited to neglect the larger modes completely in this case, since they obviously do not contribute to the dynamics at all in the case of a large cutoff. By comparing the right panels of Figs. 4.18 - 4.21 we find that the bath modes are much more displaced in the strong coupling and large cutoff case than in the other cases (note the scaling). Again this is due to the fact that more modes effectively couple to the system frequency in the sub-ohmic case than in the ohmic case, and even more for strong coupling and large cutoff. Finally, it is expected that the small frequencies

contribute to the dynamics for large times while the large frequencies contribute for short times. This expectation is accomplished in the sub-ohmic case, whereas it is not in the ohmic case.
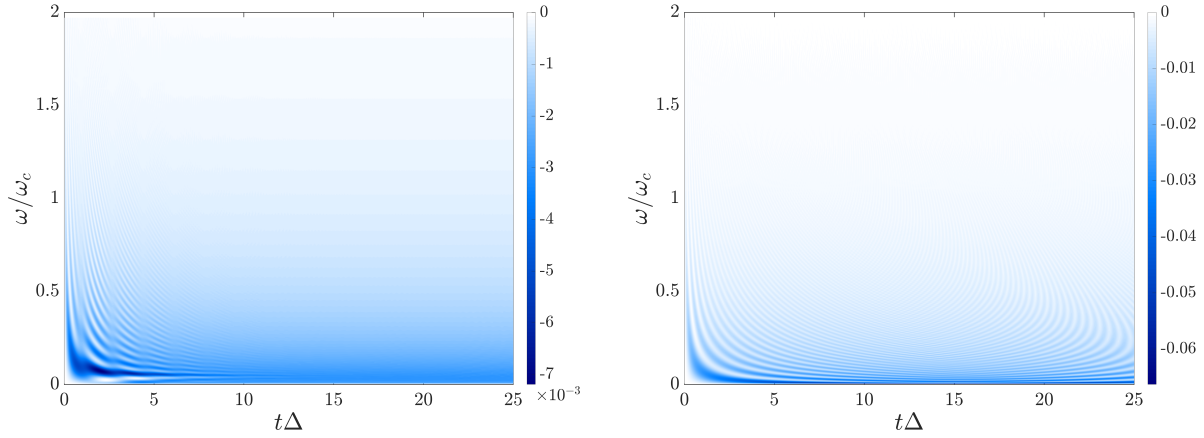

Figure 4.17.: Energy density (4.52) of the interaction as function of ω and time t. Left panel $\alpha = 0.025$, right panel $\alpha = 0.1$, with cutoff $\omega_c = 40\Delta$.

The multi D2-Ansatz has enabled us to successfully reproduce the exact dynamics of the SBM both in the ohmic as well as in the sub-ohmic regime at surprisingly humble numerical effort. While in the ohmic regime a quite large number N of modes is required in order to converge to the continuum limit, the multiplicity M turned out surprisingly low in this regime (see previous section). On the contrary, in the sub-ohmic regime a small number of modes suffices to converge to the continuum limit while a larger multiplicity M is required in order to converge with respect to the number of CS. While convergence with respect to multiplicity M is related to the complexity of the dynamics, the number N of modes required to converge to the continuum limit is intimately related to the choice for the FD. In the next section we shall address in more detail the question how to converge to the continuum limit with as few as possible environmental modes.
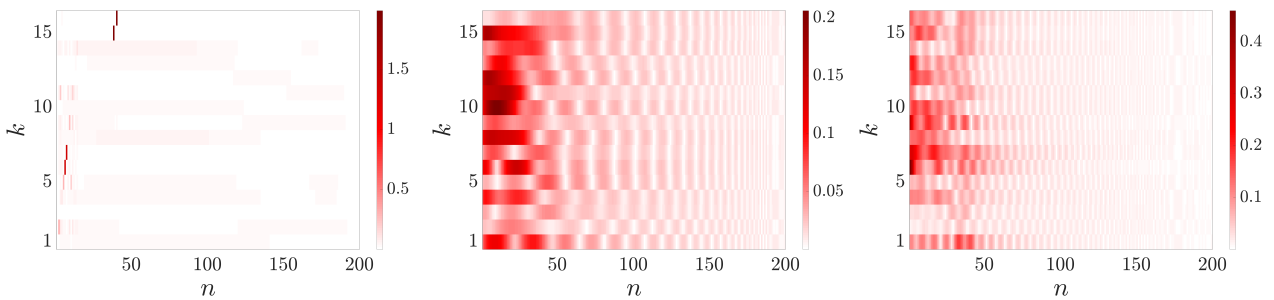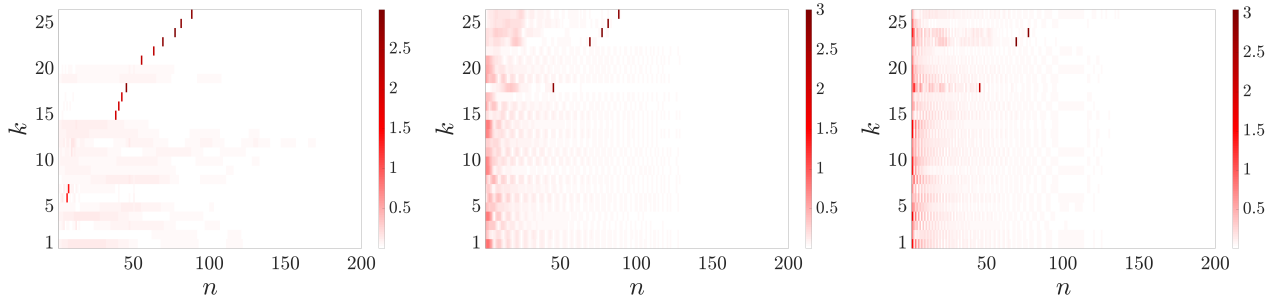

Figure 4.18.: Displacements for the subohmic case for $N = 200$ bath modes and multiplicity $M = 24$ at different times: left panel $t\Delta = 0.5$, middle panel $t\Delta = 5$, right panel $t\Delta = 15$. Further parameters read $\omega_c = 10\Delta$, $\alpha = 0.05$, $s = 0.5$.
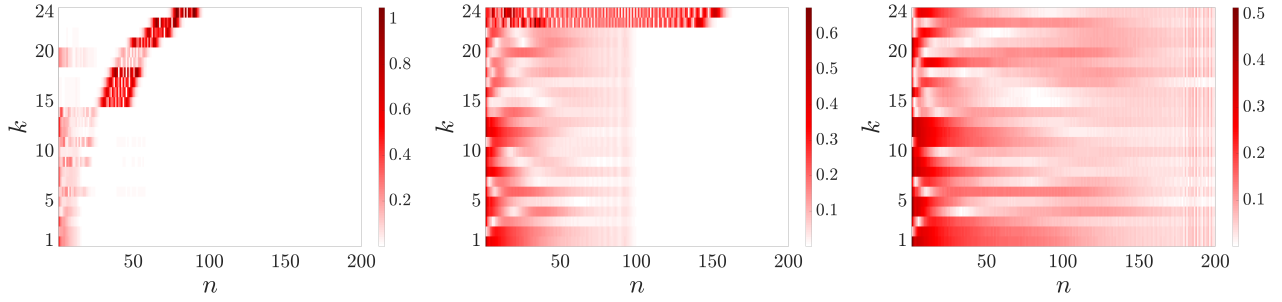
Figure 4.19.: Displacements for the subohmic case for $N = 200$ bath modes and multiplicity $M = 24$ at different times: left panel $t\Delta = 0.5$, middle panel $t\Delta = 5$, right panel $t\Delta = 15$. Further parameters read $\omega_c = 10\Delta$, $\alpha = 0.2$, $s = 0.5$.
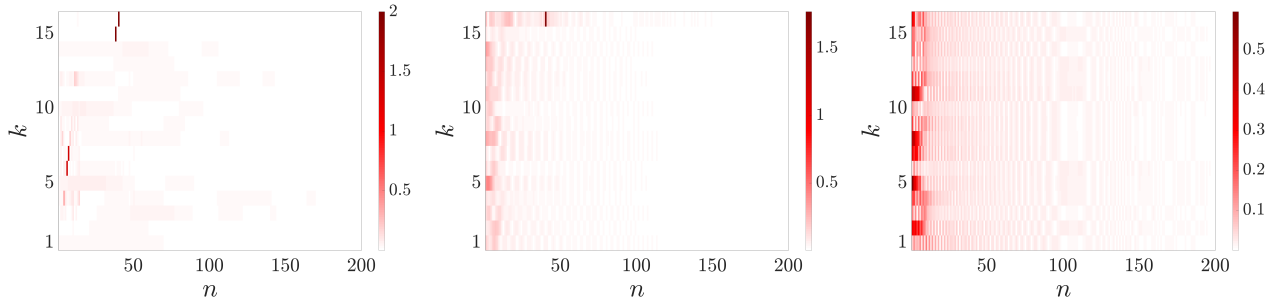
Figure 4.20.: Displacements for the subohmic case for $N = 200$ bath modes and multiplicity $M = 16$ at different times: left panel $t\Delta = 0.5$, middle panel $t\Delta = 5$, right panel $t\Delta = 15$. Further parameters read $\omega_c = 40\Delta$, $\alpha = 0.025$, $s = 0.5$.

Figure 4.21.: Displacements for the subohmic case for $N = 200$ bath modes and multiplicity $M = 16$ at different times: left panel $t\Delta = 0.5$, middle panel $t\Delta = 5$, right panel $t\Delta = 15$. Further parameters read $\omega_c = 40\Delta$, $\alpha = 0.1$, $s = 0.5$.

4.4. The Windowed Fourier Transform

In the previous section we have investigated in detail the convergence properties of the multi D2-Ansatz. In particular, we have highlighted the impact of the regularizations in the case of vanishing coefficients (see Sec. 3.3.1) and in the case of CS approaching (see Sec. 3.3.2). We have shown that these regularizations render the multi D2-Ansatz a highly stable and efficient high-precision tool with amazingly slow complexity growth with the number of environmental modes. In particular we have

shown that the linear dependency issue, based on the problem of CS approaching, can be successfully solved by apoptosis. Consequently, the multi D2-Ansatz can be converged to an arbitrary precision, and we have with the multi D2-Ansatz at hand a reliable tool to fully numerically calculate the system and environment dynamics in open quantum system settings. Building on these results, in this section we shall be concerned with the question how to optimally discretize the continuous environment in order to converge to the continuum limit with as few as possible environmental modes. In particular, we will investigate the bath correlation function (BCF) and the Windowed Fourier Transform (WFT) as a priori criteria to judge the quality of a given discretization [218].

We shall in this thesis mainly be concerned with open quantum systems where the environment is given in terms of mutually uncoupled oscillators whose coupling to the system is specified in terms of a continuous SD $J(\omega)$. The latter is again assumed to be of the general form (4.47).

For a given discretization of the frequency axis $\omega_1, \ldots, \omega_N$ the n-th mode's coupling to the system is then given by (4.8) or alternatively by (4.11) or (4.13). While the SD and its discretization (4.7) are an input to the system and hence fixed, the discretization of the frequency axis, specified in terms of a number N of frequencies and a continuous FD $\rho_f(\omega)$, is not. The only physical requirement to the discretization of the frequency axis is that in the continuum limit $N \to \infty$ *all* frequencies are included.

Obviously, although by the multi D2-Ansatz propagation of hundreds of bath modes is possible with marvellous numerical effort, reduction of the number of bath modes by a few hundred dramatically speeds up the propagation. Thus, from a numerical point of, a second requirement to the discretization of the frequency axis is the minimization of the number of modes needed to converge to the continuum limit. Hence, discretizing a SD is subject to two contrasting requirements:

(i) the discretization converges to the continuous SD in the limit of an infinite number of modes

(ii) the number of bath modes included shall be as small as possible, for the sake of numerical feasibility and efficiency.

To fulfill the first requirement, a rather arbitrary frequency density $\rho_f(\omega)$ can be chosen, which determines the distribution of the discrete frequencies. While the specific choice of the FD should not influence the result *if enough modes are included*, as shown in the following, for a finite number of modes the particular choice of the FD significantly influences the reduced dynamics. Various kinds of densities can be found in the literature [134, 162, 163, 166, 219, 220], with varying depth of detail in explaining why the particular choice was used. This raises the question for a simple and useful criterion on the FD in order to yield a good approximation for the reduced dynamics.

Reduced descriptions, where the total density matrix is traced over the (infinitely many) environmental variables with continuous spectral density [198, 221], in general lead to non-Markovian evolution equations, whose memory kernel involves the bath correlation function (BCF) $C(\tau)$, to be defined readily, as a main ingredient [221, 222]. Since they consequently require an excellent approximation of the BCF, they typically utilize the BCF as a measure of the quality of the bath discretization (see

e.g. [223] and citations therein). The BCF is defined as

$$C(\tau) = \left\langle \left\{ \hat{\mathcal{H}}_{\mathrm{I}}(\tau), \hat{\mathcal{H}}_{\mathrm{I}}(0) \right\} \right\rangle_{\mathrm{B}}, \tag{4.56}$$

where $\hat{\mathcal{H}}_{\mathrm{I}}(\tau)$ is the bath coupling operator (4.4) in the interaction picture,

$$\hat{\mathcal{H}}_{\mathrm{I}}(\tau) = \exp\left[\mathrm{i}\tau\hat{\mathcal{H}}_{\mathrm{B}}\right] \hat{\mathcal{H}}_{\mathrm{I}} \exp\left[-\mathrm{i}\tau\hat{\mathcal{H}}_{\mathrm{B}}\right], \tag{4.57}$$

and $\{\cdot, \cdot\}$ denotes the anti-commutator. The BCF thus is the correlation function of the bath coupling operator in the interaction picture.

The average $\langle\rangle_{\mathrm{B}}$ in (4.56) is taken with respect to the bath being in thermal equilibrium at temperature T,

$$\langle \hat{A} \rangle_{\mathrm{B}} = \mathrm{tr}_{\mathrm{B}} \left[Z(\beta) \exp\left(-\beta\hat{\mathcal{H}}_{\mathrm{B}}\right) \hat{A} \right]. \tag{4.58}$$

Here, β is the inverse temperature (2.54) and $Z(\beta)$ is the inverse partition function (2.57). The BCF is calculated explicitly in App. E, along with further details. It reads

$$C(\tau) = \sum_{n=1}^{N} \lambda_n^2 \mathrm{e}^{-\mathrm{i}\tau\omega_n} \coth\left(\frac{\beta\omega_n}{2}\right). \tag{4.59}$$

Especially for $T = 0$, $\beta = \infty$ and thus the zero temperature BCF is given by

$$C(\tau) = \sum_{n=1}^{N} \lambda_n^2 \mathrm{e}^{-\mathrm{i}\omega_n\tau}. \tag{4.60}$$

By insertion of the discretization (4.7) one may obtain the continuous BCF at zero temperature as the half-sided Fourier transform of the continuous SD,

$$C(\tau) = \frac{1}{\pi} \int_0^\infty \mathrm{d}\omega\, J(\omega)\mathrm{e}^{-\mathrm{i}\omega\tau}. \tag{4.61}$$

Exact numerical methods are based on numerical representations of either the SD or the BCF. However, dealing directly with a general continuous SD (or the equivalent BCF) is mostly impossible, in general. Finite representations are required by either discretizing the SD or suitably expanding the BCF. In order to calculate the reduced dynamics up to a final time T it is sufficient to know the BCF up to that time [150]. Therefore, a suitable approximation of the BCF over the time interval of interest assures the exact reduced dynamics within an error bound controlled by the accuracy of the BCF approximation. Following the same line of arguments while discretizing the SD, one realizes that the required number of discrete modes increases dramatically with the maximum propagation time T.

It is worth stressing, therefore, that methods based on a discrete SD have been used successfully

[127, 134, 162, 163, 165, 166, 183] even in a regime where the number of modes is not sufficient to reproduce the BCF over a significant time interval. However, it seems difficult to give an *a priory* criterion on how to judge the quality of the discretization with respect to the reduced dynamics. From a numerical point of view, such a criterion would be of great interest. Ideally, the large freedom on how to perform the discretization could be used to minimize the error of the reduced dynamics for a given number of environmental modes.

Under the premise that it is the BCF whose optimal reproduction ensures optimal reproduction of the system dynamics, as alternative to the FD a discretization can be obtained by employing Gauss-quadrature for the defining integral of the BCF

$$C(\tau) = \frac{1}{\pi} \int\limits_0^\infty \mathrm{d}\omega \, J(\omega) \mathrm{e}^{-\mathrm{i}\omega\tau} \approx \sum_{n=1}^N \lambda_n^2 \mathrm{e}^{-\mathrm{i}\omega_n\tau}. \tag{4.62}$$

At first sight, the integral bounds $(0, \infty)$ require Gauss-Laguerre quadrature. However, since $J(\omega)$ is effectively different from zero only in a region $\omega \in [0, \Omega]$, also other kinds of Gauss quadratures may be used. In all cases, for a given number of bath modes N the quadrature scheme gives τ-independent nodes ω_n (the zeros of the polynomial connected to the chosen quadrature) and weights $\gamma_n > 0$ such that

$$\int\limits_0^\infty \mathrm{d}\omega \, f(\omega) \approx \sum_{n=1}^N \gamma_n f(\omega_n). \tag{4.63}$$

In our case, $f(\omega) = \frac{1}{\pi} J(\omega) \mathrm{e}^{-\mathrm{i}\omega\tau}$, leading to the desired discretization (4.62) with couplings

$$\lambda_n^2 = \frac{1}{\pi} \gamma_n J(\omega_n). \tag{4.64}$$

One can show that a Gaussian quadrature with N nodes *basically exactly* [223] reproduces the BCF on a time interval $[0, T]$ if

$$T \leq \frac{4N}{\Omega}. \tag{4.65}$$

Before we turn to actual quantum dynamics, let us compare the outlined strategies with respect to the resulting BCF for zero temperature. For the continuous SD given by (4.47) it can be calculated explicitly from (4.61),

$$C(\tau) = \frac{1}{\pi} \int\limits_0^\infty \mathrm{d}\omega \, J(\omega) \mathrm{e}^{-\mathrm{i}\omega\tau} = \frac{\alpha\omega_c^2 \Gamma(s+1)}{2(1 + \mathrm{i}\omega_c\tau)^{s+1}}, \tag{4.66}$$

where $\Gamma(s+1)$ is the Gamma function.

Reduced descriptions lead to non-Markovian evolution equations whose memory kernel involves the

BCF as a main ingredient. While they consequently require an excellent approximation of the BCF, its role for an explicit approach like the multi Davydov-Ansatz is not clear. In order to draw contact between the two fundamentally different approaches, we will compare the quality of the approximation of the SD at the level of the BCF, by comparing discretized (4.60) and continuous (4.66) version. We shall see, however, that the BCF is not an appropriate measure of the quality of the approximation for the multi Davydov-Ansatz (see [218] and figures therein for further details).

For the density approach, we specifically choose $\rho_{\mathrm{f}}(\omega) \sim \mathrm{e}^{-\omega/\omega_c}$ as given in [163, 166] and $\rho_{\mathrm{f}}(\omega) \sim J(\omega)/\omega$, as given in [134] (see left panel of Fig. 4.22). In Fig. 4.23, we consider $\rho_{\mathrm{f}}(\omega) \sim J(\omega)$. For the Gauss quadrature we choose Gauss-Legendre as given in [223] and Gauss-Laguerre (see right panel of Fig. 4.22).
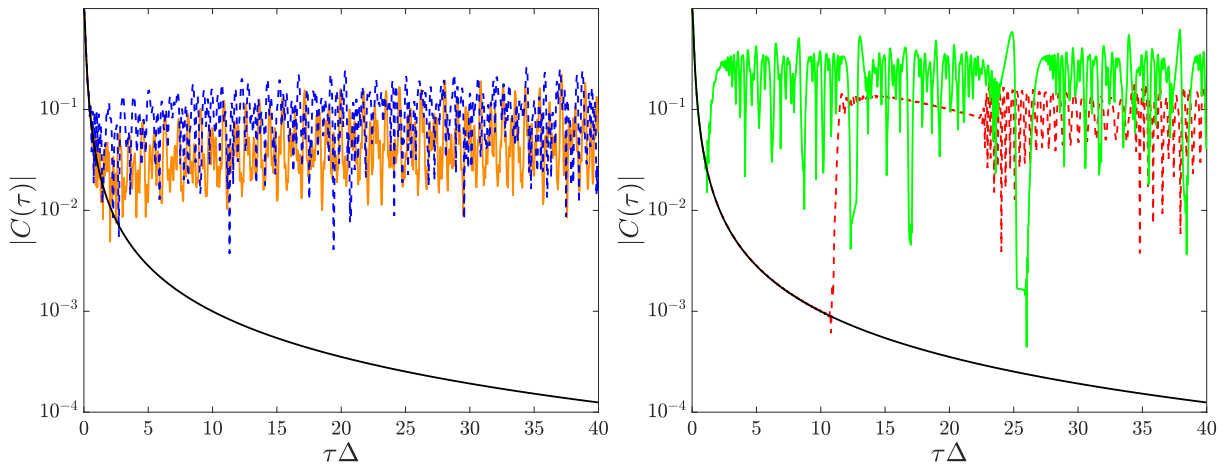
Figure 4.22.: The BCF for different discretizations with $N = 200$ for a sub-Ohmic SD with $s = 0.5$ is shown. All discretizations initially follow the algebraic decay of the BCF. The discretizations via density of frequencies (left panel) do not show obvious recurrences. The discretizations by Gauss quadrature follow the exact algebraic decay longer, but then show strong recurrences.

All discretizations lead to very good agreement with the exact BCF for short times and, for $N = 200$, to deviations of the order of 1% for long times (note the logarithmic scale of the y-axis of the figures). Among the densities, the exponential choice performs better, both in initial and longer time agreement. The Gauss quadrature methods follow the exact decay of the BCF for a longer time, but then show strong jump-like recurrences.

The Laguerre quadrature is designed to integrate over $\omega \in (0, \infty)$. Thus, only a few of the nodes ω_k are in the region of significant $J(\omega)$. The corresponding BCF therefore shows strong recurrences, as visible in the right panel of Fig. 4.22 (green line).

Most of the frequencies found from the Legendre quadrature are located at the bounds of the interval, where they have small weight λ_k^2. Consequently, for this quadrature method, too, only few frequencies effectively contribute to the BCF, explaining the strong recurrences. Nevertheless, the Legendre quadrature gives by far the best agreement for the longest initial time interval (see right panel of 4.22 (red dashed line)). In the left panel of Fig. 4.23 we have plotted the BCF resulting from a discretization in terms of Legendre quadrature, for different intervals $[0, n\omega_c]$ ($n = 3, 4, 5, 6, 7$) on

which the quadrature nodes are calculated. It is interesting to note that the longer the interval, the earlier the jump but also the better the approximation of the SD before the jump. As we will see subsequently, the jump in the BCF corresponds to a jump in the deviation of the system dynamics. Furthermore, as soon as a stronger deviation on the BCF level can be found also a stronger deviation in the system dynamics is observed. Thus, the length of the interval is another parameter entering the Legendre quadrature which determines the quality of the approximation, requiring an intermediate value optimizing between deviation and jump.

From the non Markovian quantum state diffusion equation [150] it is clear that an ideal discretization should for a long time follow the BCF without showing recurrences. As can be seen from (4.9) and (4.11), choosing $\rho_f(\omega) \sim J(\omega)$ leads to equal couplings λ_k^2 of all modes. As all modes contribute equally to the BCF, we expect this discretization to exhibit the longest recurrence time (given the irregular distribution of the ω_k as determined from (4.10)). The corresponding BCF is plotted in the right panel of Fig. 4.23 (blue dashed line), together with the discretization with the exponential density of frequencies (taken from Fig. 4.22, full orange line). As is apparent from this figure, the resulting BCF is indeed slightly improved (we tried many other discretizations, without further improvement). We will later see and discuss, however, that the corresponding quantum dynamics turns out far worse, surprisingly. In contrast to reduced density approaches, methods based on a discretized SD yield a
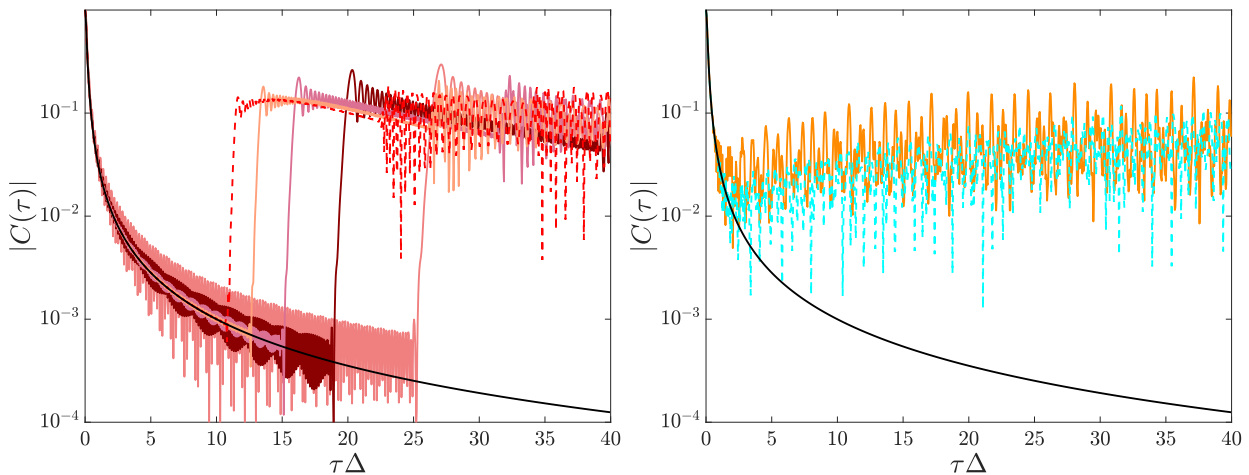

Figure 4.23.: The BCF for different discretizations with $N = 200$ for a sub-Ohmic SD with $s = 0.5$ is shown. Left panel: discretizations with Legendre quadrature, for different intervals $[0, n\omega_c]$ ($n = 3, 4, 5, 6, 7$) on which the quadrature nodes are calculated (the longer the interval, the earlier the jump). Right panel: discretization with $\rho_f(\omega) \sim J(\omega)$ is shown (blue, dashed), in comparison to an exponential FD (orange, full).

representation of the BCF with purely oscillating terms. A finite sum of such exponentials does not decay asymptotically, at all. In that sense do the multi Davydov-Ansatz as well as the ML-MCTDH method and reduced density methods approach the approximation of the bath from different ends. Nonetheless, valid results have been obtained using discrete baths, even though the BCF is only recovered for fairly short times compared to propagation time. This can be seen from Fig. 4.24, where the exact dynamics is reproduced with $N = 200$ bath modes on the time-interval $t\Delta \in [0, 25]$,

whereas the BCF (orange line in left panel of Fig. 4.22) is only reproduced exactly for $t\Delta \in [0, 2]$. Since
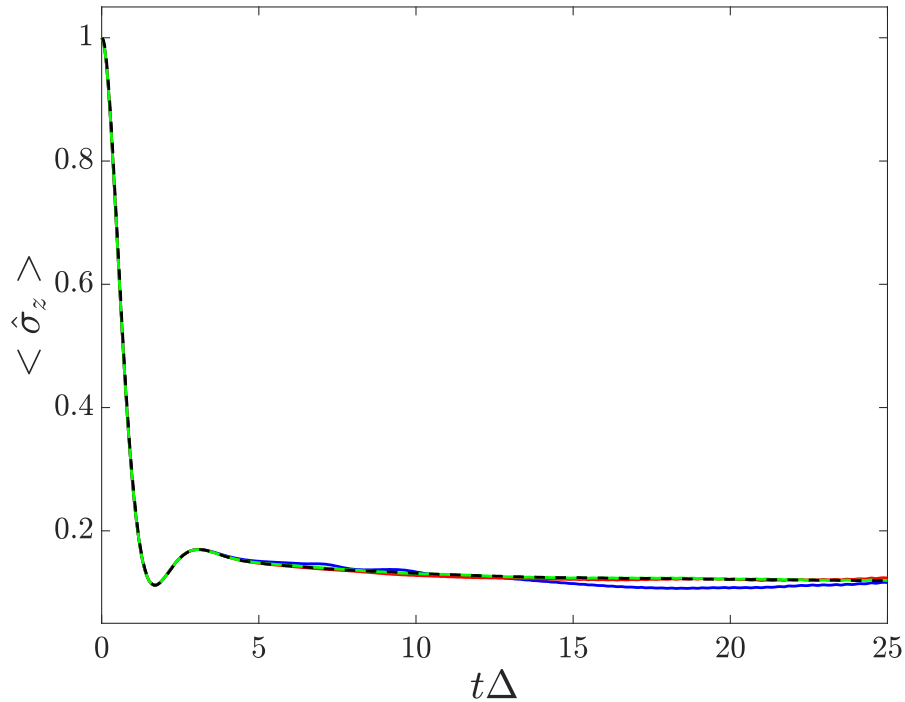
Figure 4.24.: Population dynamics of the spin for an environment with parameters $s = 0.5$, $\omega_c = 10\Delta$ and $\alpha = 0.2$ obtained via ML-MCTDH method[166] is shown (black dashed line). In addition, the dynamics gained from the multi Davydov-Ansatz is plotted for different multiplicities M ($M = 12$ blue line, $M = 18$ red line, $M = 24$ green line). As in the ML-MCTDH reference calculation, discretization of the SD was done with the exponential density of frequencies $\rho_{\mathrm{f}}(\omega) \sim \mathrm{e}^{-\omega/\omega_c}$. Convergence was reached over the time-interval of interest for $M = 24$ with $N = 200$ bath modes.

the system dynamics is nontrivial only during a short initial time span, one might conclude from this result that for explicit methods it is sufficient if the BCF is reproduced exactly in a correspondingly short time interval. The main requirement for the discretization then would be not to exhibit strong recurrences. In Fig. 4.25, the dynamics corresponding to the other discretizations considered so far reveals that this expectation fails spectacularly. The dynamics corresponding to Gauss quadrature discretizations coincides with the exact dynamics as long as the BCF is represented exactly, and the recurrences in the BCF mark the time from which on deviations from the exact dynamics can be observed. Highly surprisingly, the dynamics of the various discretizations via FD are completely different, although all FD methods apparently coincide reasonably well on the level of the BCF (see Fig. 4.22 left panel and Fig. 4.23).

Furthermore, the BCF for the Legendre method coincides much longer with the exact one than the one corresponding to the exponential FD. This is not reflected at all in the quantum dynamics of the open system. We conclude that in drastic contrast to reduced descriptions, for explicit methods based on discretized SDs, the quality of the BCF is not the appropriate measure for the choice of the discretization. Still, it is true that if the BCF is reproduced exactly up to a time T, then also the dynamics is reproduced exactly up to that time - but not vice versa.
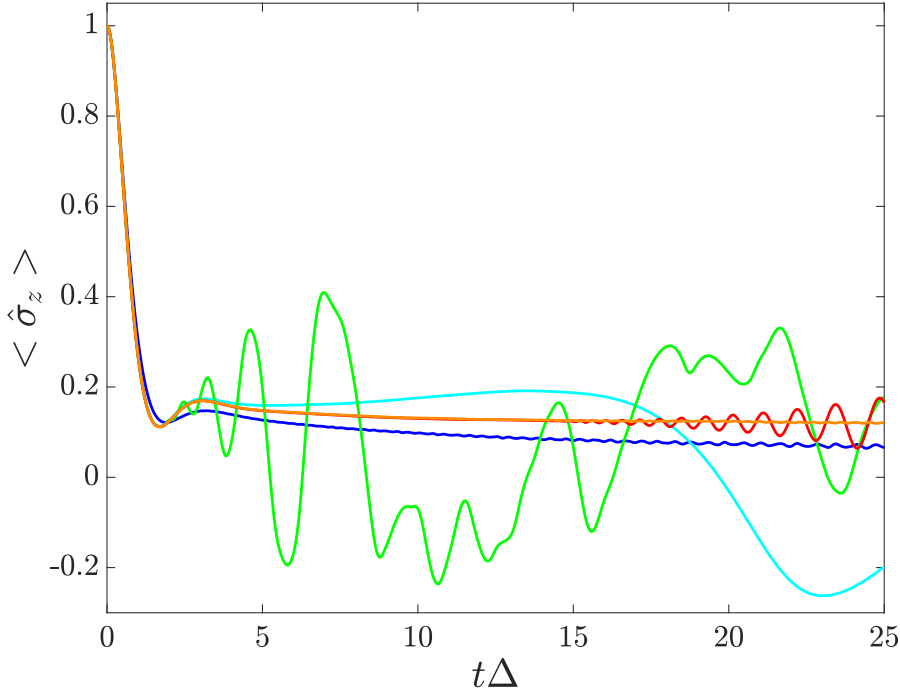
Figure 4.25.: Population dynamics of the spin for an environment with parameters $s = 0.5$, $\omega_c = 10\Delta$ and $\alpha = 0.2$ obtained with the multi Davydov-Ansatz via $\rho_{\mathrm{f}}(\omega) \sim \mathrm{e}^{-\omega/\omega_c}$ is shown (full orange line) (convergence has been checked in Fig. 4.24), in comparison with the other discretizations ($\rho_{\mathrm{f}}(\omega) \sim \frac{J(\omega)}{\omega}$ blue solid, $\sim J(\omega)$ cyan solid, Laguerre green solid, Legendre red solid). For all other discretizations except the exponential one, recurrences become apparent (the multi Davydov-Ansatz has been employed with $M = 14$ and $N = 200$ bath modes).

It seems to some extent disappointing that, under the proposition of a fixed overall number of bath modes, all effort to improve on the discretization scheme with respect to the quality of the BCF does not result in more accurate dynamics as compared to the widely used exponential FD. The conclusion that a fairly low quality approximation of the BCF for longer times does not necessarily yield low quality dynamics may also allow more freedom in approximating the BCF in the time domain. Even more crucial, the question for an a-priory criterion to judge the quality of the approximations either in time or frequency domain arises. It seems natural to introduce a quantity which interpolates between the two domains. Thus, as a-priori indicator for the quality of a discretization of the SD, we utilize a windowed Fourier transform (WFT) of the BCF (see [218]) with a Gaussian window of width σ,

$$F_\sigma(\omega, t) := \int\limits_{-\infty}^{\infty} \mathrm{d}\tau \, N_\sigma(t - \tau) C(\tau) e^{\mathrm{i}\omega\tau}, \qquad N_\sigma(t - \tau) = \frac{\sqrt{\frac{\pi}{2}}\sigma - 1}{\sqrt{2\pi}\sigma} e^{-\frac{(t-\tau)^2}{2\sigma^2}} \quad . \tag{4.67}$$

The prefactor of the Gaussian was chosen such that in the limit $\sigma \to 0$ the BCF (with the additional phase $e^{\mathrm{i}(\omega t + \pi)}$) is recovered (as a function of time), $\sigma \to \infty$ yields the SD (as a function of frequency). The WFT is thus suited to capture properties of the bath in both time- and frequency domain. We gratefully thank Prof. Dr. Walter Strunz for bringing up for discussion the idea of the WFT.

The integral in the WFT can be evaluated directly in the discrete case,

$$F_\sigma(\omega, t) = \frac{\sqrt{\frac{\pi}{2}}\sigma - 1}{\sqrt{2\pi}\sigma} \int_{-\infty}^{\infty} d\tau \, \exp\left[i\omega\tau - \frac{(t-\tau)^2}{2\sigma^2}\right] C(\tau) \tag{4.68}$$

$$= \frac{\sqrt{\frac{\pi}{2}}\sigma - 1}{\sqrt{2\pi}\sigma} \sum_{k=1}^{N} \lambda_k^2 \int_{-\infty}^{\infty} d\tau \, \exp\left[i(\omega - \omega_k)\tau - \frac{(t-\tau)^2}{2\sigma^2}\right] \tag{4.69}$$

$$= \left(\sqrt{\frac{\pi}{2}}\sigma - 1\right) \sum_{k=1}^{N} \lambda_k^2 \exp\left[it\,(\omega - \omega_k) - \frac{1}{2}\sigma^2\,(\omega - \omega_k)^2\right], \tag{4.70}$$

simplifying numerical calculations dramatically. We found that for $N = 75$, none of the methods comes close to the exact values of the WFT. This coincides with the fact that for all of the discretization methods, $N = 75$ modes are too few to reproduce the dynamics properly. For $N = 150$, the section $\sigma = 30\frac{\Delta}{\omega_c}$ outstandingly predicts that the exponential discretization gives the best results for the dynamics, since the corresponding image coincides best with the one of the exact WFT.

We see that whenever $F_\sigma(\omega, t)$ of the approximation looks similar to $F_\sigma(\omega, t)$ obtained from the exact BCF in some region close the qubit frequency $\omega \approx \Delta$, the approximate dynamics and the exact dynamics look alike. This motivates to use F_σ with an intermediate σ leading to a nontrivial image of the WFT, rather than the BCF or the SD, to estimate the quality of the discretization. Further investigations in different regimes (small s vs. large s, small coupling vs. large coupling) have shown that, up to minimal gains, no discretization outperforms the exponential FD [161]. It is clear that the FD has to be governed by a good balance between dense sampling around the system frequency, no regular distribution, and no negligence of regions where the SD has support. In particular, the failure of the discretization $\rho_f \sim J(\omega)$ may be a result of the fact that only a few modes are distributed around the system frequency. This can be seen nicely in Figs. 4.27, 4.28, where the lower edge of the red rectangle is poorly represented (system frequency is Δ).
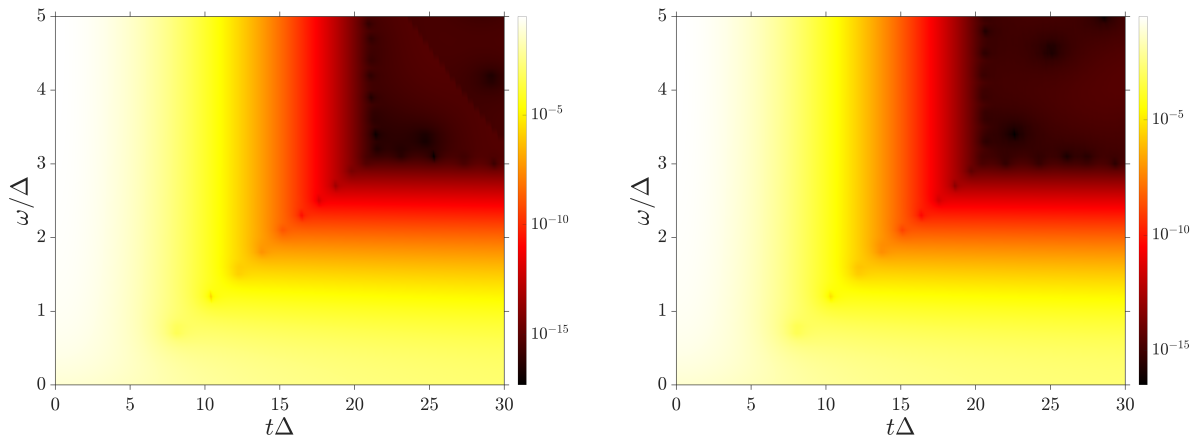
Figure 4.26.: Absolute value of the WFT for $\sigma = 100\frac{\Delta}{\omega_c}$. Exact (left panel) and for discretization with the FD $\rho_f(\omega) \sim e^{-\omega/\omega_c}$ (right panel).
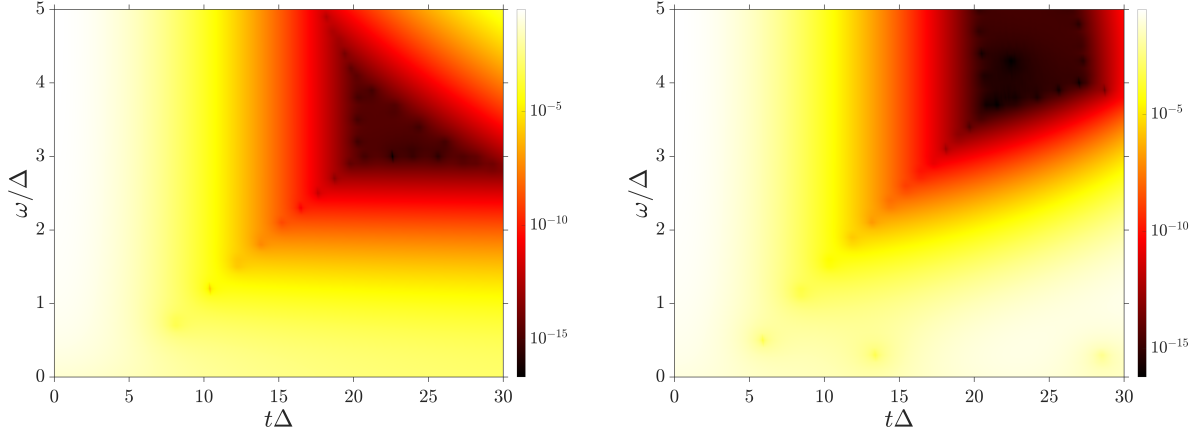
Figure 4.27.: Absolute value of the discrete WFT for $\sigma = 100\frac{\Delta}{\omega_c}$. Discretization with FD $\rho_{\mathrm{f}}(\omega) \sim J(\omega)/\omega$ (left panel) and $\rho_{\mathrm{f}}(\omega) \sim J(\omega)$ (right panel)
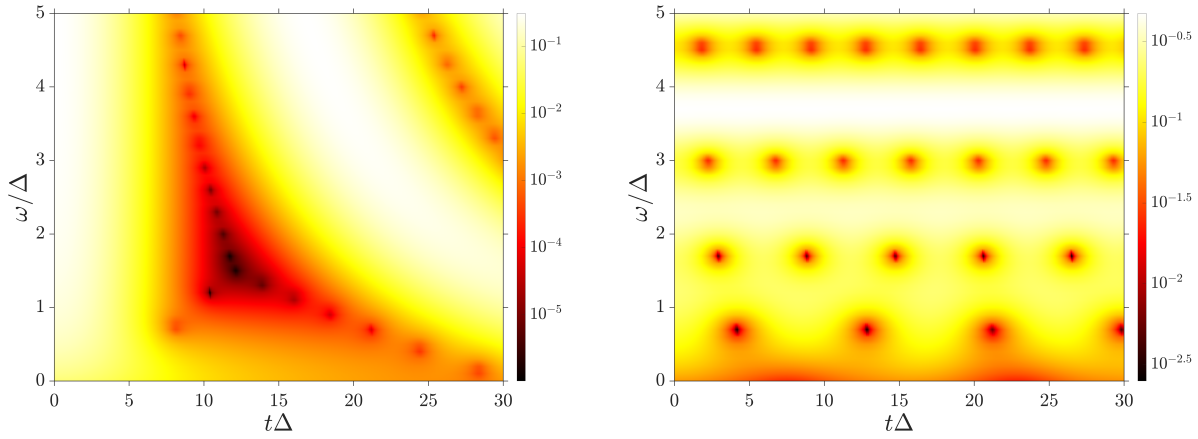
Figure 4.28.: Absolute value of the discrete WFT for $\sigma = 100\frac{\Delta}{\omega_c}$. Discretization with Laguerre quadrature (left panel) and Legendre quadrature (right panel).

It has turned out from our numerics that even if the BCF corresponding to the choice of frequencies looks very reasonable in the time domain, this does not prevent the reduced dynamics from severe, unphysical recurrences (see also [223]). We therefore found the WFT to be an alternative priori criterion to judge the quality of the reduced dynamics. By investigating its information content in the intermediate σ regime combines both, time as well as frequency domain characteristics of the bath correlation, we have found that whenever the WFT shows reasonable agreement with the exact result, also the ensuing dynamics of the open quantum system is reliably reproduced. This fact is in no way tied to the dynamical method that has been used (multi Davydov-Ansatz), because the same conclusions can be drawn from an integrable model as shown in [218]. We may thus hope that the WFT opens up a path towards even more efficient representations of general open quantum system dynamics.

In this section we have shown that in the sub-ohmic case $s < 1$, among the many discretizations

considered the exponential discretization $\rho_f(\omega) \sim e^{-\omega/\omega_c}$ is optimal in the sense that it converges the quickest to the continuum limit, i.e. with the fewest environmental modes required. Comparing discrete and continuous WFT also in the ohmic and super-ohmic regime reveals that this seems to be a universal behaviour, since we always find the exponential FD to outperform the other discretizations. However, deviations between the multi Davydov method and the quasi-adiabatic path-integral method (QUAPI) [147, 148, 196] as well as the hierarchy of pure states method (HOPS) [159] have been found in [161, 218], in the case of non-zero temperature $T \neq 0$. We found that dramatically increasing the number N of bath modes annihilates the deviations between the multi Davydov-Ansatz and the HOPS method. This firstly seems to contradict the findings of the present section, and secondly raises the question for the origin of the deviations from the QUAPI method. We give reasoning for both in the next section.

4.5. The sub-ohmic case and the problem of oversampling

Despite the thorough convergence analysis of the multi Davydov method presented so far as well as its consistency with the ML-MCTDH approach, deviations between the multi Davydov method and the quasi-adiabatic path-integral method (QUAPI) [147, 148, 196] as well as the hierarchy of pure states method (HOPS) [161] have been found in [161, 218], in the case of non-zero temperature.

As outlined in Sec. 3.7, non-zero temperature can be treated by a sampling of stochastic initial conditions. There, shifted initial conditions are propagated with the multi Davydov-Ansatz on the wave-function level, turning the total density and thermal expectation values into stochastic averages over the sampled wave functions. Since the shifted initial conditions are propagated as for zero temperature and since the WFT is independent from the initial condition (see Eq. (4.67)), we expect the considerations of the previous section to be valid also in the non-zero temperature case.

By dramatically increasing the number N of bath modes, we found coincidence between the HOPS method and the multi Davydov method for $N = 1200$ environmental modes also in the case of non-zero temperature, for an exponential discretization of the frequency axis. This seems to contradict the validity of the WFT as measure of the quality of the discretization, since it predicts the dynamics obtained from an exponential discretization of the frequency axis to coincide with the exact result for $N = 200$ modes.

In order to resolve this contradiction and to highlight the interplay between the initial condition and the number of bath modes required to converge to the continuum limit, we examine here in more detail the impact of initial shifts on the dynamics of the multi Davydov-Ansatz wave-function. To this end, we investigate the so-called polarized initial condition (to be defined readily) in the case of zero temperature.

4.5.1. On the polarized initial condition

In the case of zero temperature, we have assumed up to now the system to be in the excited state and the bath to be in its ground state initially, see Eq. (4.48). In contrast to this so-called factorized

initial condition $\hat{\rho}(0) = |+\rangle \langle+| \, |\mathbf{0}\rangle \langle\mathbf{0}|$, it is natural to assume the bath distribution to be equilibrated to the initial system state $|+\rangle$ in the case of non-zero temperature,

$$\hat{\rho}(0) = \hat{\rho}_{\mathrm{S}}(0) \left(\mathrm{tr}_{\mathrm{B}} \left[\exp\left[-\beta\left(\hat{\mathcal{H}}_{\mathrm{B}} + \hat{\mathcal{H}}_{\mathrm{I}}\right)\right]\right]\right)^{-1} \exp\left[-\beta\left(\hat{\mathcal{H}}_{\mathrm{B}} + \hat{\mathcal{H}}_{\mathrm{I}}\right)\right]. \tag{4.71}$$

In this so-called polarized initial state, β is the inverse temperature (2.54), and $\hat{\mathcal{H}}_{\mathrm{B}}$ and $\hat{\mathcal{H}}_{\mathrm{I}}$ are bath- and bath-interaction-Hamiltonian (see (4.2) and (4.4)). It is the natural ground state provided that the system is initially in the state $\hat{\rho}_{\mathrm{S}}(0)$.

Even in the case of zero temperature polarized and factorized initial condition do not coincide, since for $T = 0$ the polarized initial condition reduces to (see App. F)

$$\hat{\rho}(0) = \hat{\rho}_{\mathrm{S}}(0)\hat{D}_{\mathbf{C}}^{\dagger} |\mathbf{0}\rangle \langle\mathbf{0}| \hat{D}_{\mathbf{C}}, \tag{4.72}$$

where

$$\mathbf{C}_n = \frac{\lambda_n}{\omega_n}, \tag{4.73}$$

corresponding to a shifted initial bath state

$$\Psi_{\mathrm{B}}(0) = \hat{D}_{\mathbf{C}}^{\dagger} |\mathbf{0}\rangle. \tag{4.74}$$

Provided the bath initial state is polarized, the authors of [224] have shown that in nonequilibrium coherences exist in the case of zero temperature even when strong dissipation forces the thermodynamic state of the system to behave almost classically. Corresponding results are shown in Fig. 4.29, where the exact results are obtained for a multiplicity $M = 10$ for all given coupling strengths.

Analogous to the findings of Secs. 4.3.2 the small number of CS needed for convergence is remarkable, especially since dynamics is investigated here in the ultra-strong coupling regime where the bath dynamics is expected to be highly complicated. However, it should be noted that the time-axis is scaled here with ω_c, i.e. is x times shorter for the cutoff frequency scaled as $\omega_c = x\Delta$ compared to the results presented in Sec. 4.3.2.

The complexity of the dynamics is substantiated by the finding that CS coming close dominates the numerical calculations in this ultra strong coupling regime. It turns out that CS approaching occurs in each propagation, forcing the integrator to stop due to tiny step-sizes caused by singularities in the coefficient matrix if no apoptosis was implemented. With apoptosis implemented, propagation may be continued for times that are longer by an order of magnitude and beyond. It is remarkable that the number of CS coming close during propagation is not related to the multiplicity M nor the coupling strength in an obvious way: propagation with increased M may cope without apoptosis, or with more or fewer CS connected. Thus, in the presence of apoptosis convergence can be checked by increasing the multiplicity M in a systematic way. Furthermore, although it reduces the flexibility of the Ansatz, one infers from Fig. 4.29 that this does not negatively affect the convergence, since also
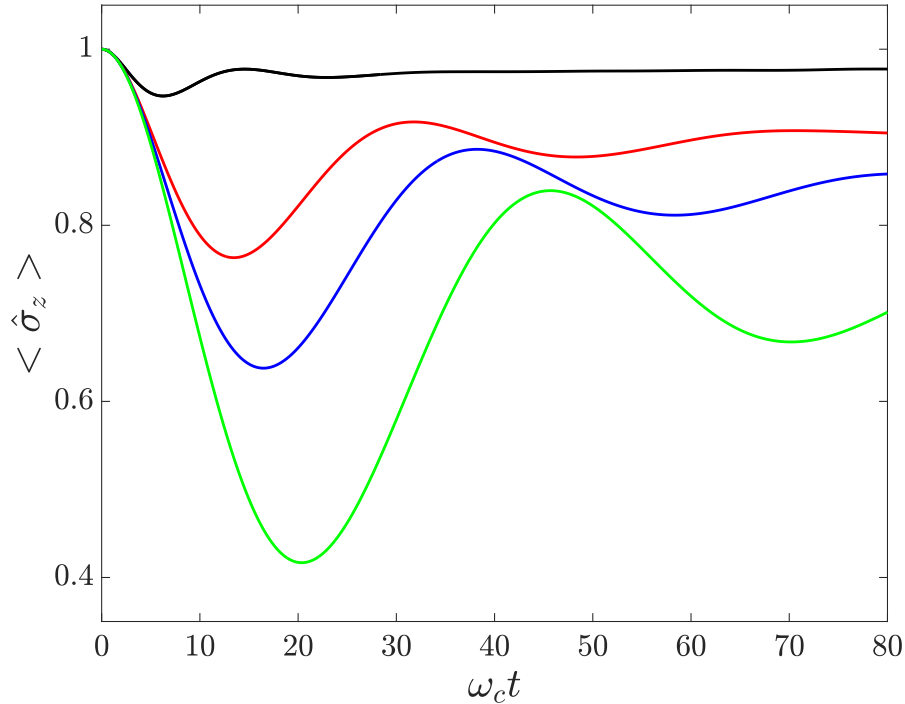
Figure 4.29.: Dynamics of the population $< \hat{\sigma}_z >$ for $N = 300$ modes for the FD $\rho_f \sim \frac{J(\omega)}{\omega}$ as well as $N = 150$ bath modes for the exponential FD. Multiplicity is $M = 10$, for different coupling strengths:, $\alpha = 0.03$: $\omega_c t = 22.3$ (green line), $\alpha = 0.04 : \omega_c t = 34.3$ (blue line), $\alpha = 0.05 : \omega_c t = 12.8$ (red line), $\alpha = 0.1 : \omega_c t = 28.6$ (black line).

after the apoptosis event the result stays converged.

It turns out that a huge number of bath modes $N = 4000$ is required to converge the result if the exponential FD $\rho_f \sim \mathrm{e}^{-\omega/\omega_c}$ is used, while only $N = 300$ modes suffice to converge the result if the FD $\rho_f \sim \frac{J(\omega)}{\omega}$ is used. This seems to contradict the findings of Sec. 4.4 since there the exponential FD turned out to outperform the FD $\rho_f \sim \frac{J(\omega)}{\omega}$, which was confirmed at the level of the WFT (see Figs. 4.26 and 4.27). Especially, the WFT (4.67) does not depend on the initial condition.

This conundrum can be resolved in the following way. It is of utmost importance that the SD $J(\omega)$ is defined for $\omega \in [0, \infty]$, while the initial shifts of the bath modes (4.74) diverge as $\omega_n \to 0$ (see Eq. (4.73)) if the couplings do not decay to zero quickly enough. This is indeed the case in the sub-ohmic regime $s < 1$ where $\lambda_n^2 \sim J(\omega_n) \sim \omega_n^s$ for $\omega_n \to 0$, see (4.7). Due to this divergence the small modes have to be vastly oversampled in order to correctly display the bath dynamics. While the FD $\sim \frac{J(\omega)}{\omega} \sim \omega^{s-1}$ equally diverges for $\omega \to 0$ in the sub-ohmic regime, leading to an appropriate oversampling of the small frequencies, this is not the case for the exponential FD $\sim \mathrm{e}^{-\omega/\omega_c}$. This explains why with the former FD one manages to converge to the continuum limit with a much smaller number of modes.

In Sec. 4.4 we found that, for the factorized initial condition, $N = 200$ modes suffice with the exponential FD to converge to the continuum limit, while $N = 300$ modes are required to converge to the continuum limit with the FD $\rho_f \sim \frac{J(\omega)}{\omega}$. We thus infer that, with an appropriate implementation,

also for the polarized initial condition convergence with at most $N = 200$ modes with the exponential FD should be attainable. We subsequently outline how to avoid the problem of oversampling of small frequencies.

Alternatively to propagating shifted initial conditions (4.74),

$$|\Psi_{\mathrm{D2}}^{\mathrm{M}}(\boldsymbol{\alpha}, t)\rangle = \mathcal{T} \exp\left[\int\limits_0^t \mathrm{d}t'\, \hat{\mathcal{H}}(t')\right] \hat{D}_{\mathbf{C}}^\dagger |\mathbf{0}\rangle , \tag{4.75}$$

the initial shifts translate to a shifted Hamiltonian even in the case where the Hamiltonian is time-dependent:

$$|\Psi(t)\rangle = \hat{D}_{\mathbf{C}}^\dagger \mathcal{T} \exp\left[\int\limits_0^t \mathrm{d}t'\, \hat{D}_{\mathbf{C}} \hat{\mathcal{H}}(t') \hat{D}_{\mathbf{C}}^\dagger\right] |\mathbf{0}\rangle . \tag{4.76}$$

While this unitary transformation leaves the system Hamiltonian $\hat{\mathcal{H}}_{\mathrm{S}}$ unchanged, it changes bath and interaction part according to

$$\hat{\mathcal{H}}_{\mathrm{B}} = \sum_{n=1}^N \omega_n (\hat{a}_n^\dagger - \mathbf{C}_n)(\hat{a}_n - \mathbf{C}_n), \tag{4.77}$$

$$\hat{\mathcal{H}}_{\mathrm{I}} = \sum_{n=1}^N \lambda_n \left(\hat{a}_n^\dagger + \hat{a}_n - 2\mathbf{C}_n\right). \tag{4.78}$$

From the interaction part $\hat{\mathcal{H}}_{\mathrm{int}} = \hat{L}\hat{\mathcal{H}}_{\mathrm{I}}$, a further term

$$-\hat{L} \sum_{n=1}^N 2\mathbf{C}_n \lambda_n = -2\hat{L} \sum_{n=1}^N \frac{\lambda_n^2}{\omega_n} \tag{4.79}$$

contributing only at the system level arises. Although they have to be oversampled if the shifted initial condition is propagated, we expect almost none of the (very) small frequencies to contribute to the dynamics. In the shifted Hamiltonian picture we thus infer that oversampling the small frequencies may be required *only* in order to correctly display the contribution (4.79) at the system level. Instead of converging it simultaneously with the number of bath modes N, we can do the limit separately by drawing contact with the continuous SD (4.7) according to

$$\sum_{n=1}^N \frac{\lambda_n^2}{\omega_n} = \frac{1}{\pi} \int\limits_0^\infty \mathrm{d}\omega\, \frac{J(\omega)}{\omega} = \Lambda, \tag{4.80}$$

resulting in the expression for the reorganization energy (4.29). Especially if the SD is of standard-form (4.47), then

$$\Lambda = \frac{\alpha \omega_c}{2} \Gamma(s). \tag{4.81}$$

In this manner the system contribution in the shifted Hamiltonian picture is replaced with its continuum limit independently of the discretization of the continuous SD. Still convergence of the dynamics with respect to the number of bath modes has to be checked. Indeed, if the dynamics is governed by the shifted Hamiltonian where the additional system contribution is replaced with its continuum limit according to (4.81), then $N = 150$ modes suffice to converge the result if the exponential FD $\rho_{\rm f}(\omega) \sim {\rm e}^{-\omega/\omega_c}$ is used to discretize the bath, in nice compliance with the results of Sec. 4.4.

Before we investigate how this finding translates to the non-zero temperature case, an important remark seems in place. Although it does not play any role for the dynamics in the SBM as studied here due to $\hat{L}^2 = 1$, an analogous procedure may be required for the counter term (4.45),

$$\hat{\mathcal{H}}_{\rm CT} = \hat{L}^2 \sum_{n=1}^{N} \frac{\lambda_n^2}{\omega_n} = \frac{\Lambda}{4} \hat{L}^2, \tag{4.82}$$

if it would be due to a system coupling operator $\hat{L}^2 \neq 1$.

4.5.2. On the treatment of non-zero temperature

While the method as outlined in Sec. 3.7 has been used successfully in the sub-ohmic case [137], from the considerations of the previous section we infer that the deviation between the HOPS and the multi Davydov-Ansatz found in [218] originates from the initial shifts, introduced by the initial value sampling in the non-zero temperature case (see Sec. 3.7). The results of the previous section directly translate to the case of finite temperature, since analogously the width σ_n^2 of the Gaussian distribution one has to sample from (see (3.71)) fulfills

$$\lim_{\omega_n \to 0} \sigma_n^2 = \infty, \tag{4.83}$$

i.e. it is large for the small frequency modes. Two important conclusions can be drawn. Firstly, in order to converge the stochastic sampling, many samples have to be drawn for the small modes. Secondly, in order to correctly display the influence of the thermal initial bath state on the dynamics, many small frequency modes have to be included in the discretization of the SD. In the spirit of the previous section, we attempt to circumvent these two issues by translating the stochastic sampling of initial conditions to a stochastic family of Hamiltonians. Instead of propagating shifted initial

conditions drawn from the distribution (3.68),

$$|\Psi_{\mathrm{D2}}^{\mathrm{M}}(\boldsymbol{\alpha}, t)\rangle = \mathcal{T} \exp\left[\int\limits_0^t \mathrm{d}t' \, \hat{\mathcal{H}}(t')\right] |\boldsymbol{\alpha}\rangle \, |\Psi_{\mathrm{sys}}(0)\rangle, \tag{4.84}$$

the initial shifts $|\boldsymbol{\alpha}\rangle = \hat{D}_{\boldsymbol{\alpha}} |\mathbf{0}\rangle$ translate to a stochastic Hamiltonian

$$|\Psi(t)\rangle = \hat{D}_{\boldsymbol{\alpha}} \mathcal{T} \exp\left[\int\limits_0^t \mathrm{d}t' \, \hat{D}_{\boldsymbol{\alpha}}^\dagger \hat{\mathcal{H}}(t') \hat{D}_{\boldsymbol{\alpha}}\right] |\mathbf{0}\rangle \, |\Psi_{\mathrm{S}}(0)\rangle, \tag{4.85}$$

introduced in the present context in [161]. Again this unitary transformation leaves the system Hamiltonian $\hat{\mathcal{H}}_{\mathrm{S}}$ unchanged, but changes bath and interaction part according to

$$\hat{\mathcal{H}}_{\mathrm{B}} = \sum_{n=1}^N \omega_n (\hat{a}_n^\dagger + \alpha_n^*)(\hat{a}_n + \alpha_n), \tag{4.86}$$

$$\hat{\mathcal{H}}_{\mathrm{I}} = \sum_{n=1}^N \lambda_n \left(\hat{a}_n^\dagger + \alpha_n^* + \hat{a}_n + \alpha_n\right). \tag{4.87}$$

From the interaction part $\hat{\mathcal{H}}_{\mathrm{int}} = \hat{L}\hat{\mathcal{H}}_{\mathrm{I}}$, a further term

$$\hat{L} \sum_{n=1}^N \lambda_n \left(\alpha_n^* + \alpha_n\right) \tag{4.88}$$

contributing only at the system level arises, and again the connection with the continuous SD may be drawn: since the α_n are Gaussian distributed with mean 0 and variance σ_n^2, the system contribution $\sum_{n=1}^N \lambda_n \alpha_n$ is also Gaussian distributed with mean 0 and variance $\sum_{n=1}^N \lambda_n^2 \sigma_n^2$. Insertion of the discretization of the SD (4.7) yields

$$\sum_{n=1}^N \lambda_n^2 \sigma_n^2 = \frac{1}{\pi} \int\limits_0^\infty \mathrm{d}\omega \, J(\omega) \sigma^2(\omega), \tag{4.89}$$

where $\sigma^2(\omega) = \frac{1}{2}\left(\mathrm{e}^{\beta\omega} - 1\right)^{-1}$. Sampling the stochastic system Hamiltonian from the continuum distribution again means that the continuum limit is performed independently of the discretization of the bath. At the same time, the contributions α_n to the bath Hamiltonian (4.86) in the shifted picture have to be drawn according to the discretized distribution. But the α_n drawn from the discretized distribution are correlated with the corresponding contribution to the discretized system contribution, and thus system and bath contributions can not be drawn independently. On the other hand, a large number of modes contributes to the continuum limit (4.89), and thus one may also argue that the resulting sum is only weakly correlated to the individual discretized values. Alternatively, however, in order to better approximate the system contribution, one may choose $N' \gg N$ and discretize the

frequency axis into N' modes $\{\tilde{\omega}_1, \ldots, \tilde{\omega}_{N'}\}$. Then a good approximation to the continuous system contribution (4.88) can be calculated with the corresponding couplings and initial displacements. Subsequently one again discretizes the frequency axis into N modes $\{\omega_1, \ldots, \omega_N\}$, and keeps only those $\tilde{\omega}_j$ which are close to the latter ones, $\{\tilde{\omega}_{i_1}, \ldots, \tilde{\omega}_{i_N}\}$. Both ideas have been implemented, the results are shown in Fig. 4.30. Indeed, *exact* coincidence of the multi Davydov-Ansatz with the HOPS
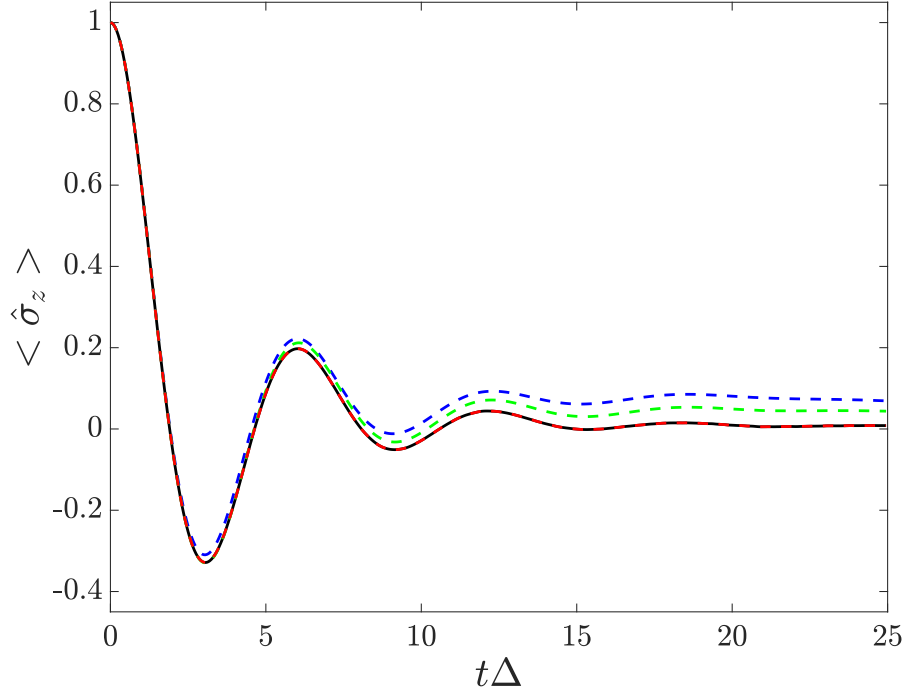
Figure 4.30.: Convergence of the multi Davydov-Ansatz to the result of the HOPS method (black solid), for $s = 0.25, \omega_c = 20\Delta, \alpha = 1.3\alpha_c)$, for non-zero temperature $T = 0.2\Delta$. Results have been converged with $M = 11$, $N = 200$. The numbers of samples are 1500 (blue dashed), 3000 (green dashed), 4500 (red dashed).

result can be achieved with both ways of translating the stochastic sampling of initial conditions to a family of stochastic Hamiltonians. The non-zero asymptotic value obtained from both methods seems reasonable, because the coupling strength was chosen larger than the critical coupling [217] $\alpha_c = 0.022$, which corresponds to dynamics in the localized phase at zero temperature.

A third possible approach, used by QUAPI, for instance, is based on a discrete evaluation of the memory integral over the BCF in the time domain. While recently QUAPI has been combined with matrix product states [225] aiming at circumvention of this issue, the long-time tails of the BCF are in the original approach necessarily poorly represented. The non-zero temperature BCF

$$C(\tau, \beta) = \frac{2\alpha\omega_c^2\Gamma(s+1)}{(\beta\omega_c)^{s+1}}\left(z^{-(s+1)} + 2\mathrm{Re}\big(\zeta(s+1, z+1)\big)\right)$$
$$z := \frac{1 + \mathrm{i}\omega_c\tau}{\beta\omega_c}, \tag{4.90}$$

where ζ denotes the Hurwitz zeta function and β is inverse temperature, decays even slower than at zero temperature, substantiating the issue. The results of [218] confirm consistency of the hierarchy of pure states (HOPS) and the multi Davydov method, while slight deviations to the QUAPI results in [226] are noticed. We believe that these deviations have their origin in the effectively finite bath correlation time which is an intrinsic feature of all methods that replace the memory integral by a finite sum. Therefore, neglecting the long-time tails in the BCF altogether might well lead to the observed discrepancies.

It is of utmost importance that in both cases, if stochastic initial conditions as well as if a family of stochastic Hamiltonians is propagated, CS approach frequently during the propagation. Thus, in order to sample in a stable and efficient way, implementation of apoptosis is unconditionally required. If it was not, the vast majority of propagations would not complete due to tiny integrator steps, and not all samples could be included. Consequently, only small temperature could be treated reliably without apoptosis. With apoptosis, all propagations complete successfully, and hence also large temperatures can be treated (see Sec. 5.4).

Finally we have verified the optimality of the exponential FD in almost any possible case, in the ohmic and sub-ohmic regime in both the zero and non-zero temperature regime. We shall therefore subsequently *always* apply the exponential FD in order to discretize the frequency axis. This allows, by means of the multi Davydov-Ansatz, for a sublime efficient convergence to the continuum limit with a small number of environmental modes.

We may, however, expect the number of CS required to exactly reproduce the reduced dynamics not to change dramatically if the bath is unitarily transformed. We have not yet utilized this gauge freedom, and we may hope that it is suited to further reduce the numerical effort required for the explicit treatment of the bath modes. In order to further minimize the number of bath modes, we shall exploit the mentioned gauge freedom in the next section where we detail the effect of a transformation of the bath into a linear chain.

4.6. The Effective Mode Representation

While typically the environment of an open quantum system is given in terms of a set of uncoupled modes each of which is coupled bilinearly to the system (see (4.6), an alternative approach to non-Markovian open system dynamics is based on the construction of a Mori-type hierarchy [227–229] of coupled effective environmental modes that is terminated by coupling the final member of the hierarchy to a Markovian bath [230–232]. The discretized spectral density is thus replaced by a series of approximate spectral densities involving an increasing number of effective modes. As the authors of [164, 233] have shown, the representation can be obtained starting from the system-bath Hamiltonian (4.6) and iteratively constructing the effective mode representation (EMR). In the final representation, the first effective mode couples to system and the second effective mode, while the second effective mode couples to the first and the third effective mode, and so forth. The construction guarantees the

accurate representation of the overall system-plus-bath dynamics for increasing time intervals with increasing chain lengths.

Formally a Markovian closure has to be included as final member of the hierarchy, but it can be shown that the Markovian closure is not necessary in order to exactly reproduce the dynamics up to a certain time, the latter depending only on the number of included modes. The transformation as given in [164, 233] can, however, not straightforwardly be reformulated in second quantization since it introduces artificial double excitations in the bath coordinates, resulting in artificial fluctuations around the exact result. The authors have furthermore pointed out that the factorized initial state of the bath modes does not remain factorized under the orthogonal transformation to the EMR. In frequency weighted coordinates, however, the factorized initial state remains factorized under the transformation. Here the EMR is rederived in (mass- and) frequency weighted coordinates which makes the reformulation of the transformed bath Hamiltonian in second quantization representation consistent. This idea has been put forward in the group of Prof. Dr. Peter Saalfrank, which will publish it soon.

Starting from the Hamiltonian (4.6), we first transform to frequency-weighted coordinates by replacing

$$Q_n := \sqrt{\omega_n} q_n, \qquad P_n := \frac{1}{\sqrt{\omega_n}} p_n. \tag{4.91}$$

The transformed creation and annihilation operators

$$\hat{A}_n^\dagger = \sqrt{\frac{1}{2\hbar}} \left(\hat{Q}_n - \mathrm{i} \hat{P}_n \right), \tag{4.92}$$

$$\hat{A}_n = \sqrt{\frac{1}{2\hbar}} \left(\hat{Q}_n + \mathrm{i} \hat{P}_n \right) \tag{4.93}$$

fulfill the standard commutation relation $\left[\hat{A}_n, \hat{A}_m^\dagger \right] = \delta_{nm}$. Their insertion into the Hamiltonian (4.1) interestingly leaves its form formally invariant. Thus we work on the same form, but keep in mind that we are working in frequency weighted coordinates.

In a first step one defines the effective coupling

$$\bar{C}_0 := \sqrt{\sum_{n=1}^N \lambda_n^2} \tag{4.94}$$

and the first effective mode creation and annihilation operator

$$\hat{B}_1^{(\dagger)} = \sum_{n=1}^N \frac{\lambda_n}{\bar{C}_0} \hat{a}_n^{(\dagger)}. \tag{4.95}$$

With these definitions, the bath interaction Hamiltonian (4.4) reads

$$\hat{\mathcal{H}}_\mathrm{I} = \bar{C}_0 \left(\hat{B}^\dagger + \hat{B} \right). \tag{4.96}$$

Thus the system couples to the first effective mode only. The transformation (4.95) does not affect the system Hamiltonian, but affects the bath Hamiltonian. In order to express the bath Hamiltonian in terms of the first effective mode, one attempts to find $N-1$ modes whose creation and annihilation operators fulfill the standard commutation relations. Thus one attempts to find an orthogonal transformation $T = t_{mn}$ with $m, n = 1, \ldots, N$ such that

$$\hat{a}_n^{(\dagger)} = \sum_{m=1}^{N} t_{nm} \hat{B}_m^{(\dagger)}. \tag{4.97}$$

While Eq. (4.95) defines the first column of the transformation T, the remaining columns are undetermined. In principle any orthogonal T with first column identical to (4.95) is a valid choice. Utilizing the Householder transformation, however, is a very natural choice since there from the first column all remaining columns are uniquely determined. For a given normalized $v \in \mathbb{R}^{N \times 1}$ the Householder matrix T is defined by $T = 1 - 2vv^T$. If v shall be such that the first column of T coincides with (4.95), one finds

$$v_1 = \sqrt{\frac{1}{2}\left(1 - \frac{\lambda_1}{\bar{C}_0}\right)}, \qquad v_j = -\frac{\lambda_j}{2v_1\bar{C}_0} \text{ for } j = 2, \ldots, N, \tag{4.98}$$

where it is easily verified that the such defined v is indeed real and normalized. Furthermore, since T is unitary,

$$\left[\hat{B}_m, \hat{B}_n^{\dagger}\right] = \delta_{mn}. \tag{4.99}$$

Insertion of (4.97) into the bath Hamiltonian leads to

$$
\begin{aligned}
\hat{\mathcal{H}}_{\text{B}} &= \sum_{n=1}^{N} \frac{\hbar\omega_n}{2}\left(\hat{a}_n^{\dagger}\hat{a}_n + \hat{a}_n\hat{a}_n^{\dagger}\right) \\
&= \sum_{m=1}^{N} \frac{\hbar}{2}\underbrace{\left(\sum_{n=1}^{N}\omega_n t_{nm}^2\right)}_{=:\tilde{\Omega}_m}\left(\hat{B}_m^{\dagger}\hat{B}_m + \hat{B}_m\hat{B}_m^{\dagger}\right) + \sum_{m<l}^{N} \hbar\underbrace{\left(\sum_{n=1}^{N}\omega_n t_{nm}t_{nl}\right)}_{=:\tilde{d}_{ml}}\left(\hat{B}_m^{\dagger}\hat{B}_l + \hat{B}_m\hat{B}_l^{\dagger}\right) \\
&= \hbar\tilde{\Omega}_1\hat{B}_1^{\dagger}\hat{B}_1 + \sum_{l=2}^{N}\hbar\tilde{d}_{1l}\left(\hat{B}_1^{\dagger}\hat{B}_l + \hat{B}_1\hat{B}_l^{\dagger}\right) + \sum_{m=2}^{N}\hbar\tilde{\Omega}_m\hat{B}_m^{\dagger}\hat{B}_m + \sum_{2=m<l}^{N}\hbar\tilde{d}_{ml}\left(\hat{B}_m^{\dagger}\hat{B}_l + \hat{B}_m\hat{B}_l^{\dagger}\right).
\end{aligned}
\tag{4.100}
$$

The first effective mode is coupled to all remaining effective modes via the second term. The last term, introducing a mutual coupling among all modes the residual bath, can be eliminated by diagonalization of the matrix $\tilde{D} = \tilde{d}_{ml}$, with $m, l = 2, \ldots, N$.

Thus we proceed as follows: The matrix containing the elements $\tilde{d}_{ml}$ is given by $D = T\text{diag}(\omega_1, \ldots, \omega_N)T$. From this matrix we extract the first effective mode $\Omega_1 := \tilde{\Omega}_1$, and

decouple the residual bath by diagonalizing $\tilde{D}$:

$$\tilde{T}^T \tilde{D} \tilde{T} = \text{diag}\left(\Omega_2, \ldots, \Omega_N\right). \tag{4.101}$$

The transformation $U^T DU$ where

$$U = \begin{pmatrix} 1 & 0 \\ 0 & \tilde{T} \end{pmatrix} \tag{4.102}$$

finally yields

$$U^T DU = \begin{pmatrix} \Omega_1 & d_{12} & \ldots & \ldots & d_{1N} \\ d_{21} & \Omega_2 & 0 & \ldots & 0 \\ \vdots & 0 & \ddots & & \vdots \\ \vdots & \vdots & & \ddots & 0 \\ d_{N1} & 0 & \ldots & 0 & \Omega_N \end{pmatrix}, \tag{4.103}$$

where

$$(d_{12}, \ldots, d_{1N}) = \left(\tilde{d}_{12}, \ldots, \tilde{d}_{1N}\right) \tilde{T}. \tag{4.104}$$

The corresponding transformed bath and interaction Hamiltonian are given by

$$\hat{\mathcal{H}}_{\text{B}} = \hbar \Omega_1 \hat{B}_1^\dagger \hat{B}_1 + \sum_{l=2}^N \hbar d_{1l} \left(\hat{B}_1^\dagger \hat{B}_l + \hat{B}_1 \hat{B}_l^\dagger\right) + \sum_{m=2}^N \hbar \Omega_m \hat{B}_m^\dagger \hat{B}_m, \tag{4.105}$$

$$\hat{\mathcal{H}}_{\text{I}} = \hat{L} \bar{C}_0 \left(\hat{B}_1^\dagger + \hat{B}_1\right). \tag{4.106}$$

Thus, the system is now coupled only to the first effective mode, while the first effective mode is coupled to all remaining effective modes. From here, we start again with $N-1$ modes $\Omega_2, \ldots, \Omega_N$ and proceed as outlined above. After n steps, we find the Hamiltonian

$$\hat{\mathcal{H}} = \hat{\mathcal{H}}_{\text{s}} + \hat{L} \bar{C}_0 \left(\hat{B}_1^\dagger + \hat{B}_1\right) + \sum_{m=1}^n \hbar \Omega_m \hat{B}_m^\dagger \hat{B}_m + \sum_{m=2}^n \bar{C}_{m-1} \left(\hat{B}_{m-1}^\dagger \hat{B}_m + \hat{B}_{m-1} \hat{B}_m^\dagger\right) + \hat{\mathcal{H}}_{\text{R}}, \tag{4.107}$$

with the residual bath Hamiltonian $\hat{\mathcal{H}}_{\text{R}}$. Again, as shown in [164], the residual bath Hamiltonian should be completed by a Markovian closure which can be neglected if enough effective modes are included.

In order to further investigate the optimality of the exponential FD which we have heuristically found in Sec. 4.4 with the help of the WFT, the EMR of the SBM is compared to results obtained with the discretization of the SD with the exponential FD. Since in the EMR the bath is transformed into a linear chain, the WFT is not meaningful for the EMR and thus can not serve as an a priori criterion

for the quality of the discretization via the effective modes. In principal the EMR allows for an exact inclusion of the continuous bath [164]. Still, for numerical purposes, one has to start from a discretized bath from which the effective modes can be calculated by subsequent orthogonal transformations. It does not make much sense if the numerical calculation of the effective modes is more demanding than the actual propagation. Thus we have chosen to start with a bath discretized with 2000 modes, from which $N = 200$ effective modes have been calculated. In all numerical calculations performed we find that the number of CS required to converge the result in the EMR is exactly the same as required in standard bath representation. This is surprising since the Hamiltonian and thus the dynamics can be expected to be rather different in the two different pictures. It once more confirms the power and reliability of the multi Davydov method. Results are shown in Fig. 4.31. They reveal that the EMR does not yield any advantage for the SBM, since results with $N = 200$ effective modes are not nearly as converged as the result in the standard bath representation (compare left panel of Fig. 4.5), if the bath is discretized with the exponential FD. Furthermore, from Fig. 4.31 we infer that the discretization from which the 2000 modes are extracted plays a dominant role for the dynamics of the effective modes. While in the standard bath representation the exponential FD yields the best approximation to the continuum limit, the FD $\sim J(\omega)/\omega$ yields the best approximation in the EMR. However, Sec. 5.1 will reveal that in stark contrast, the EMR is highly advantageous if starting from a given discretization.
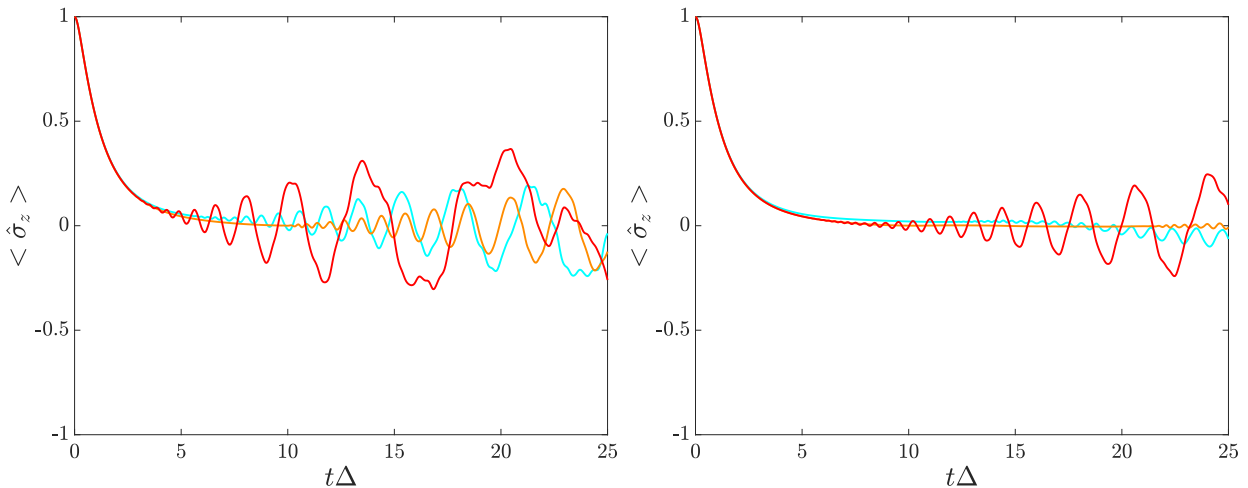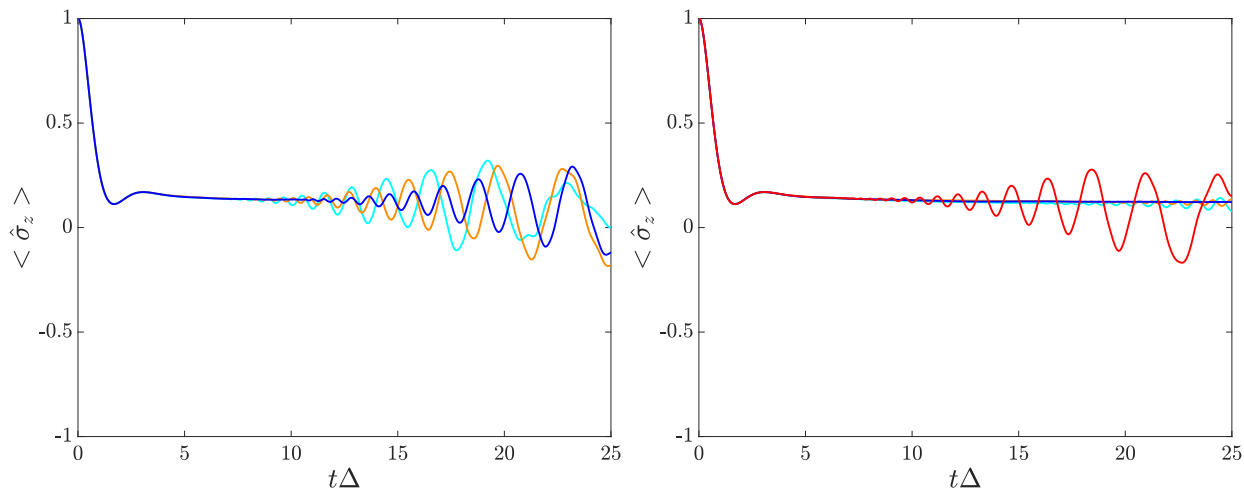

Figure 4.31.: EMR calculations compared to the numerically exact result of Sec. 4.3.2 ($s = 1, M = 6$) for $N = 100$ effective modes (left panel) and $N = 200$ effective modes (right panel), obtained from 2000 modes given by different discretizations: $\rho_f \sim e^{-\omega/\omega_c}$ (orange solid), $\rho_f \sim J(\omega)$ (cyan solid), Legendre quadrature (red solid). Further parameters are $\alpha = 0.5, \omega_c = 10\Delta$.

In this section, we have investigated in detail the effects of a transformation of the typical setup of mutually uncoupled environmental oscillators to a linear chain. In particular we found that this transformation does not yield substantial advantages in the case of the Spin-Boson model.

In this chapter we have thoroughly proven that the multi Davydov-Ansatz equipped with apoptosis (see Secs. 3.3.2 and 4.3.2.2) and the regularization in the case of vanishing coefficients (see Secs. 3.3.1 and 4.3.2.1) is a highly stable and systematically converging method suited to calculate the dynamics

Figure 4.32.: EMR calculations compared to the numerically exact result of Sec. 4.3.2 ($s = 0.5, M = 24$) for $N = 100$ effective modes (left panel) and $N = 200$ effective modes (right panel), obtained from 2000 modes given by different discretizations: $\rho_{\mathrm{f}} \sim \mathrm{e}^{-\omega/\omega_c}$ (orange solid), $\rho_{\mathrm{f}} \sim J(\omega)$ (cyan solid), $\rho_{\mathrm{f}} \sim J(\omega)/\omega$ (blue solid), Legendre quadrature (red solid). Further parameters are $\alpha = 0.2, \omega_c = 10\Delta$.

of open quantum systems in the weak as well as in the strong coupling regime. Furthermore, we have investigated various different approaches to further reduce the numerical effort required to converge to the continuum limit for different continuous spectral densities. We subsume that results obtained from the multi Davydov-Ansatz are extremely reliable and thus suited to predict physically correct conclusions also in cases where no further results are at our disposal. In the next chapter, we will venture to explore with the multi Davydov-Ansatz previously unexploited physical territory.

5. Applications

In this chapter, we apply the multi Davydov-Ansatz along with apoptosis (see Sec. 3.3.2), regularization in the case of vanishing coefficients (see Sec. 3.3.1) and the insights with respect to the discretization of continuous environments gained in the previous chapter. In particular, we will see that the regularizations are inevitably required for the method to produce reliable results. While the considerations of Sec. 4 are important in cases where the system-bath coupling is specified in terms of a continuous spectral density, we shall firstly examine two settings where the environment is already given in discretized form. There, no convergence check for the continuum limit is required.

Specifically, we shall firstly determine the vibrational relaxation dynamics of deuterium dimers in the presence of a silicon surface, utilizing a novel Hamiltonian exact up to second order in the environmental coordinates [31]. Since the model does not allow for a perturbative treatment, we will apply the multi Davydov-Ansatz in order to numerically exactly calculate the system dynamics with multiple system levels and a huge number of surface vibrations explicitly taken into account. Subsequently we will determine the channels through which the relaxation occurs. Finally we will outline how to drastically reduce the numerical effort by transforming the environment with the EMR. We will secondly investigate the relaxation dynamics of an exciton hopping on a linear molecular chain utilizing the Holstein polaron model. By investigation of the long-time dynamics for large exciton hopping elements and strong coupling strengths we will find that the relaxation dynamics is highly complicated, rendering inevitable the application of apoptosis.

In two further setups, we shall return to continuous spectral densities. Specifically, we will outline how to use the multi Davydov-Ansatz for the investigation of laser-driven molecular dynamics in dissipative environments. Firstly we will investigate the impact of environmental excitation on the transition probability in a Landau-Zener system. We will show that the multi Davydov-Ansatz is suited to reliably reproduce the analytically given long-time limit of the staying probability for multiple modes given in terms of a continuous ohmic spectral density. Finally, in a second setup we will show that the dissipative environment, given in terms of a super-ohmic continuous spectral density, can be used as a resource for population inversion if coupled strongly to a two-level system subject to chirped femtosecond laser excitations. The insights gained from the examination of the environmental dynamics are suited to open up a path for experimental realization of laser-driven population inversion even for weakly chirped laser pulses.

5.1. Vibrational relaxation dynamics at surfaces

Adsorbate-surface interactions have played an important role in both physics and chemistry for many decades [234–242]. Molecules attached to surfaces differ considerably from their gas phase counterparts since the presence of the surface leads to vibrational frequency shifts and, most importantly, opens additional decay channels for excited adsorbate vibrations which are inaccessible in free molecules. This

relaxation is of central interest in surface science [243–251] since the energy flow between adsorbed species and surfaces controls the dynamical properties of diffusion, adsorption and also desorption. Important applications include photodesorption switching [252], noncontact friction [253], tunneling microscopy [254–256] and surface-enhanced Raman scattering (SERS) [257, 258]. Especially the latter has gained new interest since the observation of giant SERS from single molecules located between closely spaced silver nanoclusters [259–261].

In particular, hydrogen adsorbed on a silicon surface has been subject to vital research [262–265]. Furthermore, complete isotope selectivity in infrared laser-induced desorption of H2 and D2 from a Si(111) surface, recently discovered experimentally [266, 267], has fueled research in the field. But while different techniques to measure surface vibrational relaxation have been put forward, the complex nature of the adsorbate-substrate couplings and surface disorder render difficult the measurement process.

Experimentally and theoretically, dynamics of Si-H bending and stretching modes has been of particular interest [268–272]. Experimental results [273, 274] hint that these vibrations are sensitive to surface structure and imperfections. The relaxation of a vibrationally excited adsorbate can be due to the coupling to substrate phonons, or to electron-hole pairs [241, 246]. We concentrate on vibrational phonon-driven multilevel relaxation since it is expected to dominate the relaxation process for semiconductors and insulators because of the large band gap.

Vibrational relaxation of adsorbates on surfaces can be done with classical molecular dynamics with on-the-fly ab initio forcefields. The classical model misses energy quantization, tunneling splittings and interference, however. Thus, quantum-mechanical treatment is a necessity. Quantum-mechanical models are often based on system-bath Hamiltonians, involving a phononic expansion of the interaction potential in terms of n-phonon terms ($n = 1, 2, \ldots$). This expansion can be derived from ab initio semi-empirical models or with further approximations.

On the contrary, here we calculate vibrational relaxation rates of a D-Si bending mode coupled to a fully D-covered Si(100)-(2 × 1) surface at zero temperature for a system-bath Hamiltonian being exact up to second order in the environmental coordinates. The authors of [31] have shown that it can be rigorously derived by an embedded cluster approach. In the sequel it is outlined briefly how this derivation unfolds, where we follow the lines given in [31].

Firstly, a small cluster based on experimental structure parameters given in [275] for D:Si(100)-2 × 1 is formed. Considering a double slab with six Si layers where only top and bottom layer are dimerized yields an unrelaxed $Si_{70}D_{54}$ cluster. The latter is relaxed with hybrid and pure density functional theory, where individual bending modes are identified. By normal mode analysis, eigenmodes corresponding to the D-Si bending modes are extracted.

The parallel antisymmetric D-Si-Si bending mode $\|, a$ given in [31] is localized at the surface which is why it will be examined in more detail here. In Born-Oppenheimer approximation, i.e. by neglecting electron-phonon coupling, the ground state potential $V(q)$ corresponding to this mode is well defined. It is calculated on a grid for different displacements of the bending mode. By solving the one-dimensional time-independent Schrödinger equation (TISE) the system eigenstates ε_j are obtained,

where the system Hamiltonian reads

$$\hat{\mathcal{H}}_{\mathrm{S}} = \sum_{j=1}^{N_S} \varepsilon_j \left| v_j \right\rangle \left\langle v_j \right|. \tag{5.1}$$

Now, a larger embedding cluster $Si_{602}D_{230}$ consisting of $N = 832$ atoms is selected. The smaller cluster is embedded in the larger one by mapping each unit of the smaller cluster to a corresponding unit in the larger one. For numerical reasons, the larger cluster is treated on a lower level of sophistication, with Brenner-type forcefields [276] containing pairwise attractive and repulsive interactions as well as many-body corrections.

Constrained normal mode analysis in the vibrational subspaces orthogonal to the transferred system modes was carried out in the Saalfrank group, resulting in $3N - 1 = 2495$ phonon modes ω_n treated in harmonic approximation. Six of these modes are rotations and translations of the whole cluster and are consequently removed from the set of modes.

The corresponding density of states of vibrational normal modes is plotted in the right panel of Fig. 5.1. As can be seen from the left panel of Fig. 5.1 does the D-Si bending mode's anharmonic frequency $\omega_{10} = 458\,\mathrm{cm}^{-1}$ lie inside the phonon bath frequency spectrum. Consequently the D-Si bending mode can efficiently couple to phonons via one-phonon channels. Thus we take into account only one-phonon system-bath couplings. Then, the couplings $\lambda_n(q)$ are calculated for several displacements along the system coordinate, on the same grid which the ground state potential is calculated on.

Finally, the coupling matrix elements $\left\langle v_i \right| \lambda_n(q) \left| v_j \right\rangle$ are calculated. By linearly approximating the couplings, $\lambda_n(q) \approx \lambda_n q$, the system coupling operator takes the form

$$\hat{L} = \sum_{i \neq j} \gamma_{ij} \left| v_i \right\rangle \left\langle v_j \right|, \tag{5.2}$$

where $\gamma_{ij} = \left\langle v_i \right| q \left| v_j \right\rangle$ are the transition matrix elements. By further taking into account only the nearest neighbor transitions, the coupling operator reads

$$\hat{L} = \sum_{j=1}^{N_S-1} \gamma_j \left(\left| v_j \right\rangle \left\langle v_{j+1} \right| + \left| v_{j+1} \right\rangle \left\langle v_j \right| \right), \tag{5.3}$$

with nearest neighbor transition matrix elements $\gamma_j = \left\langle v_j \right| q \left| v_{j+1} \right\rangle$. It is important to note that in the cluster approach presented above, no periodic boundary conditions have been imposed for numerical reasons.

Here we generalize the results obtained in [277] by application of the multi Davydov-Ansatz. It allows for a numerical exact calculation of the dynamics, allowing for accurate extraction of the lifetimes of the bending mode. Under the assumption that the system's initial state is the first excited state $\left| v_2 \right\rangle$ and that the phonons are in the ground state initially, it has been pointed out in [277] that plotting

the stick spectrum, i.e. the absolute values

$$d_j := \left| \langle v_2 | \langle \mathbf{0} | \Phi_j \rangle \right|^2 \tag{5.4}$$

of the initial state in the eigenbasis $| \Phi_j \rangle$ of the full Hamiltonian as function of the energies ε_j, reveals an important property of the dynamics of the full system. The power spectrum of the adsorbate-surface system for D-Si consists of several non-uniformly distributed peaks around the bending mode frequency $\omega_{10} = 458 \, \text{cm}^{-1}$ (see Fig. 5.1). Since the stick spectrum dictates the time-evolution of system and bath, one infers that the time-dependent survival probability of the D-Si initial vibrational state does not decay exponentially and does thus not allow for an easy extraction of the bending mode's lifetime.
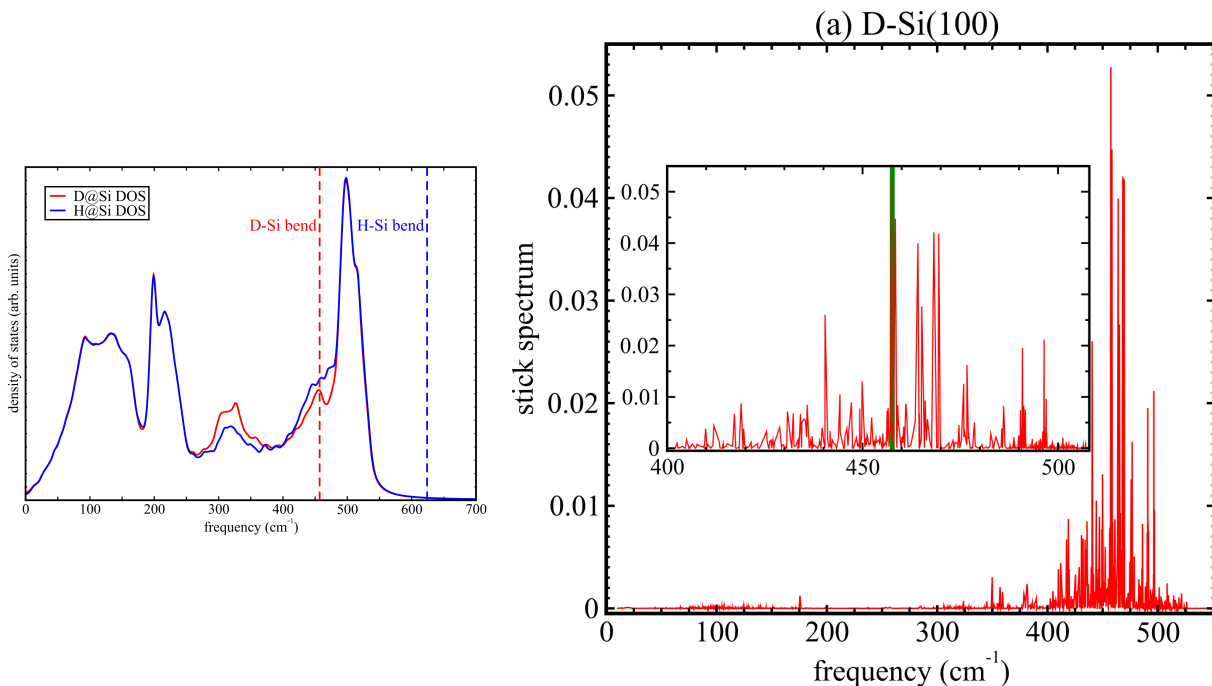
Figure 5.1.: Left panel: density of states of vibrational normal modes for $Si_{602}H_{230}$ (blue) and $Si_{602}D_{230}$ clusters (red). The vertical dashed red line indicates the D-Si bending mode frequency $\omega_{10} = 458 \, \text{cm}^{-1}$ considered here. Right panel: Stick spectrum, d_j as defined in Eq. (5.4) as function of the system energies ε_j for D-Si(100), taken from [277]. The inset is a zoom around the bending mode frequency ($458 \, \text{cm}^{-1}$), indicated by the vertical green line.

We carried out calculations with $N = 2495$ phonon modes as given in [31], for two system levels taken into account. Results were converged with a multiplicity $M = 25$ and the calculations took around a week on an 8-core machine. The results are plotted in the left panel of Fig. 5.2.

By comparing our results to the ones given in [277], where only ground and first excited states of the Fock basis were taken into account, we find that despite the simplicity of the approximation, it captures the main features of the model. While we find coincidence with the results of [277] for short times, smaller deviations are found for longer times (see left panel of Fig. 5.2 for results from the multi Davydov-Ansatz; results from [277] are not shown).

In an experimental setup one may typically aim at exciting the bending mode by an optimally tuned
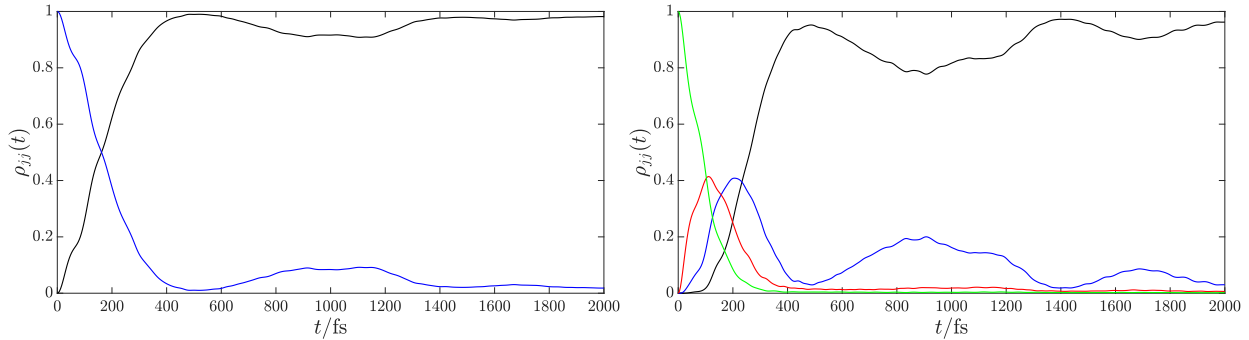
Figure 5.2.: Populations of different levels calculated with $N = 2495$ phonon modes from the multi Davydov-Ansatz with multiplicity $M = 25$. Left panel: $j = 1$ (black solid), $j = 2$ (blue solid). Right panel: $j = 1$ (black solid), $j = 2$ (blue solid) $j = 3$ (red solid), $j = 4$ (green solid). Starting in the second excited (left panel) and fourth excited (right panel) state.

laser. But since the stick spectrum shows several non-uniformly distributed peaks closely around the bending mode frequency, excitation of multiple levels will be inevitable. Thus we aim here at generalization of the results of [277] to multiple system levels taken into account.

The result for $N_S = 4$ levels taken into account where the initial system state is given by $|v_4\rangle$ is plotted in the right panel of Fig. 5.2. The dynamics shows that starting in a higher excited state changes the dynamics (compare to left panel of Fig. 5.2) since the relaxation occurs through further intermediate levels. Especially one observes further revivals and beatings in contrast to the two-level case. The displacements plotted in Figs. 5.3 - 5.5 reveal that energy between system and bath is interchanged primarily through small and large bath modes while the 'intermediate' modes do not contribute.
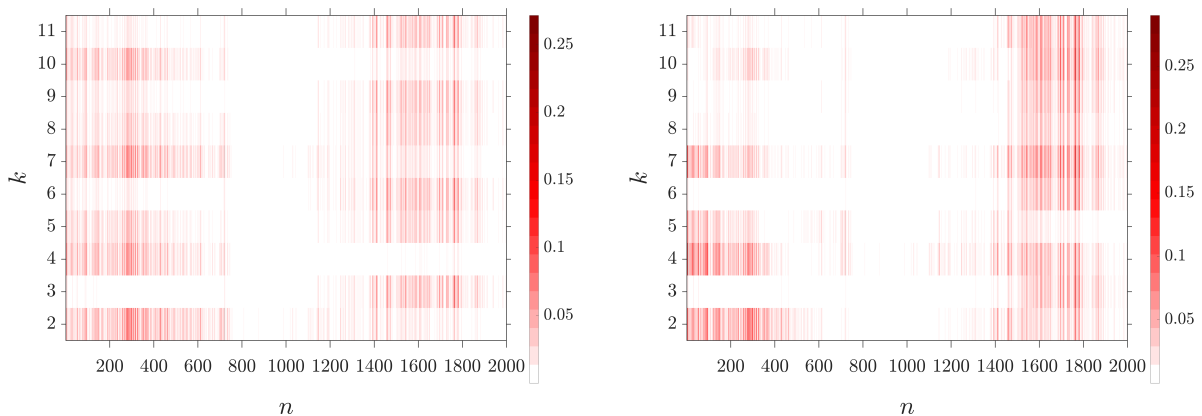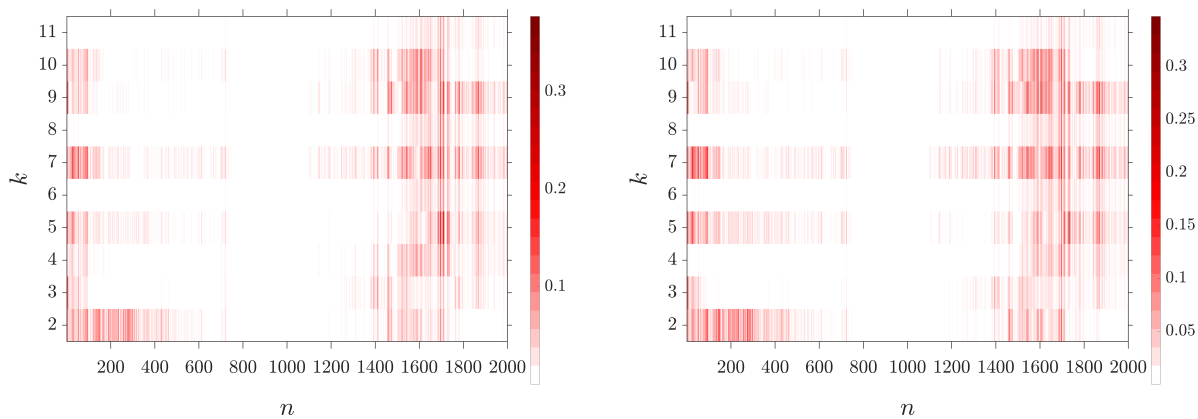

Figure 5.3.: The absolute values of the displacements at $t = 100\,\mathrm{fs}$ (left panel) and $t = 300\,\mathrm{fs}$ (right panel) as function of number of mode $n = 1 \dots 2000$ and multiplicity $k = 1, \dots, 11$.

Finally, we may infer from the structure of the stick spectrum that for short times the presence of the surface should lead to population transfer also to the higher excited states. We thus aimed at inclusion of $N_S > 4$ system levels into the model. In order to reduce the computational effort, we carried out the transformation of the Hamiltonian to the EMR outlined in Sec. 4.6. While we found
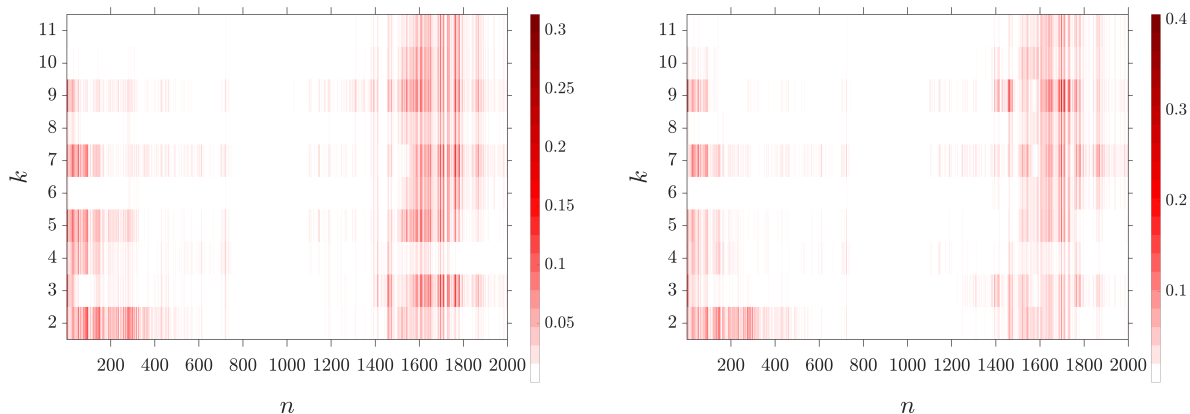
Figure 5.4.: The absolute values of the displacements at $t = 700\,\mathrm{fs}$ (left panel) and $t = 1000\,\mathrm{fs}$ (right panel) as function of number of mode $n = 1 \ldots 2000$ and multiplicity $k = 1, \ldots, 11$.

**Figure 5.5.:** The absolute values of the displacements at $t = 1500\,\mathrm{fs}$ (left panel) and $t = 2000\,\mathrm{fs}$ (right panel) as function of number of mode $n = 1 \ldots 2000$ and multiplicity $k = 1, \ldots, 11$.

in Sec. 4.6 that no noteworthy advantage arose from the EMR in the SBM, a completely different picture shows up here. It turns out that in the EMR, $N = 100$ modes are enough to obtain results identical with the ones found in the standard representation. Even more amazingly, the multiplicity needed to converge the results does not change in the EMR.

We attribute the efficiency of the EMR to the fact that from the stick spectrum 5.1 we find that there are only few frequencies which effectively couple to the system, in contrast to the SBM. Thus they can well be represented by some effective modes which are in the same region as the peaks. This is confirmed from the plots of the displacements in Figs. 5.3 - 5.4, which show that the modes which effectively contribute are centered at the borders of the frequency range, while the intermediate frequencies do not essentially contribute to the dynamics. For the SBM, on the contrary, the resulting effective modes cover the same wide frequency range as the original modes (see Sec. 4.6), and all modes effectively contribute in the dynamics (see figures for the displacements in Sec. 4.3.2).

Taking into account $N = 10$ levels with the system being initially in the fourth, fifth and sixth excited state are plotted in Figs. 5.6 and 5.7. A multiplicity of $M = 30$ was required to converge the result. As expected, mediated by the bath, population is transferred for short times also to the higher excited states. We could extract lifetimes from the calculated dynamics, but we refrain from doing so here due to the complexity of the dynamics. It is furthermore unclear how to attribute the different lifetimes found for the multiple levels a physical relevant lifetime.

The overview is rounded off by plots of entropy $S(t)$ (see Eq. (4.54)) and purity $\gamma(t)$ in Fig. 5.8.
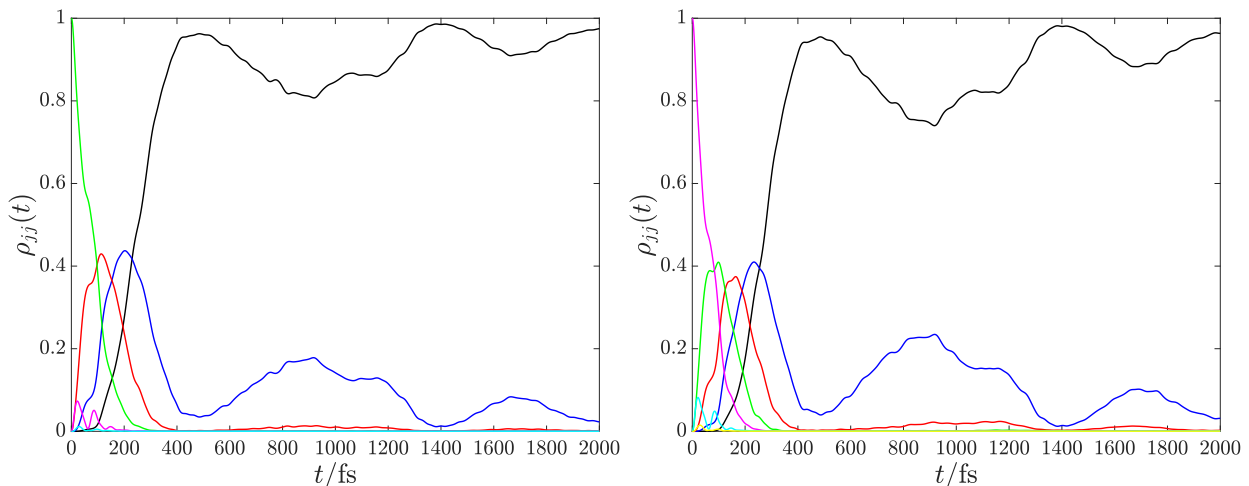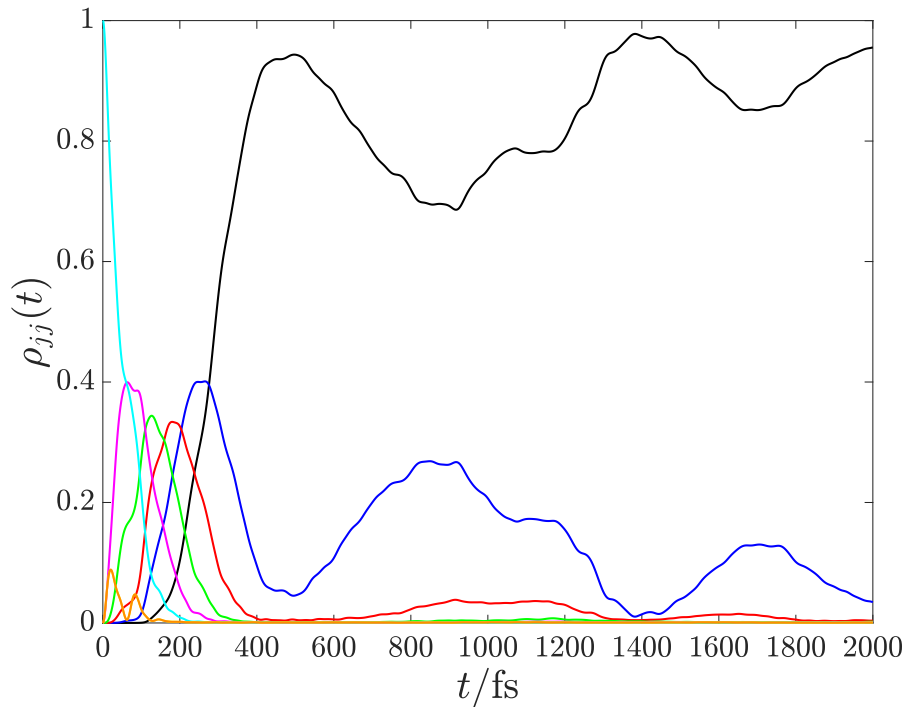

Figure 5.6.: Populations of different levels. $j = 1$ (black solid), $j = 2$ (blue solid), $j = 3$ (red solid), $j = 4$ (green solid), $j = 5$ (magenta solid), $j = 6$ (cyan solid), $j = 7$ (yellow solid). Starting in the fourth excited (left panel) and fifth excited (right panel) state.

The purity is defined as

$$\gamma(t) = \mathrm{tr}_{\mathrm{S}}\left[\hat{\rho}_{\mathrm{S}}^2(t)\right], \tag{5.5}$$

where the reduced density matrix $\hat{\rho}_{\mathrm{S}}(t)$ is given by (4.55). It measures how pure a given state is since $\gamma = 1$ iff the state is pure, and in general $0 \leq \gamma \leq 1$. We see that starting from an initially pure state, the state evolves rather quickly into a mixture where the speed of this evolution is determined by the initial system excitation. The smaller the initial excitation in the system, the slower the evolution to a mixture. Since it is the entanglement between system and bath which reduces the purity, we may view the purity as a measure for the coupling strength between system and bath. We furthermore see from the left panel of Fig. 5.8 that bath and system become finally disentangled. This is confirmed by the entropy, which as well is a measure for the entanglement between system and bath. It is thus clear that the entropy processes analogously to the purity.

To summarize, we have calculated by means of the multi Davydov-Ansatz the relaxation dynamics of deuterium dimers adsorbed on a silicon surface. While the favourable scaling of the multi Davydov-Ansatz with the number of phonon modes allows for the computation of the full system-plus-bath dynamics at comparatively low effort, we have transformed the standard bath representation into the EMR. The multi Davydov-Ansatz in combination with the EMR has turned out in the present context

Figure 5.7.: Populations of different levels. $j = 1$ (black solid), $j = 2$ (blue solid), $j = 3$ (red solid), $j = 4$ (green solid), $j = 5$ (magenta solid), $j = 6$ (cyan solid), $j = 7$ (yellow solid), $j = 8$ (orange solid). Starting in the sixth excited state.
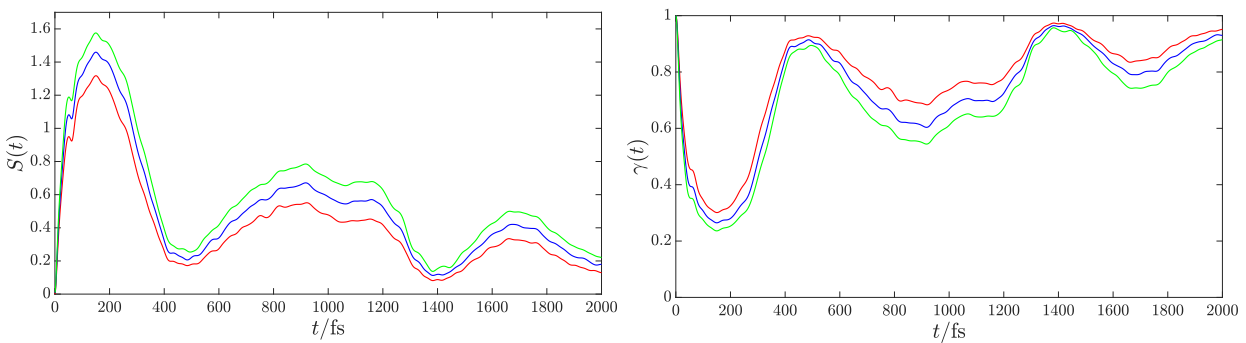
Figure 5.8.: Entropy $S(t)$ (left panel) and purity $\gamma(t)$ (right panel) as function of time, for different initial conditions. The system starts in the j-th excited state, where $j = 4$ (red solid), $j = 5$ (blue solid), $j = 6$ (green solid).

to allow the calculation of the relaxation of the dynamics of deuterium at a silicon surface at extremely low cost, since only 100 effective modes suffice in order to accurately represent the environment, while the number M of coherent states required to converge the multi Davydov-Ansatz did not increase by changing the representation.

5.2. Relaxation dynamics of the Holstein polaron

In this section, we will examine the Holstein molecular crystal, where we aim at investigation of the long-time dynamics in the strong coupling regime. The complex phonon dynamics, especially in the context of long-time propagation, inevitably leads to multiple CS approaching during propagation. Thus, without apoptosis, only short times and weak coupling could be considered. If the multi Davydov-Ansatz is equipped with apoptosis, however, reliable results can be obtained in the strong coupling limit, even for long-time propagation. Once more we will find that apoptosis allows for converged results far beyond apoptosis events although it reduces the flexibility of the Ansatz wave function.

Recent developments in ultrafast laser spectroscopy allow to study experimentally the real time nonequilibrium dynamics of photo-excited quantities [278–281]. Especially relaxation processes such as these of charge carriers in topological insulators, electron-hole pairs in light harvesting complexes [282] and polarons in anorganic liquids and solids [283–285] have been subject to intense research. The motion of such a photo-excited quantity in a molecular crystal can in many applications be theoretically described by the Holstein molecular crystal model, introduced in [286, 287].

There the crystalline medium is a linear chain of N identical point-like molecules or atoms of mass $m = 1$, where the internuclear distances of the molecules are allowed to vary. As a result of the interaction of the photo-excited quantity and the lattice, the surrounding lattice particles are displaced and the photo-excited quantity experiences a potential well. Since the photo-excited quantity is unable to move unless accompanied by the surrounding lattice deformation, photo-excited quantity and lattice deformation form a unit, which is called polaron. The lattice vibrations, given by the variation of the internuclear distances, are in the absence of the exiton quantity assumed to be uncoupled. Thus, assuming the lattice particles to stay close to their equilibrium position and consequently the potential energy curve of an individual molecule to be quadratic, the lattice Hamiltonian reads

$$\hat{\mathcal{H}}_{\mathrm{L}} = \frac{1}{2} \sum_{n=1}^{N} \left[\hat{p}_n^2 + \omega_0^2 \hat{x}_n^2 \right], \tag{5.6}$$

where $\hat{p}_n$ and $\hat{x}_n$ are momentum and position of the n-th molecule, respectively, and ω_0 is the Einstein frequency. Imposing periodic boundary conditions on the one-dimensional lattice allows for introduction of phononic creation and annihilation operators $\hat{A}_n^\dagger$ and $\hat{A}_n$, respectively. The lattice Hamiltonian then reads

$$\hat{\mathcal{H}}_{\mathrm{L}} = \sum_{n=1}^{N} \omega_n \hat{A}_n^\dagger \hat{A}_n. \tag{5.7}$$

In tight binding approximation, the exciton Hamiltonian reads

$$\hat{\mathcal{H}}_{\mathrm{ex}} = -J \sum_n \left[\hat{B}_n^\dagger \hat{B}_{n+1} + \hat{B}_{n+1}^\dagger \hat{B}_n \right] - \mu \sum_{n=1}^{N} \hat{B}_n^\dagger \hat{B}_n, \tag{5.8}$$

where J is the hopping integral between neighboring sites, and μ is the chemical potential which is set to zero for convenience. Under the assumption that the coupling is to the displacement of the atom only of the site the exciton is at, the interaction Hamiltonian reads

$$\hat{\mathcal{H}}_{\mathrm{int}} = \gamma \sum_{n=1}^{N} \hat{B}_n^\dagger \hat{B}_n \left(\hat{A}_n^\dagger + \hat{A}_n \right), \tag{5.9}$$

where γ is the phonon-exciton coupling strength. Finally, one introduces the Bloch operators

$$\hat{a}_k = \frac{1}{\sqrt{N}} \sum_{n=1}^{N} \mathrm{e}^{-ink} \hat{A}_n, \tag{5.10}$$

where $k = \frac{2\pi}{N} n$, $n = 0, \ldots, N-1$ are the lattice momenta. Then

$$\hat{A}_n = \frac{1}{\sqrt{N}} \sum_{k=1}^{N} \mathrm{e}^{ink} \hat{a}_k, \tag{5.11}$$

and one arrives at the Hamiltonian

$$\hat{\mathcal{H}} = \hat{\mathcal{H}}_{\mathrm{ex}} + \hat{\mathcal{H}}_{\mathrm{L}} + \hat{\mathcal{H}}_{\mathrm{int}}, \tag{5.12}$$

where

$$\hat{\mathcal{H}}_{\mathrm{ex}} = -J \sum_n \left[\hat{B}_n^\dagger \hat{B}_{n+1} + \hat{B}_{n+1}^\dagger \hat{B}_n \right] \tag{5.13}$$

$$\hat{\mathcal{H}}_{\mathrm{L}} = \sum_n \omega_n \hat{a}_n^\dagger \hat{a}_n \tag{5.14}$$

$$\hat{\mathcal{H}}_{\mathrm{int}} = \sum_{k,n} \lambda_k \hat{B}_n^\dagger \hat{B}_n \left(\hat{a}_n \mathrm{e}^{ikn} + \hat{a}_n^\dagger \mathrm{e}^{-ikn} \right). \tag{5.15}$$

The prefactor $\frac{1}{\sqrt{N}}$ has been absorbed into the couplings λ_k, and the coupling is allowed to depend on the phonon frequency ω_k. It is important to note that the Hamiltonian (5.12) is symmetric with respect to the site number.

The Holstein exciton has been found recently experimentally in a surface-doped layered semiconductor [288], and furthermore, an ensemble of cold polar molecules trapped in an optical lattice [289] has been shown to constitute a tunable Holstein model. The authors of [290] have presented an exact solution for two sites, and DMRG methods have been applied to it [291], and also the Zhao community has contributed valuable work with the multi Davydov-Ansatz in this field [23, 27, 137, 292–295].

It will be shown that the multi Davydov-Ansatz equipped with apoptosis allows for extension of previous results by orders of magnitude in coupling and propagation time. We find that almost every calculation has to resort to the apoptosis procedure presented in 3.3.2, which explains the small number of sites and shortness of times considered so far.

Subsequently we assume a linear dispersion phonon band

$$\omega(q) = \omega_0 + W\left(\frac{2|q|}{\pi} - 1\right), \tag{5.16}$$

where W is the half width of the phonon dispersion determining the speed of the phonon wave packets. By fixing even N and taking the lattice momenta as

$$k = \frac{2n\pi}{N}, \qquad n = -\frac{N}{2} + 1, \dots \frac{N}{2}, \tag{5.17}$$

the corresponding frequencies are given by

$$\omega_k = \omega_0 + W\left(\frac{2|k|}{\pi} - 1\right). \tag{5.18}$$

The couplings are given by the spectral density

$$J(\omega) = \frac{2S}{\pi W^2}\omega^2\sqrt{W^2 - (\omega - \omega_0)^2} \approx \sum_{n=1}^{N} \lambda_n^2 \omega_n^2 \delta(\omega - \omega_n), \tag{5.19}$$

as proposed in [296]. Here, S is the Huang-Rhys factor, $\omega_0 = 1$ is the central energy of the phonon band, and W is the phonon energy bandwidth. In the following we consider the exciton probability, i.e. the diagonal elements of the exciton reduced density matrix

$$\rho_{nn}(t) = \langle\Psi(t)|\,\hat{B}_n^\dagger \hat{B}_n\,|\Psi(t)\rangle. \tag{5.20}$$

The exciton is assumed initially at position $n = \frac{N}{2}$, $|\Psi_{\mathrm{ex}}(0)\rangle = |\frac{N}{2}\rangle_{\mathrm{ex}}$ (note that, due to the symmetry of the Hamiltonian, *any* position would yield the same result), and the phonons are initially in their ground states, $|\Psi_{\mathrm{ph}}(0)\rangle = |\mathbf{0}\rangle_{\mathrm{ph}}$. In order to obey the symmetry of the Hamiltonian, the initially unpopulated displacements have to be set such that they also obey this symmetry - otherwise unsymmetric dynamics would be observed.

In Figs. 5.9,5.10 we plot the exciton probability as function of site number and of time. All values of the density which are above 0.3 in Fig. 5.9 (above 0.5 in Fig. 5.10) have been set to 0.3 (0.5) for better visibility of the dynamics. The rendezvous which the two parts of the density have before each part reaches the chain's end is due to the rather large Huang-Rhys factor. The displacements, plotted in Fig. 5.11, show that the dynamics is highly complicated. Almost any propagation has to resort to apoptosis, which explains why, despite the small number of variables compared to previously treated settings, only short times and small chain lengths have been treated. It is the complexity of the dynamics which leads to CS coming close rather frequently. With apoptosis implemented, however, we are able to propagate smoothly for almost arbitrarily long times and large numbers of sites.

Let us now assume the couplings λ_n to be constant,

$$\lambda_n = g \tag{5.21}$$

corresponding to the setup given in [134]. The dynamics is plotted in Fig. 5.12. Again all values above the threshold 0.3 have been set to the threshold. While the influence of J is to spread the dynamics over a broader range of sites, the effect of W is to bundle the dynamics. In all cases at $t = 0$, there are no phonon deformations. The photo-excitation at $t = 0$ triggers a pair of localized phonon wave packets which travel at a group velocity given by $\pm 2W/\pi$. Thus, the larger W, the smaller the angle between the two wave-packets.
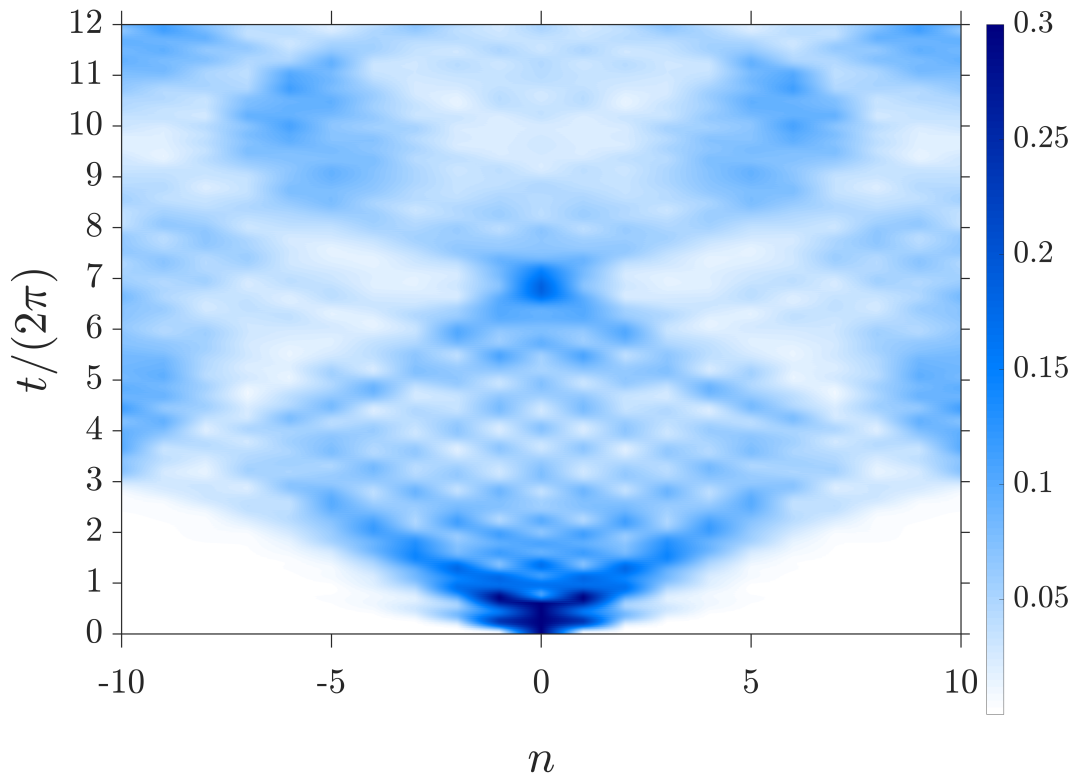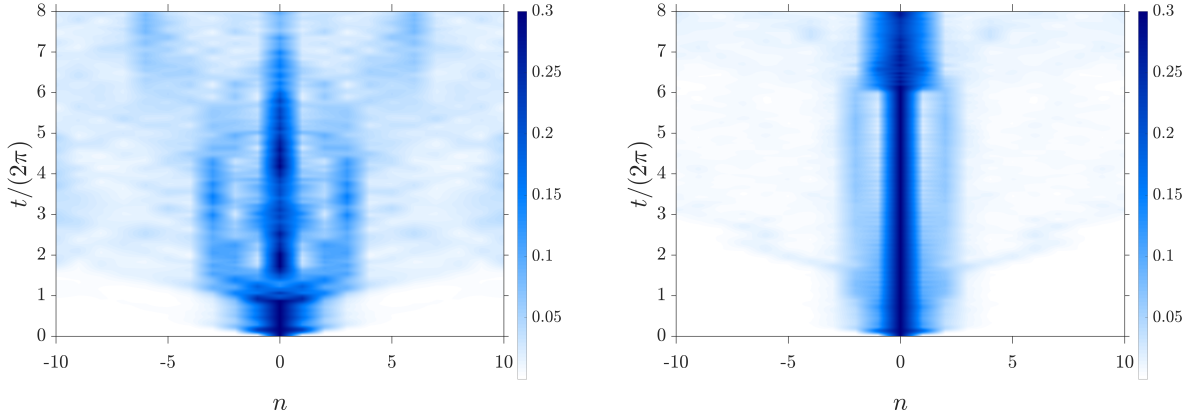

Figure 5.9.: The time evolution of the exciton probability $\rho_{jj}(t)$ as function of number of site $j = -\frac{N}{2}, \dots, \frac{N}{2}$ and of time t. The parameters read $J = -0.5$, $W = 0.8$, $S = 0.3$.
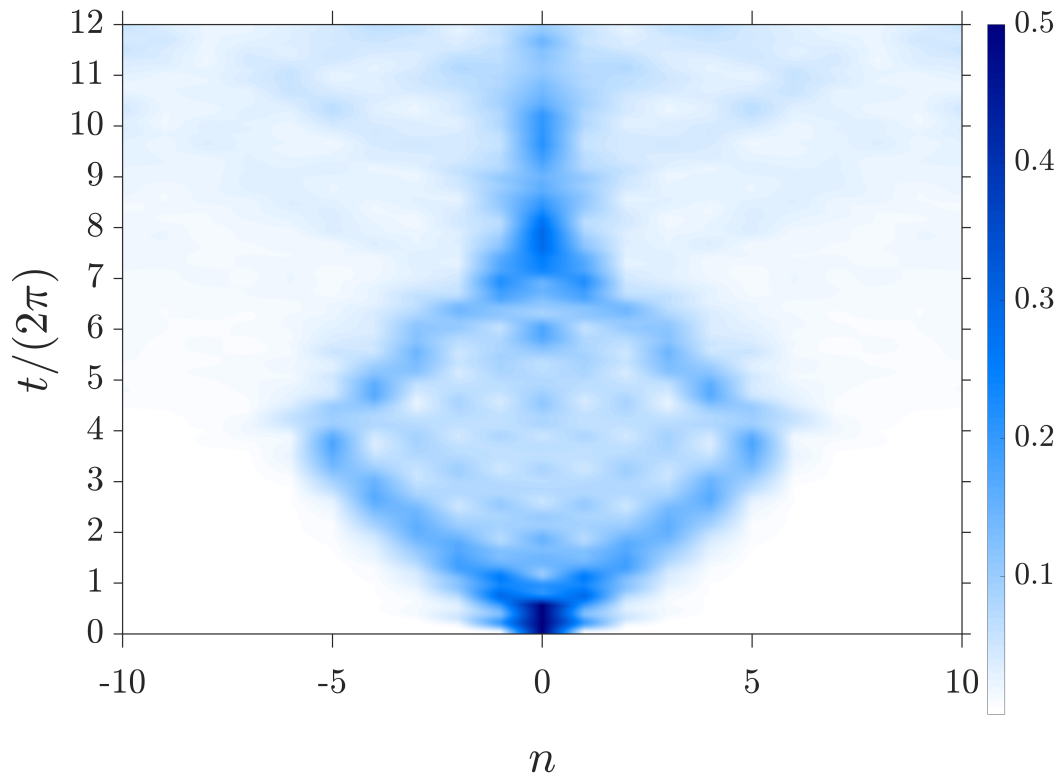
Figure 5.10.: The time evolution of the exciton probability $\rho_{jj}(t)$ as function of number of site $j = -\frac{N}{2}, \ldots, \frac{N}{2}$ and of time t. The parameters read $J = 0.5$, $W = 0.8$, $S = 0.5$.
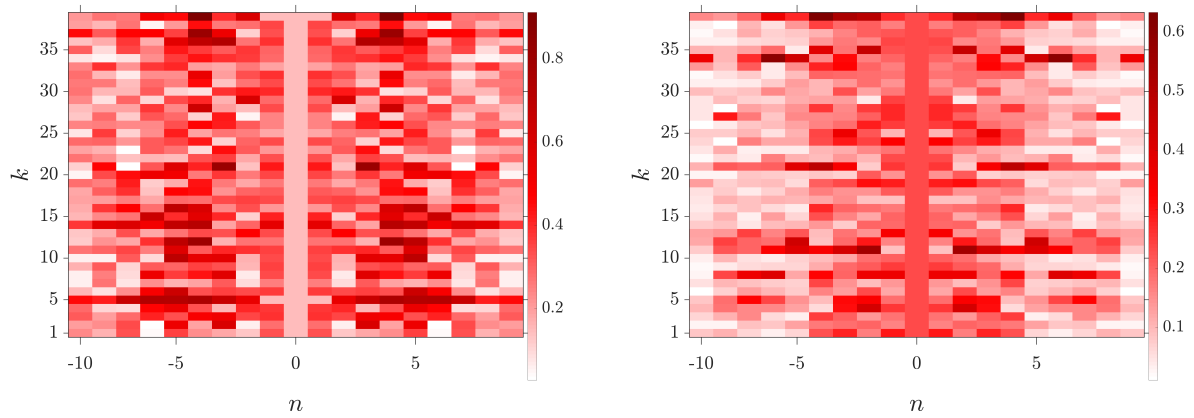
Figure 5.11.: The absolute value of the displacements as function of site index $n = -\frac{N}{2}, \ldots, \frac{N}{2}$ and multiplicity $k = 1, \ldots, 40$: at time $t = 4\frac{2\pi}{\omega_0}$ (left panel) and $t = 12\frac{2\pi}{\omega_0}$ (right panel). Further parameters read $J = 0.5$, $W = 0.8$, $S = 0.5$, $g = 0.3$.

Figure 5.12.: The effect of W on the time evolution of the exciton probability $\rho_{jj}(t)$ as function of number of site $j = -\frac{N}{2}, \ldots, \frac{N}{2}$ and of time t. Left panel: $J = 0.8$, $W = 0.1$, $g = 0.4$. Right panel: $J = 0.8$, $W = 0.8$, $g = 0.4$.

Optical spectroscopy is an important aspect of the exciton dynamics. In order to draw contact with the dynamical quantities calculated from the multi Davydov-Ansatz, the linear absorption spectrum $F(\omega)$ of the exciton dynamics is studied here. It is given by [297]

$$F(\omega) = \frac{1}{\pi} \, \mathrm{Re} \left(\int\limits_0^\infty \mathrm{d}t \, F(t) \mathrm{e}^{-\mathrm{i}\omega t} \right), \tag{5.22}$$

where the autocorrelation function $F(t)$ is defined as

$$F(t) = {}_{\mathrm{ph}}\langle \mathbf{0}| \, {}_{\mathrm{ex}}\langle 0| \hat{P} \hat{U} \hat{P}^\dagger |0\rangle_{\mathrm{ex}} |\mathbf{0}\rangle_{\mathrm{ph}}, \tag{5.23}$$

where $\hat{U}$ is the propagator of the system, and

$$\hat{P} = \mu \sum_{n=1}^N \left[|n\rangle_{\mathrm{ex}\,\mathrm{ex}}\langle 0| + |0\rangle_{\mathrm{ex}\,\mathrm{ex}}\langle n| \right] \tag{5.24}$$

is the polarization operator, where μ is the transition dipole matrix element of a single site. The autocorrelation function can be calculated as

$$F(t) = \mu^2 \sum_{m,n=1}^N {}_{\mathrm{ph}}\langle \mathbf{0}| \, {}_{\mathrm{ex}}\langle n|\hat{U}|m\rangle_{\mathrm{ex}} |\mathbf{0}\rangle_{\mathrm{ph}} = \mu^2 N \sum_{n=1}^N {}_{\mathrm{ph}}\langle \mathbf{0}| \, {}_{\mathrm{ex}}\langle n|\hat{U}|0\rangle_{\mathrm{ex}} |\mathbf{0}\rangle_{\mathrm{ph}}, \tag{5.25}$$

because of the symmetry of the Hamiltonian (5.12) with respect to the site number. By identifying

the propagated state with the multi D2 state, one obtains

$$F(t) = \mu^2 N \sum_{n=1}^{N} {}_{\text{ph}}\langle \mathbf{0}|\,{}_{\text{ex}}\langle n| \sum_{l=1}^{M} \left(\sum_{m=1}^{N} A_{lm}(t)|m\rangle_{\text{ex}} \right) |\boldsymbol{\alpha}_l(t)\rangle_{\text{ph}} = \mu^2 N \sum_{l=1}^{M} \sum_{n=1}^{N} A_{ln}(t)\,{}_{\text{ph}}\langle \mathbf{0}|\boldsymbol{\alpha}_l(t)\rangle_{\text{ph}}.$$

(5.26)

The linear absorption spectrum for the parameter setting $N = 16$, $J = 0.1$, $W = 0.1$ and $g = 0.4$ is plotted in Fig. 5.13. It differs remarkably from the result given in [27]. Huang-Rhys theory [298] predicts the phonon side bands at zero temperature to follow a Poisson distribution,

$$F(\omega) = \mathrm{e}^{-S} \sum_{n=0}^{\infty} \frac{S^n}{n!} \delta(\omega + S\omega_0 - n\omega_0).$$

(5.27)

The leftmost sideband, $n = 0$, is expected to be at $\omega = -S\omega_0$ where
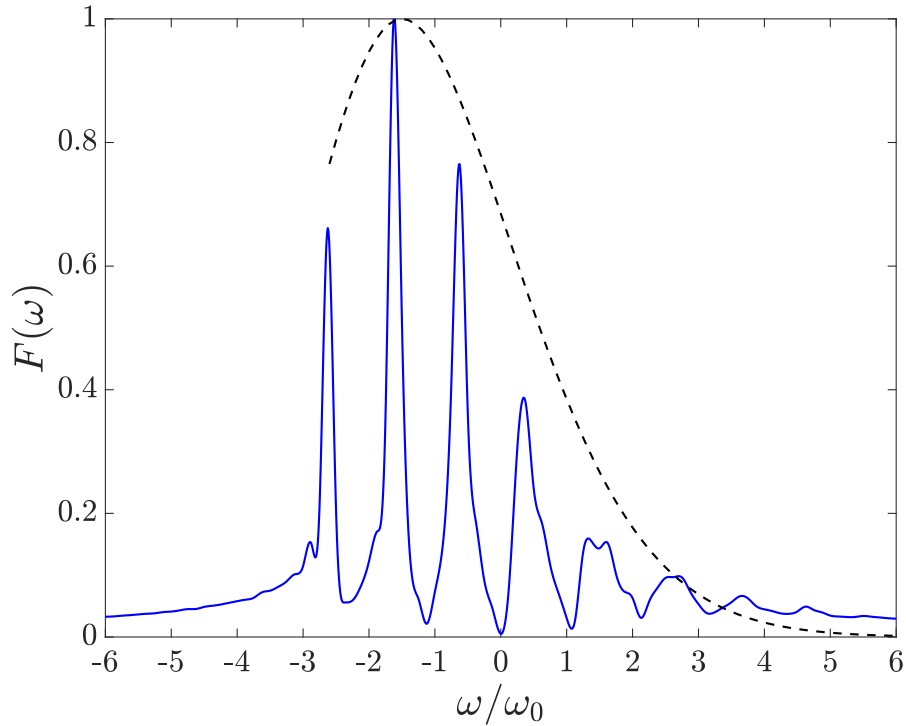
Figure 5.13.: The linear absorption spectrum (5.22) as function of ω. The result obtained from the multi Davydov-Ansatz are plotted (blue solid) vs. the Poisson distribution (5.27) (black dashed). The parameters read $N = 16$, $J = 0.1$, $W = 0.1$, $g = 0.4$.

$$S = \frac{1}{\omega_0} \sum_{n=1}^{N} \lambda_n^2 \omega_n = \frac{Ng^2}{\omega_0} = 2.56,$$

(5.28)

in nice coincidence with Fig. 5.13. Furthermore, the tallest peak is predicted to be at $n = S-1 = 1.56$, which again is nicely conform with our result since the two peaks at $n = 1$ and $n = 2$ have similar height. Furthermore, by fitting a Poisson distribution with parameter λ to the data, we find that the

fit is optimal for $\lambda \approx S$ (see dashed black line in Fig. 5.13), which again confirms our results.

We have investigated in detail the relaxation dynamics of an exciton in the Holstein molecular crystal. By considering the strong coupling regime, we have found that apoptosis is inevitable in order to obtain converged long-time results. We have shown that, despite the complexity of the phonon dynamics and despite apoptosis reduces the flexibility of the multi Davydov-Ansatz, apoptosis is suited to obtain converged results in regions far beyond those attainable without apoptosis implemented. Furthermore, we have found that special care has to be taken with respect to the initial positions of the initially unpopulated CS in order to maintain the symmetry of the model. Only if the initially unpopulated CS obey the symmetry does the Ansatz wave function obey the symmetry for all times.

5.3. The dissipative Landau Zener Model

In the course of a Landau-Zener (LZ) transition, energy levels of a two-level system undergo an avoided crossing under an action of the external drive [299, 300]. This celebrated physical phenomenon was independently studied by Landau, Zener, Stueckelberg, and Majorana in 1932, and the standard LZ model is also referred to as the Landau-Zener-Stueckelberg-Majorana (LZSM) model [299–302] which has found applications in a broad range of fields, including atomic and molecular physics [126, 303–307] quantum optics [308], solid state physics [309, 310], chemical physics [311] and quantum information science [312].

Recent experimental realizations of the LZSM as nitrogen-vacancy centers in diamond lattices [312], one-electron semiconductor double quantum dots [313], accelerated Bose-Einstein condensates which are synthetically spin-orbit coupled [314] and devices in circuit quantum electrodynamics (QED) [315–318] have revitalized scientific interest in the model. In 2004, Wallraff et al. performed an experiment in which a charge qubit is coupled to a superconducting transmission line resonator [319] and Chiorescu et al. fabricated a superconducting flux qubit coupled to a quantum interference device [320]. Such QED configurations are the solid-state analog of a two-level atom. Parameters in the super-conducting circuits can be tuned over a wide range, allowing for efficient control of the qubits and transmission line resonators. For example, Astafiev et al. built an artificial-atom maser consisting of a resonator and a Josephson-junction charge qubit coupled to it. The charge qubit is made of a superconducting Al island connected to a ground through two Josephson junctions with superconducting quantum interference device (SQUID) geometry so that the effective Josephson energy is controlled by the magnetic flux through the loop [321].

In 2004, the LZSM mechanism was observed by Izmalkov et al. in an Al three-junction qubit coupled to a Nb resonant tank circuit, and output signals were found to depend on surrounding environments [322]. Environmental effects on the QED device can be modeled by coupling a set of harmonic oscillators to the LZSM model [323]. In the framework of the dissipative LZSM model, final transition probabilities in the fast and slow sweeping limit have been studied in 1989 using time-dependent perturbation theory [324]. Inspired by the realization of LZSM physics in QED devices, Hänggi

and co-workers systematically investigated the final transition probabilities influenced by the bosonic bath at zero temperature [316, 323]. Nalbach et al. studied extensively thermal effects in the dissipative LZSM model using the quasi-adiabatic propagator path integral method and the nonequilibrium Bloch equations [325–329]. Furthermore, Sun et al. applied the hierarchy equation method [330] to the dissipative LZSM model. Recently, Huang and Zhao adopted the multiple Davydov trial states to elucidate the dissipative LZSM dynamics [331].

While much is still unknown about the underlying physics of the dissipative LZSM model, recent attention has been devoted to a superconducting qubit coupled to a single harmonic oscillator of frequency ω [321, 323, 331–334]. For example, a circuit QED device has been experimentally realized by coupling the charge qubit to the superconducting resonator through an electric field. The charge qubit and the resonator have been used to represent the standard LZSM model and the harmonic oscillator, respectively [321]. Saito et al. have revealed in their model that the dynamics at zero temperature depends strongly on the oscillator frequency only at intermediate times, if the oscillator is in its ground state at $t \to \infty$ [323]. Sun et al. compared the dynamics with rotating-wave approximation (RWA) and without RWA when the initial state of the oscillator is assumed to be a superposition of coherent states, implying that the RWA method is inaccurate for this problem. Ashhab considered the final probabilities when the harmonic oscillator mode is initially set to a finite-temperature thermal equilibrium state [333]. Huang and Zhao found two-stage LZ transitions induced by the combined effect of tunneling strength Δ and the off-diagonal qubit-oscillator coupling.

In 2018, Malla et al. aimed to find the analytical solution of slow and fast oscillators ($\omega < \Delta$ and $\omega > \Delta$, where ω is the frequency of the harmonic oscillator) when there are many quanta excited initially. Although many efforts have been devoted to understanding the LZSM model, there exist several unsettled fundamental issues: the influence on LZ transitions of an initially excited environment as well as the effect of different oscillator frequencies in the intermediate regime ($\omega \sim \Delta$) on the final probability. Moreover, the off-diagonal qubit-oscillator coupling has not been adequately treated if the initial oscillator state is not the vacuum state [332–334].

The time-dependent LZSM system Hamiltonian reads

$$\hat{\mathcal{H}}_{\mathrm{S}} = vt\hat{\sigma}_z + \Delta\hat{\sigma}_x, \tag{5.29}$$

where v is the sweeping velocity and Δ is the coupling matrix element. The instantaneous eigenvalues $E_\pm$ and eigenstates $v_\pm$ of the Hamiltonian (5.29) can be found easily by diagonalization,

$$E_\pm(t) = \pm\sqrt{(vt)^2 + \Delta^2}. \tag{5.30}$$

If the variation of the Hamiltonian (5.29) with time is adiabatic, i.e., slow enough, the Adiabatic Theorem (see e.g. [335] for details) states that the system, if initially in an instantaneous eigenstate, always stays in an instantaneous eigenstate. Thus the instantaneous eigenstates are called adiabatic eigenstates. On the contrary, the eigenstates of $\hat{\sigma}_z$, denoted as $|\pm\rangle$, are called diabatic eigenstates. While adiabatic and diabatic states coincide for $t \to \pm\infty$ since the term $vt\hat{\sigma}_z$ dominates the Hamil-

tonian (5.29) for $t \to \pm\infty$, this is not the case for $t \approx 0$. A schematic sketch is given in Fig. 5.14, where the instantaneous energies and the energy of the states $\hat{\sigma}_z$ is plotted as function of time. While at $t = 0$ the energies corresponding to the eigenstates of $\hat{\sigma}_z$ cross, it appears as an avoided crossing of spacing 2Δ in the adiabatic basis.

Under the assumption that the system is in the state $|+\rangle$ at $t \to -\infty$, Landau and Zener found independently that the probability $p(t \to \infty)$ for the system to be in the state $|+\rangle$ at $t \to \infty$ is given by

$$p(t \to \infty) = \exp\left[-\frac{\pi\Delta^2}{|v|}\right]. \tag{5.31}$$

We infer that for the probability to end up in the state $|-\rangle$ at $t \to \infty$ if the system is in the state $|+\rangle$ at $t \to -\infty$ it holds that $1 - p(t \to \infty) \to 1$ for $v \to 0$, in compliance with the Adiabatic theorem (the system stays on a red curve in Fig. 5.14 if it is there initially).

While the formula (5.31) has been known for a long time, much is still unknown about the dynamics of the LZSM-model if the system is coupled a dissipative environment. In order to illuminate the physics of the LZSM coupled to an environment, we will firstly examine the impact of initial excitation of the environment if the coupling is scaled accordingly (see Sec. 5.3.1) for a single environmental mode, as well as the impact of ohmic dissipation in the case of multiple environmental modes in Sec. 5.3.2.
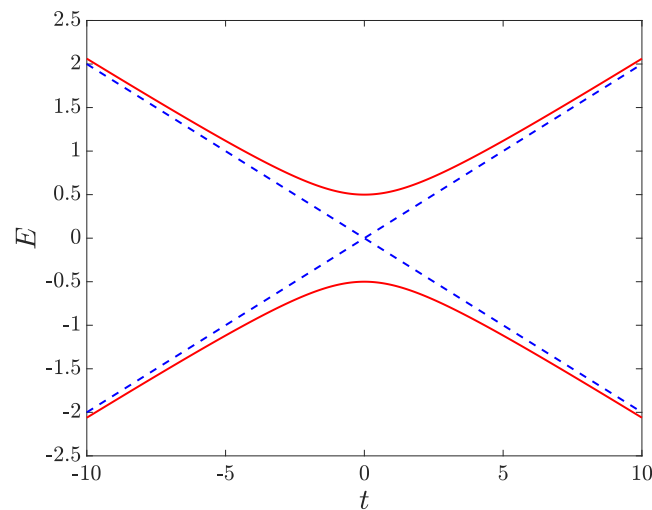
Figure 5.14.: Schematic sketch of the instantaneous energies $E_\pm$ (red solid) and the energies of the eigenstates $|\pm\rangle$ of $\hat{\sigma}_z$ (blue dashed) in arbitrary units, as function of time t in arbitrary units. Further parameters read $v = 0.2, \Delta = 0.5$.

5.3.1. Coupling to a single environmental mode

The system Hamiltonian for level transitions in the dynamics of a qubit coupled to a single harmonic degree of freedom is given by

$$\hat{\mathcal{H}}_{\mathrm{S}} = \varepsilon(t)\hat{\sigma}_z + \Delta\hat{\sigma}_z, \tag{5.32}$$

and the coupling operator is given by

$$\hat{L} = \left(\cos\theta\hat{\sigma}_z + \sin\theta\hat{\sigma}_x \right), \tag{5.33}$$

with time-dependent asymmetry parameter $\varepsilon(t) = vt$ with sweeping velocity v, and two coupling strengths

$$\lambda_z = \cos\theta, \lambda_x = \sin\theta, \tag{5.34}$$

where a change in the mixing angle θ allows us to switch between the diagonal ($\theta = 0$) and off-diagonal coupling ($\theta = \pi/2$).

In the course of the LZSM dynamics, the system energy is driven through orders of magnitude. This on the one hand is a demanding challenge for the numerics. On the other hand, system and bath can not interchange energy as long as the system frequency is above the environmental oscillator frequency. We shall see that the dynamics nicely displays this effect.

Due to the coupling to the spin, the oscillator eigenstates in the subspace of the projected Hamiltonian corresponding to spin up and spin down states are changed to

$$|n_{\pm}\rangle = \hat{D}_{\mp C}\,|n\rangle\,, \qquad C = \frac{\lambda\cos\theta}{\omega}, \tag{5.35}$$

respectively, as can be shown by a completion of the square argument [316]. In the presence of environmental coupling, the analytical result for the probability to remain in the initial state of the system is

$$p(t \to \infty) = \exp\left[\frac{-\pi\left(\left(\Delta - \frac{\lambda^2}{\omega}\sin\left(2\theta\right)\right)^2 + \lambda^2\sin^2\theta \right)}{|v|} \right]. \tag{5.36}$$

One can read off from this result that, even in the presence of coupling to the oscillator, the asymptotic result for the staying probability is unaffected, leading to the celebrated Landau-Zener result (5.31) if the coupling is purely longitudinal ($\theta = 0$). Furthermore, in combination with the no-go-theorem of Saito [316] one can read off from (5.36) the probability $P(t) = |\langle\Psi(t)|-\rangle|$ for the system to be in

the diabatic ground state if initially $|\Psi(0)\rangle = |0_+\rangle\,|+\rangle$, for $t \to \infty$,

$$P(t \to \infty) = 1 - p(t \to \infty) = 1 - \exp\left[\frac{-\pi\left(\left(\Delta - \frac{\lambda^2}{2\omega}\sin(2\theta)\right)^2 + \lambda^2\sin^2\theta\right)}{2\,|v|}\right]. \tag{5.37}$$

The general formula allows for a tuning of the steady state survival probability via several different strategies. Apart from the most obvious ones of changing the tunneling splitting and/or the sweep velocity, which are suggested by the Landau-Zener formula, another one would be to change the mixing angle θ between the diagonal and off-diagonal coupling [331] and/or the coupling strength. We note in passing that, for $\theta = 0$, a change in the oscillator frequency does not affect the asymptotic result if started from the ground state. For initially highly excited (number) states, the oscillator frequency does play a role for the steady state result, however [334].

Number states can be generated experimentally in cavities as has been shown by Haroche and co-workers. In 2007, his group fabricated an open cavity made up of two superconducting niobium mirrors facing each other and detected the birth of a photon in a cavity [336]. In detail, a small coherent field was produced after a microwave pulse was radiated by a classical source and scattered on the edges of the cavity mirrors. The field was then injected inside the cavity, leading to the creation of a superposition of photon number states [337]. Still another option for tuning the probability p, therefore, would be to change the initial excitation of the boson. This last possibility to control the steady state probability is in the focus of interest of the theoretical studies here. From the closure relation (2.26) one may infer that a number state is given in terms of an integral over the whole complex plane. As laid out in [36, 338], one may write a number state

$$|n\rangle = \frac{1}{2\pi}\sqrt{\frac{n!\mathrm{e}^{|\beta|^2}}{|\beta|^{2n}}}\int\limits_{-\pi}^{\pi}\mathrm{d}\theta\,\mathrm{e}^{-in\theta}\,||\beta|\,\mathrm{e}^{i\theta}\rangle, \tag{5.38}$$

i.e. as a one-dimensional integral along a circle in phase space. The fact that a single integral is sufficient is deeply rooted in the overcompleteness of the coherent states (see Sec. 2.3). A straightforward discretization of the integral (5.38) can be done by fixing $N \in \mathbb{N}$ and setting

$$\theta_k := -\pi + \frac{2\pi}{N_d}k, \qquad k = 0, \ldots, N_d. \tag{5.39}$$

Thus

$$|n\rangle \approx \sqrt{\frac{n!\,\mathrm{e}^{|\beta|^2}}{|\beta|^{2n}}}\frac{1}{N_d}\sum_{k=0}^{N_d}\mathrm{e}^{-in\theta_k}\,||\beta|\,\mathrm{e}^{i\theta_k}\rangle. \tag{5.40}$$

The Davydov-Ansatz with multiplicity M for the propagation of a single contribution $||\beta|\,\mathrm{e}^{i\theta_k}\rangle$ to the

sum in (5.40) reads

$$|\Psi_k(t)\rangle = \sum_{m=1}^{M} \sum_{j=\pm} A_{kjm}(t) |\alpha_{kjm}(t)\rangle |j\rangle, \tag{5.41}$$

with initial conditions

$$A_{kjm}(0) = \delta_{j,+}\delta_{m,1}, \qquad \alpha_{k,+,1}(0) = |\beta| \, \mathrm{e}^{\mathrm{i}\theta_k}. \tag{5.42}$$

The full wave function is then approximated by

$$|\Psi(t)\rangle = \sqrt{\frac{n!\mathrm{e}^{|\beta|^2}}{|\beta|^{2n}}} \frac{1}{N_d} \sum_{k=0}^{N_d} \mathrm{e}^{-\mathrm{i}n\theta_k} |\Psi_k(t)\rangle, \tag{5.43}$$

giving rise to four sums in expectation values, which is numerically demanding for large N_d. Instead, the whole expression (5.40) may be propagated with a single D2 wave function $|\Psi(t)\rangle = \sum_{k=1}^{M} \sum_{j=\pm} A_{kj} |j\rangle |\alpha_k\rangle$ of multiplicity $M \geq N_d$ with initial conditions

$$A_{k,+} = \sqrt{\frac{n!\mathrm{e}^{|\beta|^2}}{|\beta|^{2n}}} \frac{1}{N_d} \mathrm{e}^{-\mathrm{i}n\theta_k}, \qquad \alpha_k(0) = |\beta| \, \mathrm{e}^{\mathrm{i}\theta_k}, \tag{5.44}$$

for $k < N$. Numerical results show that the multiplicity required to converge a single realization (5.41) is not multiplied to the multiplicity required to converge (5.44), but is the same in both cases. The parameter space of the LZSM model with coupling to a single harmonic mode is already quite large. Because we are interested in the initial state dependence of the survival probability we first keep fixed the tunneling as well as the sweep parameter in the slow oscillator regime,

$$\Delta = 1, v = \frac{\pi \Delta^2}{4}, \omega = \frac{\Delta}{4}, \tag{5.45}$$

and only to the very end, we also change the frequency of the oscillator. We first investigate the case $n = 0$, for which we may compare the numerical results with the analytical transition probability given by (5.36). We set $n = 0$, $N = 1$, $\beta = 0$ and $|\beta|^{2n} = 1$. Multiplicity M is increased until convergence is reached. Firstly, we find from Fig. 5.15 for the three mixing angles, $\theta = 0, \pi/4, \pi/2$, that the final transition probability depends critically on the requirement that the starting time t_0 of the propagation is sufficiently early, i. e., $t_0 \ll 0$. This can be understood from the fact that (5.36) is valid only if the system starts out in its ground state $\hat{D}^\dagger[C]|0\rangle|+\rangle$ at $t_0 \to -\infty$ (see (5.35)). If t_0 is too close to $t = 0$, this state is not the system's ground state, and the dynamics will depend essentially on the precise value of t_0. We find secondly that the value of $|t_0|$ which results in the correct transition probability depends on the mixing angle θ and the largest value was found for $\theta = \pi/4$. This again follows from the same reasoning, since the off-diagonal coupling transfers the diabatic states to the adiabatic ones.
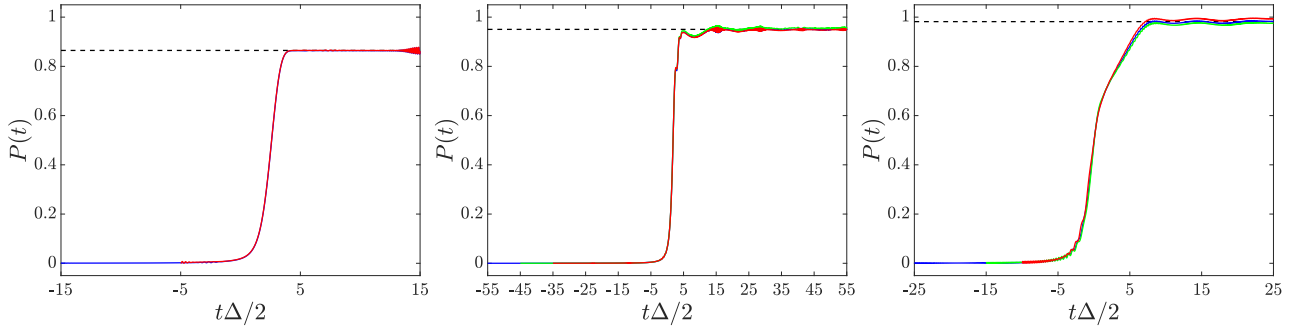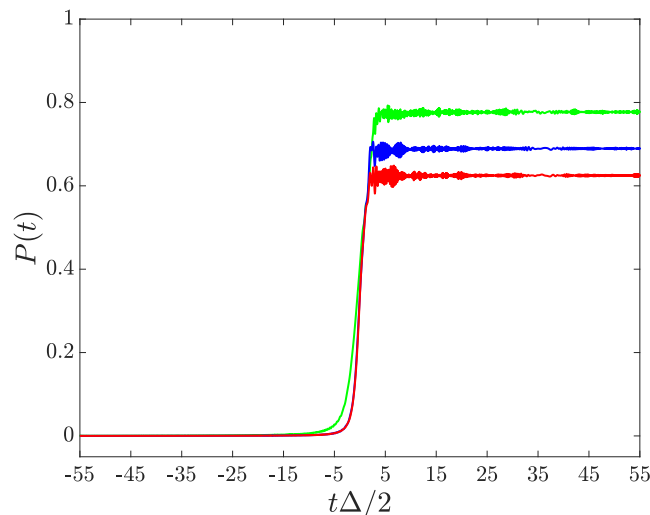
Figure 5.15.: Convergence test with respect to initial time t_0 for $\lambda = \Delta$: Dashed black lines indicate the analytical result (5.36). Different starting times indicated by different colors. For $\theta = 0$ (left panel) starting time $\frac{\Delta}{2}t = -15$ leads to converged result for $M = 15$. For $\theta = \frac{\pi}{4}$ (middle panel), starting time $\frac{\Delta}{2}t = -55$ leads to converged result for $M = 25$. For $\theta = \pi$ (right panel) starting time $\frac{\Delta}{2}t = -25$ leads to converged result for $M = 23$.

The initial times found from Figs. 5.15 are also the appropriate times to start from for higher excited states $|n\rangle$, $n > 0$. We choose $n \in [1, 100]$ for the initial excitation and a coupling strength which is renormalized by the initial excitation,

$$\lambda = \frac{\Delta}{\sqrt{n}}, \tag{5.46}$$

as given in [334]. The convergence with respect to the number N of sampling points on the circle of radius $\beta = \sqrt{n}$ is quite quick, while convergence with respect to multiplicity M occurs only slowly. Next, we choose different radii $|\beta|$ of the circle of integration, in order to examine the emphasis on the special radius $|\beta| = \sqrt{n}$ given in [36]. In Fig. 5.16 it is shown that indeed the deviation from the special radius leads to strong deterioration of the results.


Figure 5.16.: Convergence test with respect to β: $P(t)$ for $n = 4$, $\theta = \pi/4$, $N_d = 14$, $M = 18$. $\beta = 1$ (red), $\beta = 4$ (green), $\beta = \sqrt{n} = 2$ (blue) (in coincidence with the exact result).

The main finding here is that the initial oscillator excitation can be used as a parameter to tune the steady value of the staying probability, if the coupling is scaled according to $\lambda = \frac{\Delta}{\sqrt{n}}$ and the mixing angle $\theta \neq 0$. This is shown in Fig. 5.17, where a monotonic decrease of the steady state value for increasing excitation can be observed for $n > 3$. Multiplicities up to $M = 25$ have been used to obtain converged results. In [334] an (approximate) analytical reasoning for convergence of $P(t \to \infty)$ as $n \to \infty$ is given for $\theta = 0$, in conjunction with the corresponding steady state value. Although generalization of the result therein to $\theta \neq 0$ is not straightforward, our numerical calculations show that also for $\theta \neq 0$ convergence is reached as $n \to \infty$. In the absence of initial excited quanta, it is well known that longitudinal coupling ($\theta = 0$) does not contribute to the LZ transition. By gradually increasing the quanta number n, depending on the mixing angle, a more or less pronounced change of the final transition probability can be observed. Especially for a mixing angle of $\theta = \pi/4$ the effect is largest. Also, in this case the energy exchange between the system and the oscillator is largest for large quantum numbers.

We have also tried to converge results with the multi D1-Ansatz. While the method nicely converges if the $\hat{\sigma}_x$ eigenstates are chosen as basis, with the same number of CS as the D2-Ansatz, the D1-Ansatz does not converge at all if the $\hat{\sigma}_z$ eigenstates are chosen as basis. In the light of the considerations of Sec. 3.6 this is not surprising since the dynamics is here indeed such that $\langle -|\Psi(t)\rangle = 0$ for $t \ll 0$. During the long time for which $\langle -|\Psi(t)\rangle = 0$ we find in the D1-Ansatz that the CS corresponding to the $|-\rangle$ state move far away from the origin, and if the dynamics is such that the $|-\rangle$ state is populated in the vicinity of the avoided crossing, they are too far away in order to participate in the dynamics. Furthermore, the corresponding ρ-matrix is singular throughout all the time when $\langle -|\Psi(t)\rangle = 0$ and consequently a strong regularization has to be implemented for the D1-Ansatz. The D2-Ansatz is highly advantageous with respect to these issues since there they do not occur.

Finally, we investigate the transition for different oscillator frequencies for $n = 50$: slow oscillator
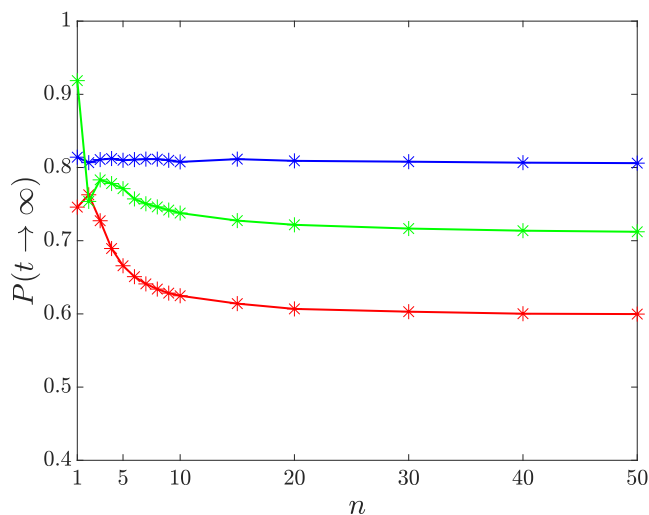
Figure 5.17.: Transition probabilities as a function of n: $\theta = 0$ (blue), $\theta = \pi/4$ (red), $\theta = \pi/2$ (green).

$\omega = 0.2\omega_0$, intermediate oscillator $\omega = \omega_0$ and fast oscillator $\omega = 2\omega_0$, where $\omega_0 = \frac{\Delta}{4}$. Further parameters for the numerics are $N = 25$ and $M = 30$. The mixing angle is $\theta = \pi/4$. As shown in Fig. 5.18, the qubits start with same initial probabilities, and end with large transition probability in the case of a slow oscillator. As expected, the transition time is longer when the oscillator is slow, and allows more transition to occur at intermediate times.

In this section, we have numerically investigated transition probabilities from the plus to the minus spin state, starting from eigenstates of the LZSM problem in the presence of an excited bosonic mode for $t \rightarrow -\infty$. In the next section, we generalize the results of this section to multiple modes. While a straightforward generalization to Fock number states is not possible (see Sec. 3.5), we shall assume that the initial bath state is a shifted coherent state.

### 5.3.2. Coupling to multiple environmental modes

In the following, we attempt to generalize the results of the previous section to multiple environmental modes. In the case of longitudinal coupling, which we assume here, the survival probability does not at all depend on the bath if the initial state is the multi-mode state corresponding to (5.35) (see [316] for details),

$$|\Psi(0)\rangle = |+\rangle \, \hat{D}_{\mathbf{C}}^{\dagger} |0\rangle \,, \qquad \mathbf{C}_n = \frac{\lambda_n}{\omega_n}. \tag{5.47}$$

The survival probability is given by $p(t \rightarrow \infty) = \exp\left[-\frac{\pi\Delta^2}{2|v|}\right]$. We sweep the detuning with velocity $v = 5\Delta^2$, and investigate the case of ohmic damping here ($s = 1$), as given in [339]. Thus it is not necessary to include the initial shift (5.47) in the bath coordinates to an effective system contribution as outlined in Sec. 4.5.1.
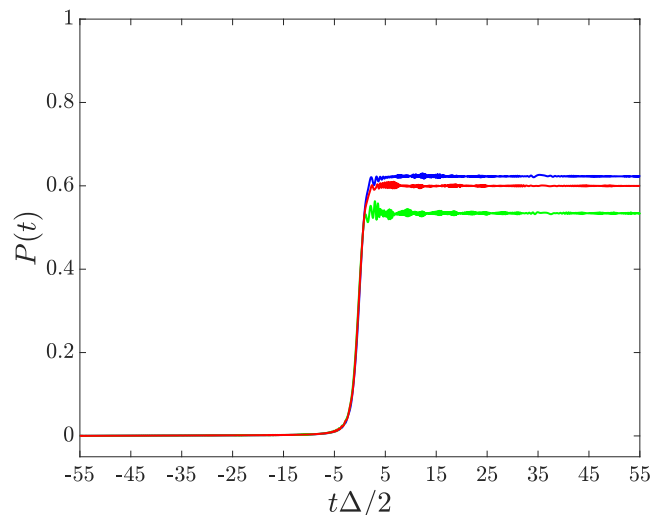
Figure 5.18.: Transition probabilities $P(t)$ as a function of ω: $\omega = 1 \times \omega_0$ (blue), $\omega = 0.2 \times \omega_0$ (green), and $\omega = 2 \times \omega_0$ (red), where $\omega_0 = \Delta/4$; mixing angle $\theta = \pi/4$.
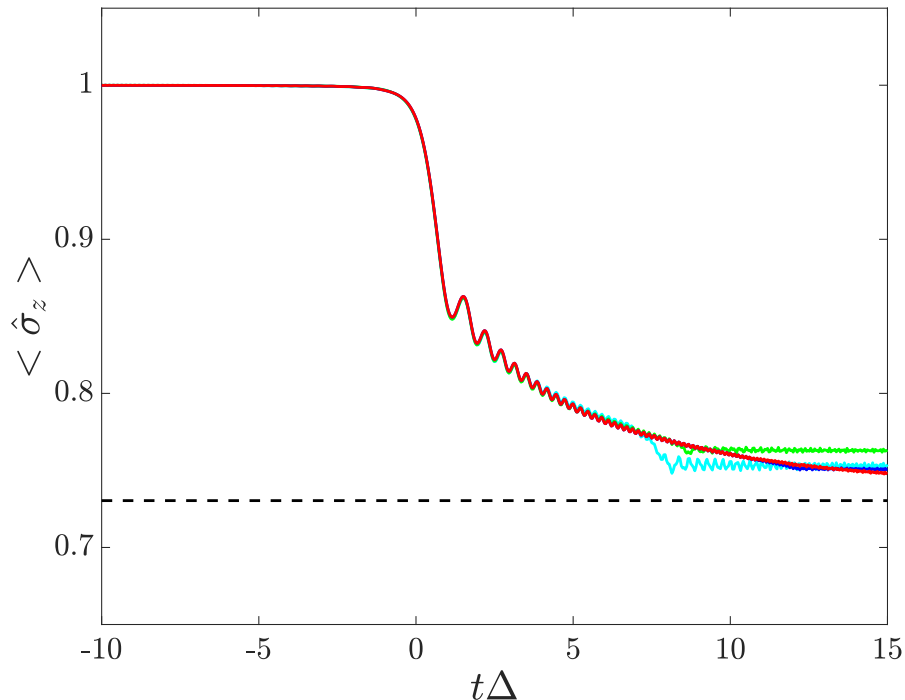
Figure 5.19.: Convergence of the multi Davydov-Ansatz for coupling strength $\alpha = 0.2$ and $\omega_c = 50\Delta$. $M = 20$ (cyan solid), $M = 35$ (green solid), $M = 50$ (blue solid), $M = 65$ (red dashed). Convergence is rather slow.

The cutoff frequency, taken here to be large, $\omega_c = 50\Delta$, has another important property here. While the system frequency is swept through orders of magnitude in the course of the LZSM model, system and bath can not interchange energy if the system energy is far above the cutoff ω_c. Thus, the larger ω_c, the earlier is the time for which system and bath start to interact, and the later is the time at which they cease to interact. This can be nicely seen from Fig. 5.19, where the convergence to the final transition probability is ultra slow, corresponding to the large value of ω_c.

The convergence with respect to the multiplicity is rather slow. The result has been converged with $M = 65$ coherent states where the bath is discretized with $N = 200$ modes according to the exponential FD. An exponential fit from the data calculated with the multi D2-Ansatz with $M = 65$ predicts a staying probability of $p(t \to \infty) = 0.7397$ while the exact value is given by $\exp\left[-\frac{\pi}{10}\right] = 0.7304$. In order to illuminate the slowness of the convergence in more detail, we plot the distribution of the displacements α_{kn} as a function of $n \in \{1, \ldots, 200\}$ and $k \in \{1, \ldots, 60\}$ at time $t\Delta = 11.5$ in Fig. 5.20, and in Fig. 5.21 the coefficients $A_{jk}(t)$ as function of k and t. The visual representation reveals that the bath stays coherent as long as the system is far away from the avoided crossing $t \ll 0$. In contrast to the undriven SBM, multiple modes effectively participate in the dynamics in the vicinity of the avoided crossing. This is deeply rooted in the sweeping of the system frequency since it leads to a sweep through resonance with multiple bath modes causing strong decoherence in the bath. As soon as the vicinity of the avoided crossing is left, the bath becomes coherent again as can be seen from the coefficients' time evolution in Fig. 5.21. In the light of the chaotic dynamics encountered

in the vicinity of the avoided crossing, it is even more surprising that the final transition probability does not depend on the bath at all.
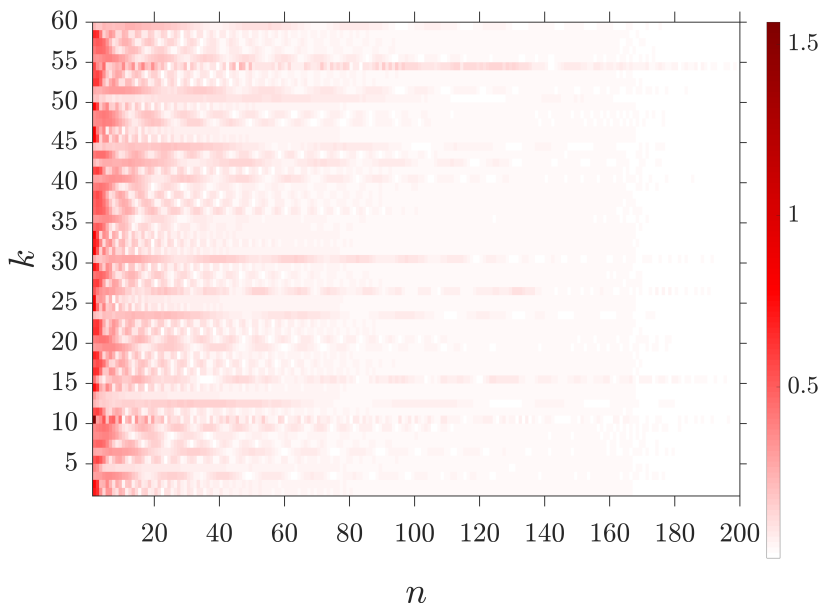
Figure 5.20.: The absolute value of the displacements at $t\Delta = 11.5$ as function of number of mode $n = 1\ldots 200$ and multiplicity $k = 1,\ldots,60$.
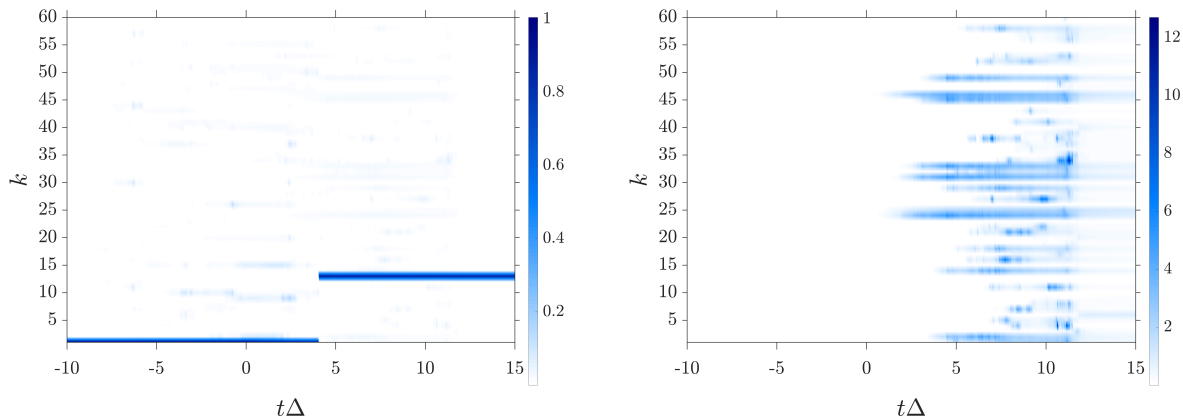
Figure 5.21.: The absolute value of the coefficients as function of number of time $t\Delta$ and multiplicity $k = 1,\ldots,60$: $A_{+,k}(t)$ (left panel), $A_{-,k}(t)$ (right panel).

We have shown that with apoptosis, the multi Davydov-Ansatz numerically exactly predicts the dynamics of system and bath in driven systems even in highly demanding regimes. While without apoptosis the possible number of CS which can be employed in the Ansatz is limited, no such limit exists with apoptosis implemented. In particular, we have shown that the method can be converged also in cases where convergence is rather slow due to the complexity of the bath dynamics. In the

next section, we shall thus confidently apply the method to a dissipative laser-driven system in the strong coupling regime which has so far remained occlusive due to its complexity.

5.4. Rapid Adiabatic Passage with a dissipative environment

It is well known that coupling a quantum system to an environment leads to dissipation and deco-
herence. While they are mostly considered as a nuisance, it has been shown recently that quantum
dissipation can be exploited as a resource for the preparation and control of quantum states [340–
351]. Furthermore, the continuous progress in laser technology has led to a wealth of theoretical and
experimental studies on the interaction of matter with laser light (see e.g. [126] and [352] for in-depth
reviews). Quantum mechanical experiments rely on the ability to start with a pure initial state or
an ensemble of identical initial states, and thus especially the problem of laser-induced population
transfer in multi-level systems has been subject to intense research. For two-level systems, population
transfer can theoretically be achieved if the laser frequency is tuned linearly through resonance with
the system, as in the LZSM model (see Sec. 5.3). This requires, however, adiabatic dynamics, $v \to 0$
in (5.31), rendering virtually impossible the corresponding practical implementation. Alternatively,
population transfer can be achieved if highly coherent radiation is tuned to the resonance frequency
of the system. In principal, complete population transfer can be achieved independently of the pulse
shape if the pulse area is equal to π [126]. Unfortunately the robustness of this method of population
transfer under variations of the pulse area away from π and due to inhomogeneities of the sample is
in general experimentally not satisfactory [353, 354]. Furthermore, for multi-level systems in which
many states lie within the bandwidth of the excitation source, it is virtually impossible for a single
pulse to satisfy the π-condition for all transitions simultaneously. This is the reason why a lot of
effort has been put into the investigation of the rapid adiabatic passage (RAP) scenario, that is less
prone to external disturbances. There the frequency of the radiation is a slowly varying function
of time, which is swept through resonance with the system [353]. Subsequently, we will investigate
both the π-pulse as well as the RAP scenario, for a semiconductor quantum dot in the presence of an
environmental phononic heat bath. Theoretical investigation of this model in the ultra weak coupling
regime has been carried out in [355], utilizing a second order perturbation theory in the system bath
interaction. Not surprisingly, very good agreement with the experimental results was found, although
for high temperatures and low chirp parameters far from optimal population transfer was reported
(away from odd integer multiples of π of pulse areas in the case of small chirp). Here, we will focus
on large system bath couplings. This is especially of high relevance since recent advances in the field
of cold atomic gases have revealed that it is indeed possible to accurately tune the coupling between
a quantum dot and the bath [356].

In the following, we consider the interaction of a two-level system, characterized by system energies
$\omega_1 < \omega_2$, with the electric field $E(t)$ of an external laser. We assume that the polarization of the field
is in the direction of the system's dipole matrix element μ, and that the latter is constant. Let $|1, 2\rangle$
be the diabatic basis, i.e. the standard basis of $\mathbb{R}^2$, then the TDSE for the two-level system, written
in terms of the coefficients of $|\Psi\rangle = c_1 |1\rangle + c_2 |2\rangle$, reads

$$\mathrm{i} \begin{pmatrix} \dot{c}_1 \\ \dot{c}_2 \end{pmatrix} = \begin{pmatrix} \omega_1 & \mu E(t) \\ \mu E^*(t) & \omega_2 \end{pmatrix} \begin{pmatrix} c_1 \\ c_2 \end{pmatrix}. \tag{5.48}$$

The real electric field of the chirped excitation pulse can be written as

$$E(t) = \frac{1}{2} f(t) \left(\exp\left[-\mathrm{i}\omega_0 t - \mathrm{i}\alpha t^2\right] + cc. \right), \tag{5.49}$$

where ω_0 is the laser frequency and α is the linear temporal chirp and $f(t)$ is the time-dependent envelope of the electric field. We now take three commonly applied steps that lead to simplified equations. Firstly, we transfer into the rotating frame (interaction picture) by using the factorization Ansatz

$$c_1 = d_1 \exp\left[-\mathrm{i}\omega_1 t + \mathrm{i}\alpha t^2\right],$$
$$c_2 = d_2 \exp\left[-\mathrm{i}\omega_2 t\right]. \tag{5.50}$$

Secondly, by applying the rotating wave approximation (RWA) we neglect fast oscillating exponential terms $\sim \exp\left[\pm\mathrm{i}\left(\omega_0 + \omega_2 - \omega_1\right)t \pm \mathrm{i}\alpha t^2\right]$. Thirdly and finally we assume laser and system to be resonant at $t = 0$, i.e. $\omega_2 - \omega_1 = \omega_0$. Then the system of equations

$$\mathrm{i} \begin{pmatrix} \dot{d}_1 \\ \dot{d}_2 \end{pmatrix} = \begin{pmatrix} 2\alpha t & \frac{1}{2}\mu f(t) \\ \frac{1}{2}\mu f(t) & 0 \end{pmatrix} \begin{pmatrix} d_1 \\ d_2 \end{pmatrix} \tag{5.51}$$

emerges from system (5.48).

We assume that the pulse has the Gaussian shape

$$f(t) = \frac{\Theta}{\mu\sqrt{\pi}\tau_p} \exp\left(-\frac{t^2}{\tau_p^2}\right), \tag{5.52}$$

where τ_p is the pulse duration (including the numerical FWHM factor $\sqrt{\ln 16}$), and the peak amplitude $\frac{\Theta}{\mu\sqrt{\pi}\tau_p}$ is scaled with the dipole matrix element μ and characterized by the pulse area Θ. The frequency bandwidth Γ and the spectral chirp ϕ'' are related to the pulse duration and the temporal chirp via [354]

$$\tau_p^2 = \frac{1}{\Gamma^2} \left(1 + (2\phi'')^2\Gamma^4\right), \tag{5.53}$$

$$\alpha = \frac{2\phi''\Gamma^4}{1 + (2\phi'')^2\Gamma^4}. \tag{5.54}$$

Experimentally, the chirped laser pulse is created by passing a Fourier-limited source pulse through a pulse-shaping device [357]. The transform-limited pulse duration τ_0 of the source pulse is set to $\tau_0 = 5\,\mathrm{ps}$ as reported in [355]. It is related to the above quantities via $\Gamma = \frac{1}{\tau_0}$.

In an experimental setup, the laser-driven system is not isolated, and it is thus natural to couple it to an environmental bath of phonons. The corresponding total Hamiltonian is then given by (4.6). The

system Hamiltonian is given by (5.51),

$$\hat{\mathcal{H}}_{\text{s}} = \begin{pmatrix} 2\alpha t & \frac{1}{2}\mu f(t) \\ \frac{1}{2}\mu f(t) & 0 \end{pmatrix}, \tag{5.55}$$

and we assume the bath to be coupled to the diabatic state $|1\rangle$,

$$\hat{L} = \begin{pmatrix} 0 & 0 \\ 0 & 1 \end{pmatrix}. \tag{5.56}$$

For the 3D solid state quantum dot investigated in [355], interaction of excitons with acoustical phonons is dominant [355]. Thus the continuous spectral density $J(\omega)$, specifying the phonon bath, is assumed to be superohmic with exponent 3,

$$J(\omega) = A\omega^3 \exp\left[-\frac{\omega^2}{\omega_c^2}\right] \approx \sum_{k=1}^{N} \lambda_k^2 \delta(\omega - \omega_k), \tag{5.57}$$

where A specifies the system-bath coupling strength and ω_c is the cutoff frequency. Based on an estimate of the size of the quantum dot, the cutoff frequency induced by the electron-phonon coupling form factor is set to $\omega_c = 0.72\,\text{meV}$. In a slight deviation from Eq. (4.7) and previous considerations, we assume the discretization of the SD in (5.57) without the π-prefactor.

Because we want to treat strong coupling strengths, special care has to be taken with respect to the initial conditions for the quantum dynamics. The quantum dot is assumed to be in its ground state initially, $|\Psi_{\text{s}}(0)\rangle = |1\rangle$. In the interaction picture, however, the sign of ϕ'' determines whether the energy of the state $|1\rangle$ is above or below the energy of state $|2\rangle$. This is schematically sketched in Fig. 5.22 , where the energies of the diabatic basis $|1, 2\rangle$ are plotted as function of time in the interaction picture versus the energies of the adiabatic basis (the instantaneous eigenstates of the Hamiltonian (5.55))

$$E_{\pm}^{\text{ad}}(t) = \alpha t \pm \sqrt{(\alpha t)^2 + \left(\frac{1}{2}\mu f(t)\right)^2}, \tag{5.58}$$

for $\phi'' = -7\,\text{ps}^2$ and pulse area $\theta = \pi$. For negative chirp $\phi'' < 0$, the energy of $|1\rangle$ is above the energy of state $|2\rangle$ in the interaction picture, for $t < 0$. In the presence of a dissipative bath, however, the ground state of the environment is determined by those states which diagonalize $\langle\Psi_{\text{s}}(0)|\hat{\mathcal{H}}|\Psi_{\text{s}}(0)\rangle$, see [316] for details. Thus, the initial bath state at $T = 0$ is given by the ground state $|\Psi_{\text{B}}(0)\rangle = |\mathbf{0}\rangle$. The sign of the chirp will be chosen to be negative [357], such that the passage proceeds on the upper red line in Fig. 5.22. The coupling strength has been chosen as $A = 10^j A_0$ with $j = 0, 1, 2$ and $A_0 = 0.022\,\text{ps}^{-2}$ as given in [355]. Converged results have been found for the phonon bath being discretized with $N = 200$ modes by the FD $\rho_{\text{f}}(\omega) \sim \text{e}^{-\omega/\omega_c}$. In the light of the consideration of Sec. 5.3.1 we have taken special care with respect to the initial time of the propagation. In order to converge the results with respect to the time axis, propagation has been carried out from $-T$ to T
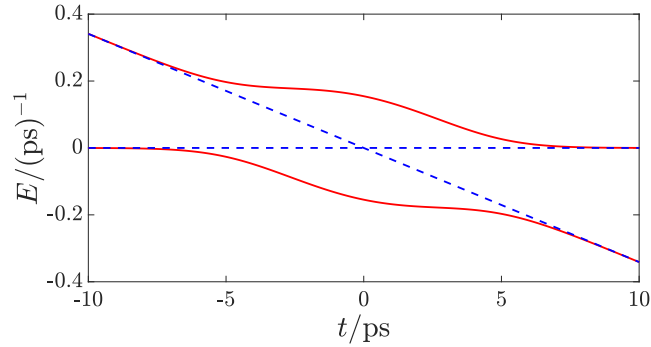
Figure 5.22.: Energies of the diabatic basis $|1,2\rangle$ (blue dashed) vs. the energies of the adiabatic basis (5.58) (red solid) of the Hamiltonian (5.55) as function of time. Further parameters read $\phi'' = -7\,\mathrm{ps}^2$, $\theta = \pi$.

where $T = \frac{10}{\sqrt{2|\alpha|}} = 54.15\,\mathrm{ps}$.
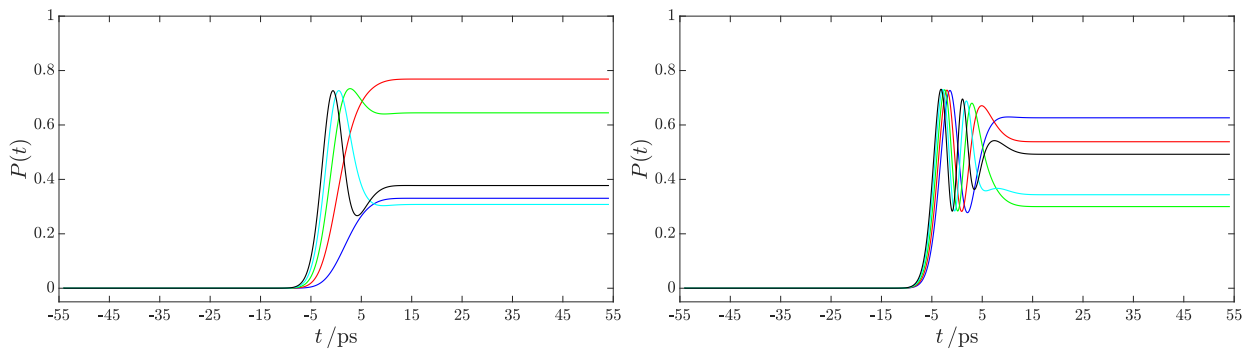
Figure 5.23.: Dynamics of the population $P(t) = \langle\Psi(t)|2\rangle\,\langle 2|\Psi(t)\rangle$, for small chirp $\phi'' = -7\,\mathrm{ps}^2$ and different pulse areas: Left panel $\theta = \pi/2$ (blue solid), $\theta = \pi$ (red solid), $\theta = 3\pi/2$ (green solid), $\theta = 2\pi$ (cyan solid), $\theta = 5\pi/2$ (black solid). Right panel $\theta = 3\pi$ (blue solid), $\theta = 7\pi/2$ (red solid), $\theta = 4\pi$ (green solid), $\theta = 9\pi/2$ (cyan solid), $\theta = 5\pi$ (black solid). The coupling strength is $A = 0.22\,\mathrm{ps}^{-2}$.

Firstly we see from Figs. 5.23-5.26 that, as expected, system and bath do not interact as long as the laser is off. Only after the $|2\rangle$ state has been populated by the laser-matter interaction does the bath interact with the system. For large $t \to \infty$ the system frequency $\omega_{\mathrm{S}} \sim |\alpha|t$ is above the cutoff frequency ω_c and thus system and bath do not interact. We stress that the dynamics is such that $\langle 2|\Psi(t)\rangle = 0$ for $t \ll 0$, hence the corresponding coefficients in the Ansatz wave function are zero for long times and application of the D1-Ansatz would fail to converge. This is, however, not the case for the D2-Ansatz.

By comparing Figs. 5.23 and 5.24 it is nicely revealed that for small chirp $\phi'' = -7\,\mathrm{ps}^2$ the dynamics changes its very nature in the presence of strong coupling to the phonon bath. The presence of spontaneous decay channels between system and bath corrects, for small as well as for large chirp, for the decay channel in the system, in the strong coupling regime.

While for small chirp the transition probability is already above 90% for pulse areas $\theta > 3\pi/2$ (see Figs. 5.23 and 5.24), for large chirp the transition probability is enhanced but does not exceed 80%
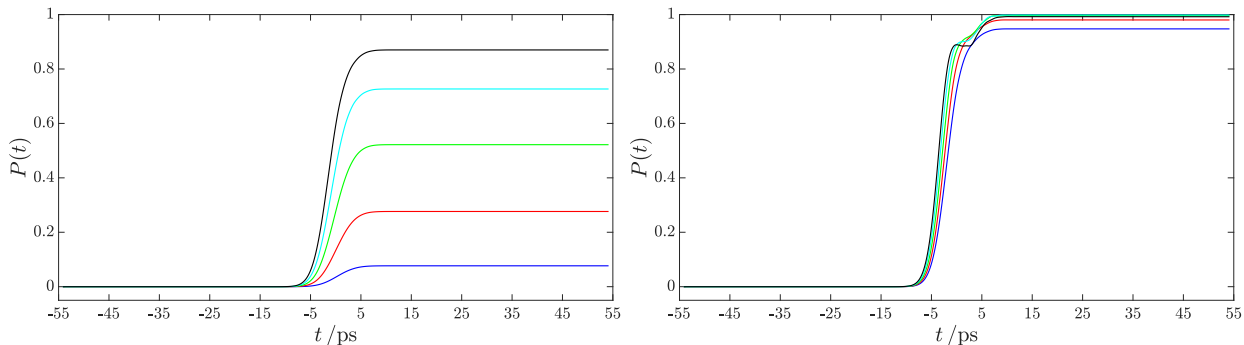
Figure 5.24.: Dynamics of the population $P(t) = \langle\Psi(t)|2\rangle\langle2|\Psi(t)\rangle$, for small chirp $\phi'' = -7\,\mathrm{ps}^2$ and different pulse areas: Left panel $\theta = \pi/2$ (blue solid), $\theta = \pi$ (red solid), $\theta = 3\pi/2$ (green solid), $\theta = 2\pi$ (cyan solid), $\theta = 5\pi/2$ (black solid). Right panel $\theta = 3\pi$ (blue solid), $\theta = 7\pi/2$ (red solid), $\theta = 4\pi$ (green solid), $\theta = 9\pi/2$ (cyan solid), $\theta = 5\pi$ (black solid). The coupling strength is $A = 2.2\,\mathrm{ps}^{-2}$.
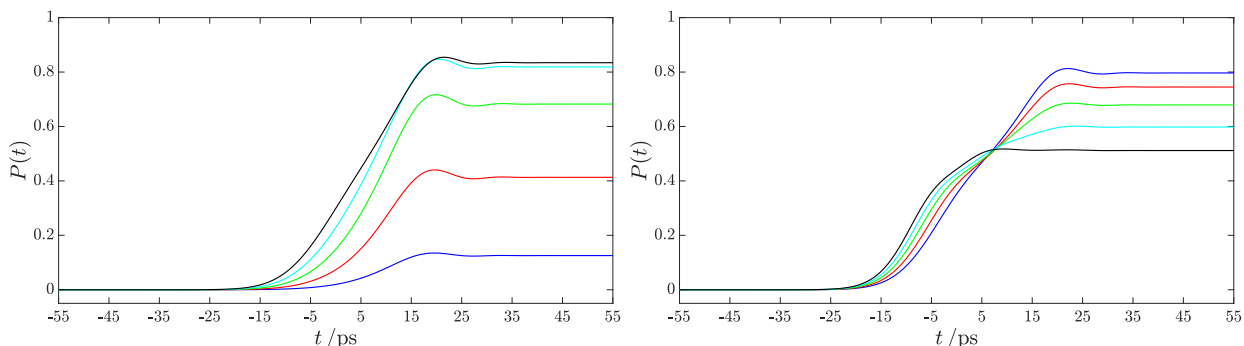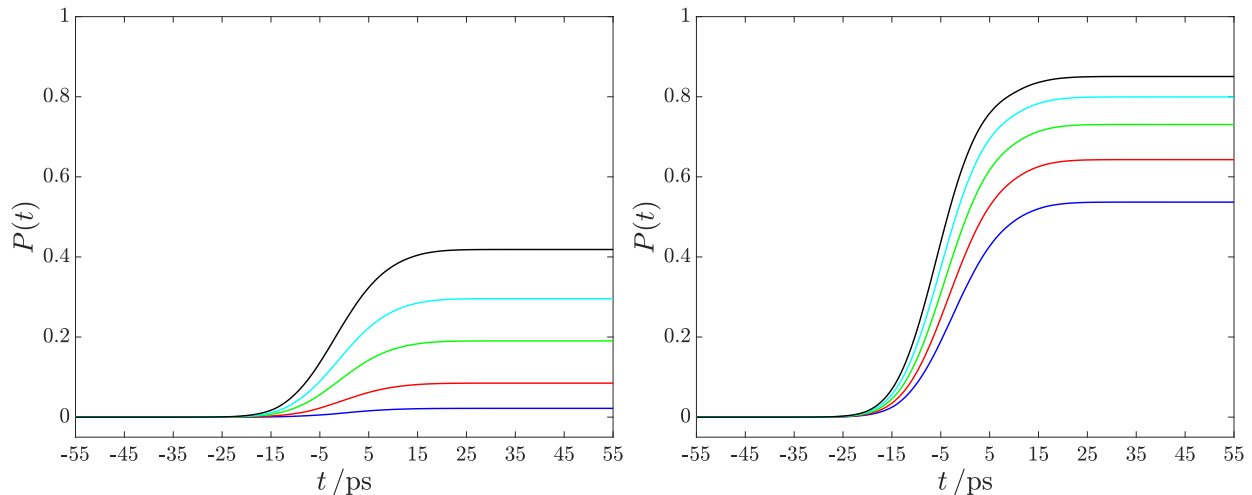

Figure 5.25.: Dynamics of the population $P(t) = \langle\Psi(t)|2\rangle\langle2|\Psi(t)\rangle$, for large chirp $\phi'' = -40\,\mathrm{ps}^2$ and different pulse areas: Left panel $\theta = \pi/2$ (blue solid), $\theta = \pi$ (red solid), $\theta = 3\pi/2$ (green solid), $\theta = 2\pi$ (cyan solid), $\theta = 5\pi/2$ (black solid). Right panel $\theta = 3\pi$ (blue solid), $\theta = 7\pi/2$ (red solid), $\theta = 4\pi$ (green solid), $\theta = 9\pi/2$ (cyan solid), $\theta = 5\pi$ (black solid). The coupling strength is $A = 0.22\,\mathrm{ps}^{-2}$.

even for $\theta = 5\pi$ (see Figs. 5.25 and 5.25). In addition, we have plotted the final transition probability as a function of pulse area and coupling strength at $T = 0$ in Fig. 5.27. The plot nicely shows how with increasing coupling strength the oscillations in the final transition probability cease. Although we can not quantify it, it is obvious that the presence of spontaneous decay channels between system and bath corrects for the decay channel in the system in the strong coupling regime.

We have also investigated the effect of finite temperature on the found results. While moderate temperature does not essentially influence the effect, our results confirm the results given in [355] in regard to a diminishing effect on the population transfer, see Figs. 5.28 and 5.29. Temperature sampling has been converged with up to 4000 samples. We find, analogously to 4.5.2, that in order to converge the samples of the temperature sampling, apoptosis occurs at almost any calculation and is thus once more confirmed to be indispensable for the functionality of the multi Davydov method.

The multi Davydov-Ansatz has enabled us to calculated the dynamics of a laser-driven system coupled strongly to a dissipative environment. In this context, firstly, we have shown that with apoptosis
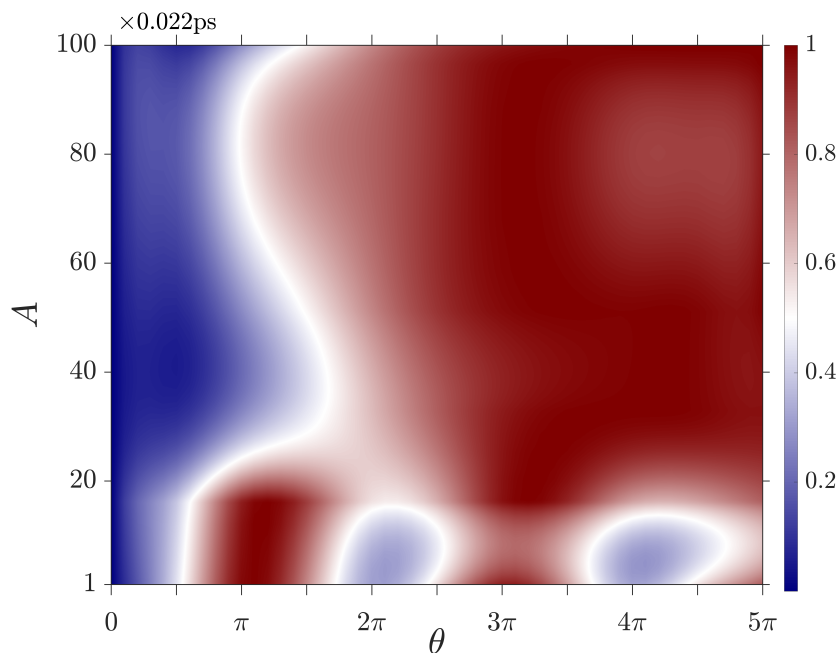
Figure 5.26.: Dynamics of the population $P(t) = \langle\Psi(t)|2\rangle\langle 2|\Psi(t)\rangle$, for large chirp $\phi'' = -40\,\mathrm{ps}^2$ and different pulse areas: Left panel $\theta = \pi/2$ (blue solid), $\theta = \pi$ (red solid), $\theta = 3\pi/2$ (green solid), $\theta = 2\pi$ (cyan solid), $\theta = 5\pi/2$ (black solid). Right panel $\theta = 3\pi$ (blue solid), $\theta = 7\pi/2$ (red solid), $\theta = 4\pi$ (green solid), $\theta = 9\pi/2$ (cyan solid), $\theta = 5\pi$ (black solid). The coupling strength is $A = 2.2\,\mathrm{ps}^{-2}$.

Figure 5.27.: The final transition probability as function of pulse area $\theta = 0, \ldots, 5\pi$ and coupling $A = A_0 \times 0.022\,\mathrm{ps}^{-2}$ for $A_0 = 1, \ldots, 100$.

the temperature sampling, required in order to treat the non-zero temperature case, can efficiently be converged. The stochastically sampled shifted Hamiltonians render complex the bath dynamics, leading to coherent states approaching frequently. On the contrary, without apoptosis, almost none of the samples could be propagated.

We have furthermore shown that in the context of RAP, coupling a system to a dissipative environ-
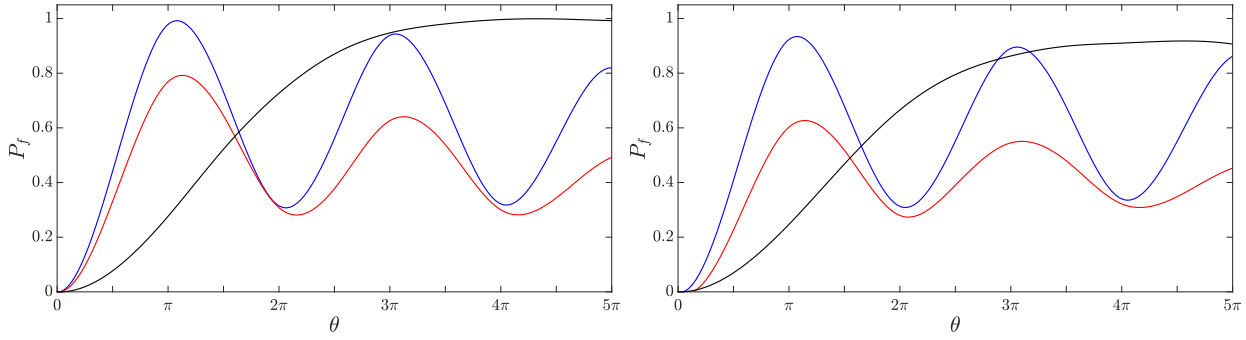
Figure 5.28.: Temperature dependence of the final transition probability, for small chirp $\phi'' = -7\,\text{ps}$: $T = 0\,\text{K}$ (left panel), $T = 20\,\text{K}$ (right panel). Colors indicate the magnitude 10^j of the coupling ($A = 10^j \times 0.022\,\text{ps}^{-2}$): $j = 0$ blue solid, $j = 1$ red solid, $j = 2$ black solid.
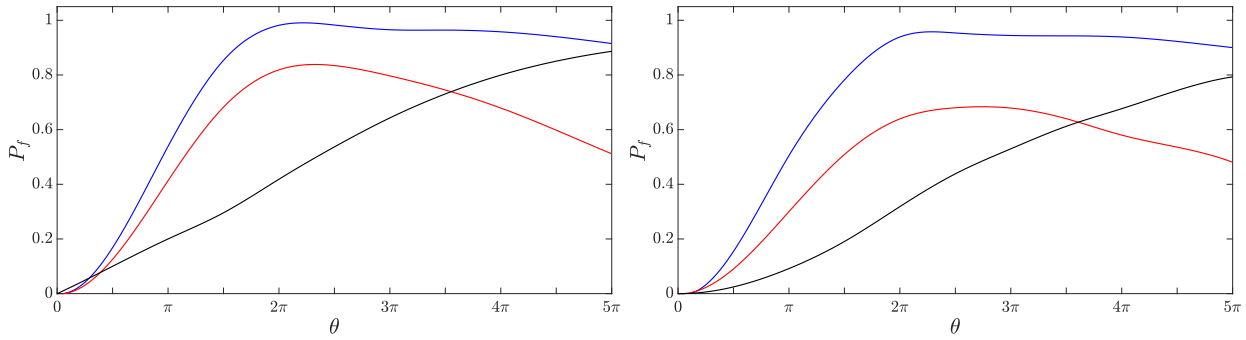
Figure 5.29.: Temperature dependence of the final transition probability, for large chirp $\phi'' = -20\,\text{ps}$: $T = 0\,\text{K}$ (left panel), $T = 20\,\text{K}$ (right panel). Colors indicate the magnitude 10^j of the coupling ($A = 10^j \times 0.022\,\text{ps}^{-2}$): $j = 0$ blue solid, $j = 1$ red solid, $j = 2$ black solid.

ment may serve as a resource for laser-driven population inversion. Even in cases where the laser is only weakly chirped, almost full population inversion can be achieved. This holds true even for non-zero temperature and may thus allow for experimental realization.

6. Summary And Outlook

We have theoretically investigated an Ansatz of the bosonic many-body wave function of several complex composite quantum systems in terms of freely moving Gaussian basis functions. We have shown how to circumvent severe weaknesses of the method, based on non-orthogonal coherent states, because of which it is traditionally considered ill-behaved. By detailing how to proceed in the case of vanishing coefficients by regularization and by apoptosis in the case of closeness of CS we have dispelled these prejudices once and for all.

Based on the foundations presented in the first section, in the second chapter we have investigated general aspects of the real-time propagation in terms of the variational multi-configurational Gaussian (vMCG) Ansatz, a parametrization of the wave function by means of coherent states. By exploitation of a gauge freedom of the Ansatz, we have firstly shown that all variational principles introduced in the first chapter are equivalent for the vMCG Ansatz. By means of the gauge freedom we have secondly outlined how to thoroughly derive from the variational principle a system of equations of motion for the Ansatz parameters in standard form, even in the case where normalized coherent states are applied. Based on a rigorous translation of the equations of motion to linear algebra language, we have detailed subsequently how to carefully regularize the equations of motion for the Ansatz parameters in the event of two major issues related to the vMCG Ansatz: the regularization of the ρ-matrix in the case of vanishing coefficients, and apoptosis in the case of coherent states approaching. As completion of the discourse on previous attempts to circumvent these issues, we have rounded out this part by an excursion to semiclassical methods. In this context we have isolated the variational principle as root of the widely differing numbers of basis functions required for converged results between semiclassical methods and the full variational approach. Furthermore, possible generalizations of the vMCG method by means of displaced number states (DNS) and squeezed states have discussed. While we found that an extension in terms of DNS along the variational principle is impossible due to the emergence of an inappropriate number of equations of motion, generalization by squeezed states is possible in principle. Yet the complexity of the formulation of squeezed states in terms of creation and annihilation operators inevitably requires to work in position representation, where the formulation is much simpler. Thereof work is in progress in our group, and we hope that the insights and regularizations found in this thesis may help to overcome the issues related to squeezed states, allowing for the application of even more powerful basis sets. In order to tackle open quantum system settings, we have highlighted how to generalize the vMCG Ansatz to the multi D1 and D2-Ansatz. Finally we have theoretically argued that the multi D2-Ansatz should be preferred over the multi D1-Ansatz and shown how to treat nonzero bath setups by the multi D2-Ansatz on the wave function level.

In the third chapter we have thoroughly proven that the multi Davydov Ansatz equipped with apoptosis and the regularization in the case of vanishing coefficients is a highly stable and systematically converging method suited to calculate the dynamics of open quantum systems in the weak as well as in the strong coupling regime at extremely low computational effort. To this end, we have considered

the quantum Rabi model, as well as the Spin-Boson model in the ohmic and in the sub-ohmic regime. We have demonstrated for the quantum Rabi model that the regularization of the ρ-matrix in the case of (almost) vanishing coefficients as outlined in the second chapter clearly outperforms other possible regularizations. Secondly, while a surprisingly small number of basis functions has been shown to suffice in order to be close to convergence, we have demonstrated for the Spin-Boson model that apoptosis is inevitably required in order to fully converge to the exact result. While without apoptosis still some propagations may complete successfully, only the implementation of apoptosis allows for a systematic convergence of the multi Davydov Ansatz.

In addition we have shown for the Spin-Boson model that in the ohmic regime most of the environmental modes participate in the dynamics, the sub-ohmic regime is dominated by the dynamics of the small frequency modes. Thus, it is more complicated to reproduce the model's dynamics for the ohmic case in the ultra-strong coupling regime. In both the ohmic as well as in the sub-ohmic case, energy is mainly transferred from the system to the environment through small frequencies.

In order to further reduce the numerical effort required to converge to the continuum limit for continuous spectral densities, we have firstly investigated various different discretizations of the frequency axis. We have shown that, for the multi Davydov Ansatz, the bath correlation function is not an appropriate criterion to estimate the quality of the discretization. By studying the Windowed Fourier Transform we have found such an a priori criterion for the quality of the discretization of continuous spectral densities in the frequency domain. We think that it is well suited to help other researchers to quantify the quality of a given discretization without having to resort to the dynamics. It will for sure straighten up the disorder reigning currently in the field of discretizations of spectral densities in the frequency domain.

Subsequently, by borrowing ideas from the hierarchy of pure states (HOPS) method, we have demonstrated how to avoid an oversampling of small frequencies for polarized initial conditions in the sub-ohmic regime as well as for the treatment of non-zero temperature settings. In this context, translation of the initial conditions to a shifted Hamiltonian have proven highly advantageous.

Finally, we have investigated in detail the advantageousness for the numerical effort of a transformation of the environment of mutually uncoupled oscillators to a (Mori-type) linear chain of effective modes. While this effective representation in principle allows for reproduction of the exact system-plus-bath dynamics, for the Spin-Boson model with continuous ohmic and sub-ohmic spectral density the effective mode representation has been shown to be of no advantage.

The findings of the third chapter show that results obtained from the multi Davydov Ansatz are extremely reliable and thus suited to predict physically correct conclusions also in cases where no further results are at our disposal. Thus, in the fourth chapter, we have explored by its means physically unexploited territory.

Firstly we have calculated by means of the multi Davydov Ansatz the relaxation dynamics of deuterium dimers adsorbed on a silicon surface. To this end, we have taken into account 2495 phonon modes and multiple system levels of the discretized parallel antisymmetric D-Si-Si bending mode. The favourable scaling of the multi Davydov Ansatz with the number of phonon modes has allowed for the

computation of the full system-plus-bath dynamics at comparatively low effort. By investigating in detail their dynamics we found that only certain small frequency-ranges of the environmental modes effectively participate in the dynamics. By transforming the standard bath representation into the effective mode representation (EMR), we found that indeed only approximately 100 effective modes suffice in order to accurately represent the environment, while the number M of coherent states required to converge the multi Davydov Ansatz did not increase by changing the representation. Thus, the multi Davydov Ansatz in combination with the EMR has turned out in the present context to allow the calculation of the relaxation of the dynamics of deuterium at a silicon surface at extremely low cost. However, also in this context apoptosis has turned out to be indispensable in order to obtain converged results.

By inclusion of further energetically higher-lying system-levels we have shown that initial population transfer occurred also to these higher-lying levels, rendering more complex the overall relaxation dynamics. The results presented in this chapter have the potential to reliably predict the relaxation dynamics. While they shed light on the channels through which the relaxation occurs, they may allow to isolate possible approaches to enhance reactions in the presence of surfaces. Future research is required in order to illuminate in more detail the relaxation dynamics in the presence of an external laser, responsible for the initial excitation of the deuterium dimers. In particular, possible further theoretical research comprises the treatment of continuous system degrees of freedom [358].

Secondly, we have investigated in detail the relaxation dynamics of an exciton on a one-dimensional molecular chain in the Holstein molecular crystal. By considering the strong coupling regime, we have found that apoptosis is inevitable in order to obtain converged long-time results. We have shown that, despite the complexity of the phonon dynamics and despite apoptosis reduces the flexibility of the multi Davydov Ansatz, apoptosis is suited to obtain converged results in regions far beyond those attainable without apoptosis implemented.

Furthermore, we have found that special care has to be taken with respect to the initial positions of the initially unpopulated CS in order to maintain the symmetry of the model. Only if the initially unpopulated CS obey the symmetry does the Ansatz wave function obey the symmetry for all times. Finally, we leave for further applications the extension of the presented results to larger chain lengths and even longer times. As pointed out in Sec. 3.5, a straightforward generalization to multiple excitons is, however, not in sight.

Thirdly we have shown how to tune the transition probability in the Landau-Zener-Stückelberg-Majorana model (LZSM) coupled to an environment. By investigating in detail the dynamics of the system, we have illuminated several aspects of diagonal and off-diagonal coupling. The main finding of this section has been the fact that if the coupling is scaled appropriately, a consistent limit for the excitation $n \to \infty$ can be found.

To this end, we have numerically investigated transition probabilities from the plus to the minus spin state, starting from eigenstates of the LZSM problem in the presence of an excited bosonic mode $|n\rangle$ for $t \to -\infty$. We have demonstrated how the reduction of the integral occurring in the representation of the excited state by coherent states to an integral over a circle of radius β, and of the corresponding

initial value sampling to a single wave-function allows for an extremely efficient propagation scheme. Although the circle's radius β is in principle arbitrary, numerical calculations show that correct results are obtained with reasonable numerical effort only if the radius is chosen as $\beta = \sqrt{n}$, in coincidence with theoretical considerations in [36]. With the avoided crossing (of the bare system) at $t = 0$, we found from a thorough convergence study that, especially for non-zero mixing angle θ (see Eq. (5.29)), in the numerics, we have to start from rather early times $t_0 \ll 0$. Furthermore, in order to compare results for different initial excitation numbers of the bosonic mode, we had to scale the coupling strength with $1/\sqrt{n}$. Then, we found convergence of the transition probability $P(t \to \infty)$ for large n. The asymptotic values are non-trivially dependent on the mixing angle θ. For $\theta = 0$, the diagonal coupling shows little effect on the transition probabilities at long times even in the presence of the initial excited quanta. For $\theta = \pi/4$, both channels of coupling are open, and it turns out that for large n, larger amounts of energy are exchanged between the spin and the oscillator as if one of the channels was closed. Furthermore, we have shown that also the oscillator frequency allows for a tuning of the final probability. If the oscillator is slower, more transitions occur at intermediate times, leading to larger transition probability at long times. It would be an interesting topic for future studies to investigate if interference between the diagonal and off-diagonal coupling channels is responsible for the enhanced energy exchange between the spin and oscillator. This could be done by adding additional bath degrees of freedom with continuous spectral densities, leading to decoherence. For multiple environmental modes, we have investigated the effect of an ohmic bath of large cutoff on the LZSM dynamics by pushing the number of coherent states employed to reproduce the exact dynamics into unexplored territory. We have shown that with apoptosis, the multi Davydov-Ansatz numerically exactly predicts the dynamics of system and bath in driven systems even in highly demanding regimes. While without apoptosis the possible number of CS which can be employed in the Ansatz is limited, no such limit exists with apoptosis implemented. In particular, we have shown that the method can be converged also in cases where convergence is rather slow due to the complexity of the bath dynamics.

Fourthly and finally, in a study of rapid adiabatic passage coupled to an environment we have shown that strongly coupling a system subject to chirped laser excitation to an environmental bath is suited to enhance the final transition probability by orders of magnitude, and that consequently the environmental degrees of freedom may serve as a resource. This was shown to hold true even for non-zero temperature, and thus we hope that experimental realizations will underpin this finding in the future. In this context, the multi Davydov-Ansatz has enabled us to calculated the dynamics of a laser-driven system coupled strongly to a dissipative environment. We have shown that with apoptosis the temperature sampling, required in order to treat the non-zero temperature case, can efficiently be converged. The stochastically sampled shifted Hamiltonians render complex the bath dynamics, leading to coherent states approaching frequently. On the contrary, without apoptosis, almost none of the samples could be propagated.

To summarize, we have shown that even in highly demanding regimes as for laser driven systems at non-zero temperature in dissipative environments, the multi Davydov-Ansatz equipped with apoptosis

and the regularization of the ρ-matrix is a highly reliable and stable numerical tool which allows to calculate the system and bath dynamics at extremely low numerical effort. We hope that the results of this thesis will enable other researchers to reliably predict the properties of various further physical systems.

List of abbreviations

BCF	bath correlation function
CS	coherent state
CCS	coupled coherent states method
DFVP	Dirac-Frenkel variational principle
DMRG	density-matrix renormalization group method
DNS	displaced number states
EMR	effective mode representation
EOM	equations of motion
FD	density of frequencies
FWHM	full-width half-maximum
HEOM	hierarchy of equations of motion method
HK	Herman-Kluk
HOPS	hierarchy of pure states method
LZ	Landau-Zener
LZSM	Landau-Zener-Stüeckelberg-Majorana model
(ML-) MCTDH	(multi-layer) multi-configurational time-dependent Hartree method
MVP	McLachlan variational principle
QED	quantum electrodynamics
QUAPI	quasi-adiabatic path-integral method
RAP	rapid adiabatic passage
RWA	rotating-wave approximation
SBM	Spin Boson model
SD	spectral density
TDSE	time-dependent Schrödinger equation
TDVP	time-dependent variational principle
TISE	time-independent Schrödinger equation
vMCG	variational multi-configurational Gaussian method
WFT	Windowed Fourier Transform

Appendix

A. Closure relation of displaced number states

We want to show that unity can be represented by

$$\hat{1} = \frac{1}{\pi} \int_{\mathbb{C}} d\alpha \, \hat{D}_\alpha \ket{n} \bra{n} \hat{D}_\alpha^\dagger. \tag{A.1}$$

First, we calculate the matrix elements $\bra{m} \hat{D}_\alpha \ket{n}$ by utilization of

$$\exp\left[-\alpha^* \hat{a}\right] \ket{n} = \sum_{k=0}^{n} \frac{(-\alpha^*)^k}{k!} \sqrt{\frac{n!}{(n-k)!}} \ket{n-k} = \sum_{k=0}^{n} \frac{(-\alpha^*)^k}{(n-k)!} \sqrt{\frac{n!}{k!}} \ket{k}. \tag{A.2}$$

Using the disentangled form of the displacement operator (2.33), one easily derives

$$\bra{m} \hat{D}_\alpha \ket{n} = \exp\left(-\frac{1}{2}|\alpha|^2\right) \sum_{k=0}^{\min\{m,n\}} \frac{\alpha^{m-k}(-\alpha^*)^{n-k}}{(m-k)!(n-k)!k!} \sqrt{m!n!} \tag{A.3}$$

$$= \exp\left(-\frac{1}{2}|\alpha|^2\right) \begin{cases} \sqrt{\frac{n!}{m!}} \alpha^{m-n} L_n^{m-n}\left(|\alpha|^2\right), & m \geq n \\ \sqrt{\frac{m!}{n!}} (-\alpha^*)^{n-m} L_m^{n-m}\left(|\alpha|^2\right), & n \geq m \end{cases}, \tag{A.4}$$

where the generalized Laguerre polynomials $L_n^{(j)}$ are given by

$$L_n^{(j)}(x) = \sum_{k=0}^{n} (-1)^k \binom{n+j}{n-k} \frac{x^k}{k!}. \tag{A.5}$$

They fulfill the orthogonality condition

$$\int_0^\infty dx \, x^j e^{-x} L_n^{(j)}(x) L_m^{(j)}(x) = \frac{(n+j)!}{n!} \delta_{nm}. \tag{A.6}$$

By twice insertion of the identity in terms of number states (2.11), eq. (A.1) is equivalent to

$$\hat{1} = \frac{1}{\pi} \sum_{k,l=0}^{\infty} \int_{\mathbb{C}} d\alpha \, \ket{k} \bra{k} \hat{D}_\alpha \ket{n} \bra{n} \hat{D}_\alpha^\dagger \ket{l} \bra{l}. \tag{A.7}$$

From (A.4) we infer that it is crucial to split the summations into four parts: (i) $k, l \leq n$, (ii) $k < n, l > n$, (iii) $k > n, l < n$, (iv) $k, l > n$. While the parts (ii) and (iii) give 0, the parts (i) and (iv)

give $\sum\limits_{k=0}^{n} |k\rangle \langle k|$ and $\sum\limits_{k=n+1}^{\infty} |k\rangle \langle k|$, respectively. We show exemplarily (i) and (ii). Suppose $k, l \leq n$:

$$\frac{1}{\pi} \sum_{k,l=0}^{n} \int_{\mathbb{C}} \mathrm{d}\alpha \, |k\rangle \langle k| \, \hat{D}_\alpha \, |n\rangle \langle n| \, \hat{D}_\alpha^\dagger \, |l\rangle \langle l| \tag{A.8}$$

$$= \frac{1}{\pi} \sum_{k,l=0}^{n} |k\rangle \langle l| \, \frac{\sqrt{k!l!}}{n!} \int_{\mathbb{C}} \mathrm{d}\alpha \, \mathrm{e}^{-|\alpha|^2} (-\alpha^*)^{n-k} (-\alpha)^{n-l} L_k^{(n-k)}\left(|\alpha|^2\right) L_l^{(n-l)}\left(|\alpha|^2\right) \tag{A.9}$$

$$= \sum_{k=0}^{n} |k\rangle \langle k| \, \frac{k!}{n!} \int_0^\infty \mathrm{d}r \, 2r \left(r^2\right)^{n-k} \mathrm{e}^{-r^2} L_k^{n-k}\left(r^2\right) L_k^{n-k}\left(r^2\right) \tag{A.10}$$

$$= \sum_{k=0}^{n} |k\rangle \langle k| \,, \tag{A.11}$$

In (A.9) we have introduced polar coordinates, where the integration over the angle gives $2\pi\delta_{kl}$. In (A.10) we have used the orthogonality of the Laguerre polynomials (A.6). Now suppose $k < n, l > n$. Along similar lines, the integration over the angle gives 0. This completes the proof.

B. Hamilton equations: classical vs. CCS for a Morse oscillator

Here we show that Eq. (3.45),

$$i\dot{\alpha} = \frac{\partial H(\alpha^*, \alpha)}{\partial \alpha^*},$$ (B.1)

arising for the special case of multiplicity $M = 1$ from system (3.43,3.44), differs from classical Hamilton equations for the 1D Morse potential

$$V(q) = D\left(1 - e^{-\alpha_1 q}\right)^2.$$ (B.2)

The Hamilton equations for a particle of mass $m = 1$ in the 1D Morse potential read

$$\dot{q} = p,$$ (B.3)

$$\dot{p} = -V'(q) = -2D\alpha_1 \left(e^{-\alpha_1 q} - e^{-2\alpha_1 q}\right).$$ (B.4)

Here, D is the well-depth and α_1 is the potential width.
Quantization of the potential, done via (2.5), yields

$$\hat{\mathcal{H}} = \frac{\omega}{4}\left(\hat{a}^\dagger - \hat{a}\right)^2 + D\left(1 - e^{-\alpha_2(\hat{a}^\dagger + \hat{a})}\right)^2$$ (B.5)

where

$$\alpha_2 = \frac{\alpha_1}{\sqrt{2\omega}}.$$ (B.6)

Here, ω can be considered as a further free parameter. The ordered form of the kinetic energy operator is found to be

$$T(\hat{a}^\dagger, \hat{a}) = \frac{\hat{p}^2}{2} = -\frac{\omega}{4}\left(\hat{a}^\dagger - \hat{a}\right)^2 = -\frac{\omega}{4}\left[\left(\hat{a}^\dagger\right)^2 - 2\hat{a}^\dagger\hat{a} - 1 + \hat{a}^2\right]$$ (B.7)

and the ordered form of the potential energy is

$$V(\hat{a}^\dagger, \hat{a}) = D\left(1 - 2e^{\alpha_2^2/2}e^{-\alpha_2\hat{a}^\dagger}e^{-\alpha_2\hat{a}} + e^{2\alpha_2^2}e^{-2\alpha_2\hat{a}^\dagger}e^{-2\alpha_2\hat{a}}\right),$$ (B.8)

where the Baker-Campbell-Hausdorff formula has been used to order the exponentials. Consequently, equation (B.1) reads

$$i\dot{\alpha} = \frac{\partial H(\alpha^*, \alpha)}{\partial \alpha^*} = -\frac{\omega}{2}(\alpha^* - \alpha) + 2D\alpha_2\left[e^{\alpha_2^2/2}e^{-\alpha_2(\alpha^* + \alpha)} - e^{2\alpha_2^2}e^{-2\alpha_2(\alpha^* + \alpha)}\right].$$ (B.9)

Using

$$\alpha = \sqrt{\frac{\omega}{2}} \left(q + \frac{\mathrm{i}}{\omega} p \right), \tag{B.10}$$

according to (2.20), we finally arrive at

$$\dot{q} = p \tag{B.11}$$

$$\dot{p} = -2D\alpha_1 \left(\mathrm{e}^{\alpha_1^2/(4\omega)} \mathrm{e}^{-\alpha_1 q} - \mathrm{e}^{\alpha_1^2/\omega} \mathrm{e}^{-2\alpha_1 q} \right). \tag{B.12}$$

Eq. (B.12) differs from (B.4) in the two exponential prefactors which stem from disentanglement of creation and annihilation operator. However, usually these factors are close to unity.

C. Equations of motion for the multi Davydov-Ansatz

In order to express the equations of motion, arising from the variational principle for the multi Davydov-Ansatz, we consider a physical system which is bipartite: while one part has finite Hilbert space dimension (the 'system'), the other one does not (the environment or 'bath'). Clearly they have to be coupled in order not to behave as if they were isolated. Thus, let us assume a Hamiltonian

$$\hat{\mathcal{H}} = \hat{\mathcal{H}}_{\text{sys}} + \hat{\mathcal{H}}_{\text{bath}} + \hat{\mathcal{H}}_{\text{int}} \tag{C.1}$$

split into system-, bath- and interaction parts. The system is of finite Hilbert space dimension N_S, such that we can choose a finite basis $\{|v_j\rangle \,|\, j = 1, \ldots, N_S\}$ and write

$$\hat{\mathcal{H}}_{\text{sys}} = \sum_{i,j=1}^{N_S} Z_{ij} |v_i\rangle \langle v_j| \,. \tag{C.2}$$

Writing

$$\hat{\mathcal{H}}_{\text{int}} = \hat{L}\hat{\mathcal{H}}_{\text{I}} \tag{C.3}$$

with $\hat{L}$ acting only on the system and $\hat{\mathcal{H}}_{\text{I}}$ only acting on the environment, we may also expand

$$\hat{L} = \sum_{i,j=1}^{N_S} L_{ij} |v_i\rangle \langle v_j| \,. \tag{C.4}$$

The corresponding multi D2-Ansatz reads (see Sec. 3.6)

$$|\Psi_{\text{D2}}^{\text{M}}(t)\rangle = \sum_{k=1}^{M} \left(\sum_{j=1}^{N_S} A_{kj}(t) |v_j\rangle \right) |\mathbf{F}_k(t)\rangle \,, \tag{C.5}$$

where $A_{kj}(t)$ are complex coefficients and $|\mathbf{F}_k(t)\rangle = \bigotimes_{n=1}^{N_b} |F_{kn}(t)\rangle$ are N_b-mode coherent states. The multi D1-Ansatz (see Sec. 3.6 corresponding to the chosen system basis reads

$$|\Psi_{\text{D1}}^{\text{M}}(t)\rangle = \sum_{k=1}^{M} \sum_{j=1}^{N_S} A_{kj}(t) |v_j\rangle |\mathbf{F}_{kj}(t)\rangle \,, \tag{C.6}$$

where again $A_{kj}(t)$ are complex coefficients and $|\mathbf{F}_{kj}(t)\rangle = \bigotimes_{n=1}^{N_b} |F_{kjn}(t)\rangle$ are N_b-mode coherent states. In the sequel we will suppress the explicit notion of time-dependence for the sake of simplicity. We shall derive the equations of motion for the D2-Ansatz in Sec. C.1 and subsequently outline how to formulate the system of equations of motion in terms of matrix operations. In Sec. C.2 we do the same for the D1-Ansatz.

C.1. D2-Ansatz

The time-derivative of the multi D2-Ansatz wave function (C.5) reads

$$\frac{\partial}{\partial t} \left|\Psi_{\mathrm{D2}}^{\mathrm{M}}\right\rangle = \sum_{j=1}^{N_S} \sum_{k=1}^{M} \left[\dot{A}_{kj} + A_{kj} \sum_{m=1}^{N_b} \left(-\frac{1}{2}\dot{F}_{km}F_{km}^* - \frac{1}{2}F_{km}\dot{F}_{km}^* + \dot{F}_{km}\hat{a}_m^\dagger\right)\right] \left|\mathbf{F}_k\right\rangle \left|v_j\right\rangle, \qquad (C.7)$$

and the variation similarly reads

$$\left\langle\delta\Psi_{\mathrm{D2}}^{\mathrm{M}}\right| = \sum_{j=1}^{N_S} \sum_{k=1}^{M} \left\langle v_j\right| \left\langle\mathbf{F}_k\right| \left[\delta A_{kj}^* + A_{kj}^* \sum_{m=1}^{N_b} \left(\left(-\frac{1}{2}F_{km} + \hat{a}_m\right)\delta F_{km}^* - \frac{1}{2}F_{km}^*\delta F_{km}\right)\right]. \qquad (C.8)$$

Under the assumption that all appearing variations are mutually independent, MN_S equations can be obtained by projection of the TDSE onto $\left\langle v_j\right| \left\langle\mathbf{F}_l\right|$, which yields

$$\left\langle v_j\right| \left\langle\mathbf{F}_l\right| \frac{\partial}{\partial t} \left|\Psi_{\mathrm{D2}}^{\mathrm{M}}\right\rangle = \sum_{k=1}^{M} \left[\dot{A}_{kj} + A_{kj} \sum_{m=1}^{N_b} \left(-\frac{1}{2}\dot{F}_{km}F_{km}^* - \frac{1}{2}F_{km}\dot{F}_{km}^*\right)\right] \left\langle\mathbf{F}_l|\mathbf{F}_k\right\rangle$$

$$+ \sum_{k=1}^{M} \left[A_{kj} \sum_{m=1}^{N_b} \dot{F}_{km}F_{lm}^*\right] \left\langle\mathbf{F}_l|\mathbf{F}_k\right\rangle$$

$$= -\,\mathrm{i}\left\langle v_j\right| \left\langle\mathbf{F}_l\right| \hat{\mathcal{H}} \left|\Psi_{\mathrm{D2}}^{\mathrm{M}}\right\rangle. \qquad (C.9)$$

We define the expression

$$X_{kj} := \dot{A}_{kj} + A_{kj} \sum_{m=1}^{N_b} \left(-\frac{1}{2}\dot{F}_{km}F_{km}^* - \frac{1}{2}F_{km}\dot{F}_{km}^*\right) \qquad (C.10)$$

according to Sec. 3.2. With this abbreviation, equation (C.9) reads

$$\sum_{k=1}^{M} \left[X_{kj} + A_{kj} \sum_{m=1}^{N_b} \dot{F}_{km}F_{lm}^*\right] \left\langle\mathbf{F}_l|\mathbf{F}_k\right\rangle = -\mathrm{i}\left\langle v_j\right| \left\langle\mathbf{F}_l\right| \hat{\mathcal{H}} \left|\Psi_{\mathrm{D2}}^{\mathrm{M}}\right\rangle. \qquad (C.11)$$

Additional MN_b equations are obtained by projection onto $\sum_{j=1}^{N_S} A_{lj}^* \left\langle v_j\right| \left\langle\mathbf{F}_l\right| \hat{a}_r$, which yields

$$\sum_{j=1}^{N_S} A_{lj}^* \left\langle v_j\right| \left\langle\mathbf{F}_l\right| \hat{a}_r \frac{\partial}{\partial t} \left|\Psi_{\mathrm{D2}}^{\mathrm{M}}\right\rangle = \sum_{j=1}^{N_S} \left\{A_{lj}^* \sum_{k=1}^{M} \left[F_{kr}\left(X_{kj} + A_{kj} \sum_{m=1}^{N_b} \dot{F}_{km}F_{lm}^*\right)\right] \left\langle\mathbf{F}_l|\mathbf{F}_k\right\rangle\right.$$

$$+ \sum_{k=1}^{M} A_{kj}\dot{F}_{kr} \left\langle\mathbf{F}_l|\mathbf{F}_k\right\rangle \Bigg\}$$

$$= -\,\mathrm{i}\sum_{j=1}^{N_S} A_{lj}^* \left\langle v_j\right| \left\langle\mathbf{F}_l\right| \hat{a}_r\hat{\mathcal{H}} \left|\Psi_{\mathrm{D2}}^{\mathrm{M}}\right\rangle. \qquad (C.12)$$

We denote the Hadamard product by $\circ$, the tensor product by $\otimes$, by $\mathbb{1}_n$ the $n \times n$ unit matrix, and by $1_{m \times n}$ the matrix in $\mathbb{C}^{m \times n}$ which consists of only ones. Furthermore, we denote by $\mathbf{vec}(\boldsymbol{M})$ the vectorization of a matrix $\boldsymbol{M}$, which converts the matrix into a column vector,

$$\mathbf{vec}(\boldsymbol{M}) = (a_{11}, \ldots, a_{m1}, a_{12}, \ldots, a_{m2}, \ldots, a_{1n}, \ldots, a_{mn})^T \in \mathbb{C}^{mn \times 1} \tag{C.13}$$

for

$$\boldsymbol{M} = \begin{pmatrix} a_{11} & a_{12} & \cdots & a_{1n} \\ \vdots & \vdots & \cdots & \vdots \\ a_{m1} & a_{m2} & \cdots & a_{mn} \end{pmatrix} \in \mathbb{C}^{m \times n}. \tag{C.14}$$

Define the matrix of displacements

$$\boldsymbol{F} \in \mathbb{C}^{M \times N_b}, \qquad \boldsymbol{F}_{kn} = F_{kn}, \tag{C.15}$$

the matrix of coefficients

$$\boldsymbol{A} \in \mathbb{C}^{M \times N_S}, \qquad \boldsymbol{A}_{kj} = A_{kj}, \tag{C.16}$$

and the matrix of auxiliary variables

$$\boldsymbol{X} \in \mathbb{C}^{M \times N_S}, \qquad \boldsymbol{X}_{kj} = X_{kj}. \tag{C.17}$$

The vectors of coefficients are

$$\overrightarrow{A_j} := (A_{1j}, \ldots, A_{Mj})^T \in \mathbb{C}^{M \times 1}, \qquad \boldsymbol{A}_j := \mathrm{diag}\left(\overrightarrow{A_j}\right) \in \mathbb{C}^{M \times M}. \tag{C.18}$$

Furthermore, we set

$$\overrightarrow{X_j} := (X_{1j}, \ldots, X_{Mj})^T \in \mathbb{C}^{M \times 1}, \qquad \boldsymbol{X}_j := \mathrm{diag}\left(\overrightarrow{X_j}\right) \in \mathbb{C}^{M \times M}, \tag{C.19}$$

and

$$\boldsymbol{D} := \boldsymbol{F}\boldsymbol{F}^\dagger \in \mathbb{C}^{M \times M}, \qquad \boldsymbol{d} := \mathrm{diag}\left(\boldsymbol{D}\right) \otimes 1_{1 \times M} \in \mathbb{R}^{M \times M} \tag{C.20}$$

With the matrices

$$\boldsymbol{S} := \mathrm{e}^{\boldsymbol{D}^* - \frac{1}{2}\left(\boldsymbol{d} + \boldsymbol{d}^T\right)} \in \mathbb{C}^{M \times M}, \qquad \boldsymbol{S}_{lk} = \langle \mathbf{F}_l | \mathbf{F}_k \rangle \tag{C.21}$$

it is immediate that

$$\langle v_j| \langle \mathbf{F}_l| \frac{\partial}{\partial t} |\Psi_{\mathrm{D2}}^{\mathrm{M}}\rangle = \sum_{k=1}^{M} \left[X_{kj} + A_{kj} \sum_{m=1}^{N_b} \dot{F}_{km} F_{lm}^* \right] \langle \mathbf{F}_l|\mathbf{F}_k\rangle$$
$$= \left[\boldsymbol{S}\overrightarrow{X_j} + \left(\boldsymbol{F}^* \dot{\boldsymbol{F}}^T \circ \boldsymbol{S} \right) \overrightarrow{A_j} \right]_l , \tag{C.22}$$

and

$$\sum_{j=1}^{N_S} A_{lj}^* \langle v_j| \langle \mathbf{F}_l| \hat{a}_r \frac{\partial}{\partial t} |\Psi_{\mathrm{D2}}^{\mathrm{M}}\rangle = \sum_{j=1}^{N_S} \left\{ A_{lj}^* \sum_{k=1}^{M} \left[F_{kr} \left(X_{kj} + A_{kj} \sum_{m=1}^{N_b} \dot{F}_{km} F_{lm}^* \right) \right] \langle \mathbf{F}_l|\mathbf{F}_k\rangle \right.$$
$$\left. + \sum_{k=1}^{M} A_{kj} \dot{F}_{kr} \langle \mathbf{F}_l|\mathbf{F}_k\rangle \right\}$$
$$= \left[\sum_{j=1}^{N_S} \left(\boldsymbol{A}_j^* \left(\boldsymbol{S}\boldsymbol{X}_j + \left(\boldsymbol{F}^* \dot{\boldsymbol{F}}^T \circ \boldsymbol{S} \right) \boldsymbol{A}_j \right) \boldsymbol{F} + \boldsymbol{A}_j^* \boldsymbol{S} \boldsymbol{A}_j \dot{\boldsymbol{F}} \right) \right]_{lr} . \tag{C.23}$$

Obtaining vectorized expressions from these ones is tedious. We end up with a system which has the structure

$$\begin{pmatrix} \boldsymbol{S} & & & \boldsymbol{L}_{21} \\ & \ddots & & \vdots \\ & & \boldsymbol{S} & \boldsymbol{L}_{2N_S} \\ \boldsymbol{L}_{21}^\dagger & \dots & \boldsymbol{L}_{2N_S}^\dagger & \boldsymbol{L}_3 \end{pmatrix} \begin{pmatrix} \mathbf{vec}\,\boldsymbol{X} \\ \mathbf{vec}\,\dot{\boldsymbol{F}} \end{pmatrix} = -\mathrm{i} \begin{pmatrix} \mathbf{vec}\,\boldsymbol{R}_1 \\ \mathbf{vec}\,\boldsymbol{R}_2 \end{pmatrix} \tag{C.24}$$

where

$$\boldsymbol{L}_{2j} = \left(\boldsymbol{F}^* \otimes \overrightarrow{A_j}^T \right) \circ (1_{1\times N_b} \otimes \boldsymbol{S}) \in \mathbb{C}^{M \times M N_b} \tag{C.25}$$
$$\boldsymbol{L}_3 = \left(\left[1_{1\times N_b} \otimes \boldsymbol{F}^T \otimes 1_{M\times 1} \right] \circ \left[1_{N_b \times 1} \otimes \boldsymbol{F}^* \otimes 1_{1\times M} \right] \right) \circ \left[1_{N_b \times N_b} \otimes \left(\left(\boldsymbol{A}^* \boldsymbol{A}^T \right) \circ \boldsymbol{S} \right) \right]$$
$$+ \mathbb{1}_{N_b} \otimes \left(\left(\boldsymbol{A}^* \boldsymbol{A}^T \right) \circ \boldsymbol{S} \right) \in \mathbb{C}^{M N_b \times M N_b}. \tag{C.26}$$

The right-hand sides are given by

$$\boldsymbol{R}_1 \in \mathbb{C}^{M \times N_S}, \qquad (\boldsymbol{R}_1)_{lj} := \langle v_j| \langle \mathbf{F}_l| \hat{\mathcal{H}} |\Psi_{\mathrm{D2}}^{\mathrm{M}}\rangle , \tag{C.27}$$

and

$$\boldsymbol{R}_2 \in \mathbb{C}^{M \times N_b}, \qquad (\boldsymbol{R}_2)_{lr} := \sum_{j=1}^{N_S} A_{lj}^* \langle v_j| \langle \mathbf{F}_l| \hat{a}_r \hat{\mathcal{H}} |\Psi_{\mathrm{D2}}^{\mathrm{M}}\rangle \tag{C.28}$$

Define the matrices

$$\boldsymbol{Z} \in \mathbb{C}^{N_S \times N_S}, \qquad \boldsymbol{Z}_{ij} = Z_{ij} \quad (\text{see(C.2)}), \tag{C.29}$$

and

$$\boldsymbol{L} \in \mathbb{C}^{N_S \times N_S}, \qquad \boldsymbol{L}_{ij} = L_{ij} \quad (\text{see(C.4)}). \tag{C.30}$$

For the system part,

$$\langle v_j | \langle \mathbf{F}_l | \hat{\mathcal{H}}_{\text{sys}} | \Psi_{\text{D2}}^{\text{M}} \rangle = \sum_{k=1}^{M} \sum_{i=1}^{N_S} \langle v_j | \hat{\mathcal{H}}_{\text{S}} | v_i \rangle A_{ki} S_{lk} = \left(\mathbf{S} \mathbf{A} \mathbf{Z}^T \right)_{lj}, \tag{C.31}$$

and

$$\sum_{j=1}^{N_S} A_{lj}^* \langle v_j | \langle \mathbf{F}_l | \hat{a}_r \hat{\mathcal{H}}_{\text{sys}} | \Psi_{\text{D2}}^{\text{M}} \rangle = \sum_{j=1}^{N_S} \sum_{k=1}^{M} \sum_{i=1}^{N_S} A_{lj}^* F_{kr} \langle v_j | \hat{\mathcal{H}}_{\text{sys}} | v_i \rangle A_{ki} S_{lk}$$
$$= \left(\left[\left(\boldsymbol{A}^* \boldsymbol{Z} \boldsymbol{A}^T \right) \circ \mathbf{S} \right] \mathbf{F} \right)_{lr}. \tag{C.32}$$

Assume $\hat{\mathcal{H}}_{\text{bath}}$ and $\hat{\mathcal{H}}_{\text{I}}$ to be in normal-ordered form,

$$\hat{\mathcal{H}}_{\text{bath}} = H_{\text{bath}}(\hat{\mathbf{a}}^\dagger, \hat{\mathbf{a}}), \qquad \hat{\mathcal{H}}_{\text{I}} = H_{\text{I}}(\hat{\mathbf{a}}^\dagger, \hat{\mathbf{a}}). \tag{C.33}$$

Then

$$\langle \mathbf{F}_l | \hat{\mathcal{H}}_{\text{bath}} | \mathbf{F}_k \rangle = H_{\text{bath}}(\mathbf{F}_l^*, \mathbf{F}_k) S_{lk} =: B_{lk} S_{lk},$$
$$\langle \mathbf{F}_l | \hat{\mathcal{H}}_{\text{I}} | \mathbf{F}_k \rangle = H_{\text{I}}(\mathbf{F}_l^*, \mathbf{F}_k) S_{lk} =: I_{lk} S_{lk}. \tag{C.34}$$

and consequently

$$\langle v_j | \langle \mathbf{F}_l | \hat{\mathcal{H}}_{\text{bath}} | \Psi_{\text{D2}}^{\text{M}} \rangle = \sum_{k=1}^{M} A_{kj} B_{lk} S_{lk} = \left(\underbrace{\left(\mathbf{B} \circ \mathbf{S} \right)}_{=:\mathbf{U}} \mathbf{A} \right)_{lj}, \tag{C.35}$$

and

$$\langle v_j | \langle \mathbf{F}_l | \hat{\mathcal{H}}_{\text{I}} | \Psi_{\text{D2}}^{\text{M}} \rangle = \sum_{k=1}^{M} \sum_{i=1}^{N_S} A_{ki} L_{ji} I_{lk} S_{lk} = \left(\underbrace{\left(\mathbf{I} \circ \mathbf{S} \right)}_{=:\boldsymbol{V}} \underbrace{\left(\mathbf{A} \mathbf{L}^T \right)}_{=:\boldsymbol{W}} \right)_{lj}. \tag{C.36}$$

Furthermore, for a normal-ordered Hamiltonian $H(\hat{\mathbf{a}}^\dagger, \hat{\mathbf{a}})$:

$$\left[\hat{a}_r, H(\hat{\mathbf{a}}^\dagger, \hat{\mathbf{a}}) \right] = \frac{\partial H(\hat{\mathbf{a}}^\dagger, \hat{\mathbf{a}})}{\partial \hat{a}_r^\dagger} \tag{C.37}$$

Thus, if we set

$$\frac{\partial H_{\text{bath}}(\mathbf{F}_l^*, \mathbf{F}_k)}{\partial F_{lr}^*} = \alpha_{lkr}, \qquad \frac{\partial H_{\text{I}}(\mathbf{F}_l^*, \mathbf{F}_k)}{\partial F_{lr}^*} = \beta_{lkr}, \tag{C.38}$$

then for the bath part:

$$\sum_{j=1}^{N_S} A_{lj}^* \langle v_j | \langle \mathbf{F}_l | \hat{a}_r \hat{\mathcal{H}}_{\text{B}} | \Psi_{\text{D2}}^{\text{M}} \rangle = \sum_{j=1}^{N_S} \sum_{k=1}^{M} A_{lj}^* A_{kj} \left(B_{lk} F_{kr} + \alpha_{lkr} \right) S_{lk}$$

$$= \left(\left[\left(\boldsymbol{A}^* \boldsymbol{A}^T \right) \circ \mathbf{U} \right] \mathbf{F} + \text{sum} \left[\left(\left(\boldsymbol{A}^* \boldsymbol{A}^T \right) \circ \boldsymbol{S} \right) \circ \boldsymbol{\alpha}, 2 \right] \right)_{lr}, \tag{C.39}$$

and for the interaction part:

$$\sum_{j=1}^{N_S} A_{lj}^* \langle v_j | \langle \mathbf{F}_l | \hat{a}_r \hat{\mathcal{H}}_{\text{I}} | \Psi_{\text{D2}}^{\text{M}} \rangle = \sum_{j=1}^{N_S} \sum_{k=1}^{M} \sum_{i=1}^{N_S} A_{lj}^* A_{ki} L_{ji} \left(I_{lk} F_{kr} + \beta_{lkr} \right) S_{lk}$$

$$= \left(\left[\left(\boldsymbol{A}^* \boldsymbol{W}^T \right) \circ \mathbf{V} \right] \mathbf{F} + \text{sum} \left[\left(\left(\boldsymbol{A}^* \boldsymbol{L} \boldsymbol{A}^T \right) \circ \boldsymbol{S} \right) \circ \boldsymbol{\beta}, 2 \right] \right)_{lr}. \tag{C.40}$$

Here, $\text{sum}[\cdot, 2]$ denotes summation over the second component, i.e. the rows of the matrix.

C.2. D1-Ansatz

The time-derivative of the multi D1-Ansatz wave function (C.6) reads

$$\frac{\partial}{\partial t} | \Psi_{\text{D1}}^{\text{M}} \rangle = \sum_{j=1}^{N_S} \sum_{k=1}^{M} \left[\dot{A}_{kj} + A_{kj} \sum_{m=1}^{N_b} \left(-\frac{1}{2} \dot{F}_{kjm} F_{kjm}^* - \frac{1}{2} F_{kjm} \dot{F}_{kjm}^* + \dot{F}_{kjm} \hat{a}_m^\dagger \right) \right] | \mathbf{F}_{kj} \rangle | v_j \rangle, \tag{C.41}$$

and the variation similarly reads

$$\langle \delta \Psi_{\text{D1}}^{\text{M}} | = \sum_{j=1}^{N_S} \sum_{k=1}^{M} \langle v_j | \langle \mathbf{F}_{kj} | \left[\delta A_{kj}^* + A_{kj}^* \sum_{m=1}^{N_b} \left(\left(-\frac{1}{2} F_{kjm} + \hat{a}_m \right) \delta F_{kjm}^* - \frac{1}{2} F_{kjm}^* \delta F_{kjm} \right) \right]. \tag{C.42}$$

Under the assumption that all appearing variations are mutually independent, MN_S equations can be obtained by projection of the TDSE onto $\langle v_j | \langle \mathbf{F}_{lj} |$, which yields

$$\langle v_j | \langle \mathbf{F}_{lj} | \frac{\partial}{\partial t} | \Psi_{\mathrm{D1}}^{\mathrm{M}} \rangle = \sum_{k=1}^{M} \left[\dot{A}_{kj} + A_{kj} \sum_{m=1}^{N_b} \left(-\frac{1}{2} \dot{F}_{kjm} F_{kjm}^* - \frac{1}{2} F_{kjm} \dot{F}_{kjm}^* \right) \right] \langle \mathbf{F}_{lj} | \mathbf{F}_{kj} \rangle$$

$$+ \sum_{k=1}^{M} \left[A_{kj} \sum_{m=1}^{N_b} \dot{F}_{kjm} F_{ljm}^* \right] \langle \mathbf{F}_{lj} | \mathbf{F}_{kj} \rangle$$

$$= -\mathrm{i} \langle v_j | \langle \mathbf{F}_{lj} | \hat{\mathcal{H}} | \Psi_{\mathrm{D1}}^{\mathrm{M}} \rangle . \tag{C.43}$$

We define the expression

$$X_{kj} := \dot{A}_{kj} + A_{kj} \sum_{m=1}^{N_b} \left(-\frac{1}{2} \dot{F}_{kjm} F_{kjm}^* - \frac{1}{2} F_{kjm} \dot{F}_{kjm}^* \right) \tag{C.44}$$

according to Sec. 3.2. With this abbreviation, equation (C.43) reads

$$\sum_{k=1}^{M} \left[X_{kj} + A_{kj} \sum_{m=1}^{N_b} \dot{F}_{kjm} F_{ljm}^* \right] \langle \mathbf{F}_{lj} | \mathbf{F}_{kj} \rangle = -\mathrm{i} \langle v_j | \langle \mathbf{F}_{lj} | \hat{\mathcal{H}} | \Psi_{\mathrm{D1}}^{\mathrm{M}} \rangle . \tag{C.45}$$

Additional $MN_S N_b$ equations are obtained by projection onto $A_{lj}^* \langle v_j | \langle \mathbf{F}_{lj} | \hat{a}_r$, which yields

$$A_{lj}^* \langle v_j | \langle \mathbf{F}_{lj} | \hat{a}_r \frac{\partial}{\partial t} | \Psi_{\mathrm{D1}}^{\mathrm{M}} \rangle = A_{lj}^* \sum_{k=1}^{M} \left[F_{kjr} \left(X_{kj} + A_{kj} \sum_{m=1}^{N_b} \dot{F}_{kjm} F_{ljm}^* \right) \right] \langle \mathbf{F}_{lj} | \mathbf{F}_{kj} \rangle$$

$$+ \sum_{k=1}^{M} A_{kj} \dot{F}_{kjr} \langle \mathbf{F}_{lj} | \mathbf{F}_k \rangle$$

$$= -\mathrm{i} A_{lj}^* \langle v_j | \langle \mathbf{F}_{lj} | \hat{a}_r \hat{\mathcal{H}} | \Psi_{\mathrm{D1}}^{\mathrm{M}} \rangle . \tag{C.46}$$

We again denote the Hadamard product by $\circ$, the tensor product by $\otimes$, the vectorization of a matrix $\boldsymbol{M}$ by $\mathbf{vec}(\boldsymbol{M})$, by $\mathbb{1}_n$ the $n \times n$ unit matrix, and by $1_{m \times n}$ the matrix in $\mathbb{C}^{m \times n}$ which consists of only ones. Define the matrix of displacements

$$\boldsymbol{F}_j \in \mathbb{C}^{M \times N_b}, \qquad (\boldsymbol{F}_j)_{kn} = F_{kjn}, \tag{C.47}$$

The vectors of coefficients are

$$\overrightarrow{A_j} := (A_{1j}, \dots, A_{Mj})^T \in \mathbb{C}^{M \times 1}, \qquad \boldsymbol{A}_j := \mathrm{diag}\left(\overrightarrow{A_j} \right) \in \mathbb{C}^{M \times M}. \tag{C.48}$$

and the matrix of auxiliary variables

$$\boldsymbol{X} \in \mathbb{C}^{M \times N_S}, \qquad \boldsymbol{X}_{kj} = X_{kj}. \tag{C.49}$$

Furthermore, we set

$$\overrightarrow{X_j} := (X_{1j}, \ldots, X_{Mj})^T \in \mathbb{C}^{M \times 1}, \qquad \boldsymbol{X}_j := \mathrm{diag}\left(\overrightarrow{X_j}\right) \in \mathbb{C}^{M \times M}, \tag{C.50}$$

and

$$\boldsymbol{D}_j := \boldsymbol{F}_j \boldsymbol{F}_j^\dagger \in \mathbb{C}^{M \times M}, \qquad \boldsymbol{d}_j := \mathrm{diag}\left(\boldsymbol{D}_j\right) \otimes 1_{1 \times M} \in \mathbb{R}^{M \times M} \tag{C.51}$$

With the matrices

$$\boldsymbol{S}_j := \mathrm{e}^{\boldsymbol{D}_j^* - \frac{1}{2}\left(\boldsymbol{d}_j + \boldsymbol{d}_j^T\right)} \in \mathbb{C}^{M \times M}, \qquad (\boldsymbol{S}_j)_{lk} = \langle \mathbf{F}_{lj} | \mathbf{F}_{kj} \rangle \tag{C.52}$$

it is immediate that

$$
\begin{aligned}
\langle v_j | \langle \mathbf{F}_{lj} | \frac{\partial}{\partial t} | \Psi_{\mathrm{D1}}^{\mathrm{M}} \rangle &= \sum_{k=1}^{M} \left[X_{kj} + A_{kj} \sum_{m=1}^{N_b} \dot{F}_{kjm} F_{ljm}^* \right] \langle \mathbf{F}_{lj} | \mathbf{F}_{kj} \rangle \\
&= \left[\boldsymbol{S}_j \overrightarrow{X_j} + \left(\boldsymbol{F}_j^* \dot{\boldsymbol{F}}_j^T \circ \boldsymbol{S}_j \right) \overrightarrow{A_j} \right]_l,
\end{aligned}
\tag{C.53}
$$

and

$$
\begin{aligned}
A_{lj}^* \langle v_j | \langle \mathbf{F}_{lj} | \hat{a}_r \frac{\partial}{\partial t} | \Psi_{\mathrm{D1}}^{\mathrm{M}} \rangle &= A_{lj}^* \sum_{k=1}^{M} \left[F_{kjr} \left(X_{kj} + A_{kj} \sum_{m=1}^{N_b} \dot{F}_{kjm} F_{ljm}^* \right) \right] \langle \mathbf{F}_{lj} | \mathbf{F}_{kj} \rangle \\
&\quad + \sum_{k=1}^{M} A_{kj} \dot{F}_{kr} \langle \mathbf{F}_{lj} | \mathbf{F}_{kj} \rangle \\
&= \left[\left(\boldsymbol{A}_j^* \left(\boldsymbol{S}_j \boldsymbol{X}_j + \left(\boldsymbol{F}_j^* \dot{\boldsymbol{F}}_j^T \circ \boldsymbol{S}_j \right) \boldsymbol{A}_j \right) \boldsymbol{F}_j + \boldsymbol{A}_j^* \boldsymbol{S}_j \boldsymbol{A}_j \dot{\boldsymbol{F}}_j \right) \right]_{lr}.
\end{aligned}
\tag{C.54}
$$

Obtaining vectorized expressions from these ones is tedious. We end up with N_S systems which have the structure

$$\begin{pmatrix} \boldsymbol{S}_j & \boldsymbol{L}_{2j} \\ \boldsymbol{L}_{21}^\dagger & \boldsymbol{L}_{3j} \end{pmatrix} \begin{pmatrix} \overrightarrow{X_j} \\ \mathbf{vec}\, \dot{\boldsymbol{F}}_j \end{pmatrix} = -\mathrm{i} \begin{pmatrix} \vec{R}_{1j} \\ \mathbf{vec}\, \boldsymbol{R}_{2j} \end{pmatrix} \tag{C.55}$$

where

$$\boldsymbol{L}_{2j} = \left(\boldsymbol{F}_j^* \otimes \overrightarrow{A_j^T} \right) \circ \left(1_{1 \times N_b} \otimes \boldsymbol{S}_j \right) \in \mathbb{C}^{M \times M N_b} \tag{C.56}$$

$$
\begin{aligned}
\boldsymbol{L}_{3j} &= \left(\left[1_{1 \times N_b} \otimes \boldsymbol{F}_j^T \otimes 1_{M \times 1} \right] \circ \left[1_{N_b \times 1} \otimes \boldsymbol{F}_j^* \otimes 1_{1 \times M} \right] \right) \circ \left[1_{N_b \times N_b} \otimes \left(\left(\overrightarrow{A_j^*} \overrightarrow{A_j^T} \right) \circ \boldsymbol{S}_j \right) \right] \\
&\quad + \mathbb{1}_{N_b} \otimes \left(\left(\overrightarrow{A_j^*} \overrightarrow{A_j^T} \right) \circ \boldsymbol{S}_j \right) \in \mathbb{C}^{M N_b \times M N_b}.
\end{aligned}
\tag{C.57}
$$

The right-hand sides are given by

$$\vec{R}_{1j} \in \mathbb{C}^{M \times 1}, \qquad (\boldsymbol{R}_{1j})_l := \langle v_j | \langle \mathbf{F}_{lj} | \hat{\mathcal{H}} | \Psi_{\mathrm{D1}}^{\mathrm{M}} \rangle, \tag{C.58}$$

and

$$\boldsymbol{R}_{2j} \in \mathbb{C}^{M \times N_b}, \qquad (\boldsymbol{R}_{2j})_{lr} := A_{lj}^* \langle v_j | \langle \mathbf{F}_l | \hat{a}_r \hat{\mathcal{H}} | \Psi_{\mathrm{D1}}^{\mathrm{M}} \rangle . \tag{C.59}$$

Unlike in the multi D2 equations of motion (see Sec. C.1), it is not straightforwardly possible to easily express the right-hand sides in an analogous general form in terms of matrix operations. This is, apart from further complications, mainly due to the fact that the Hamiltonian may couple the different system eigenstates, and thus overlaps $(\boldsymbol{S}_{ij})_{lk} := \langle \mathbf{F}_{li} | \mathbf{F}_{kj} \rangle$ enter the equations requiring tensor contractions which can not easily be formulated in terms of matrix operations. If the model comprises a two-level system (as e.g. the Spin-Boson model, for which we have implemented the equations of motion (see Sec. 4.3.2.1) for the multi D1-Ansatz), the implementation yet being tedious can rely on direct implementation of the required sums.

D. Details of implementation

We shall address important details regarding the implementation of the multi D2-Ansatz here. In particular, positions of initially unpopulated CS, implementation of apoptosis especially with treatment of cases where multiple CS approach at the same time, and further details with respect to the regularization of vanishing coefficients are discussed.

Let us assume an open quantum system setting as given in Sec. 4, with a Hamiltonian given by (4.6). In most settings encountered in this thesis the initial state is a product state, $|\Psi(0)\rangle = |\Psi\rangle_{\mathrm{B}}(0)|\Psi\rangle_{\mathrm{S}}(0)$, with an arbitrary system initial state $|\Psi\rangle_{\mathrm{S}}(0)$ and the bath initial state $|\Psi\rangle_{\mathrm{B}}(0) = |\boldsymbol{\alpha}_0\rangle$ being a multi-mode coherent state at $\boldsymbol{\alpha}_0 \in \mathbb{C}^N$. If a multitude of $M > 1$ coherent states are employed in the multi D2-Ansatz (3.54), the initial condition fixes only one of the M initial positions of the coherent states, i.e. $M - 1$ CS are initially unpopulated. Their positions are in principle arbitrary. In contrast to numerical details given in [168], our calculations hint that the mutual distances of the CS should not be too close (then the overlap matrix $\mathbf{S}$ given in Eq. (3.35) becomes singular) but also not too large (then the unpopulated CS which are far away from the initially populated one do not take part in the action). An appropriate distance can be extracted from the theoretical considerations in Sec. 2.3: if the unpopulated CS are placed on *arbitrary* grid points on the (multi-dimensional) regular grid $\left\{ (c_1, \ldots, c_N) \in \mathbb{C}^N \,|\, c_j = \sqrt{\pi}(m_j + i n_j), j = 1, \ldots, N, m_j, n_j \in \mathbb{Z} \right\}$ around the initial CS $\boldsymbol{\alpha}_0$, then both requirements are fulfilled. Furthermore, as long as neighbouring points of the initial CS on this grid are chosen, it is of no relevance where exactly the initially unpopulated CS are placed.

In order to implement the apoptosis procedure outlined in Sec. 3.3.2, the mutual distances $d(\boldsymbol{\alpha}_1, \boldsymbol{\alpha}_2)$ in phase space of the multi-mode CS have to be monitored in each time step. If the distance

$$d(\boldsymbol{\alpha}_1, \boldsymbol{\alpha}_2) = \sqrt{\sum_{n=1}^{N} |\alpha_{1n} - \alpha_{2n}|^2} < \varepsilon \tag{D.1}$$

undershoots a given threshold ε at a certain time t_0 for two CS $|\boldsymbol{\alpha}_1\rangle$ and $|\boldsymbol{\alpha}_2\rangle$, then we need to connect these two CS by replacing

$$\boldsymbol{\alpha}_2(t) \to \boldsymbol{\alpha}_1(t) + \mathbf{C}, \qquad \mathbf{C} = \boldsymbol{\alpha}_2(t_0) - \boldsymbol{\alpha}_1(t_0). \tag{D.2}$$

This connection is implemented as follows.

It is possible that the criterion (D.1) is fulfilled for multiple CS $|\boldsymbol{\alpha}_i\rangle$, $i = 1, \ldots, I$ at the same time, requiring all of them to be connected but with not any two of them fulfilling condition (D.1). To be more specific, say $I = 3$ and $d(\boldsymbol{\alpha}_1, \boldsymbol{\alpha}_2) < \varepsilon$ and $d(\boldsymbol{\alpha}_2, \boldsymbol{\alpha}_3) < \varepsilon$. Then not necessarily $d(\boldsymbol{\alpha}_1, \boldsymbol{\alpha}_3) < \varepsilon$ but still it is required to connect $|\boldsymbol{\alpha}_1\rangle$ with $|\boldsymbol{\alpha}_3\rangle$. Thus, finding all CS which have to be connected to $|\boldsymbol{\alpha}_1\rangle$ is a connected component search. Specifically, in each time step we store the distance information in

an adjacency matrix $\mathbf{D} \in \mathbb{R}^{M \times M}$ whose elements are defined by the distance d,

$$\mathbf{D}_{ij} = \begin{cases} 1, & d(\boldsymbol{\alpha}_i, \boldsymbol{\alpha}_j) < \varepsilon \\ 0, & d(\boldsymbol{\alpha}_i, \boldsymbol{\alpha}_j) \geq \varepsilon \end{cases}. \tag{D.3}$$

On this adjacency matrix we perform a weakly connected component search (also known as Union Find algorithm), resulting in the number N_C of connected components (excluding the components of size one, i.e. the CS which are not connected to any other CS) together with a list of arrays containing the numbers of the connected CS.

For each array $(a_1, \ldots, a_n)$ in the list, we choose the first element as the one which replaces the other ones according to (D.2). This effectively means that the columns in $\mathbf{L}_2$ and $\mathbf{R}_2$ as well as the rows and columns in $\mathbf{L}_3$ (see Eq. (3.34) and Sec. C) corresponding to the entries $a_1, \ldots, a_n$ of the array have respectively to be summed up, and the matrix entries corresponding to a_1 be replaced with the sum while the matrix entries corresponding to $a_2, \ldots, a_n$ be deleted. Finally, the results of the subsequent solution of the linear system (3.18) have to be refilled into the corresponding entries of the input to the integrator.

Finally, details of the implementation with respect to the regularization in the case of vanishing coefficients are discussed. The required strength of the regularization depends on the setting, specifically on the number N of bath modes and the number M of CS employed in the multi D2-Ansatz. A strong regularization of the $\boldsymbol{\rho}$-matrix (see Sec. 3.3 and Eq. (3.28)) is required in cases where $N \approx 1$ and $M \gg 10$ (in these cases even a regularization of the $\mathbf{S}$-matrix may be required). On the contrary, the calculations we have executed show that in problems where many modes are included, $N \gg 1$, regularization of the ρ-matrix is not necessarily required if a small noise is included for the the coefficients corresponding to the initially unpopulated CS. This substantiates the theoretical considerations of Secs. 3.3.1 and 3.3.2 which hints that the closeness of CS and not the regularization of vanishing coefficients is the dominant issue for large systems. Thus, the closeness of CS is the dominant issue in the systems whose dynamics we are mostly interested in. If the integration is implemented as outlined here, the propagation proceeds highly stable and without further instabilities.

E. Calculation of the BCF

We aim here at the derivation of the BCF $C(\tau) = \mathrm{tr}_\mathrm{B}\left[Z(\beta)\exp\left[-\beta\hat{\mathcal{H}}_\mathrm{B}\right]\left\{\hat{\mathcal{H}}_\mathrm{I}(\tau),\hat{\mathcal{H}}_\mathrm{I}(0)\right\}\right]$ where $\beta = (k_B T)^{-1}$ is the inverse temperature (2.54), $Z(\beta)$ is the inverse partition function (2.57), $\hat{\mathcal{H}}_\mathrm{B} = \sum_{n=1}^{N}\omega_n\hat{a}_n^\dagger\hat{a}_n$ is the bath Hamiltonian (4.2) and $\hat{\mathcal{H}}_\mathrm{I}(\tau) = \exp\left[\mathrm{i}\tau\hat{\mathcal{H}}_\mathrm{B}\right]\hat{\mathcal{H}}_\mathrm{I}\exp\left[-\mathrm{i}\tau\hat{\mathcal{H}}_\mathrm{B}\right]$ is the bath part of the interaction Hamiltonian $\hat{\mathcal{H}}_\mathrm{I} = \sum_{n=1}^{N}\lambda_n\left(\hat{a}_n^\dagger + \hat{a}_n\right)$ (see (4.4)) in the interaction picture. The bracket $\{\cdot,\cdot\}$ denotes the anti-commutator, $\{A,B\} = AB + BA$ for operators A,B. Let us first consider the case $N = 1$.

One easily calculates from (2.10) that

$$\mathrm{e}^{\mathrm{i}\tau\omega\hat{a}^\dagger\hat{a}}\hat{a}\,\mathrm{e}^{-\mathrm{i}\tau\omega\hat{a}^\dagger\hat{a}}\left|n\right\rangle = \mathrm{e}^{-\mathrm{i}\tau\omega n}\mathrm{e}^{\mathrm{i}\tau\omega\hat{a}^\dagger\hat{a}}\hat{a}\left|n\right\rangle = \mathrm{e}^{-\mathrm{i}\tau\omega n}\sqrt{n}\,\mathrm{e}^{\mathrm{i}\tau\omega\hat{a}^\dagger\hat{a}}\left|n-1\right\rangle = \mathrm{e}^{-\mathrm{i}\tau\omega}\sqrt{n}\left|n-1\right\rangle, \qquad \text{(E.1)}$$

for all n. The $\left|n\right\rangle$ constitute a complete set of states (see Sec. 2.1) and thus we infer

$$\mathrm{e}^{\mathrm{i}\tau\omega\hat{a}^\dagger\hat{a}}\hat{a}\,\mathrm{e}^{-\mathrm{i}\tau\omega\hat{a}^\dagger\hat{a}} = \mathrm{e}^{-\mathrm{i}\tau\omega}\hat{a}, \qquad \text{(E.2)}$$

since both operators act on all number states in the same way. From this by Hermitian conjugation it readily follows

$$\mathrm{e}^{\mathrm{i}\tau\omega\hat{a}^\dagger\hat{a}}\hat{a}^\dagger\mathrm{e}^{-\mathrm{i}\tau\omega\hat{a}^\dagger\hat{a}} = \mathrm{e}^{\mathrm{i}\tau\omega}\hat{a}^\dagger. \qquad \text{(E.3)}$$

Thus for a single environmental mode

$$\hat{\mathcal{H}}_\mathrm{I}(\tau) = \lambda\left(\mathrm{e}^{\mathrm{i}\tau\omega}\hat{a}^\dagger + \mathrm{e}^{-\mathrm{i}\tau\omega}\hat{a}\right). \qquad \text{(E.4)}$$

Consequently the first part $C_1(\tau)$ of the bath correlation function reads for $N = 1$

$$C_1(\tau) := \mathrm{tr}_\mathrm{B}\left[Z(\beta)\exp\left[-\beta\hat{\mathcal{H}}_\mathrm{B}\right]\hat{\mathcal{H}}_\mathrm{I}(\tau)\hat{\mathcal{H}}_\mathrm{I}(0)\right] \qquad \text{(E.5)}$$

$$= Z(\beta)\lambda^2\sum_{n=0}^{\infty}\left\langle n\right|\left[\mathrm{e}^{-\beta\omega\hat{a}^\dagger\hat{a}}\left(\mathrm{e}^{\mathrm{i}\tau\omega}\hat{a}^\dagger + \mathrm{e}^{-\mathrm{i}\tau\omega}\hat{a}\right)\left(\hat{a}^\dagger + \hat{a}\right)\right]\left|n\right\rangle. \qquad \text{(E.6)}$$

In the sum only these terms survive where a creation and an annihilation operator act on the number states (otherwise the overlap with the same number state from both sides yields zero). Thus

$$C_1(\tau) = Z(\beta)\lambda^2\sum_{n=0}^{\infty}\left\langle n\right|\left[\mathrm{e}^{-\beta\omega\hat{a}^\dagger\hat{a}}\left(\mathrm{e}^{\mathrm{i}\tau\omega}\hat{a}^\dagger\hat{a} + \mathrm{e}^{-\mathrm{i}\tau\omega}\hat{a}\hat{a}^\dagger\right)\right]\left|n\right\rangle \qquad \text{(E.7)}$$

$$= Z(\beta)\lambda^2\sum_{n=0}^{\infty}\left[\mathrm{e}^{-\beta\omega n}\left(n\mathrm{e}^{\mathrm{i}\tau\omega} + (n+1)\mathrm{e}^{-\mathrm{i}\tau\omega}\right)\right] \qquad \text{(E.8)}$$

$$= Z(\beta)\lambda^2\left[\mathrm{e}^{\mathrm{i}\tau\omega}\sum_{n=0}^{\infty}n\mathrm{e}^{-\beta\omega n} + \mathrm{e}^{-\mathrm{i}\tau\omega}\sum_{n=0}^{\infty}(n+1)\mathrm{e}^{-\beta\omega n}\right]. \qquad \text{(E.9)}$$

From the geometric series $\sum\limits_{n=0}^{\infty} x^n = (1-x)^{-1}$ for $|x| < 1$ we infer

$$\sum_{n=0}^{\infty} n x^n = x \sum_{n=0}^{\infty} n x^{n-1} = x \frac{d}{dx} \sum_{n=0}^{\infty} x^n = \frac{x}{(1-x)^2}. \tag{E.10}$$

Consequently we obtain for the first part of the BCF for $N = 1$ that

$$C_1(\tau) = Z(\beta)\lambda^2 \left[e^{\mathrm{i}\tau\omega} \frac{e^{-\beta\omega}}{(1 - e^{-\beta\omega})^2} + e^{-\mathrm{i}\tau\omega} \left(\frac{e^{-\beta\omega}}{(1 - e^{-\beta\omega})^2} + \frac{1}{1 - e^{-\beta\omega}} \right) \right] \tag{E.11}$$

$$= \frac{Z(\beta)\lambda^2}{(1 - e^{-\beta\omega})^2} \left[e^{\mathrm{i}\tau\omega} e^{-\beta\omega} + e^{-\mathrm{i}\tau\omega} \right] \tag{E.12}$$

$$= \frac{\lambda^2}{1 - e^{-\beta\omega}} \left[e^{\mathrm{i}\tau\omega} e^{-\beta\omega} + e^{-\mathrm{i}\tau\omega} \right]. \tag{E.13}$$

Analogously for the second part

$$C_2(\tau) := \mathrm{tr}_{\mathrm{B}} \left[Z(\beta) \exp\left[-\beta\hat{\mathcal{H}}_{\mathrm{B}} \right] \hat{\mathcal{H}}_{\mathrm{I}}(0) \hat{\mathcal{H}}_{\mathrm{I}}(\tau) \right] \tag{E.14}$$

$$= \frac{\lambda^2}{1 - e^{-\beta\omega}} \left[e^{\mathrm{i}\tau\omega} + e^{-\mathrm{i}\tau\omega} e^{-\beta\omega} \right]. \tag{E.15}$$

Thus we finally arrive at

$$C(\tau) = C_1(\tau) + C_2(\tau) = \lambda^2 \frac{1 + e^{-\beta\omega}}{1 - e^{-\beta\omega}} \left[e^{\mathrm{i}\tau\omega} + e^{-\mathrm{i}\tau\omega} \right]. \tag{E.16}$$

By inferring that each of the summands contains all the information of the BCF, we arbitrarily keep only the second one and have

$$C(\tau) = \lambda^2 \coth\left(\frac{\beta\omega}{2} \right) e^{-\mathrm{i}\omega\tau}. \tag{E.17}$$

This result straightforwardly generalizes to the case of multiple modes $N > 1$ where we have

$$C(\tau) = \sum_{n=1}^{N} \lambda_n^2 \coth\left(\frac{\beta\omega_n}{2} \right) e^{-\mathrm{i}\omega_n\tau}. \tag{E.18}$$

Especially for temperature $T \to 0$, the inverse temperature $\beta = (k_B T)^{-1} \to \infty$. Due to $\lim\limits_{\beta\to\infty} \coth\left(\frac{\beta\omega_n}{2} \right) = 1$ the zero temperature BCF reads

$$C(\tau) = \sum_{n=1}^{N} \lambda_n^2 e^{-\mathrm{i}\omega_n\tau}. \tag{E.19}$$

F. Calculation of the polarized initial condition for $T = 0$

We examine the density $\left(\mathrm{tr_B} \left[\exp \left[-\beta \left(\hat{\mathcal{H}}_\mathrm{B} + \hat{\mathcal{H}}_\mathrm{I} \right) \right] \right] \right)^{-1} \exp \left[-\beta \left(\hat{\mathcal{H}}_\mathrm{B} + \hat{\mathcal{H}}_\mathrm{I} \right) \right]$ for $\hat{\mathcal{H}}_\mathrm{B}$ and $\hat{\mathcal{H}}_\mathrm{I}$ given by (4.2) and (4.4) respectively. For $N = 1$ we obtain from the commutation relation (2.37) of the displacement operator (see Sec. 2.2) and creation and annihilation operator as well as insertion of the closure relation (2.11) of the number states

$$\exp \left[-\beta \left(\hat{\mathcal{H}}_\mathrm{B} + \hat{\mathcal{H}}_\mathrm{I} \right) \right] = \exp \left[-\beta(\omega \hat{a}^\dagger \hat{a} + \lambda(\hat{a}^\dagger + \hat{a})) \right] \tag{F.1}$$

$$= \exp \left[\beta \frac{\lambda^2}{\omega} \right] \exp \left[-\beta\omega \left(\hat{a}^\dagger + \frac{\lambda}{\omega} \right) \left(\hat{a} + \frac{\lambda}{\omega} \right) \right] \tag{F.2}$$

$$\stackrel{(2.37)}{=} \exp \left[\beta \frac{\lambda^2}{\omega} \right] \exp \left[-\beta\omega \hat{D}_C^\dagger \hat{a}^\dagger \hat{D}_C \hat{D}_C^\dagger \hat{a} \hat{D}_C \right], \qquad C = \frac{\lambda}{\omega} \tag{F.3}$$

$$= \exp \left[\beta \frac{\lambda^2}{\omega} \right] \exp \left[\hat{D}_C^\dagger \left(-\beta\omega \hat{a}^\dagger \hat{a} \right) \hat{D}_C \right] \tag{F.4}$$

$$= \exp \left[\beta \frac{\lambda^2}{\omega} \right] \left(\hat{D}_C^\dagger \sum_{n=0}^\infty |n\rangle \langle n| \hat{D}_C \right) \times$$
$$\times \exp \left[\hat{D}_C^\dagger \left(-\beta\omega \hat{a}^\dagger \hat{a} \right) \hat{D}_C \right] \left(\hat{D}_C^\dagger \sum_{m=0}^\infty |m\rangle \langle m| \hat{D}_C \right), \tag{F.5}$$

where we have used the unitarity (2.35) of the displacement operator. Since for any unitary operator A, any operator B and any $k \in \mathbb{N}$ it holds that $\left(A^\dagger B A \right)^k = A^\dagger B^k A$, we conclude

$$\exp \left[A^\dagger B A \right] = \sum_{k=0}^\infty \frac{1}{k!} \left(A^\dagger B A \right)^k = \sum_{k=0}^\infty \frac{1}{k!} A^\dagger B^k A = A^\dagger \left(\sum_{k=0}^\infty \frac{1}{k!} B^k \right) A = A^\dagger \exp \left[B \right] A. \tag{F.6}$$

Hence

$$\exp \left[-\beta \left(\hat{\mathcal{H}}_\mathrm{B} + \hat{\mathcal{H}}_\mathrm{I} \right) \right] = \exp \left[\beta \frac{\lambda^2}{\omega} \right] \hat{D}_C^\dagger \sum_{n,m=0}^\infty |n\rangle \langle n| \exp \left[-\beta\omega \hat{a}^\dagger \hat{a} \right] |m\rangle \langle m| \hat{D}_C \tag{F.7}$$

$$= \exp \left[\beta \frac{\lambda^2}{\omega} \right] \hat{D}_C^\dagger \sum_{n=0}^\infty \mathrm{e}^{-\beta\omega n} |n\rangle \langle n| \hat{D}_C. \tag{F.8}$$

Since the trace is invariant under cyclic permutation we conclude

$$\mathrm{tr}_\mathrm{B}\left[\exp\left[-\beta\left(\hat{\mathcal{H}}_\mathrm{B}+\hat{\mathcal{H}}_\mathrm{I}\right)\right]\right] = \mathrm{tr}_\mathrm{B}\left[\exp\left[\beta\frac{\lambda^2}{\omega}\right]\hat{D}_C^\dagger\sum_{n=0}^\infty \mathrm{e}^{-\beta\omega n}\,|n\rangle\,\langle n|\,\hat{D}_C\right] \tag{F.9}$$

$$= \mathrm{tr}_\mathrm{B}\left[\exp\left[\beta\frac{\lambda^2}{\omega}\right]\sum_{n=0}^\infty \mathrm{e}^{-\beta\omega n}\,|n\rangle\,\langle n|\right] \tag{F.10}$$

$$= \exp\left[\beta\frac{\lambda^2}{\omega}\right]\sum_{m=0}^\infty \langle m|\left(\sum_{n=0}^\infty \mathrm{e}^{-\beta\omega n}\,|n\rangle\,\langle n|\right)|m\rangle \tag{F.11}$$

$$= \exp\left[\beta\frac{\lambda^2}{\omega}\right](Z(\beta))^{-1}. \tag{F.12}$$

Here, we have used the inverse partition function $Z(\beta)$ (see (2.57)). Thus, from (F.8) and (F.12) the final expression for the density reads

$$\left(\mathrm{tr}_\mathrm{B}\left[\exp\left[-\beta\left(\hat{\mathcal{H}}_\mathrm{B}+\hat{\mathcal{H}}_\mathrm{I}\right)\right]\right]\right)^{-1}\exp\left[-\beta\left(\hat{\mathcal{H}}_\mathrm{B}+\hat{\mathcal{H}}_\mathrm{I}\right)\right] = Z(\beta)\hat{D}_C^\dagger\sum_{n=0}^\infty \mathrm{e}^{-\beta\omega n}\,|n\rangle\,\langle n|\,\hat{D}_C. \tag{F.13}$$

Now we may transition to the case $T \to 0$, i.e. $\beta = (k_B T)^{-1} \to \infty$. Although in (F.8) the pre-factor $\exp\left[\beta\frac{\lambda^2}{\omega}\right] \to \infty$ in this case, it is cancelled by an appropriate pre-factor in the trace (F.12). Since $Z(\beta) \to 1$ for $\beta \to \infty$ we finally find that in (F.13) only the first summand survives for $T \to 0$,

$$\left(\mathrm{tr}_\mathrm{B}\left[\exp\left[-\beta\left(\hat{\mathcal{H}}_\mathrm{B}+\hat{\mathcal{H}}_\mathrm{I}\right)\right]\right]\right)^{-1}\exp\left[-\beta\left(\hat{\mathcal{H}}_\mathrm{B}+\hat{\mathcal{H}}_\mathrm{I}\right)\right] = \hat{D}_C^\dagger\,|0\rangle\,\langle 0|\,\hat{D}_C. \tag{F.14}$$

This result straightforwardly generalizes to (4.74) in the case $N > 1$.

Bibliography

[1] A. S. Davydov and N. I. Kislukha: *Solitary excitons in one-dimensional molecular chains*, Physica Status Solidi (b) **59** (1973), 465–470.

[2] A. Davydov: *The theory of contraction of proteins under their excitation*, Journal of Theoretical Biology **38** (1973), 559–569.

[3] A. S. Davydov and N. I. Kislukha: *Solitons in One-Dimensional Molecular Chains*, physica status solidi (b) **75** (1976), 735–742.

[4] A. S. Davydov: *Solitons in Molecular Systems*, Physica Scripta **20** (1979), 387–394.

[5] N. J. Zabusky and M. D. Kruskal: *Interaction of "Solitons" in a Collisionless Plasma and the Recurrence of Initial States*, Physical Review Letters **15** (1965), 240–243.

[6] E. Schroedinger: *Der stetige Uebergang von der Mikro- zur Makromechanik*, Die Naturwissenschaften **14** (1926), 664–666.

[7] A. S. Davydov: *Soliton motion in a one-dimensional molecular lattice with account taken of thermal oscillations*, Sov. Phys. JETP **51** (1980), 397–400.

[8] P. S. Lomdahl and W. C. Kerr: *Do Davydov Solitons Exist at 300 K?*, Physical Review Letters **55** (1985), 1235–1238.

[9] G. van Velzen and J. Tjon: *Numerical studies on the stability of Davydov solitons*, Physics Letters A **116** (1986), 167–171.

[10] J. P. Cottingham and J. W. Schweitzer: *Calculation of the lifetime of a Davydov soliton at finite temperature*, Physical Review Letters **62** (1989), 1792–1795.

[11] W. Rhodes and A. Nicholls: *Localization versus delocalization of the Davydov soliton: Dispersive collapse under the Schrödinger equation*, Physical Review Letters **64** (1990), 1174–1177.

[12] L. Cruzeiro-Hansson: *Two Reasons Why the Davydov Soliton May Be Thermally Stable After All*, Physical Review Letters **73** (1994), 2927–2930.

[13] P. L. Christiansen and A. C. Scott (eds.): *Davydov's Soliton Revisited*, vol. 243 of *NATO ASI Series*, (Springer US, Boston, MA), (1990).

[14] X.-F. Pang, H.-W. Zhang, J.-F. Yu, and Y.-H. Luo: *Thermal stability of the new soliton transported bio-energy under influence of fluctuations of characteristic parameters at biological temperature in the protein molecules*, International Journal of Modern Physics B **19** (2005), 4677–4699.

[15] D. D. Georgiev and J. F. Glazebrook: *Quantum tunneling of Davydov solitons through massive barriers*, Chaos, Solitons & Fractals **123** (2019), 275–293.

[16] D. W. Brown, B. J. West, and K. Lindenberg: *Davydov solitons: New results at variance with standard derivations*, Physical Review A **33** (1986), 4110–4120.

[17] H. Fröhlich: *Electrons in lattice fields*, Advances in Physics **3** (1954), 325–361.

[18] D. W. Brown, B. J. West, and K. Lindenberg: *Applicability of Hamilton's equations in the quantum soliton problem*, Physical Review A **37** (1988), 642–643.

[19] Q. Zhang, V. Romero-Rochin, and R. Silbey: *Variational approach to the Davydov soliton*, Physical Review A **38** (1988), 6409–6415.

[20] D. W. Brown, K. Lindenberg, and B. J. West: *Nonlinear Density-Matrix Approach for the Finite-Temperature Soliton Problem*, Physical Review Letters **57** (1986), 2341–2343.

[21] L. Cruzeiro, J. Halding, P. L. Christiansen, O. Skovgaard, and A. C. Scott: *Temperature effects on the Davydov soliton*, Physical Review A **37** (1988), 880–887.

[22] W. Forner: *Quantum and temperature effects on Davydov soliton dynamics: averaged Hamiltonian method*, Journal of Physics: Condensed Matter **4** (1992), 1915–1923.

[23] J. Sun, B. Luo, and Y. Zhao: *Dynamics of a one-dimensional Holstein polaron with the Davydov ansätze*, Physical Review B **82** (2010), 014305.

[24] B. Luo, J. Ye, and Y. Zhao: *Variational study of polaron dynamics with the Davydov Ansätze*, physica status solidi (c) **8** (2011), 70–73.

[25] Y. Zhao, B. Luo, Y. Zhang, and J. Ye: *Dynamics of a Holstein polaron with off-diagonal coupling*, The Journal of Chemical Physics **137** (2012), 084113.

[26] N. Wu, L. Duan, X. Li, and Y. Zhao: *Dynamics of the sub-Ohmic spin-boson model: A time-dependent variational study*, The Journal of Chemical Physics **138** (2013), 84111.

[27] N. Zhou, Z. Huang, J. Zhu, V. Chernyak, and Y. Zhao: *Polaron dynamics with a multitude of Davydov D 2 trial states*, The Journal of Chemical Physics **143** (2015), 014113.

[28] I. Burghardt, H. D. Meyer, and L. S. Cederbaum: *Approaches to the approximate treatment of complex molecular systems by the multiconfiguration time-dependent Hartree method*, Journal of Chemical Physics **111** (1999), 2927–2939.

[29] G. A. Worth and I. Burghardt: *Full quantum mechanical molecular dynamics using Gaussian wavepackets*, Chemical Physics Letters **368** (2003), 502–508.

[30] G. A. Worth, M. A. Robb, and I. Burghardt: *A novel algorithm for non-adiabatic direct dynamics using variational Gaussian wavepackets*, Faraday Discussions **127** (2004), 307.

[31] U. Lorenz and P. Saalfrank: *A novel system-bath Hamiltonian for vibration-phonon coupling: Formulation, and application to the relaxation of Si–H and Si–D bending modes of H/D:Si(100)-(2x1)*, Chemical Physics **482** (2017), 69–80.

[32] C. Tannoudji: *Quantum mechanics*, (Wiley, New York), (1977).

[33] N. Dunford and J. T. Schwartz: *Linear operators 1 General theory*, (Wiley Interscience Publ., New York), (1988).

[34] M. Abramowitz and I. Stegun: (Dover Publ., New York), 10th edn., (1972).

[35] W. H. Louisell: *Quantum statistical properties of radiation*, Wiley series in pure and applied optics, (Wiley, New York), (1973).

[36] W. P. Schleich: *Quantum Optics in Phase Space*, (Wiley-VCH Verlag GmbH & Co. KGaA, Weinheim, FRG), (2001).

[37] F. Grossmann, M. Werther, L. Chen, and Y. Zhao: *Generalization of the Davydov Ansatz by squeezing*, Chemical Physics **481** (2016), 99–107.

[38] J.-P. Gazeau: *Coherent States in Quantum Physics*, (Wiley, Weinheim, Germany), (2009).

[39] M. H. Stone: *Linear Transformations in Hilbert Space: III. Operational Methods and Group Theory*, Proceedings of the National Academy of Sciences **16** (1930), 172–175.

[40] J. v. Neumann: *Die Eindeutigkeit der Schrödingerschen Operatoren*, Mathematische Annalen **104** (1931), 570–578.

[41] V. Bargmann: *On a Hilbert space of analytic functions and an associated integral transform part I*, Communications on Pure and Applied Mathematics **14** (1961), 187–214.

[42] B. C. Hall: *Quantum Theory for Mathematicians*, vol. 267 of *Graduate Texts in Mathematics*, (Springer New York, New York, NY), (2013).

[43] V. Bargmann, P. Butera, L. Girardello, and J. R. Klauder: *On the completeness of the coherent states*, Reports on Mathematical Physics **2** (1971), 221–228.

[44] K. E. Cahill: *Coherent-State Representations for the Photon Density Operator*, Physical Review **138** (1965), B1566–B1576.

[45] I. Daubechies, A. Grossmann, and Y. Meyer: *Painless nonorthogonal expansions*, Journal of Mathematical Physics **27** (1986), 1271–1283.

[46] C. W. Gardiner and P. Zoller: *Quantum Noise*, (Springer, Berlin; Heidelberg; New York), 3rd edn., (2010).

[47] R. J. Glauber: *Coherent and Incoherent States of the Radiation Field*, Physical Review **131** (1963), 2766–2788.

[48] E. C. G. Sudarshan: *Equivalence of Semiclassical and Quantum Mechanical Descriptions of Statistical Light Beams*, Physical Review Letters **10** (1963), 277–279.

[49] R. J. Glauber: *Quantum Theory of Optical Coherence*, (Wiley), (2006).

[50] M. Werther and F. Grossmann: *Including temperature in a wavefunction description of the dynamics of the quantum Rabi model*, Journal of Physics A: Mathematical and Theoretical **51** (2018), 014001.

[51] W. Vogel, D.-G. Welsch, and S. Wallentowitz: *Quantum optics an introduction*, (Wiley-VCH, Berlin), 2nd edn., (2001).

[52] F. Hong-Yi, H. R. Zaidi, and J. R. Klauder: *New approach for calculating the normally ordered form of squeeze operators*, Physical Review D **35** (1987), 1831–1834.

[53] M. M. Nieto: *Displaced and squeezed number states*, Physics Letters A **229** (1997), 135–143.

[54] G. S. Agarwal: *Quantum optics*, (Cambridge Univ. Press, Cambridge, Mass.), (2013).

[55] A. Perelomov: *Generalized Coherent States and Their Applications*, vol. 53, (Springer, Berlin; Heidelberg), (1986).

[56] M. S. Kim, F. A. M. de Oliveira, and P. L. Knight: *Properties of squeezed number states and squeezed thermal states*, Physical Review A **40** (1989), 2494–2503.

[57] A. Chizhov and B. Murzakhmetov: *Photon statistics and phase properties of two-mode squeezed number states*, Physics Letters A **176** (1993), 33–40.

[58] T. G. Philbin: *Generalized coherent states*, American Journal of Physics **82** (2014), 742–748.

[59] H.-D. Meyer, U. Manthe, and L. Cederbaum: *The multi-configurational time-dependent Hartree approach*, Chemical Physics Letters **165** (1990), 73–78.

[60] U. Manthe, H. Meyer, and L. S. Cederbaum: *Wave-packet dynamics within the multiconfiguration Hartree framework: General aspects and application to NOCl*, The Journal of Chemical Physics **97** (1992), 3199–3213.

[61] H. Wang and M. Thoss: *Multilayer formulation of the multiconfiguration time-dependent Hartree theory*, The Journal of Chemical Physics **119** (2003), 1289–1299.

[62] U. Manthe: *A multilayer multiconfigurational time-dependent Hartree approach for quantum dynamics on general potential energy surfaces*, The Journal of Chemical Physics **128** (2008), 164116.

[63] P. Griffiths and J. Harris: *Principles of Algebraic Geometry*, (John Wiley & Sons, Inc., Hoboken, NJ, USA), (1994).

[64] A. McLachlan: *A variational solution of the time-dependent Schrodinger equation*, Molecular Physics **8** (1964), 39–44.

[65] P. Kramer and M. Saraceno: *Geometry of the Time-Dependent Variational Principle in Quantum Mechanics*, vol. 140 of *Lecture Notes in Physics*, (Springer, Berlin; Heidelberg), (1981).

[66] J. Frenkel: *Waves Mechanics: Advanced General Theory*, (Oxford University Press, Oxford), (1934).

[67] C. Lubich: *From Quantum to Classical Molecular Dynamics: Reduced Models and Numerical Analysis*, (European Mathematical Society Publishing House, Zuerich, Switzerland), (2008).

[68] J. Broeckhove, L. Lathouwers, E. Kesteloot, and P. Van Leuven: *On the equivalence of time-dependent variational principles*, Chemical Physics Letters **149** (1988), 547–550.

[69] A. R. Forsyth: *Calculus of variations*, (Dover, New York, NY), unabr. and unalt. republ. edn., (1960).

[70] M. Werther and F. Grossmann: *The Davydov D1.5 Ansatz for the quantum Rabi model*, Physica Scripta **93** (2018), 074001.

[71] I. Burghardt, K. Giri, and G. A. Worth: *Multimode quantum dynamics using Gaussian wavepackets: The Gaussian-based multiconfiguration time-dependent Hartree (G-MCTDH) method applied to the absorption spectrum of pyrazine*, Journal of Chemical Physics **129** (2008).

[72] M. C. Gutzwiller: *Phase-Integral Approximation in Momentum Space and the Bound States of an Atom*, Journal of Mathematical Physics **8** (1967), 1979–2000.

[73] M. C. Gutzwiller: *Phase-Integral Approximation in Momentum Space and the Bound States of an Atom. II*, Journal of Mathematical Physics **10** (1969), 1004–1020.

[74] M. C. Gutzwiller: *Energy Spectrum According to Classical Mechanics*, Journal of Mathematical Physics **11** (1970), 1791–1806.

[75] M. C. Gutzwiller: *Periodic Orbits and Classical Quantization Conditions*, Journal of Mathematical Physics **12** (1971), 343–358.

[76] W. H. Miller: *Semiclassical Theory of Atom–Diatom Collisions: Path Integrals and the Classical S Matrix*, The Journal of Chemical Physics **53** (1970), 1949–1959.

[77] W. H. Miller: *Classical S Matrix: Numerical Application to Inelastic Collisions*, The Journal of Chemical Physics **53** (1970), 3578–3587.

[78] W. H. Miller: *Classical S Matrix for Rotational Excitation; Quenching of Quantum Effects in Molecular Collisions*, The Journal of Chemical Physics **54** (1971), 5386–5397.

[79] C. C. Rankin and W. H. Miller: *Classical S Matrix for Linear Reactive Collisions of H+Cl2*, The Journal of Chemical Physics **55** (1971), 3150–3156.

[80] R. Marcus: *Extension of the WKB method to wave functions and transition probability amplitudès (S-matrix) for inelastic or reactive collisions*, Chemical Physics Letters **7** (1970), 525–532.

[81] R. A. Marcus: *Theory of Semiclassical Transition Probabilities (S Matrix) for Inelastic and Reactive Collisions*, The Journal of Chemical Physics **54** (1971), 3965–3979.

[82] J. N. L. Connor and R. A. Marcus: *Theory of Semiclassical Transition Probabilities for Inelastic and Reactive Collisions. II Asymptotic Evaluation of the S Matrix*, The Journal of Chemical Physics **55** (1971), 5636–5643.

[83] W. H. Wong and R. A. Marcus: *Semiclassical Transition Probabilities (S Matrix) of Vibrational—Translational Energy Transfer*, The Journal of Chemical Physics **55** (1971), 5663–5667.

[84] R. A. Marcus: *Theory of Semiclassical Transition Probabilities for Inelastic and Reactive Collisions. V. Uniform Approximation in Multidimensional Systems*, The Journal of Chemical Physics **57** (1972), 4903–4909.

[85] D. E. Fitz and R. A. Marcus: *Semiclassical theory of molecular spectral line shapes in gases*, The Journal of Chemical Physics **59** (1973), 4380–4392.

[86] E. J. Heller: *Time-dependent approach to semiclassical dynamics*, The Journal of Chemical Physics **62** (1975), 1544–1555.

[87] M. F. Herman and E. Kluk: *A semiclasical justification for the use of non-spreading wavepackets in dynamics calculations*, Chemical Physics **91** (1984), 27–34.

[88] M. F. Herman: *Time reversal and unitarity in the frozen Gaussian approximation for semiclassical scattering*, The Journal of Chemical Physics **85** (1986), 2069–2076.

[89] E. Kluk, M. F. Herman, and H. L. Davis: *Comparison of the propagation of semiclassical frozen Gaussian wave functions with quantum propagation for a highly excited anharmonic oscillator*, The Journal of Chemical Physics **84** (1986), 326–334.

[90] K. G. Kay: *Integral expressions for the semiclassical time-dependent propagator*, The Journal of Chemical Physics **100** (1994), 4377–4392.

[91] K. G. Kay: *Numerical study of semiclassical initial value methods for dynamics*, The Journal of Chemical Physics **100** (1994), 4432–4445.

[92] M. J. Davis and E. J. Heller: *Semiclassical Gaussian basis set method for molecular vibrational wave functions*, The Journal of Chemical Physics **71** (1979), 3383–3395.

[93] E. J. Heller: *Frozen Gaussians: A very simple semiclassical approximation*, The Journal of Chemical Physics **75** (1981), 2923–2931.

[94] S. Sawada, R. Heather, B. Jackson, and H. Metiu: *A strategy for time dependent quantum mechanical calculations using a Gaussian wave packet representation of the wave function*, The Journal of Chemical Physics **83** (1985), 3009–3027.

[95] G. Richings, I. Polyak, K. Spinlove, G. Worth, I. Burghardt, and B. Lasorne: *Quantum dynamics simulations using Gaussian wavepackets: the vMCG method*, International Reviews in Physical Chemistry **34** (2015), 269–308.

[96] D. Picconi and I. Burghardt: *Open system dynamics using Gaussian-based multiconfigurational time-dependent Hartree wavefunctions: Application to environment-modulated tunneling*, The Journal of Chemical Physics **150** (2019), 224106.

[97] W. Koch, M. Bonfanti, P. Eisenbrandt, A. Nandi, B. Fu, J. Bowman, D. Tannor, and I. Burghardt: *Two-layer Gaussian-based MCTDH study of the S1-S0 vibronic absorption spectrum of formaldehyde using multiplicative neural network potentials*, The Journal of Chemical Physics **151** (2019), 064121.

[98] S. Römer, M. Ruckenbauer, and I. Burghardt: *Gaussian-based multiconfiguration time-dependent Hartree: A two-layer approach. I. Theory*, The Journal of Chemical Physics **138** (2013), 064106.

[99] M. Bonfanti, J. Petersen, P. Eisenbrandt, I. Burghardt, and E. Pollak: *Computation of the S1-S0 Vibronic Absorption Spectrum of Formaldehyde by Variational Gaussian Wavepacket and Semiclassical IVR Methods*, Journal of Chemical Theory and Computation **14** (2018), 5310–5323.

[100] P. Eisenbrandt, M. Ruckenbauer, S. Römer, and I. Burghardt: *Gaussian-based multiconfiguration time-dependent Hartree: A two-layer approach. II. Application to vibrational energy transport in a molecular chain*, The Journal of Chemical Physics **149** (2018), 174101.

[101] U. Manthe: *The multi-configurational time-dependent Hartree approach revisited*, The Journal of Chemical Physics **142** (2015), 244109.

[102] H.-D. Meyer and H. Wang: *On regularizing the MCTDH equations of motion*, The Journal of Chemical Physics **148** (2018), 124105.

[103] H. Wang and H.-D. Meyer: *On regularizing the ML-MCTDH equations of motion*, The Journal of Chemical Physics **149** (2018), 044119.

[104] B. Poirier and J. C. Light: *Efficient distributed Gaussian basis for rovibrational spectroscopy calculations*, The Journal of Chemical Physics **113** (2000), 211–217.

[105] S. Habershon: *Linear dependence and energy conservation in Gaussian wavepacket basis sets*, The Journal of Chemical Physics **136** (2012), 014109.

[106] W. Koch and T. J. Frankcombe: *Basis Expansion Leaping: A New Method to Solve the Time-Dependent Schrödinger Equation for Molecular Quantum Dynamics*, Physical Review Letters **110** (2013), 263202.

[107] G. A. Hagedorn: *Semiclassical quantum mechanics. III. The large order asymptotics and more general states*, Annals of Physics **135** (1981), 58–70.

[108] R. Borrelli and A. Peluso: *Quantum dynamics of electronic transitions with Gauss-Hermite wave packets*, The Journal of Chemical Physics **144** (2016), 114102.

[109] H. R. Larsson, B. Hartke, and D. J. Tannor: *Efficient molecular quantum dynamics in coordinate and phase space using pruned bases*, The Journal of Chemical Physics **145** (2016), 204108.

[110] M. Bonfanti and I. Burghardt: *Tangent space formulation of the Multi-Configuration Time-Dependent Hartree equations of motion: The projector-splitting algorithm revisited*, Chemical Physics **515** (2018), 252–261.

[111] M. Werther and F. Grossmann: *Apoptosis of moving, non-orthogonal basis functions in many-particle quantum dynamics* (2019).

[112] J. Hopcroft and R. Tarjan: *Algorithm 447: efficient algorithms for graph manipulation* (1973).

[113] D. V. Shalashilin and I. Burghardt: *Gaussian-based techniques for quantum propagation from the time-dependent variational principle: Formulation in terms of trajectories of coupled classical and quantum variables*, Journal of Chemical Physics **129** (2008).

[114] V. M. Pérez-García, H. Michinel, J. I. Cirac, M. Lewenstein, and P. Zoller: *Low Energy Excitations of a Bose-Einstein Condensate: A Time-Dependent Variational Analysis*, Physical Review Letters **77** (1996), 5320–5323.

[115] D. O'Dell, S. Giovanazzi, G. Kurizki, and V. M. Akulin: *Bose-Einstein Condensates with 1/r Interatomic Attraction: Electromagnetically Induced "Gravity"*, Physical Review Letters **84** (2000), 5687–5690.

[116] D. V. Shalashilin and M. S. Child: *Time dependent quantum propagation in phase space*, The Journal of Chemical Physics **113** (2000), 10028–10036.

[117] D. V. Shalashilin and M. S. Child: *Description of tunneling with the help of coupled frozen Gaussians*, The Journal of Chemical Physics **114** (2001), 9296–9304.

[118] S. H. Strogatz: *Nonlinear Dynamics and Chaos*, (CRC Press), (2018).

[119] D. V. Shalashilin: *Quantum mechanics with the basis set guided by Ehrenfest trajectories: Theory and application to spin-boson model*, The Journal of Chemical Physics **130** (2009), 244101.

[120] M. S. Child and D. V. Shalashilin: *Locally coupled coherent states and Herman–Kluk dynamics*, The Journal of Chemical Physics **118** (2003), 2061–2071.

[121] B. Gu and S. Garashchuk: *Quantum Dynamics with Gaussian Bases Defined by the Quantum Trajectories*, The Journal of Physical Chemistry A **120** (2016), 3023–3031.

[122] I. Polyak, C. S. M. Allan, and G. A. Worth: *A complete description of tunnelling using direct quantum dynamics simulation: Salicylaldimine proton transfer*, The Journal of Chemical Physics **143** (2015), 084121.

[123] J. Liouville: *Note sur la Théorie de la Variation des constantes arbitraires.*, Journal de Mathématiques Pures et Appliquées (1838), 342–349.

[124] F. Grossmann and A. L. Xavier: *From the coherent state path integral to a semiclassical initial value representation of the quantum mechanical propagator*, Physics Letters A **243** (1998), 243–248.

[125] W. H. Miller: *On the relation between the semiclassical initial value representation and an exact quantum expansion in time-dependent coherent states*, The Journal of Physical Chemistry B **106** (2002), 8132–8135.

[126] F. Grossmann: *Theoretical Femtosecond Physics*, Graduate Texts in Physics, (Springer International Publishing, Cham), (2018).

[127] M. Buchholz, F. Grossmann, and M. Ceotto: *Mixed semiclassical initial value representation time-averaging propagator for spectroscopic calculations*, Journal of Chemical Physics **144** (2016), 094102.

[128] C. Harabati, J. M. Rost, and F. Grossmann: *Long-time and unitary properties of semiclassical initial value representations*, The Journal of Chemical Physics **120** (2004), 26–30.

[129] S. V. Isakov, M. B. Hastings, and R. G. Melko: *Topological entanglement entropy of a Bose–Hubbard spin liquid*, Nature Physics **7** (2011), 772–775.

[130] W. S. Cole, S. Zhang, A. Paramekanti, and N. Trivedi: *Bose-Hubbard Models with Synthetic Spin-Orbit Coupling: Mott Insulators, Spin Textures, and Superfluidity*, Physical Review Letters **109** (2012), 085302.

[131] S. Trotzky, Y.-A. Chen, A. Flesch, I. P. McCulloch, U. Schollwöck, J. Eisert, and I. Bloch: *Probing the relaxation towards equilibrium in an isolated strongly correlated one-dimensional Bose gas*, Nature Physics **8** (2012), 325–330.

[132] J. C. Budich, B. Trauzettel, and G. Sangiovanni: *Fluctuation-driven topological Hund insulators*, Physical Review B **87** (2013), 235104.

[133] V. Chernyak, S. Choi, and S. Mukamel: *Generalized coherent state representation of Bose-Einstein condensates*, Physical Review A **67** (2003), 053604.

[134] L. Chen, R. Borrelli, and Y. Zhao: *Dynamics of Coupled Electron–Boson Systems with the Multiple Davydov D 1 Ansatz and the Generalized Coherent State*, The Journal of Physical Chemistry A **121** (2017), 8757–8770.

[135] M. Werther, F. Grossmann, Z. Huang, and Y. Zhao: *Davydov-Ansatz for Landau-Zener-Stueckelberg-Majorana transitions in an environment: Tuning the survival probability via number state excitation*, The Journal of Chemical Physics **150** (2019), 234109.

[136] L. Chen, M. Gelin, and Y. Zhao: *Dynamics of the spin-boson model: A comparison of the multiple Davydov D1, D1.5, D2 Ansätze*, Chemical Physics **515** (2018), 108–118.

[137] L. Wang, Y. Fujihashi, L. Chen, and Y. Zhao: *Finite-temperature time-dependent variation with multiple Davydov states*, The Journal of Chemical Physics **146** (2017), 124127.

[138] P. Bocchieri and A. Loinger: *Quantum recurrence theorem*, Physical Review **107** (1957), 337–338.

[139] M. A. Nielsen and I. L. Chuang: *Quantum Computation and Quantum Information*, vol. 52, (Cambridge University Press, Cambridge), (2010).

[140] G.-Y. Xiang, Z.-B. Hou, C.-F. Li, G.-C. Guo, H.-P. Breuer, E.-M. Laine, and J. Piilo: *Entanglement distribution in optical fibers assisted by nonlocal memory effects*, EPL (Europhysics Letters) **107** (2014), 54006.

[141] B. Bylicka, D. Chruściński, and S. Maniscalco: *Non-Markovianity and reservoir memory of quantum channels: a quantum information theory perspective*, Scientific Reports **4** (2015), 5720.

[142] R. Kubo: *The fluctuation-dissipation theorem*, Reports on Progress in Physics **29** (1966), 306.

[143] H.-P. Breuer and F. Petruccione: *The Theory of Open Quantum Systems*, (Oxford University Press, Oxford, New York), (2007).

[144] A. Redfield: *The Theory of Relaxation Processes*, in: *Advances in Magnetic Resonance* (Ed. J. S. Waugh), vol. 1 of *Advances in Magnetic and Optical Resonance*, 1–32, (Academic Press), (1965).

[145] G. Lindblad: *On the Generators of Quantum Dynamical Semigroups*, Commun.Math. Phys. **48** (1976), 119–130.

[146] Y. Tanimura and S. Mukamel: *Optical Stark Spectroscopy of a Brownian Oscillator in Intense Fields*, Journal of the Physical Society of Japan **63** (1994), 66–77.

[147] N. Makri: *Numerical Path Integral Techniques for Long Time Dynamics of Quantum Dissipative Systems*, Journal of Mathematical Physics **36** (1995), 2430–2457.

[148] N. Makri and D. E. Makarov: *Tensor Propagator for Iterative Quantum Time Evolution of Reduced Density Matrices. I. Theory*, J. Chem. Phys. **102** (1995), 4600–4610.

[149] L. Diósi, N. Gisin, and W. T. Strunz: *Non-Markovian quantum state diffusion*, Phys. Rev. A **58** (1998), 1699–1712.

[150] W. T. Strunz, L. Diósi, and N. Gisin: *Open System Dynamics with Non-Markovian Quantum Trajectories*, Phys. Rev. Lett. **82** (1999), 1801–1805.

[151] C. Meier and D. J. Tannor: *Non-Markovian evolution of the density operator in the presence of strong laser fields*, Journal of Chemical Physics **111** (1999), 3365–3376.

[152] W. T. Strunz and T. Yu: *Convolutionless Non-Markovian Master Equations and Quantum Trajectories: Brownian Motion*, Phys. Rev. A **69** (2004), 052115.

[153] M. Schröder, U. Kleinekathöfer, and M. Schreiber: *Calculation of absorption spectra for light-harvesting systems using non-Markovian approaches as well as modified Redfield theory*, Journal of Chemical Physics **124** (2006), 084903.

[154] Y. Tanimura: *Stochastic Liouville, Langevin, Fokker–Planck, and Master Equation Approaches to Quantum Dissipative Systems*, J. Phys. Soc. Jpn. **75** (2006), 082001.

[155] T. Mori and S. Miyashita: *Dynamics of the Density Matrix in Contact with a Thermal Bath and the Quantum Master Equation*, J. Phys. Soc. Jpn. **77** (2008), 124005.

[156] G. Schaller and T. Brandes: *Preservation of Positivity by Dynamical Coarse Graining*, Phys. Rev. A **78** (2008), 022106.

[157] U. Weiss: *Quantum Dissipative Systems*, (World Scientific, Singapore), (2008).

[158] J. M. Moix and J. Cao: *A Hybrid Stochastic Hierarchy Equations of Motion Approach to Treat the Low Temperature Dynamics of Non-Markovian Open Quantum Systems*, J. Chem. Phys. **139** (2013), 134106.

[159] D. Suess, A. Eisfeld, and W. T. Strunz: *Hierarchy of Stochastic Pure States for Open Quantum System Dynamics*, Phys. Rev. Lett. **113** (2014), 150403.

[160] D. Suess, W. T. Strunz, and A. Eisfeld: *Hierarchical Equations for Open System Dynamics in Fermionic and Bosonic Environments*, Journal of Statistical Physics **159** (2015), 1408–1423.

[161] R. Hartmann and W. T. Strunz: *Exact Open Quantum System Dynamics Using the Hierarchy of Pure States (HOPS)*, Journal of Chemical Theory and Computation **13** (2017), 5834–5845.

[162] H. Wang, M. Thoss, and W. H. Miller: *Systematic convergence in the dynamical hybrid approach for complex systems: A numerically exact methodology*, Journal of Chemical Physics **115** (2001), 2979–2990.

[163] H. Wang and M. Thoss: *From coherent motion to localization: dynamics of the spin-boson model at zero temperature*, New Journal of Physics **10** (2008), 115005.

[164] K. H. Hughes, C. D. Christ, and I. Burghardt: *Effective-mode representation of non-Markovian dynamics: A hierarchical approximation of the spectral density. I. Application to single surface dynamics*, Journal of Chemical Physics **131** (2009), 024109.

[165] C.-M. Goletz and F. Grossmann: *Decoherence and dissipation in a molecular system coupled to an environment: An application of semiclassical hybrid dynamics*, Journal of Chemical Physics **130** (2009), 244107.

[166] H. Wang and M. Thoss: *From coherent motion to localization: II. Dynamics of the spin-boson model with sub-Ohmic spectral density at zero temperature*, Chemical Physics **370** (2010), 78–86.

[167] D. Conte and C. Lubich: *An error analysis of the multi-configuration time-dependent Hartree method of quantum dynamics*, ESAIM: Mathematical Modelling and Numerical Analysis **44** (2010), 759–780.

[168] L. Wang, L. Chen, N. Zhou, and Y. Zhao: *Variational dynamics of the sub-Ohmic spin-boson model on the basis of multiple Davydov D1 states*, Journal of Chemical Physics **144** (2016), 1–12.

[169] U. Manthe and T. Weike: *On the multi-layer multi-configurational time-dependent Hartree approach for bosons and fermions*, Journal of Chemical Physics **146** (2017), 064117.

[170] I. de Vega and D. Alonso: *Dynamics of non-Markovian open quantum systems*, Reviews of Modern Physics **89** (2017), 015001.

[171] S. Gröblacher, A. Trubarov, N. Prigge, G. D. Cole, M. Aspelmeyer, and J. Eisert: *Observation of non-Markovian micromechanical Brownian motion*, Nature Communications **6** (2015), 7606.

[172] K. H. Madsen, S. Ates, T. Lund-Hansen, A. Löffler, S. Reitzenstein, A. Forchel, and P. Lodahl: *Observation of Non-Markovian Dynamics of a Single Quantum Dot in a Micropillar Cavity*, Physical Review Letters **106** (2011), 233601.

[173] X. Mi, J. V. Cady, D. M. Zajac, P. W. Deelman, and J. R. Petta: *Strong coupling of a single electron in silicon to a microwave photon*, Science **355** (2017), 156–158.

[174] A. Potočnik, A. Bargerbos, F. A. Y. N. Schröder, S. A. Khan, M. C. Collodo, S. Gasparinetti, Y. Salathé, C. Creatore, C. Eichler, H. E. Türeci, A. W. Chin, and A. Wallraff: *Studying light-harvesting models with superconducting circuits*, Nature Communications **9** (2018), 904.

[175] I. Aharonovich, D. Englund, and M. Toth: *Solid-state single-photon emitters*, Nature Photonics **10** (2016), 631–641.

[176] A. W. Chin, J. Prior, R. Rosenbach, F. Caycedo-Soler, S. F. Huelga, and M. B. Plenio: *The role of non-equilibrium vibrational structures in electronic coherence and recoherence in pigment–protein complexes*, Nature Physics **9** (2013), 113–118.

[177] P. Kaer, T. R. Nielsen, P. Lodahl, A.-P. Jauho, and J. Mørk: *Non-Markovian Model of Photon-Assisted Dephasing by Electron-Phonon Interactions in a Coupled Quantum-Dot–Cavity System*, Physical Review Letters **104** (2010), 157401.

[178] D. P. S. McCutcheon and A. Nazir: *Coherent and incoherent dynamics in excitonic energy transfer: Correlated fluctuations and off-resonance effects*, Physical Review B **83** (2011), 165101.

[179] D. P. S. McCutcheon, N. S. Dattani, E. M. Gauger, B. W. Lovett, and A. Nazir: *A general approach to quantum dynamics using a variational master equation: Application to phonon-damped Rabi rotations in quantum dots*, Physical Review B **84** (2011), 081305.

[180] J. E. Subotnik, A. Jain, B. Landry, A. Petit, W. Ouyang, and N. Bellonzi: *Understanding the Surface Hopping View of Electronic Transitions and Decoherence*, Annual Review of Physical Chemistry **67** (2016), 387–417.

[181] D. Segal and B. K. Agarwalla: *Vibrational Heat Transport in Molecular Junctions*, Annual Review of Physical Chemistry **67** (2016), 185–209.

[182] A. O. Caldeira and A. J. Leggett: *Quantum tunnelling in a dissipative system*, Annals of Physics **149** (1983), 374–456.

[183] T. Deng, Y. Yan, L. Chen, and Y. Zhao: *Dynamics of the two-spin spin-boson model with a common bath*, The Journal of Chemical Physics **144** (2016), 144102.

[184] R. Marcus and N. Sutin: *Electron transfers in chemistry and biology*, Biochimica et Biophysica Acta (BBA) - Reviews on Bioenergetics **811** (1985), 265–322.

[185] L. Mühlbacher and R. Egger: *Crossover from nonadiabatic to adiabatic electron transfer reactions: Multilevel blocking Monte Carlo simulations*, Journal of Chemical Physics **118** (2003), 179–191.

[186] P. F. Barbara, T. J. Meyer, and M. A. Ratner: *Contemporary Issues in Electron Transfer Research*, The Journal of Physical Chemistry **100** (1996), 13148–13168.

[187] I. I. Rabi: *On the Process of Space Quantization*, Physical Review **49** (1936), 324–328.

[188] I. I. Rabi: *Space Quantization in a Gyrating Magnetic Field*, Physical Review **51** (1937), 652–654.

[189] A. Crespi, S. Longhi, and R. Osellame: *Photonic Realization of the Quantum Rabi Model*, Physical Review Letters **108** (2012), 163601.

[190] J. Larson: *Dynamics of the Jaynes–Cummings and Rabi models: old wine in new bottles*, Physica Scripta **76** (2007), 146–160.

[191] Q. Xie, H. Zhong, M. T. Batchelor, and C. Lee: *The quantum Rabi model: solution and dynamics*, Journal of Physics A: Mathematical and Theoretical **50** (2017), 113001.

[192] D. Braak: *Integrability of the Rabi model*, Physical Review Letters **107** (2011), 2–5.

[193] C. Moler and C. Van Loan: *Nineteen Dubious Ways to Compute the Exponential of a Matrix*, SIAM Review **20** (1978), 801–836.

[194] C. Moler and C. Van Loan: *Nineteen Dubious Ways to Compute the Exponential of a Matrix, Twenty-Five Years Later*, SIAM Review **45** (2003), 3–49.

[195] M. Grifoni, E. Paladino, and U. Weiss: *Dissipation, Decoherence and Preparation Effects in the Spin-Boson System*, Eur. Phys. J. B **10** (1999), 719–729.

[196] M. Thorwart, E. Paladino, and M. Grifoni: *Dynamics of the Spin-Boson Model with a Structured Environment*, Chem. Phys. **296** (2004), 333–344.

[197] F. B. Anders, R. Bulla, and M. Vojta: *Equilibrium and Nonequilibrium Dynamics of the Sub-Ohmic Spin-Boson Model*, Phys. Rev. Lett. **98** (2007), 210402.

[198] A. J. Leggett, S. Chakravarty, A. T. Dorsey, M. P. A. Fisher, A. Garg, and W. Zwerger: *Dynamics of the Dissipative Two-State System*, Rev. Mod. Phys. **59** (1987), 1–85.

[199] B. Golding, M. N. Zimmerman, and S. N. Coppersmith: *Dissipative quantum tunneling of a single microscopic defect in a mesoscopic metal*, Physical Review Letters **68** (1992), 998–1001.

[200] B. Golding, J. E. Graebner, A. B. Kane, and J. L. Black: *Relaxation of Tunneling Systems by Conduction Electrons in a Metallic Glass*, Physical Review Letters **41** (1978), 1487–1491.

[201] R. I. Cukier and M. Morillo: *Solvent effects on proton-transfer reactions*, The Journal of Chemical Physics **91** (1989), 857–863.

[202] S. Han, J. Lapointe, and J. E. Lukens: *Observation of incoherent relaxation by tunneling in a macroscopic two-state system*, Physical Review Letters **66** (1991), 810–813.

[203] M. Thorwart, J. Eckel, J. Reina, P. Nalbach, and S. Weiss: *Enhanced quantum entanglement in the non-Markovian dynamics of biomolecular excitons*, Chemical Physics Letters **478** (2009), 234–237.

[204] S. Huelga and M. Plenio: *Vibrations, quanta and biology*, Contemporary Physics **54** (2013), 181–207.

[205] J. Tang: *Superexchange electron-transfer reactions in a three-component system. The spin-boson model for photosynthesis*, Chemical Physics Letters **217** (1994), 55–60.

[206] M. Merkli, G. P. Berman, and R. Sayre: *Electron transfer reactions: generalized spin-boson approach*, Journal of Mathematical Chemistry **51** (2013), 890–913.

[207] D. P. DiVincenzo: *Two-bit gates are universal for quantum computation*, Physical Review A **51** (1995), 1015–1022.

[208] S. Chakravarty: *Quantum Fluctuations in the Tunneling between Superconductors*, Physical Review Letters **49** (1982), 681–684.

[209] A. J. Bray and M. A. Moore: *Influence of Dissipation on Quantum Coherence*, Physical Review Letters **49** (1982), 1545–1549.

[210] F. Guinea, V. Hakim, and A. Muramatsu: *Bosonization of a two-level system with dissipation*, Physical Review B **32** (1985), 4410–4418.

[211] G. Kotliar and Q. Si: *Toulouse points and non-Fermi-liquid states in the mixed-valence regime of the generalized Anderson model*, Physical Review B **53** (1996), 12373–12388.

[212] T. A. Costi and G. Zaránd: *Thermodynamics of the dissipative two-state system: A Bethe-ansatz study*, Physical Review B **59** (1999), 12398–12418.

[213] P. Forn-Díaz, J. J. García-Ripoll, B. Peropadre, J.-L. Orgiazzi, M. A. Yurtalan, R. Belyansky, C. M. Wilson, and A. Lupascu: *Ultrastrong coupling of a single artificial atom to an electromagnetic continuum in the nonperturbative regime*, Nature Physics **13** (2017), 39–43.

[214] B. Peropadre, D. Zueco, D. Porras, and J. J. García-Ripoll: *Nonequilibrium and Nonperturbative Dynamics of Ultrastrong Coupling in Open Lines*, Physical Review Letters **111** (2013), 243602.

[215] F. Yoshihara, T. Fuse, S. Ashhab, K. Kakuyanagi, S. Saito, and K. Semba: *Superconducting qubit–oscillator circuit beyond the ultrastrong-coupling regime*, Nature Physics **13** (2017), 44–47.

[216] H. Liu, L. Zhu, S. Bai, and Q. Shi: *Reduced quantum dynamics with arbitrary bath spectral densities: Hierarchical equations of motion based on several different bath decomposition schemes*, Journal of Chemical Physics **140** (2014), 134106.

[217] A. Winter, H. Rieger, M. Vojta, and R. Bulla: *Quantum Phase Transition in the Sub-Ohmic Spin-Boson Model: Quantum Monte Carlo Study with a Continuous Imaginary Time Cluster Algorithm*, Phys. Rev. Lett. **102** (2009), 030601.

[218] R. Hartmann, M. Werther, F. Grossmann, and W. T. Strunz: *Exact open quantum system dynamics: Optimal frequency vs time representation of bath correlations*, The Journal of Chemical Physics **150** (2019), 234105.

[219] H. Wang, X. Song, D. Chandler, and W. H. Miller: *Semiclassical study of electronically nonadiabatic dynamics in the condensed-phase: Spin-boson problem with Debye spectral density*, Journal of Chemical Physics **110** (1999), 4828–4840.

[220] C. M. Goletz, W. Koch, and F. Grossmann: *Semiclassical dynamics of open quantum systems: Comparing the finite with the infinite perspective*, Chemical Physics **375** (2010), 227–233.

[221] R. P. Feynman and F. L. Vernon: *The theory of a general quantum system interacting with a linear dissipative system*, Annals of Physics **173** (1963), 118–173.

[222] Y. Tanimura and P. G. Wolynes: *Quantum and classical Fokker-Planck equations for a Gaussian-Markovian noise bath*, Phys. Rev. A **43** (1991), 4131–4142.

[223] I. De Vega, U. Schollwöck, and F. A. Wolf: *How to discretize a quantum bath for real-time evolution*, Physical Review B - Condensed Matter and Materials Physics **92** (2015), 1–14.

[224] D. Kast and J. Ankerhold: *Persistence of Coherent Quantum Dynamics at Strong Dissipation*, Physical Review Letters **110** (2013), 010402.

[225] S. Suzuki, H. Oshiyama, and N. Shibata: *Quantum Annealing of Pure and Random Ising Chains Coupled to a Bosonic Environment*, Journal of the Physical Society of Japan **88** (2019), 061003.

[226] P. Nalbach and M. Thorwart: *Ultraslow Quantum Dynamics in a Sub-Ohmic Heat Bath*, Phys. Rev. B **81** (2010), 054308.

[227] H. Mori: *A Continued-Fraction Representation of the Time-Correlation Functions*, Progress of Theoretical Physics **34** (1965), 399–416.

[228] M. Dupuis: *Moment and Continued Fraction Expansions of Time Autocorrelation Functions*, Progress of Theoretical Physics **37** (1967), 502–537.

[229] P. Grigolini and G. P. Parravicini: *Phonon thermal baths: A treatment in terms of reduced models*, Physical Review B **25** (1982), 5180–5187.

[230] E. Gindensperger, I. Burghardt, and L. S. Cederbaum: *Short-time dynamics through conical intersections in macrosystems. I. Theory: Effective-mode formulation*, The Journal of Chemical Physics **124** (2006), 144103.

[231] E. Gindensperger and L. S. Cederbaum: *Quantum dynamics in macrosystems with several coupled electronic states: Hierarchy of effective Hamiltonians*, The Journal of Chemical Physics **127** (2007), 124107.

[232] E. Gindensperger, H. Köppel, and L. S. Cederbaum: *Hierarchy of effective modes for the dynamics through conical intersections in macrosystems*, The Journal of Chemical Physics **126** (2007), 034106.

[233] K. H. Hughes, C. D. Christ, and I. Burghardt: *Effective-mode representation of non-Markovian dynamics: A hierarchical approximation of the spectral density. II. Application to environment-induced nonadiabatic dynamics*, The Journal of Chemical Physics **131** (2009), 124108.

[234] B. N. J. Persson: *Vibrational energy and phase relaxation at surfaces*, Journal of Physics C: Solid State Physics **17** (1984), 4741–4750.

[235] R. Franchy, M. Wuttig, and H. Ibach: *Anharmonic effects on adsorbate vibrations*, Surface Science **203** (1988), 489–499.

[236] H. Kasai and A. Okiji: *Non-adiabatic effects on electronic damping of adsorbate vibrations on metal surfaces*, Journal of Electron Spectroscopy and Related Phenomena **54-55** (1990), 163–171.

[237] E. Rotenberg, J. Schaefer, and S. D. Kevan: *Coupling Between Adsorbate Vibrations and an Electronic Surface State*, Physical Review Letters **84** (2000), 2925–2928.

[238] K. Watanabe, N. Takagi, and Y. Matsumoto: *Direct Time-Domain Observation of Ultrafast Dephasing in Adsorbate-Substrate Vibration under the Influence of a Hot Electron Bath: Cs Adatoms on Pt(111)*, Physical Review Letters **92** (2004), 057401.

[239] R. Arafune, K. Hayashi, S. Ueda, Y. Uehara, and S. Ushioda: *Inelastic Photoemission due to Scattering by Surface Adsorbate Vibrations*, Physical Review Letters **95** (2005), 207601.

[240] S. Sakong, P. Kratzer, X. Han, T. Balgar, and E. Hasselbrink: *Isotope effects in the vibrational lifetime of hydrogen on germanium(100): Theory and experiment*, The Journal of Chemical Physics **131** (2009), 124502.

[241] H. Arnolds: *Vibrational dynamics of adsorbates – Quo vadis?*, Progress in Surface Science **86** (2011), 1–40.

[242] G. Füchsel, J. C. Tremblay, T. Klamroth, and P. Saalfrank: *Selective Excitation of Molecule-Surface Vibrations in H2 and D2 Dissociatively Adsorbed on Ru(0001)*, Israel Journal of Chemistry **52** (2012), 438–451.

[243] T. C. Shen, C. Wang, G. C. Abeln, J. R. Tucker, J. W. Lyding, P. Avouris, and R. E. Walkup: *Atomic-Scale Desorption Through Electronic and Vibrational Excitation Mechanisms*, Science **268** (1995), 1590–1592.

[244] H. Guo, P. Saalfrank, and T. Seideman: *Theory of photoinduced surface reactions of admolecules*, Progress in Surface Science **62** (1999), 239–303.

[245] K. Laß, X. Han, and E. Hasselbrink: *The surprisingly short vibrational lifetime of the internal stretch of CO adsorbed on Si(100)*, The Journal of Chemical Physics **123** (2005), 051102.

[246] P. Saalfrank: *Quantum Dynamical Approach to Ultrafast Molecular Desorption from Surfaces*, Chemical Reviews **106** (2006), 4116–4159.

[247] N. Shenvi, S. Roy, and J. C. Tully: *Nonadiabatic dynamics at metal surfaces: Independent-electron surface hopping*, The Journal of Chemical Physics **130** (2009), 174107.

[248] B. Lepetit, D. Lemoine, Z. Medina, and B. Jackson: *Sticking and desorption of hydrogen on graphite: A comparative study of different models*, The Journal of Chemical Physics **134** (2011), 114705.

[249] O. Galparsoro, R. Pétuya, J. I. Juaristi, C. Crespos, M. Alducin, and P. Larrégaray: *Energy Dissipation to Tungsten Surfaces upon Eley–Rideal Recombination of N_2 and H_2*, The Journal of Physical Chemistry C **119** (2015), 15434–15442.

[250] G.-J. Kroes and C. Díaz: *Quantum and classical dynamics of reactive scattering of H_2 from metal surfaces*, Chemical Society Reviews **45** (2016), 3658–3700.

[251] M. Bonfanti and R. Martinazzo: *Classical and quantum dynamics at surfaces: Basic concepts from simple models*, International Journal of Quantum Chemistry **116** (2016), 1575–1602.

[252] K. Stokbro, U. J. Quaade, R. Lin, C. Thirstrup, and F. Grey: *Electronic mechanism of STM-induced diffusion of hydrogen on Si(100)*, Faraday Discussions **117** (2000), 231–240.

[253] A. I. Volokitin and B. N. J. Persson: *Adsorbate-Induced Enhancement of Electrostatic Noncontact Friction*, Physical Review Letters **94** (2005), 086104.

[254] B. Persson and P. Avouris: *Local bond breaking via STM-induced excitations: the role of temperature*, Surface Science **390** (1997), 45–54.

[255] E. T. Foley, A. F. Kam, J. W. Lyding, and P. Avouris: *Cryogenic UHV-STM Study of Hydrogen and Deuterium Desorption from Si(100)*, Physical Review Letters **80** (1998), 1336–1339.

[256] J. I. Pascual, J. J. Jackiw, Z. Song, P. S. Weiss, H. Conrad, and H.-P. Rust: *Adsorbate-Substrate Vibrational Modes of Benzene on Ag(110) Resolved with Scanning Tunneling Spectroscopy*, Physical Review Letters **86** (2001), 1050–1053.

[257] P. Gao and M. J. Weaver: *Surface-enhanced Raman spectroscopy as a probe of adsorbate-surface bonding: benzene and monosubstituted benzenes adsorbed at gold electrodes*, The Journal of Physical Chemistry **89** (1985), 5040–5046.

[258] B. N. J. Persson, K. Zhao, and Z. Zhang: *Chemical Contribution to Surface-Enhanced Raman Scattering*, Physical Review Letters **96** (2006), 207401.

[259] H. Xu, E. J. Bjerneld, M. Käll, and L. Börjesson: *Spectroscopy of Single Hemoglobin Molecules by Surface Enhanced Raman Scattering*, Physical Review Letters **83** (1999), 4357–4360.

[260] A. M. Michaels, M. Nirmal, and L. E. Brus: *Surface Enhanced Raman Spectroscopy of Individual Rhodamine 6G Molecules on Large Ag Nanocrystals*, Journal of the American Chemical Society **121** (1999), 9932–9939.

[261] Jiang, K. Bosnick, M. Maillard, and L. Brus: *Single Molecule Raman Spectroscopy at the Junctions of Large Ag Nanocrystals*, The Journal of Physical Chemistry B **107** (2003), 9964–9972.

[262] P. Dumas, Y. J. Chabal, and G. S. Higashi: *Coupling of an adsorbate vibration to a substrate surface phonon: H on Si(111)*, Physical Review Letters **65** (1990), 1124–1127.

[263] P. Guyot-Sionnest, P. Dumas, Y. J. Chabal, and G. S. Higashi: *Lifetime of an adsorbate-substrate vibration: H on Si(111)*, Physical Review Letters **64** (1990), 2156–2159.

[264] P. Guyot-Sionnest, P. H. Lin, and E. M. Hiller: *Vibrational dynamics of the Si–H stretching modes of the Si(100)/H:2x1 surface*, The Journal of Chemical Physics **102** (1995), 4269–4278.

[265] C. Thirstrup, M. Sakurai, T. Nakayama, and K. Stokbro: *Temperature suppression of STM-induced desorption of hydrogen on Si(100) surfaces*, Surface Science **424** (1999), L329–L334.

[266] J. C. Tully: *Mode-Selective Control of Surface Reactions*, Science **312** (2006), 1004–1005.

[267] Z. Liu: *Desorption of H from Si(111) by Resonant Excitation of the Si-H Vibrational Stretch Mode*, Science **312** (2006), 1024–1026.

[268] J. C. Tully, Y. J. Chabal, K. Raghavachari, J. M. Bowman, and R. R. Lucchese: *Infrared linewidths and vibrational lifetimes at surfaces: H on Si(100)*, Physical Review B **31** (1985), 1184–1186.

[269] Y. Chabal, P. Dumas, P. Guyot-Sionnest, and G. Higashi: *Vibrational dynamics of the ideally H-terminated Si(111) surface*, Surface Science **242** (1991), 524–530.

[270] K. Kuhnke, M. Morin, P. Jakob, N. J. Levinos, Y. J. Chabal, and A. L. Harris: *Vibrational energy transfer among adsorbate modes: Picosecond dynamics on stepped H/Si(111)*, The Journal of Chemical Physics **99** (1993), 6114–6125.

[271] C.-S. Tsai, C.-E. Lin, J.-C. Lin, and J.-K. Wang: *Vibrational dephasing dynamics of the hydrogenated Si(100)-2x1 surface revisited: multi-mode dephasing model*, Chemical Physics Letters **295** (1998), 509–515.

[272] R. Honke, P. Jakob, Y. J. Chabal, A. Dvořák, S. Tausendpfund, W. Stigler, P. Pavone, A. P. Mayer, and U. Schröder: *Anharmonic adlayer vibrations on the Si(111):H surface*, Physical Review B **59** (1999), 10996–11013.

[273] S. Watanabe: *Chemical structure and surface phonons associated with H on Si*, The Journal of Chemical Physics **108** (1998), 5965–5974.

[274] S. Watanabe: *Isotopic shift and broadening of Si–D bending vibration on Si(111)*, Applied Surface Science **162-163** (2000), 146–151.

[275] K. Stokbro: *Electric field dependent structural and vibrational properties of the Si(100)-H(2x1) surface and its implications for STM induced hydrogen desorption*, Surface Science **429** (1999), 327–337.

[276] D. W. Brenner and B. J. Garrison: *Dissociative valence force field potential for silicon*, Physical Review B **34** (1986), 1304–1307.

[277] F. Bouakline, U. Lorenz, G. Melani, G. K. Paramonov, and P. Saalfrank: *Isotopic effects in vibrational relaxation dynamics of H on a Si(100) surface*, The Journal of Chemical Physics **147** (2017), 144703.

[278] V. Zorba, J. Syzdek, X. Mao, R. E. Russo, and R. Kostecki: *Ultrafast laser induced breakdown spectroscopy of electrode/electrolyte interfaces*, Applied Physics Letters **100** (2012), 234101.

[279] M. Eisele, T. L. Cocker, M. A. Huber, M. Plankl, L. Viti, D. Ercolani, L. Sorba, M. S. Vitiello, and R. Huber: *Ultrafast multi-terahertz nano-spectroscopy with sub-cycle temporal resolution*, Nature Photonics **8** (2014), 841–845.

[280] F. Ceballos and H. Zhao: *Ultrafast Laser Spectroscopy of Two-Dimensional Materials Beyond Graphene*, Advanced Functional Materials **27** (2017), 1604509.

[281] C. Ferrante, A. Virga, L. Benfatto, M. Martinati, D. De Fazio, U. Sassi, C. Fasolato, A. K. Ott, P. Postorino, D. Yoon, G. Cerullo, F. Mauri, A. C. Ferrari, and T. Scopigno: *Raman spectroscopy of graphene under ultrafast laser excitation*, Nature Communications **9** (2018), 308.

[282] C. Bronner and P. Tegeder: *Relaxation dynamics of photoexcited charge carriers at the Bi(111) surface*, Physical Review B **89** (2014), 115105.

[283] Z. An, C. Q. Wu, and X. Sun: *Dynamics of Photogenerated Polarons in Conjugated Polymers*, Physical Review Letters **93** (2004), 216407.

[284] C.-L. Lee, I.-W. Hwang, C. C. Byeon, B. H. Kim, and N. C. Greenham: *Triplet Exciton and Polaron Dynamics in Phosphorescent Dye Blended Polymer Photovoltaic Devices*, Advanced Functional Materials **20** (2010), 2945–2950.

[285] E. Mozafari and S. Stafström: *Polaron dynamics in a two-dimensional Holstein-Peierls system*, The Journal of Chemical Physics **138** (2013), 184104.

[286] T. Holstein: *Studies of polaron motion*, Annals of Physics **8** (1959), 343–389.

[287] T. Holstein: *Studies of polaron motion*, Annals of Physics **8** (1959), 325–342.

[288] M. Kang, S. W. Jung, W. J. Shin, Y. Sohn, S. H. Ryu, T. K. Kim, M. Hoesch, and K. S. Kim: *Holstein polaron in a valley-degenerate two-dimensional semiconductor*, Nature Materials **17** (2018), 676–680.

[289] F. Herrera and R. V. Krems: *Tunable Holstein model with cold polar molecules*, Physical Review A **84** (2011), 051401.

[290] A. Tayebi and V. Zelevinsky: *The Holstein polaron problem revisited*, Journal of Physics A: Mathematical and Theoretical **49** (2016), 255004.

[291] O. R. Tozer and W. Barford: *Localization of large polarons in the disordered Holstein model*, Physical Review B **89** (2014), 155434.

[292] D. Golež, J. Bonča, L. Vidmar, and S. A. Trugman: *Relaxation Dynamics of the Holstein Polaron*, Physical Review Letters **109** (2012), 236402.

[293] L. Chen, Y. Zhao, and Y. Tanimura: *Dynamics of a One-Dimensional Holstein Polaron with the Hierarchical Equations of Motion Approach*, Journal of Physical Chemistry Letters **6** (2015), 3110–3115.

[294] N. Zhou, L. Chen, Z. Huang, K. Sun, Y. Tanimura, and Y. Zhao: *Fast, Accurate Simulation of Polaron Dynamics and Multidimensional Spectroscopy by Multiple Davydov Trial States*, The Journal of Physical Chemistry A **120** (2016), 1562–1576.

[295] Z. Huang, L. Wang, C. Wu, L. Chen, F. Grossmann, and Y. Zhao: *Polaron dynamics with off-diagonal coupling: beyond the Ehrenfest approximation*, Phys. Chem. Chem. Phys. **19** (2017), 1655–1668.

[296] S. Tanaka: *Ultrafast relaxation dynamics of the one-dimensional molecular chain: The time-resolved spontaneous emission and exciton coherence*, The Journal of Chemical Physics **119** (2003), 4891–4904.

[297] E. J. Heller: *The semiclassical way to molecular spectroscopy*, Acc. Chem. Res. **14** (1981), 368.

[298] K. Huang and A. Rhys: *Theory of light absorption and non-radiative transitions in F-centres*, Proc. R. Soc. London **Ser. A** (1950), 406.

[299] L. D. Landau: *A Theory of Energy Transfer II*, Phys. Z. Soviet Union **2** (1932), 46.

[300] C. Zener: *Non-adiabatic crossing of energy levels*, Proceedings of the Royal Society of London. Series A, Containing Papers of a Mathematical and Physical Character **137** (1932), 696–702.

[301] E. C. G. Stueckelberg: *Theorie der unelastischen Stösse zwischen Atomen*, Hel. Phys. Acta **5** (1932), 369.

[302] E. Majorana: *Atomi orientati in campo magnetico variabile*, Il Nuovo Cimento **9** (1932), 43–50.

[303] M. S. Child: *Molecular collision theory*, (Academic Press London ; New York), (1974).

[304] R. J. Lipert, G. Bermudez, and S. D. Colson: *Pathways of S1 decay in phenol, indoles, and water complexes of phenol and indole in a free jet expansion*, The Journal of Physical Chemistry **92** (1988), 3801–3805.

[305] A. Thiel: *The Landau-Zener effect in nuclear molecules*, Journal of Physics G: Nuclear and Particle Physics **16** (1990), 867–910.

[306] W. Wernsdorfer and R. Sessoli: *Quantum Phase Interference and Parity Effects in Magnetic Molecular Clusters*, Science **284** (1999), 133–135.

[307] W. Xie and W. Domcke: *Accuracy of trajectory surface-hopping methods: Test for a two-dimensional model of the photodissociation of phenol*, The Journal of Chemical Physics **147** (2017), 184114.

[308] D. Bouwmeester, N. H. Dekker, F. E. v. Dorsselaer, C. A. Schrama, P. M. Visser, and J. P. Woerdman: *Observation of Landau-Zener dynamics in classical optical systems*, Physical Review A **51** (1995), 646–654.

[309] W. Wernsdorfer, R. Sessoli, A. Caneschi, D. Gatteschi, A. Cornia, and D. Mailly: *Landau–Zener method to study quantum phase interference of Fe8 molecular nanomagnets*, Journal of Applied Physics **87** (2000), 5481–5486.

[310] W. Wernsdorfer, R. Sessoli, A. Caneschi, D. Gatteschi, and A. Cornia: *Nonadiabatic Landau-Zener tunneling in Fe8molecular nanomagnets*, Europhysics Letters (EPL) **50** (2000), 552–558.

[311] L. Zhu, A. Widom, and P. M. Champion: *A multidimensional Landau-Zener description of chemical reaction dynamics and vibrational coherence*, The Journal of Chemical Physics **107** (1997), 2859–2871.

[312] G. D. Fuchs, G. Burkard, P. V. Klimov, and D. D. Awschalom: *A quantum memory intrinsic to single nitrogen–vacancy centres in diamond*, Nature Physics **7** (2011), 789–793.

[313] T. Ota, K. Hitachi, and K. Muraki: *Landau-Zener-Stückelberg interference in coherent charge oscillations of a one-electron double quantum dot*, Scientific Reports **8** (2018), 5491.

[314] A. J. Olson, S.-J. Wang, R. J. Niffenegger, C.-H. Li, C. H. Greene, and Y. P. Chen: *Tunable Landau-Zener transitions in a spin-orbit-coupled Bose-Einstein condensate*, Physical Review A **90** (2014), 013616.

[315] W. D. Oliver, Y. Yu, J. C. Lee, K. K. Berggreen, L. S. Levitov, and T. P. Orlando: *Mach-Zehnder Interferometry in a Strongly Driven Superconducting Qubit*, Science **310** (2005), 1653–1657.

[316] K. Saito, M. Wubs, S. Kohler, Y. Kayanuma, and P. Hänggi: *Dissipative Landau-Zener transitions of a qubit: Bath-specific and universal behavior*, Physical Review B **75** (2007), 214308.

[317] D. Zueco, P. Hänggi, and S. Kohler: *Landau–Zener tunnelling in dissipative circuit QED*, New Journal of Physics **10** (2008), 115012.

[318] T. Niemczyk, F. Deppe, H. Huebl, E. P. Menzel, F. Hocke, M. J. Schwarz, J. J. Garcia-Ripoll, D. Zueco, T. Hümmer, E. Solano, A. Marx, and R. Gross: *Circuit quantum electrodynamics in the ultrastrong-coupling regime*, Nature Physics **6** (2010), 772–776.

[319] A. Wallraff, D. I. Schuster, A. Blais, L. Frunzio, R.-S. Huang, J. Majer, S. Kumar, S. M. Girvin, and R. J. Schoelkopf: *Strong coupling of a single photon to a superconducting qubit using circuit quantum electrodynamics*, Nature **431** (2004), 162–167.

[320] I. Chiorescu, P. Bertet, K. Semba, Y. Nakamura, C. J. P. M. Harmans, and J. E. Mooij: *Coherent dynamics of a flux qubit coupled to a harmonic oscillator*, Nature **431** (2004), 159–162.

[321] O. Astafiev, K. Inomata, A. O. Niskanen, T. Yamamoto, Y. A. Pashkin, Y. Nakamura, and J. S. Tsai: *Single artificial-atom lasing*, Nature **449** (2007), 588–590.

[322] A. Izmalkov, M. Grajcar, E. Ilichev, N. Oukhanski, T. Wagner, H.-G. Meyer, W. Krech, M. H. S. Amin, A. M. van den Brink, and A. M. Zagoskin: *Observation of macroscopic Landau-Zener transitions in a superconducting device*, Europhysics Letters **65** (2004), 844–849.

[323] M. Wubs, K. Saito, S. Kohler, P. Hänggi, and Y. Kayanuma: *Gauging a Quantum Heat Bath with Dissipative Landau-Zener Transitions*, Physical Review Letters **97** (2006), 200404.

[324] P. Ao and J. Rammer: *Influence of dissipation on the Landau-Zener transition*, Physical Review Letters **62** (1989), 3004–3007.

[325] P. Nalbach and M. Thorwart: *Landau-Zener Transitions in a Dissipative Environment: Numerically Exact Results*, Physical Review Letters **103** (2009), 220401.

[326] P. Nalbach, J. Knörzer, and S. Ludwig: *Nonequilibrium Landau-Zener-Stueckelberg spectroscopy in a double quantum dot*, Physical Review B **87** (2013), 165425.

[327] P. Nalbach: *Adiabatic-Markovian bath dynamics at avoided crossings*, Physical Review A **90** (2014), 042112.

[328] P. Nalbach, C. A. Mujica-Martinez, and M. Thorwart: *Vibronically coherent speed-up of the excitation energy transfer in the Fenna-Matthews-Olson complex*, Physical Review E **91** (2015), 022706.

[329] P. Nalbach, N. Klinkenberg, T. Palm, and N. Müller: *Environmental rocking ratchet: Environmental rectification by a harmonically driven avoided crossing*, Physical Review E **96** (2017), 042134.

[330] Z. Sun, L. Zhou, G. Xiao, D. Poletti, and J. Gong: *Finite-time Landau-Zener processes and counterdiabatic driving in open systems: Beyond Born, Markov, and rotating-wave approximations*, Physical Review A **93** (2016), 012121.

[331] Z. Huang and Y. Zhao: *Dynamics of dissipative Landau-Zener transitions*, Physical Review A **97** (2018), 013803.

[332] Z. Sun, J. Ma, X. Wang, and F. Nori: *Photon-assisted Landau-Zener transition: Role of coherent superposition states*, Physical Review A **86** (2012), 012107.

[333] S. Ashhab: *Superradiance transition in a system with a single qubit and a single oscillator*, Physical Review A **87** (2013), 013826.

[334] R. K. Malla and M. E. Raikh: *Landau-Zener transition in a two-level system coupled to a single highly excited oscillator*, Physical Review B **97** (2018), 035428.

[335] T. Kato: *On the Adiabatic Theorem of Quantum Mechanics*, Journal of the Physical Society of Japan **5** (1950), 435–439.

[336] S. Gleyzes, S. Kuhr, C. Guerlin, J. Bernu, S. Deleglise, U. Busk Hoff, M. Brune, J.-M. Raimond, and S. Haroche: *Quantum jumps of light recording the birth and death of a photon in a cavity*, Nature **446** (2007), 297–300.

[337] S. Haroche: *Nobel Lecture: Controlling photons in a box and exploring the quantum to classical boundary*, Reviews of Modern Physics **85** (2013), 1083–1102.

[338] P. Domokos, P. Adam, and J. Janszky: *One-dimensional coherent-state representation on a circle in phase space*, Physical Review A **50** (1994), 4293–4297.

[339] P. P. Orth, A. Imambekov, and K. Le Hur: *Nonperturbative stochastic method for driven spin-boson model*, Physical Review B **87** (2013), 014305.

[340] M. B. Plenio and S. F. Huelga: *Entangled Light from White Noise*, Physical Review Letters **88** (2002), 197901.

[341] C. Marr, A. Beige, and G. Rempe: *Entangled-state preparation via dissipation-assisted adiabatic passages*, Physical Review A - Atomic, Molecular, and Optical Physics **68** (2003), 11.

[342] A. S. Parkins, E. Solano, and J. I. Cirac: *Unconditional Two-Mode Squeezing of Separated Atomic Ensembles*, Physical Review Letters **96** (2006), 053602.

[343] S. Diehl, A. Micheli, A. Kantian, B. Kraus, H. P. Büchler, and P. Zoller: *Quantum states and phases in driven open quantum systems with cold atoms*, Nature Physics **4** (2008), 878–883.

[344] J. Li and G. S. Paraoanu: *Generation and propagation of entanglement in driven coupled-qubit systems*, New Journal of Physics **11** (2009), 113020.

[345] F. Verstraete, M. M. Wolf, and J. Ignacio Cirac: *Quantum computation and quantum-state engineering driven by dissipation*, Nature Physics **5** (2009), 633–636.

[346] M. J. Kastoryano, F. Reiter, and A. S. Sørensen: *Dissipative Preparation of Entanglement in Optical Cavities*, Physical Review Letters **106** (2011), 090502.

[347] C. A. Muschik, E. S. Polzik, and J. I. Cirac: *Dissipatively driven entanglement of two macroscopic atomic ensembles*, Physical Review A **83** (2011), 052312.

[348] H. Krauter, C. A. Muschik, K. Jensen, W. Wasilewski, J. M. Petersen, J. I. Cirac, and E. S. Polzik: *Entanglement Generated by Dissipation and Steady State Entanglement of Two Macroscopic Objects*, Physical Review Letters **107** (2011), 080503.

[349] K. Koga and N. Yamamoto: *Dissipation-induced pure Gaussian state*, Physical Review A **85** (2012), 022103.

[350] J. C. Budich, P. Zoller, and S. Diehl: *Dissipative preparation of Chern insulators*, Physical Review A **91** (2015), 042117.

[351] S. Lüker, T. Kuhn, and D. E. Reiter: *Phonon-assisted dark exciton preparation in a quantum dot*, Physical Review B **95** (2017), 1–8.

[352] P. van der Straten and H. Metcalf: *Atoms and Molecules Interacting with Light*, (Cambridge University Press, Cambridge), (2016).

[353] J. S. Melinger, S. R. Gandhi, A. Hariharan, D. Goswami, and W. S. Warren: *Adiabatic population transfer with frequency-swept laser pulses*, The Journal of Chemical Physics **101** (1994), 6439–6454.

[354] V. Malinovsky and J. Krause: *General theory of population transfer by adiabatic rapid passage with intense, chirped laser pulses*, The European Physical Journal D **14** (2001), 147–155.

[355] A. Debnath, C. Meier, B. Chatel, and T. Amand: *Chirped laser excitation of quantum dot excitons coupled to a phonon bath*, Physical Review B - Condensed Matter and Materials Physics **86** (2012), 1–5.

[356] I. Bloch, J. Dalibard, and W. Zwerger: *Many-body physics with ultracold gases*, Reviews of Modern Physics **80** (2008), 885–964.

[357] C.-M. Simon, T. Belhadj, B. Chatel, T. Amand, P. Renucci, A. Lemaitre, O. Krebs, P. A. Dalgarno, R. J. Warburton, X. Marie, and B. Urbaszek: *Robust Quantum Dot Exciton Generation via Adiabatic Passage with Frequency-Swept Optical Pulses*, Physical Review Letters **106** (2011), 166801.

[358] R. Binder, D. Lauvergnat, and I. Burghardt: *Conformational Dynamics Guides Coherent Exciton Migration in Conjugated Polymer Materials: First-Principles Quantum Dynamical Study*, Physical Review Letters **120** (2018), 227401.

List of publications

F. Grossmann, M. Werther, L. Chen, and Y. Zhao: *Generalization of the Davydov Ansatz by squeezing*, Chemical Physics **481** (2016), 99–107.

M. Werther and F. Grossmann: *Including temperature in a wavefunction description of the dynamics of the quantum Rabi model*, Journal of Physics A: Mathematical and Theoretical **51** (2018), 014001.

M. Werther and F. Grossmann: *The Davydov D1.5 Ansatz for the quantum Rabi model*, Physica Scripta **93** (2018), 074001.

R. Hartmann, M. Werther, F. Grossmann, and W. T. Strunz: *Exact open quantum system dynamics: Optimal frequency vs time representation of bath correlations*, The Journal of Chemical Physics **150** (2019), 234105.

M. Werther, F. Grossmann, Z. Huang, and Y. Zhao: *Davydov-Ansatz for Landau-Zener-Stueckelberg-Majorana transitions in an environment: Tuning the survival probability via number state excitation*, The Journal of Chemical Physics **150** (2019), 234109.

M. Werther and F. Grossmann: *Apoptosis of moving, non-orthogonal basis functions in many- particle quantum dynamics*, Physical Review B **101** (2020), 174315.

Erklärung

Diese Arbeit wurde am Institut für Theoretische Physik der Technischen Universität Dresden unter der wissenschaftlichen Betreuung PD. Dr. Frank Großmanns, Prof. Dr. Jan Carl Budichs und Prof. Dr. Matthias Vojtas durchgeführt.

Hiermit versichere ich, dass ich die vorliegende Arbeit ohne unzulässige Hilfe Dritter und ohne Benutzung anderer als der angegebenen Hilfsmittel angefertigt habe; die aus fremden Quellen direkt oder indirekt übernommenen Gedanken sind als solche kenntlich gemacht. Die Arbeit wurde bisher weder im Inland noch im Ausland in gleicher oder ähnlicher Form einer anderen Prüfungsbehörde vorgelegt. Darüber hinaus erkenne ich die Promotionsordnung der Fakultät Mathematik und Naturwissenschaften der Technischen Universität Dresden vom 23. Februar 2011 an.

Dresden, 21.04.2020 _____

Michael Werther